N-Heterocyclic Metallocenes of the Lanthanides based on the 4-azapentalenyl anion.

by

Lauren Emily Wise

BSc (Hons)

Submitted in fulfilment of the requirements for the Degree of

Doctor of Philosophy in Chemistry

School of Chemistry

University of Tasmania

November, 2009

DECLARATION OF ORIGINALITY

This thesis contains no material which has been accepted for a degree or diploma by the University or any other institution, except by way of background information and duly acknowledged in the thesis, and to the best of the candidate's knowledge and belief no material previously published or written by another person except where due acknowledgement is made in the text of the thesis.

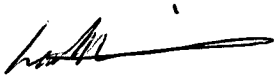

Lauren E. Wise

November, 2009

STATEMENT OF AUTHORITY OF ACCESS

ACKNOWLEDGEMENTS

To my supervisors Dr Michael Gardiner and Professor Brian Yates I thank for their time, support, patience, ongoing encouragement and advise through out the course of my PhD. Their sharing of their knowledge in their particular areas has allowed me to develop my scientific skills and widen my interest in the field of chemistry. I am forever grateful for their belief in my ability in allowing me to undertake this project and their persistence when the going was hampered. I would especially like to thank Dr Michael Gardiner for the opportunity he provided me with to go and study in the group of Professor Reiner Anwander at the Technische Universität München during my PhD, this was invaluable and for this I am truly grateful.

I thank the members of the organometallic (Lab 308) and computational (Room 314) groups whom I have had the pleasure of working with during the course of my studies in particular Dr Vicki-Anne Tolhurst, Dr Jun Wang, Dr Alistair Frey, Dr David Graham, Dr Alison Magill, Dr Melanie Denney and Dr Thomas Rodemann. Along with various other members of the group, which would take up far too much space. I thank you for the fun and enjoyment as well as the help and ideas you have shared with me along the way. I would also like to thank Professor Reiner Anwander, Dr Andreas Fischbach and Dr Frank Estler for the memorable experience at the Technische Universität München, the time spent here and the sharing of their knowledge with me.

To the multitude of people from the School of Chemistry at the University of Tasmania, past and present, thank you for the support over the course of my undergraduate and postgraduate studies as well as providing me with a good environment in which to work and learn in. To Dr Emily Hilder my Post Graduate Research coordinator I thank you for your support and words of encouragement. Thank you also goes to Associate Professor Noel Davies from the CSL for mass spectroscopy studies carried out and Professor Allan White, Dr Brian Skelton, Dr P.B. Hitchcock, Professor Peter Junk and Dr Gary Fallon for the X-Ray diffraction studies carried out.

Finally I thank my family and friends for their continuing support in what sometimes seemed an endless journey. To my parents, thank you so much for your support and words of wisdom, without you I may have not got here.

ABSTRACT

This thesis describes synthetic and density functional (DFT) investigations of organometallic complexes of the 4-azapentalenyl anion featuring Group 1, 3 and 4 metals. Included are ligand development methods and organometallic complexes of various extended ring systems, built by benzannulation of the parent 3*H*-pyrrolizine ring system. Emphasis was directed towards applications in alkene polymerisation.

The ring extension of the bicyclic 3*H*-pyrrolizine core led to the successful synthesis and characterisation of 5*H*-pyrrolo[2,1-a]isoindole and 6*H*-isoindolo[2,1-a]isoindole. Both were prepared using intramolecular Heck coupling reactions. The attempted synthesis of two other systems, 9*H*-pyrrolo[1,2-a]indole, an isomer of 5*H*-pyrrolo[2,1-a]isoindole, and a methylated derivative of 5*H*-pyrrolo[2,1-a]isoindole were unsuccessful. Subsequent reactions of the modified heterocyclic systems with Group 1 metals led to the identification *via* NMR spectroscopy of formation of the corresponding anions in the case of lithium, sodium and potassium salts. Crystalline salts of the novel potassium 5*H*-pyrrolo[2,1-a]isoindenyl complexes with coordinated Lewis bases were isolated and characterised by NMR spectroscopy, microanalysis and single crystal X-ray diffraction studies. The structural studies revealed the anion to display some cyclopentadienyl-like tendencies, as well as allowing for further metal-ligand interactions, in the same way that the indenyl and fluorenyl anions relate to the cyclopentadienyl anion itself. Other complexes proved too unstable to isolate via decomposition routes described below. Similarly, attempts to prepare Group 3 and 4 metal complexes led to reprotonation of the heterocycle or reductive coupling outcomes.

The effects of extending the ring system of the 4-azapentalenyl anion by benzannulation was investigated using DFT. Studies of the deprotonated 5*H*-pyrrolo[2,1-a]isoindole indicated an uneven charge distribution over the three ringed heterocyclic system. When comparing the highest occupied molecular orbitals (HOMO) of this system it was observed that a large HOMO was present at position 5 of the deprotonated 5*H*-pyrrolo[2,1-a]isoindole. The combination of these findings, along with calculated pK_a values, aided in the understanding of the instability of many of the Group 1, 3 and 4 metal complexes with respect to reprotonation and

reductive coupling. This was supported *via* reacting a potassium salt of 5*H*-pyrrolo[2,1-a]isoindole with mercuric chloride resulting in the reductively coupled dimer bis(5*H*-pyrrolo[2,1-a]isoindole), which was identified by ^{1}H NMR spectroscopy and GC-MS analysis.

DFT studies of unsolvated complexes of 5*H*-pyrrolo[2,1-a]isoindole Group 1 metal salts indicated that the size and nature of the metal centre influences the type of bonding interaction observed and the extent to which the ligand can "fold" along the N-C bridgehead vector of the anion in allowing for higher hapticity of the metal-ligand interaction in the complex. Similar studies were carried out on Group 1, 3 and 4 metal complexes of the parent 4-azapentalenyl anion system. These complexes either, i, exhibited a folding of the anion along the bridgehead vector, with dihedral angles between 17 – 26 $^{\circ}$ for potassium and sodium, respectively, varying in accord with the size of the metal to achieve increased hapticity, ii, or resulted in η^5-interactions with a non-folded anion for lithium as, presumably, the necessarily increased extent of folding that would be needed in the more symmetrically bound structure comes at too great an expense of aromatic behaviour of the fused ring system of the anion.

DFT studies on the insertion of ethylene into the scandium – hydride bond of bis(4–azapentalenyl)scandium hydride showed the ability of the 4-azapentalenyl anion to alter its binding mode via a η^8-folded/η^5-planar fluctional process during the insertion process in accord with the binding of catalysis substrates. This process results in the ethylene polymerisation chain growth step having a very low energy barrier, indicating that such fluctional processes are potentially of major interest to this industrially important reaction. However, synthetic access to such transition metal complexes remains a challenge for future work on this interesting ligand system that has been shown by this study to have high potential in a niche area of major industrial importance.

CONTENTS

CHAPTER 1
INTRODUCTION

CHAPTER 2

SYNTHESIS OF 3*H*-PYRROLIZINE SYSTEMS

CHAPTER 3

GROUP 1 METAL MODIFIED 4-AZAPENTALENYL COMPLEXES

CHAPTER 4

DENSITY FUNCTIONAL STUDIES OF UNSOLVATED GROUP 1, 3 AND 4 METAL 4-AZAPENTALENYL COMPLEXES

CHAPTER 5

COMPUTATIONAL STUDIES OF CATALYTICALLY RELEVANT SYSTEMS

CHAPTER 6

pK_A STUDIES OF MODIFIED 3*H*-PYRROLIZINES

CHAPTER 7

CONCLUSIONS

ABBREVIATIONS

Å	Ångstrom, 10^{-10} metre
Anal.	Microanalysis
Bu^n	Normal butyl
Calcd.	Calculated
CCl_4	Carbon tetrachloride
Cp	Cyclopentadienyl
Cp*	Pentamethylcyclopentadienyl
δ	Chemical shift in NMR (ppm)
Δ	Heat
d	Doublet
DFT	Density functional theory
DMAc	N,N-Dimethylacetimide
DME	1,2-dimethoxyethane
DMF	N,N-Dimethylformamide
18-crown-6	1,4,7,10,13,16-hexaoxacyclooctadecane
dibenzo-18-crown-6	2,3,11,12-dibenzo-1,4,7,10,13,16-hexaoxacyclooctadeca-2,11-diene
Et	Ethyl
Et_2O	Diethyl ether
EtOAc	Ethyl acetate
gCOSY	Gradient correlation spectroscopy
gHMBC	Gradient heteronuclear multiple bond correlation
gHMQC	Gradient heteronuclear quantum correlation
gNOESY	Gradient nuclear overhauser effect spectroscopy
hartree	$4.3597842 \times 10^{-18}$ J

Herrmann's catalyst	*trans*-Di(μ-acetato)-bis[*o*-(di-*o*-tolylphosphino)benzyl]dipalladium(II)
Hz	Hertz
$kcalmol^{-1}$	4.184 $kJmol^{-1}$
KH	Potassium hydride
Ln	Lanthanide
M	Metal
m	Multiplet
Me	Methyl
m.p.	Melting point
NaH	Sodium hydride
NBS	N-bromosuccinimide
NMR	Nuclear magnetic resonance
P(*o*-tol)$_3$	Tri-*o*-tolylphosphine
$Pd(OAc)_2$	Palladium acetate
PMDETA	N,N,N',N",N"-Pentamethyldiethylenetriamine
ppm	Parts per million
q	Quartet
s	Singlet
t	Triplet
THF	Tetrahydrofuran
TMEDA	N, N, N',N'-Tetramethylethylenediamine

CHAPTER 1

INTRODUCTION

1.1 GENERAL CONSIDERATIONS

Within the field of organometallic chemistry the terminology metallocene refers to a compound of the formula η^5-$(C_5H_5)_2M$.[1] The key feature of metallocenes and derivatives such as $[\eta^5$-$(C_5H_5)_2MCl_2]$ is the π-bound aromatic ligands. The first reported metallocene was bis(cyclopentadienyl)iron(II), commonly referred to as ferrocene, **(I)**, in 1951 by Pauson and Keely.[2] However, the unique structure and its subsequent chemistry was not determined until a few years later. The "sandwich" type structural characteristic of metallocene complexes was proposed by the Harvard University group of Wilkinson in 1952.[3] They postulated a "pentagonal anti-prismatic structure"[4] where the iron metal centre was "sandwiched" between two cyclopentadienyl units, Figure 1. Their theoretical structure was subsequently confirmed in 1956 when the first X-ray crystal structure of ferrocene was published by Dunitz *et al.*[5]

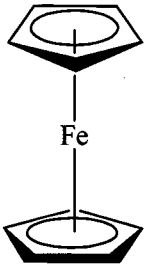

Figure 1. "Sandwich" structure of ferrocene **(I)**.

The discovery of ferrocene saw the rapid expansion of cyclopentadienyl metal chemistry with the majority of research in this area being carried out in two different laboratories: Wilkinson now at Imperial College, London, and E. O. Fisher at the Technical University of Munich, who jointly shared the 1973 Noble Prize in Chemistry for their pioneering work done in this particular field of organometallic chemistry.[4] Within ten years of the first report of ferrocene analogous complexes had been synthesised and reported for most of the first row transition metals, all of

which, with the exception of ferrocene, are sensitive to air. Analogous complexes containing cyclopentadienyl and substituted cyclopentadienyl ligands, such as the pentamethylcyclopentadienyl and fluorenyl anions, are now known for many s and p block metals, other transition metals and the lanthanoids.

Structurally, all metallocene complexes of the cyclopentadienyl anion and pentamethylcyclopentadienyl anion type exhibit the same sandwich structure observed in ferrocene, the cyclopentadienyl rings are either in an eclipsed or staggered orientation, Figure 2. It has been shown experimentally that the rotation barrier between the staggered and eclipsed conformations of non-substituted metallocenes is between 8 to 20 kJ/mol.[6] At low temperatures ferrocene and osmocene take on eclipsed conformations, at room temperature crystalline ferrocene is known to have molecules of both configurations present.[5,6]

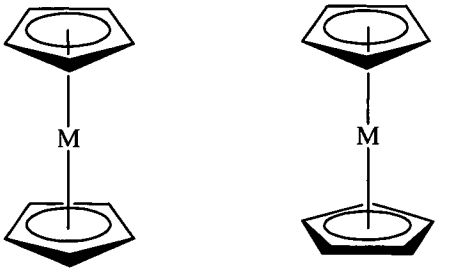

Eclipsed Staggered

Figure 2. Orientation of cyclopentadienyl anions in metallocene complexes.

1.2 METAL CYCLOPENTADIENYL CHEMISTRY

1.2.1 Introduction

The cyclopentadienyl anion **(II)** and its substituted derivatives, such as pentamethylcyclopentadienyl **(III),** indenyl **(IV)** and fluorenyl **(V)** are some of the most widely utilised ligands in transition metal and organolanthanide research.[7,8] The π electrons of these aromatic systems have made them ideal ligands for transition and lanthanide metal complexes as the aromatic π electrons are able to overlap effectively with the relevant orbitals of the metal.

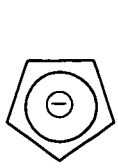

(II)

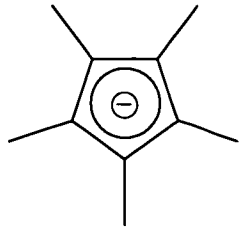

(III)

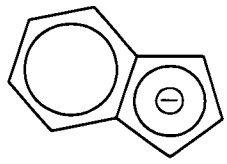

(IV)

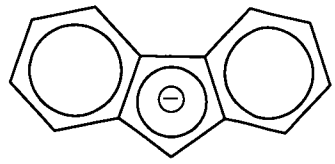

(V)

The discovery of ferrocene by Pauson and Kealy in 1951 was one of pure chance. It was the unexpected product of the reaction shown in Equation 1, they had been trying to synthesise the coupled dihydrofulvalene, **(VI)**.[4] Whilst they may not have achieved their desired target, they had stumbled across a compound that would see the resurgence of transition metal chemistry in the form of metallocene complexes and the development of the chemistry of the cyclopentadienyl anion.

$$2\,(C_5H_5)MgBr \;+\; FeCl_3 \xrightarrow{Et_2O} (C_5H_5)_2Fe$$

Equation 1. Original synthesis of ferrocene

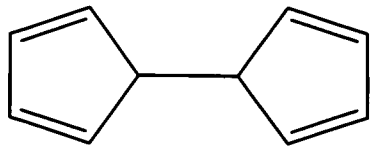

(VI)

Since the initial synthesis of ferrocene a variety of methods have been developed for the preparation of the bis(cyclopentadienyl) complexes, including new synthetic schemes to obtain ferrocene. These newer methods exploit the chemical property that cyclopentadiene is a weak acid with a pK_a of approximately 20.[6] Due to its pK_a value it is easily deprotonated with the use of a strong base giving the symmetrical aromatic stabilised anion. A general method for the formation of the cyclopentadienyl anion is by forming the Group 1 metal complex, an example reaction is given in Equation 2 for the formation of sodium cyclopentadienide. This can be subsequently reacted in metathetical exchange reactions allowing for the desired cyclopentadienyl metal complexes to be obtained, examples of these are shown in Scheme 1.

$$C_5H_6 + NaH \xrightarrow{THF} (C_5H_5)Na + H_2$$

Equation 2. Formation of the cyclopentadienyl anion

$$2\,(C_5H_5)Na + FeCl_2 \xrightarrow{THF} (C_5H_5)_2Fe + 2\,NaCl$$

$$2\,(C_5H_5)Na + TiCl_4 \xrightarrow{THF} (C_5H_5)_2TiCl_2 + 2\,NaCl$$

$$2\,(C_5H_5)Na + [(C_2H_4)_2RhCl]_2 \xrightarrow{THF} 2\,(C_5H_5)Rh(C_2H_4)_2 + 2\,NaCl$$

Scheme 1. Examples of salt metathesis reactions in metallocene synthesis

1.2.2 BONDING IN METAL HETEROCYCLIC SYSTEMS

The hapticity of a ligand may be defined as the "number of atoms which are within bonding distance of the metal atom", (Cotton 1968).[9] A ligand may have the potential to interact with the metal *via* more than one hapticity, for example the cyclopentadienyl anion exhibits η^1, monohaptic, through to η^5, pentahaptic, binding modes. Figure 3 shows the range of hapticities possible in complexes which contain the cyclopentadienyl ligand. Note there are two types of η^1 M-C_5H_5 interactions possible. Multihaptic ligands such as the cyclopentadienyl, indenyl and fluorenyl are attractive for use in metallocene chemistry especially in the field of catalysis due to their fluxional binding mode potential.

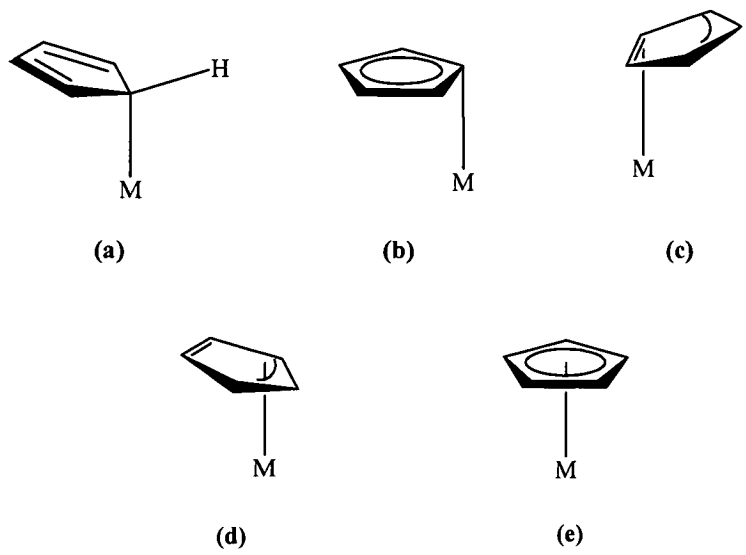

Figure 3. Possible binding modes exhibited by the cyclopentadienyl anion (a) $\eta^1(\delta)$, (b) $\eta^1(\pi)$, (c) η^2, (d) η^3 and (c) η^5.

The knowledge of this range of hapticities in complexes of the cyclopentadienyl anion has been successfully utilised in the catalytic polymerisation of olefins. The ability of the cyclopentadienyl system to form various bonding modes comes about from a phenomenon known as ring slippage. In 1987 O'Connor and Casey reviewed the literature on ring slippage chemistry of transition metal cyclopentadienyl and indenyl complexes.[7] Their review indicated that one of the

main interests in using these particular systems was their interconversion chemistry. The ability of the cyclopentadienyl system to interconvert from η^5, η^3 and η^1 forms was originally determined though physical studies, such as infra red and ^1H NMR spectroscopies. The first transition metal complexes with an η^1 bound cyclopentadienyl were reported three years after the determination of the solid state structure of ferrocene.[10,11] These studies indicated that the cyclopentadienyl ring was nearly planar and the angle (θ, see Figure 4) between the metal, the sp^3 ring carbon and the ring centre was about 120 °.

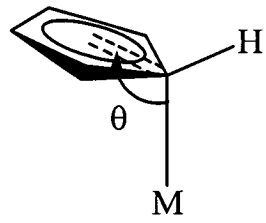

Figure 4. η^1 interaction between metal and cyclopentadienyl anion.

Whilst X-ray crystal structure determination confirmed the ability of the cyclopentadienyl system to form η^1 and η^5 binding modes in the 1950s, it was not until two decades later in 1978 that the η^3 binding mode was shown to be plausible when the X-ray crystal structure of $[(\eta^5\text{-}C_5H_5)(\eta^3\text{-}C_5H_5)W(CO)_2]$, **(VII)**, was reported.[12] The synthesis of **(VII)** also gave the first reported interconversion between an η^5-C_5H_5 complex to an η^3-C_5H_5 complex during the carbonylation reaction, as shown in Scheme 2.

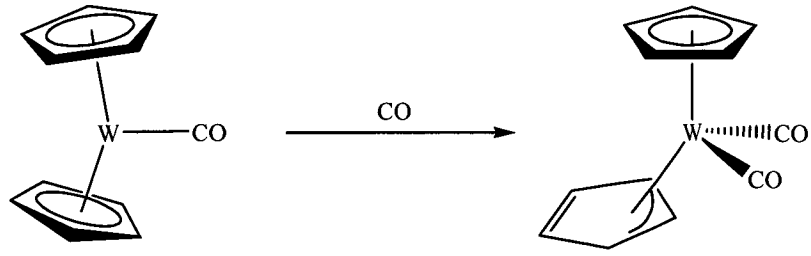

Scheme 2. Interconversion of cyclopentadienyl from an η^5 complex to η^1 complex.

The first reports of an interconversion between the η^5 and η^1 interactions were made in 1968 by Ustynyuk *et al.*, who postulated that the reaction of $[(\eta^5\text{-}(C_5H_5)_2)Ni]$ with triphenylphosphine at room temperature gave $[(\eta^1\text{-}C_5H_5)(\eta^5\text{-}C_5H_5)Ni(PPh_3)]$.[7,13] In the following years several reports provided spectroscopic data (infra red and ^1H NMR) that supported the fluxional behaviour of the cyclopentadienyl ligand showing interconversion of the metal anion interaction from η^1 to η^5.[7,14,15] During the 1970s many theories were put forward concerning the interconversion from η^1 to η^5 or vice versa. Cotton reported the observation of the interconversion from η^1 to η^5 for $[Ti(C_5H_5)_4]$. He postulated that the interconversion in the complex goes *via* an η^4 interaction.[7,16] He also later proposed a bis(η^4-C_5H_5) intermediate for the η^5 to η^1 interconversion on the basis of variable temperature ^1H NMR spectroscopic studies of the heteroleptic molybdenum complex, **(VIII)**, carried out by McCleverty, who later postulated an η^3 intermediate.[7,17,18] The theory that these interconversions go *via* an η^3 intermediate was also proposed by Werner and Kraus for a palladium cyclopentadienyl complex.[19]

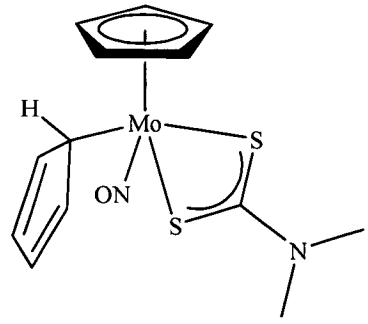

(VIII)

It was not until 1978 that the first conversion of an η^5-cyclopentadienyl complex to an isolated and well characterised η^1-cyclopentadienyl complex was reported.[7] During the same year Atwood and co-workers structurally characterised the $(\eta^1\text{-}C_5H_5^-)$ containing complex **(IX)**, where the zirconium centre interacted with four cyclopentadienyl moieties, three *via* an η^5 interaction and one in an η^1 fashion.[20] In 1979 Werner and Kühn isolated an η^1-cyclopentadienyl intermediate, **(XI)**, by the addition of a neutral two electron donor trialkylphosphine ligand, Scheme 3.[7] The X-

ray crystal structure of **(XI)** confirmed the η^1-cyclopentadienyl interaction to the palladium centre.[21]

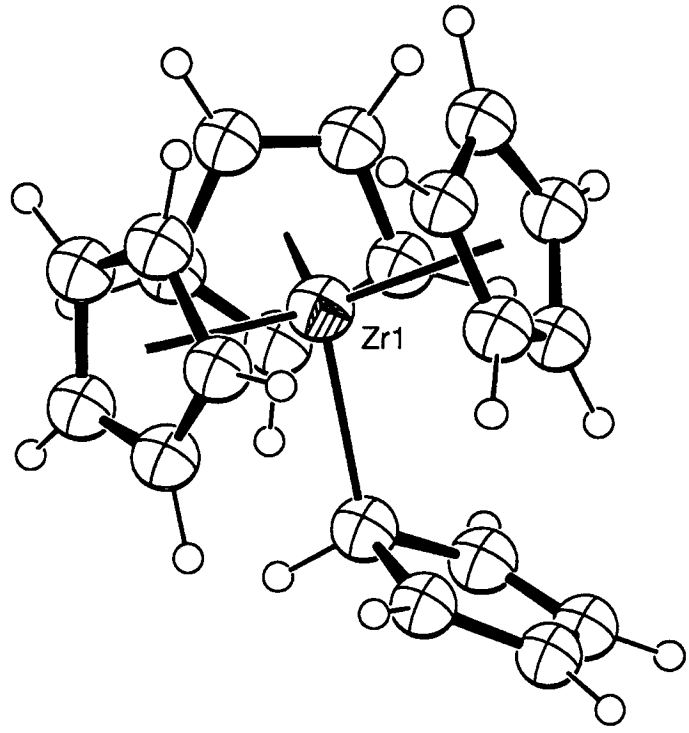

Figure 5. Single crystal X-ray structure of $[(\eta^5\text{-}C_5H_5)_3Zr(\eta^1\text{-}C_5H_5)]$, **(IX)**,[20] X-ray crystal structure reproduced from the CCDC database.[22,23] Thermal ellipsoids and hydrogens are shown with arbitrary radii.

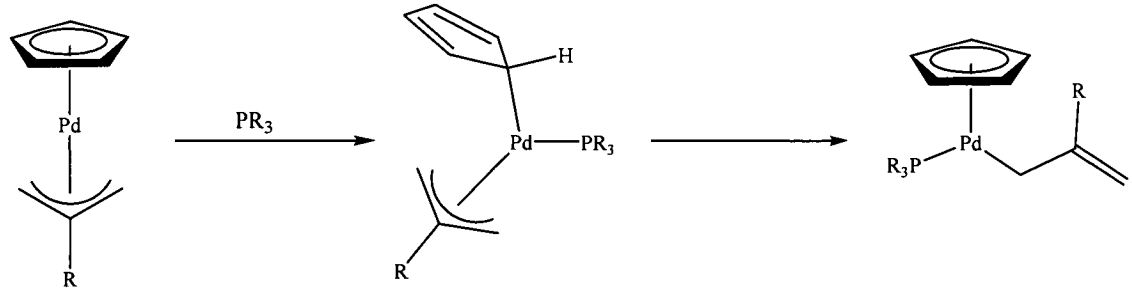

(X) **(XI)** **(XII)**

Scheme 3.

Similar interconversions between binding modes are known for indenyl and fluorenyl complexes, which contain "localised allyl-ene structures"[7] similar to that of slipped ring η^3 cyclopentadienyl complexes. The presence of the phenylene substituents of indenyl in η^5 complexes leads to the increased interconversion between η^5 to η^3 interactions in comparison to that observed for cyclopentadienyl ligands. This increased tendency for isomerisation between the binding modes was named the "indenyl effect" by Basolo[22] and is known in cyclopentadienyl chemistry as "ring slippage" or "ring folding".[23] This particular type of interconversion was first noted by Hart-Davis and Mawbay in 1969 in the reaction of **(XIII)** with triphenylphosphine, PPh_3, Scheme 4.[24] This change in bonding mode occurs in these particular complexes when a reduction or the addition of a donor ligand increases the valence electron count of the metal by two.[23]

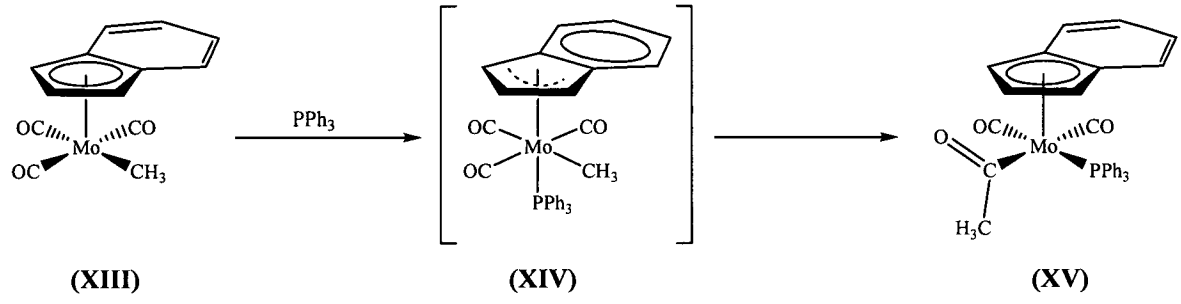

(XIII) **(XIV)** **(XV)**

Scheme 4. The Indenyl Effect.

It has been shown that the interconversion between different interaction modes of the cyclopentadienyl anion, and indeed other similar heterocyclic systems such as the pentamethylcyclopentadienyl anion and the indenyl anion, can be induced photochemically. Crichton and colleagues reported the successful photolysis induced conversion of $[(\eta^5\text{-}C_5H_5)Co(CO)_2]$, **(XVI)**, to $[(\eta^3\text{-}C_5H_5)Co(CO)_3]$, **(XVII)**, in a matrix of CO.[7,25] They determined the formation of the new complex *via* infra red spectroscopy which showed a decrease in the IR bands of the η^5 complex and the appearance of new bands that were attributed to the η^3 complex, these showed similarity to the IR bands observed for $[(\eta^3\text{-}C_3H_5)Co(CO)_3]$, which were known *via* a previous synthesis.[7]

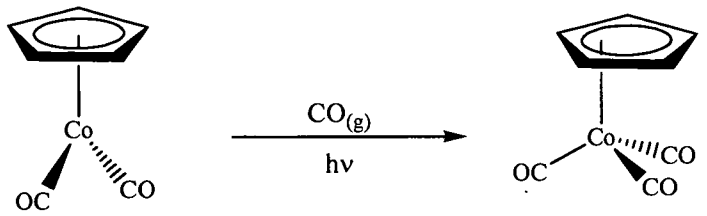

(XVI) **(XVII)**

Scheme 5.

The stability of the various binding modes between the metal centre and the indenyl and cyclopentadienyl anions has been explored through computational chemistry. In 2002 Veiros *et al.* published their work regarding the computational study of the η^5 to η^3 haptotropic shift of the molybdenum indenyl and cyclopentadienyl complexes, **(XVIII)** and **(XIX)** respectively, Figure 6.[23] They were able to show that η^5-cyclopentadienyl transition metal complexes are more stable than the same η^3 complex, whilst the reverse is true for complexes containing the indenyl ligand. Hart-Davies and Mawby through their earlier theoretical work suggested that this preference and subsequent stability of an η^3 indenyl – transition metal complex was due to the aromaticity of the six membered ring.[24] However the work by Verios *et al.* suggested that the preference for the η^3 binding mode in the molybdenum indenyl complexes was directly related to the molybdenum – indenyl bond strength and not as a result of the aromaticity gain in the η^3 indenyl complexes as previously proposed by Hart-Davies and Mawby.

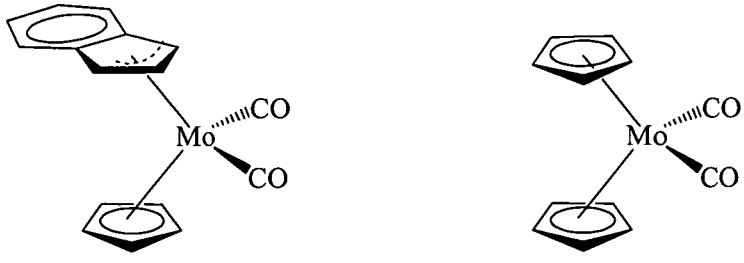

(VIII) **(XIX)**

Figure 6.

Verios and his colleagues showed that the energy required to fold the indenyl ligands, during ligand exchange, is less than 4.18 $kJmol^{-1}$, Figure 7 with this difference having little influence on the interaction between metal and ligand. Instead they found that the metal – anion bond strength influences the stability of the metal – anion interaction. The metal – anion bond strengths for each ligand were studied using a natural population analysis which has been shown to provide reliable charge calculations.[26] The bond strengths were then evaluated using two different methods, known as the Wiberg indices and the extended Hückel overlap population. The results from the evaluations indicated that for the η^5 metal anion complexes the cyclopentadienyl – M bond is stronger than the indenyl – M bond. Whilst for the η^3 metal anion complexes the indenyl – M bond is stronger than that of the cyclopentadienyl –M bond.[23] This was reflected in the metal – carbon distances in the complexes with the more stable bonding interaction occurring were the bond distances were the shortest.

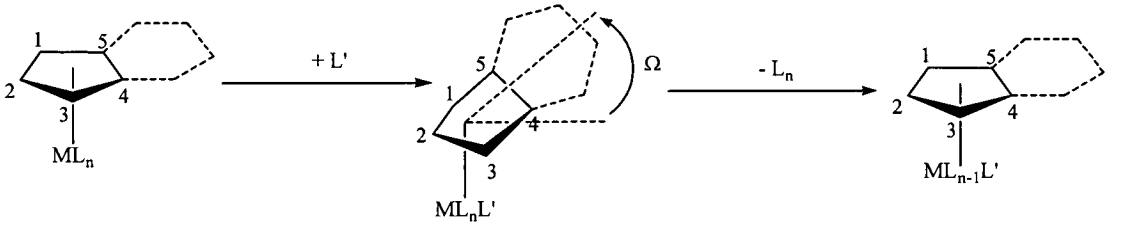

Figure 7. Folding of the cyclopentadienyl/indenyl ligand during ligand exchange, where Ω is the degree of folding of the anion of interest.

Extension of metallocene chemistry beyond the highly successful cyclopentadienyl anion has led to the use of other systems including the pentalendiyl ligand. The first complexes of pentalendiyl were reported during the 1960s and 190s by Katz and colleagues.[27,28] These complexes were composed of two pentalendiyl moieties bridged by two transition metal centres, as shown in Figure 8, where the metal centres were either nickel or cobalt. Since the report of these first pentalendiyl complexes, the research into this system as a ligand in metallocene chemistry was limited due to the difficultly in accessing the parent dihydropentalene. The synthesis of dihydropentalene involves the flash vacuum pyrrolysis (FVP) of cyclooctatetraene at temperatures between 550 – 600 °C to produce a mixture of isomeric

dihydropentalenes.[29] These mixtures are then deprotonated, typically with *n*-BuLi, to yield pentalendiyldilithium.

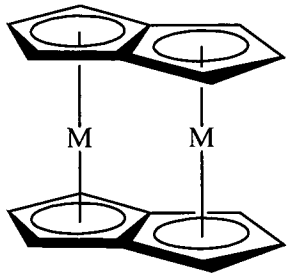

Figure 8.

It wasn't until the late 1990s when the chemistry of the pentalene dianion was once again explored in greater depth. The majority of the research on transition metal and actinide pentalendiyl complexes has been carried out by the groups of Jonas at the Max Plank Institute for Carbon Research and Cloke at the University of Sussex. Both groups have successfully synthesised mononuclear metallocene type pentalendiyl complexes. In 1997 Jonas *et al.* reported the synthesis of bis(pentalendiyl) complexes for the Group 4 metals titanium, zirconium and hafnium, Scheme 6.[30] Prior to the report of these homoleptic pentalendiyl complexes, Jonas also reported the synthesis of heteroleptic vanadium complexes containing one pentalendiyl dianion and either a cyclopentadienyl, a pentamethylcyclopentadienyl or an indenyl anion.[31]

Jonas and his colleagues reported the X-ray crystal structures of complexes **(XX)** - **(XXII)** along with the heteroleptic vanadium complexes **(XXIII)** – **(XXVI)**. These studies showed that the pentalendiyl anion adopts a different geometry to that which had been reported earlier in X-ray diffraction structure studies of the binuclear complexes. In the binuclear complexes the pentalendiyl had been observed to be nearly planar or planar. In comparison the pentalendiyl dianions of the mononuclear complexes **(XX)** – **(XXVI)** exhibited folded geometries,[31] as shown in the X-ray crystal structure of **(XXIII)**, Figure 9.[32,33] The folding of the dianion is seen to occur along the bridgehead dihedral vector with the four adjacent carbons to the bridgehead atoms and the "wingtip" carbons folding towards the metal centre. The observed

folding in **(XXIII)**, Figure 9, is characteristic of all the complexes reported by Jonas in 1997, including the Group 4 metal complexes shown in Scheme 6. Single crystal X-ray structures of **(XXIII) - (XXV)** allowed for the determination of the interaction between the metal centre and the pentalendiyl, these were described by Jonas and his colleagues as η^8 interactions.[30]

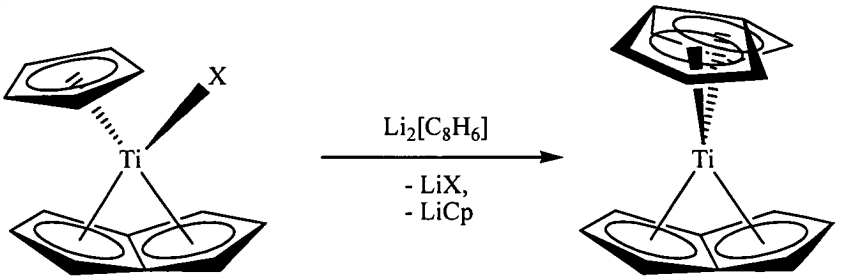

(XX) **(XXI)**

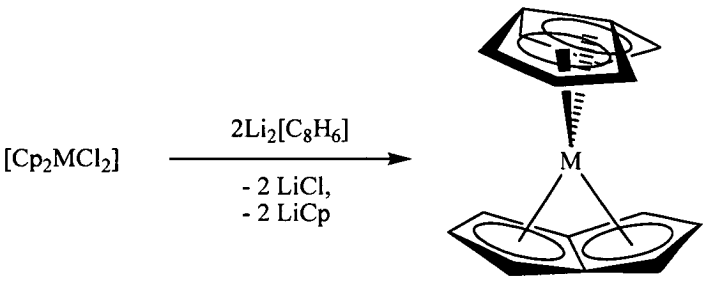

M = Zr, Hf

(XXII)

Scheme 6. Synthesis of pentalendiyl Group 4 metal complexes.

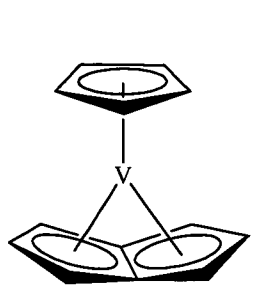

(XXIII)

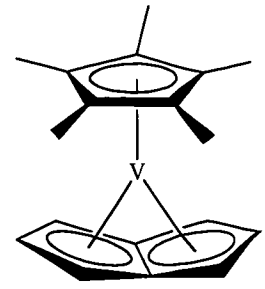

(XXIV)

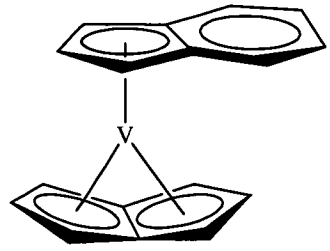

(XXV)

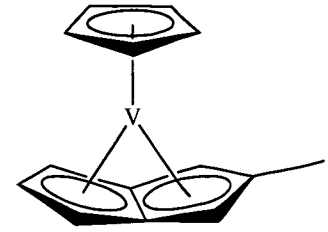

(XXVI)

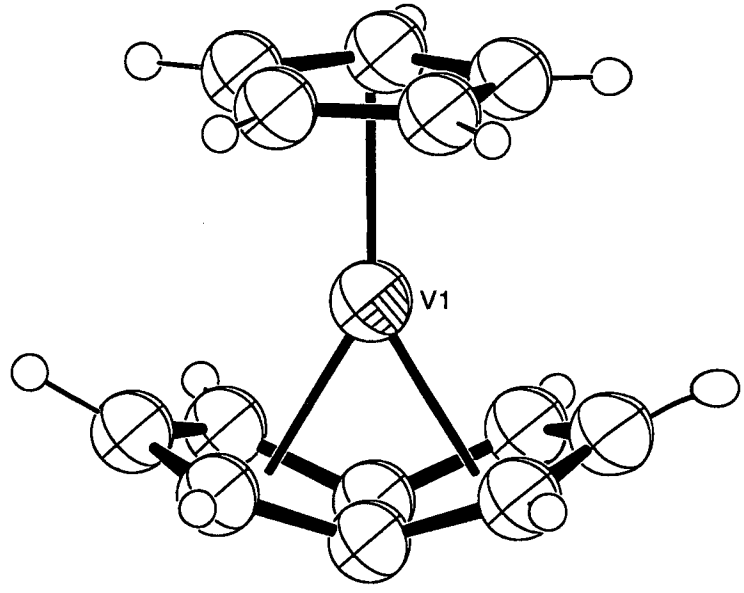

Figure 9. Single crystal X-ray structure of the mixed ligand metallocene, $[V(C_8H_6)(C_5H_5)]$, **(XXIII),**[32] X-ray crystal structure reproduced from the CCDC database.[22,23] Thermal ellipsoids and hydrogens are shown with arbitrary radii.

In 1997 Cloke reported the first actinide bis(pentalendiyl) complex, $[Th\{C_8H_4(Si^iPr_3\text{–}1,5)_2\}_2]$, **(XXVII)**.[34] The thorium complex was synthesised using the reaction outlined in Scheme 7, the analogous uranium complex **(XXVIII)** was synthesised some two years later by Cloke *et al.* using the same procedure.[35] As was the case for the previously mentioned Group 4 and vanadium complexes of Jonas *et al.*, the actinide complexes synthesised by Cloke exhibited the same folding of the pentalendiyl towards the metal centre.

$$[ThCl_4] + 2\,K_2[C_8H_4(Si^iPr_3\text{-}1,5)_2] \xrightarrow{THF} [Th\{C_8H_4(Si^iPr_3\text{-}1,5)_2\}_2] + 4\,KCl$$

(XXVII)

Scheme 7. Synthesis of the bis(pentalendiyl)thorium complex, **(XXVII)**.

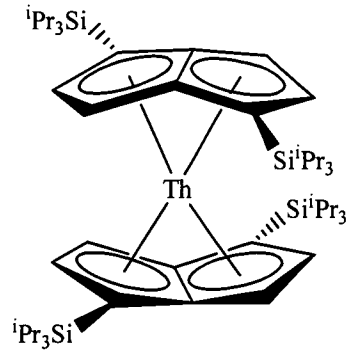

(XXVII)

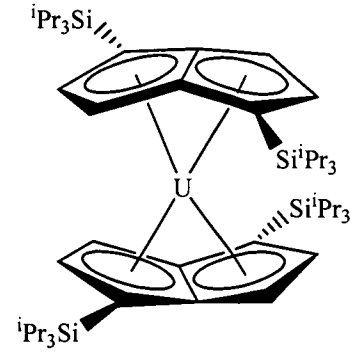

(XXVIII)

In order to determine whether the interaction between the metal centre and pentalendiyl was η^8 or η^6, Cloke collaborated with Green from Oxford to study **(XXVII)** and **(XXVIII)** using density functional theory, DFT.[35] In order for an η^8 interaction between the metal centre and the pentalendiyl to be present, Cloke stated that "the wingtip carbons must interact with the metal. This necessitates a folding of the ligand toward the metal, which must be stabilised by a bonding interaction to counteract the loss of aromaticity in the ring".[35] Cloke and Green found that for an η^8 interaction to exist between the metal and the anion the Highest Occupied Molecular

Orbital (HOMO) of the pentalendiyl had to have sigma symmetry with respect to the coordinated metal. Cloke, Green and Jardine found that "The HOMO of the pentalene dianion is an orbital of δ symmetry with respect to an η^8-coordinated metal." (Cloke *et al.* 1999).[35] Their work indicated that the 5*f* and 6*d* orbitals in bispentalendiyl actinide complexes of D_{2d} symmetry can overlap with the HOMOs of the pentalene dianion allowing the formation of covalent bonds. They found that the 6d orbitals of the metal were more effective in covalent bonding than the 5*f* orbitals therefore they concluded that the 6*d* orbitals had a greater contribution to the bonding in the complex.[35]

In 2002 Cloke and Hitchcock reported the preparation and reactivity of a mixed sandwich uranium(III) complex, **(XXIX)**.[36] The determined single crystal structure of **(XXIX)** showed the pentalendiyl to adopt a folded geometry related to those reported by Cloke and Hitchcock in 1999 in their bis(pentalendiyl)thorium and uranium complexes.[35] The increase of this fold angle suggests that the mixed ligand complex is less sterically congested than **(XXVII)**. The fold angle about the bridgehead of **(XXIX)** was found to be 26 °,[36] which is similar to that of $[Th\{C_8H_4(Si^iPr_3\text{–}1,5)_2\}_2]$, **(XXVII)**, which was reported to be 24 °.[34] The heteroleptic metallocene was synthesised *via* the reaction of uranium(III) iodide with $K(C_5Me_5)$ in diethyl ether which was subsequently reacted *in situ* with $K_2[C_8H_4\{Si^iPr_3\text{–}1,5\}_2]$ to yield **(XXIX)**.

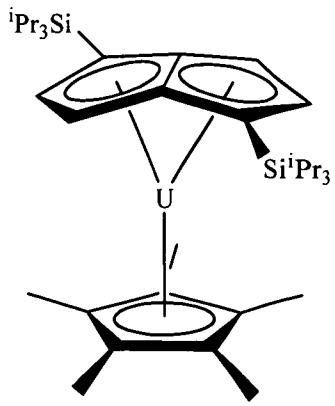

(XXIX)

On exposing **(XXIX)** to nitrogen at atmospheric pressure Cloke and Hitchcock noted that additional peaks were observed in the ^{1}H and the ^{29}Si NMR spectra. Subsequent freezing and thawing of the sample saw the disappearance of these signals to give the spectra of **(XXIX)**. Further spectroscopic studies and the determined single crystal X-ray structure of the nitrogen exposed product revealed it to be a binuclear complex which is bridged by a dinitrogen unit, **(XXX)**. They found that the N-N bond length of the dinitrogen unit was comparable to that observed for a N-N double bond but was significantly longer than that expected for a N-N triple bond. The ability to reversibly bind dinitrogen in complex **(XXX)** and form **(XXIX)** was determined to occur due to the instability of **(XXX)** due to steric crowding.

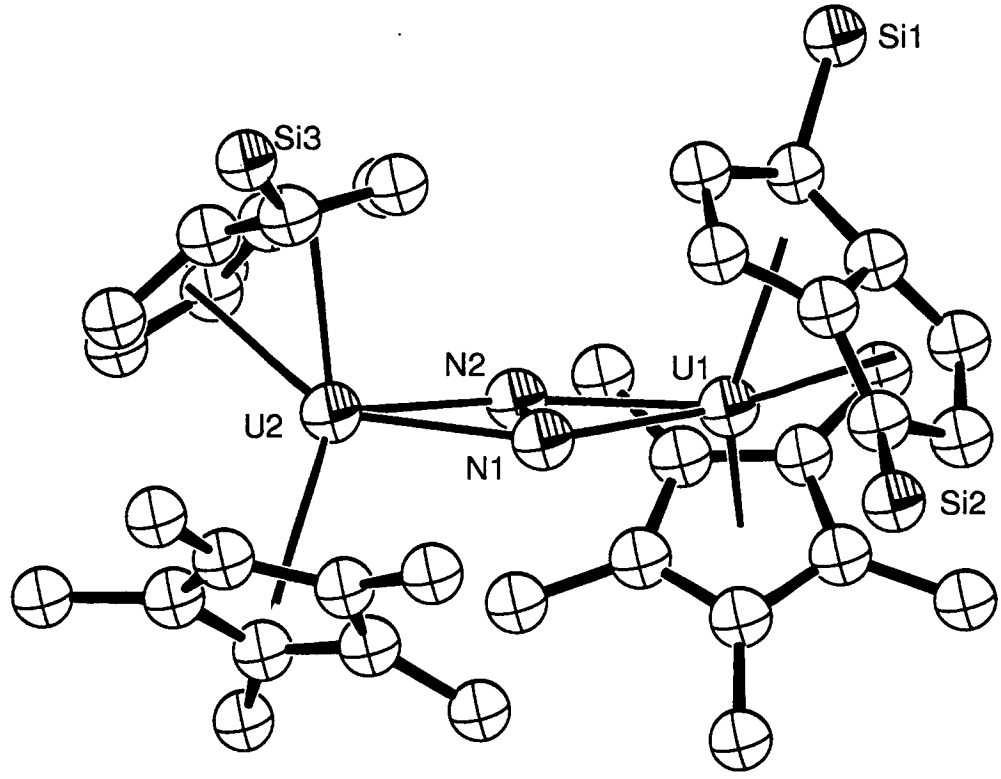

Figure 10. Single crystal X-ray structure of $[U_2(\mu^2\text{-}N)(\eta^5\text{-}C_5Me_5)_2(\eta^8\text{-}C_8H_4\{Si^iPr_3\text{-}1,5\}_2)_2]$, **(XXX)**,[37] X-ray crystal structure reproduced from the CCDC database.[22,23] Thermal ellipsoids are shown with arbitrary radii, hydrogens and isopropyl groups have been removed for clarity.

1.2.3 METAL PYRROLIDE CHEMISTRY

The ligands in the metallocenes and organometallic complexes discussed thus far do not contain any heteroatoms. The incorporation of a heteroatom such as nitrogen, oxygen, sulphur or phosphorus into aromatic systems allows for changes in aromaticity to occur. This variation in aromaticity in turn can influence the interaction between the ligand and a metal centre in an organometallic complex.[37] The inclusion of a heteroatom into the five membered cyclopentadienyl ligand leads to a dissymmetry in the ring electron density with the heteroatom bearing a greater percentage of the total electronic density in comparison to the carbon atoms.[38] These deprotonated heteroatom containing ligands can be divided into two groups: single ligands such as pyrrole, **(XXXI)**, phosphole, **(XXXII)** and arsole, **(XXXIII)** and multi-ring bridged ligands such as indole, **(XXXIV)**, 3*H*-pyrrolizine, **(XXXV)**, phosphinole, **(XXXVI)** and calix[4]pyrrole, **(XXXVII)**. The focus of this thesis was the development of aromatic ligand systems containing a nitrogen heteroatom.

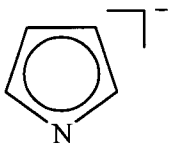

(XXXI)

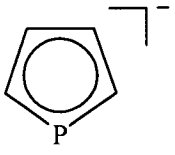

(XXXII)

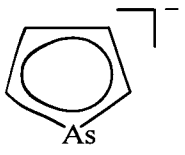

(XXXIII)

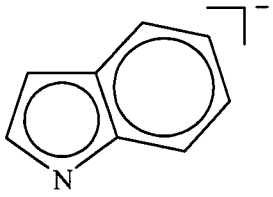

(XXXIV)

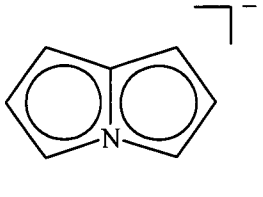

(XXXV)

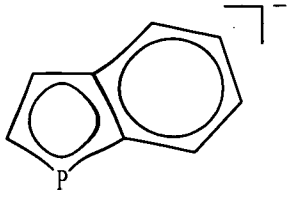

(XXXVI)

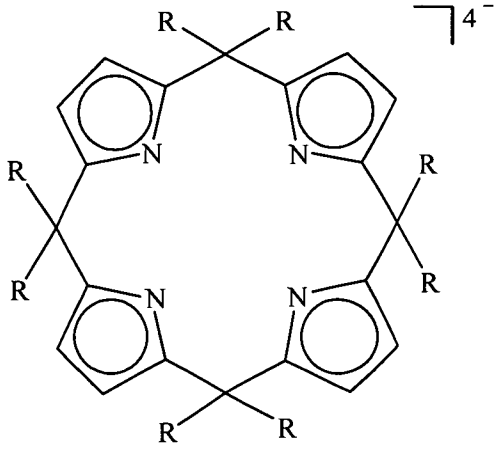

(XXXVII)

One of the simplest five membered aromatic nitrogen containing heterocycles is pyrrole, **(XXXI)**. This particular heterocycle which contains a nitrogen atom has been extensively investigated and used as an alternative to cyclopentadiene based systems. Pyrrole contains a nitrogen centre which has a relatively acidic proton (the pK_a of pyrrole is 23.3[39]), this readily reacts with various bases such as: Na; NaH, *n*-BuLi and K to form the pyrrolide anion, **(XXXI)**. A lone pair of electrons occupies the sp^2 hybridised atomic orbital of the nitrogen centre of the pyrrolide anion that is readily available for interacting with metal centres in complexes. The availability of this lone pair means that the pyrrolide anion often preferentially interacts with the metal centre by a σ-binding mode. This differs from cyclopentadienyl complexes where η^5-bound metal complexes are commonly formed.

In order to achieve pyrrolide complexes where the metal is π bound to the ligand the electron pair must be either shielded by placing bulky substituents at the 2 and 5 positions of the pyrrole, **(XXXIIII)**, or be unavailable for interaction with the metal centre, as in **(XXXIX)**. It is possible to achieve a π pyrrolide complex without the incorporation of bulky substituents, however this can only occur if a favourable electronic structure for the metal centre is present. One of the earliest examples of the pyrrolyl anion interacting with the metal in an organometallic complex *via* a π binding mode is the heteroleptic azaferrocene $[(\eta^5\text{-}C_5H_5)Fe(\eta^5\text{-}NC_4H_4)$, **(XL)**, whose synthesis was reported in 1964 by King and Bisnette.[40] They concluded that the electronic requirements of the iron(II) centre to achieve an 18 electron count lead to the η^5- π interaction with the pyrrolyl anion being favoured over a σ interaction.

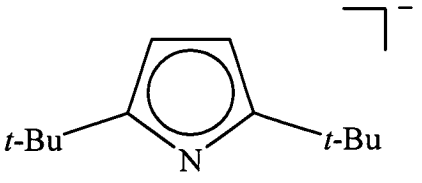

(XXXVIII)

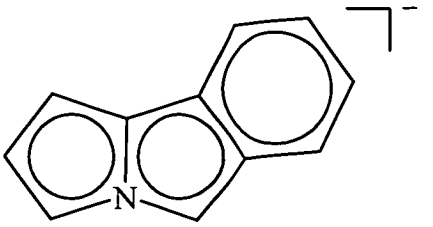

(XXXIX)

The azaferrocene complex is an example of a heteroleptic metallocene which contains a π bound pyrrolide, however some of the first π bound pyrrolide complexes were monocyclic complexes. The first successful synthesis of the π bound pyrrolide complex pyrrolylmanganese tricarbonyl, **(XLI)**, was reported some two years earlier than that of **(XL)** by Joshi and Pauson in 1962.[41] Their synthesis involved the heating of manganese decacarbonyl with pyrrole to obtain the π bound complex, **(XLI)**

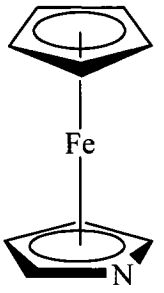

(XL)

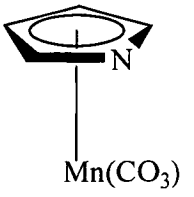

(XLI)

Pyrrolide complexes of Group 3 and lanthanide metal complexes are most likely to form an η^1 interaction between the pyrrolyl and the metal due to the highly electrophilic nature of the metal centre. In order to prepare complexes of these metals where the pyrrolyl anion bonds to the metal centre *via* a π interaction the pyrrolide must contain bulky substituents at the 2 and 5 positions of the anion in order to block any possibility of a σ interaction occurring. During the early and mid 1990s the group of Schumann utilised tertiary-butyl substituted pyrrolides, at positions 2 and 5, to obtain π bound complexes of Group 3 and lanthanide metals, Figure 11.[38]

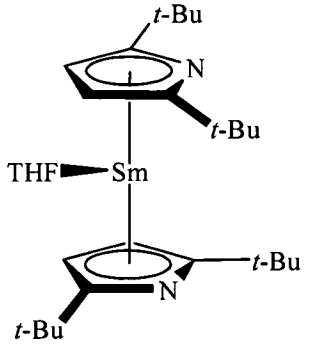

(XLII)

Figure 11.

The pyrrolide complexes described thus far are only those which contain one π bound pyrrolide anion, however complexes are known which contain two π bound pyrrolides are known which are similar to those of the cyclopentadienyl metallocene complexes. These types of homoleptic complexes have been prepared by the reaction of various transition[42-44] and main group[45-47] metals with the 2,5-di(*tert*-butyl)substituted pyrrolide anion to give diazametallocene complexes, examples of which are shown in Figure 12. Due to the steric bulk of these particular substituted pyrrolides, the formation of π interactions is highly favoured over σ interactions between the metal centre and the anion.

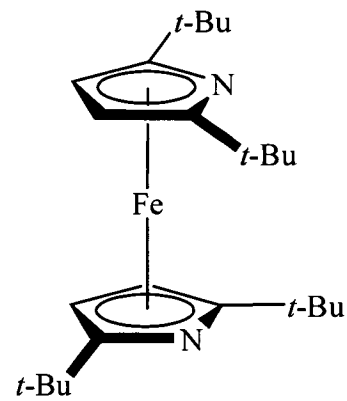

(XLIII)

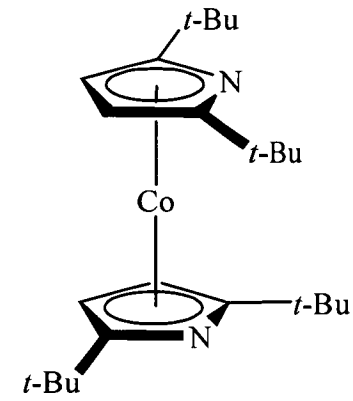

(XLIV)

Figure 12.

To eliminate any possibility of σ interactions in pyrrolide complexes the lone pair of electrons on the nitrogen must be unavailable for bonding. One such way of achieving this is evident in a group of compounds known as the pyrrolizines, where the nitrogen heteroatom is situated at the bridgehead of the fused heterocyclic system, for example in the *3H*-pyrrolizine precursor, **(XLV)**. These systems are easily deprotonated using Group 1 metals to give the 4-azapentalenyl anion, Scheme 8. The 4-azapentalenyl anion system is a nitrogen heterocycle which contains a π electron system that is isoelectronic with the ten electron pentalene dianion commented on earlier in this Chapter.

Metal complexes of the 4-azapentalenyl anion were first reported in 1967 by Okamura and Katz,[48] who prepared the lithium, sodium and potassium 4-azapentalenyl complexes using the method outlined in Scheme 8. The formation of these complexes was identified *via* the absence of the methylene signal in the ^{1}H NMR spectra, which was present in the ^{1}H NMR spectrum of the parent 3*H*-pyrrolizine. Okamura and Katz also investigated the acidity of the parent compound *via* measuring the rate at which its protons exchanged with D_2O in N,N-dimethyl formamide which contained triethylamine. Using the rate of exchange of the protons, along with the formula shown in Equation 3, Okumura and Katz determined the pK_a of 3*H*-pyrrolizine to be 29.[48]

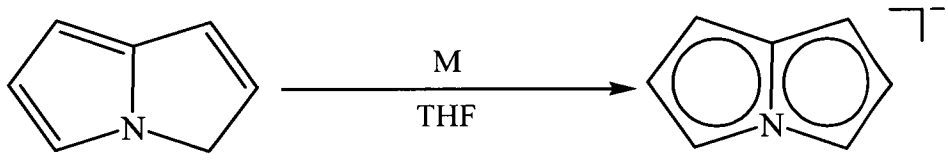

(XLV) **(XLVI)** M = *n*-BuLi, NaH, Na, K

Scheme 8. Preparation of the 4-azapentalenyl anion *via* the deprotonation of 3*H*-pyrrolizine using Group 1 metals.

$$pK_a = 19.09 - 2.139 \log (\text{Relative Exchange Rates})$$

Equation 3. Determination of the pK_a of 3*H*-pyrrolizine.

While the chemistry of metal complexes of the cyclopentadienyl anion and the pentalenyl dianion continued to be developed from the 1960s onwards, the chemistry of the 4-azapentalenyl anion remained relatively dormant. Continued interest still surrounded the 3*H*-pyrrolizine system due to research into a family of compounds known as the mitomycins which are comprised of an edge fused 5:5 bridgehead *N*-heterocycle, Figure 13. Compounds belonging to the mitomycin family have been shown to be of importance as intermediates in organic synthesis and as structural motifs in many natural products.

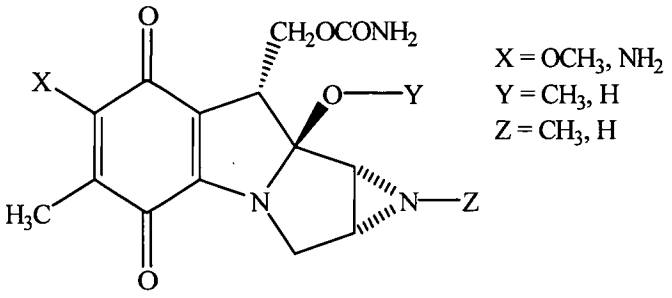

Figure 13.

While research continued on the mitomycin family of compounds, the chemistry of the 4-azapentalenyl system remained relatively quiet in comparison. It was not until 1998 when Kissounko and his colleagues reported the isolation of the lithium and thallium 4-azapentalenide complexes, **(XLVII)** and **(XLVIII)** as well as the lithium salt of the substituted 3*H*-pyrrolizine 1-methyl-3*H*-pyrrolizine, **(IL)**.[49] Kissounko *et al.* also reported the synthesis of range of Group 14 substituted derivatives of the 4-azapentalenyl anion synthesised from the lithium 4-azapentalenide, **(XLVII)**, Scheme 9. These compounds were characterised *via* ^{1}H NMR and $^{13}C\{^{1}H\}$ NMR spectroscopies except for **(XLVIII)** which, due to its decreased stability in solution, was limited to characterisation by mass spectrometry. To date no solid state structures are known for metal complexes of the 4-azapentyalenyl anion and, therefore, the metal-anion binding mode variability is still yet to be determined.

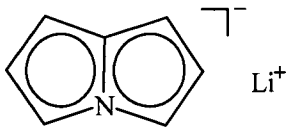

(XLVII)

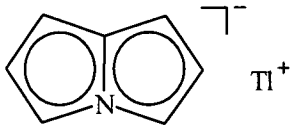

(XLVIII)

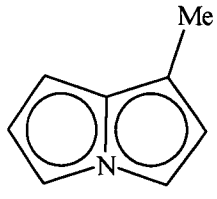

(IL)

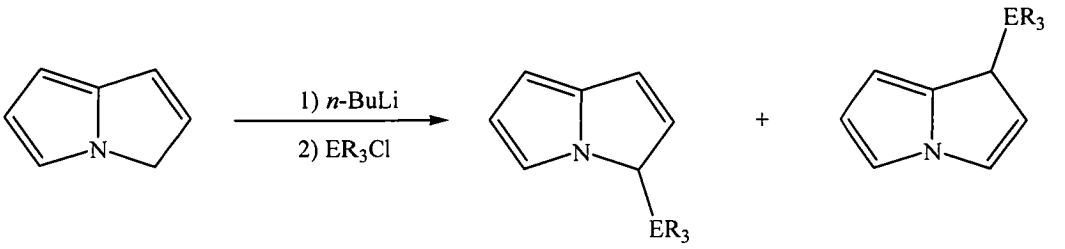

R = Me, Ph.
E = Si, Sn.

Scheme 9. Synthesis of Group 14 substituted 3*H*-pyrrolizines.

1.3 LANTHANOCENCES: A BRIEF OVERVIEW

The development and study of metallocene complexes of the lanthanides stemmed from the investigation into cyclopentadienyl as an appropriate ligand in organometallic chemistry. Prior to the synthesis of the first lanthanide metallocenes in the 1950s, the organometallic chemistry of the lanthanides was limited due to their extremely sensitive nature towards oxygen and water and the preparative techniques available at the time. The development of suitable handling techniques saw the expansion of lanthanide chemistry to include a variety of classes of compounds where the lanthanides were found to have 3+ oxidation states, later it would be found that the oxidation states of Ln^0, Ln^{2+} and Ln^{4+} were also possible.

The first organolanthanide cyclopentadienyl complexes to be synthesised and characterised were those of the type shown in Equation 4 by Birmingham and Wilkinson in 1956.[50] In order to obtain lanthanocenes a lanthanide trihalide was reacted with an alkali metal cyclopentadienide, as shown in Equation 4.[50,51] The cyclopentadienyl anion and its derivatives, such as the pentamethylcyclopentadienyl anion, have been shown to provide stability to organolanthanide complexes by satisfying the coordination sphere of the lanthanide metal. The properties of these complexes are influenced by the relationship between the size of the lanthanide and the steric demands of the cyclopentadienyl group.[6] The cyclopentadienyl ligands therefore are able to provide the electrostatic and steric stability required while only occupying one anionic ligand site of the metal centre.

$$3\ (C_5H_5)Na + LnCl_3 \xrightarrow[-\ 3NaCl]{THF} (C_5H_5)_3Ln$$

Equation 4. Synthesis of tris(cyclopentadienyl) lanthanide complexes

The first lanthanocenes synthesised were the solvent free tris(cyclopentadienyl) complexes achieved by subliming the compounds *in vacuo* at temperatures above 200 °C.[52] Complexes of this type for the lanthanides including scandium, yttrium and lanthanum were obtained *via* the reaction shown in Equation 4, with the smaller lanthanides utilising either NaC_5H_5 or KC_5H_5 in diethyl ether or benzene. The only exception to this is the synthesis of the radioactive promethium analogue, which was obtained by the neutron bombardment of tris(cyclopentadienyl)neodymium(III).[52] Many of the solid state structures of those $Ln(C_5H_5)_3$ complexes have been determined by single crystal X-ray structure determination, an example of this is shown for tris(cyclopentadienyl)luteium(III), **(L)**.[53] In the solid state these compounds exist as polymeric structures with slight variances in the binding modes between the lanthanide centre and the cyclopentadienyl ligands observed in accordance with variations in the size of the metal centre.

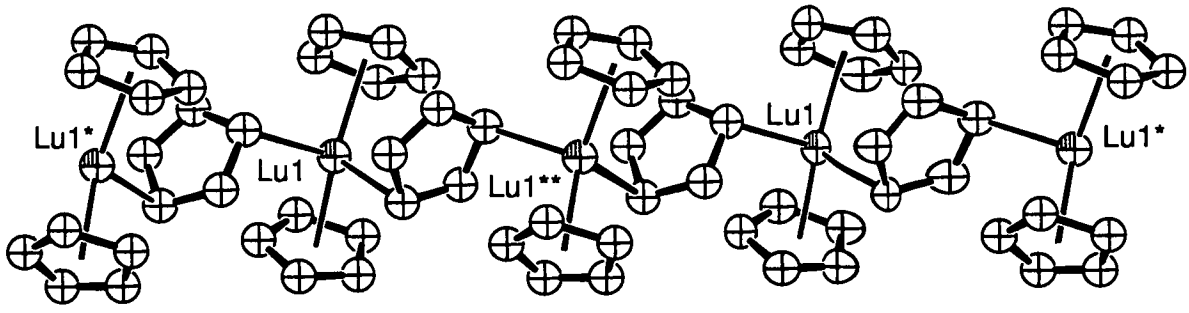

Figure 14. Single crystal X-ray structure of $[(\eta^5\text{-}C_5H_5)_2Lu(\eta^1\text{-}C_5H_5)]_n$, **(L)**,[53] X-ray crystal structure reproduced from the CCDC database.[22,23] Thermal ellipsoids are shown with arbitrary radii, hydrogens have been removed for clarity.

Another class of lanthanocenes that have been widely explored are the bis(cyclopentadienyl)lanthanide halides. Complexes of this type have been obtained in a variety of ways, two of which are given for the synthesis of $(C_5H_5)_2LnCl$ complexes in Scheme 10.[6] It should be noted that isolable complexes of this type for lanthanides with a large ionic radii, La – Nd, could not be obtained *via* these synthetic routes.[52] The first crystal structure of this type compound was reported in 1972 by Atwood and Smith for $[(C_5H_5)_2ScCl]$, **(LI)**.[54] This complex exists as a dimer comprised of two $(C_5H_5)_2Sc$ moieties that are bridged by two chlorides. Changes to the solid state structures are observed for the lanthanides with small or ionic radii, for example the X-ray crystal structure of the analogous dysprosium complex, **(LII)**, shows each $(C_5H_5)_2Dy$ unit being bridged to another *via* a single chloride.[52]

$$2\,(C_5H_5)M + LnCl_3 \longrightarrow (C_5H_5)_2LnCl + 2\,MCl$$

$$2\,(C_5H_5)_3Ln + LnCl_3 \longrightarrow 3\,(C_5H_5)_2LnCl$$

Scheme 10. Synthesis of bis(cyclopentadienyl)lanthanide(III) chloride complexes.

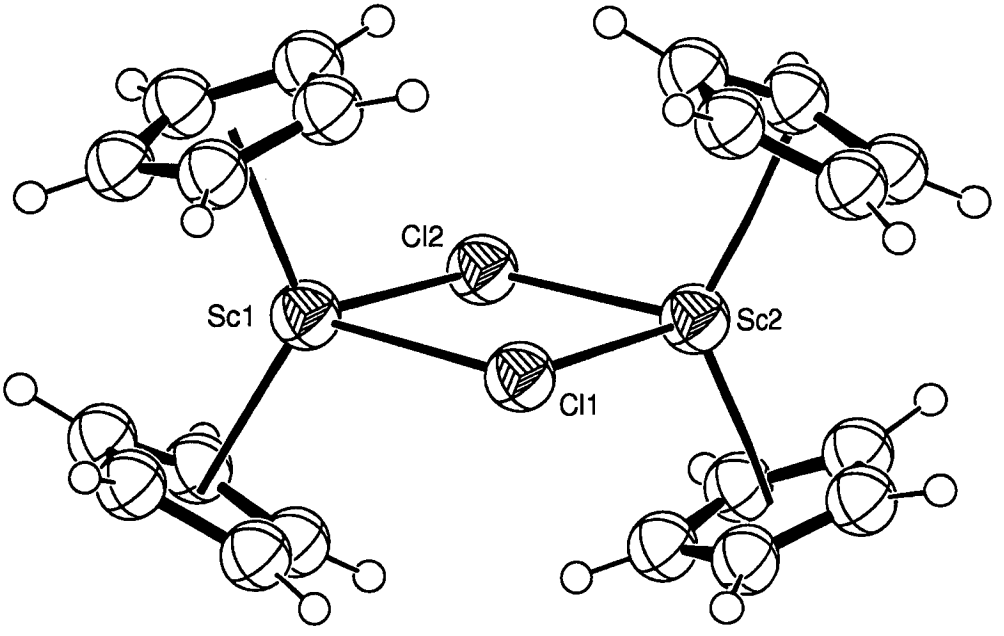

Figure 15. Single crystal X-ray structure of $[(\eta^5\text{-}C_5H_5)_2ScMe]_2$, **(LI)**,[54] X-ray crystal structure reproduced from the CCDC database.[22,23] Thermal ellipsoids are shown with arbitrary radii.

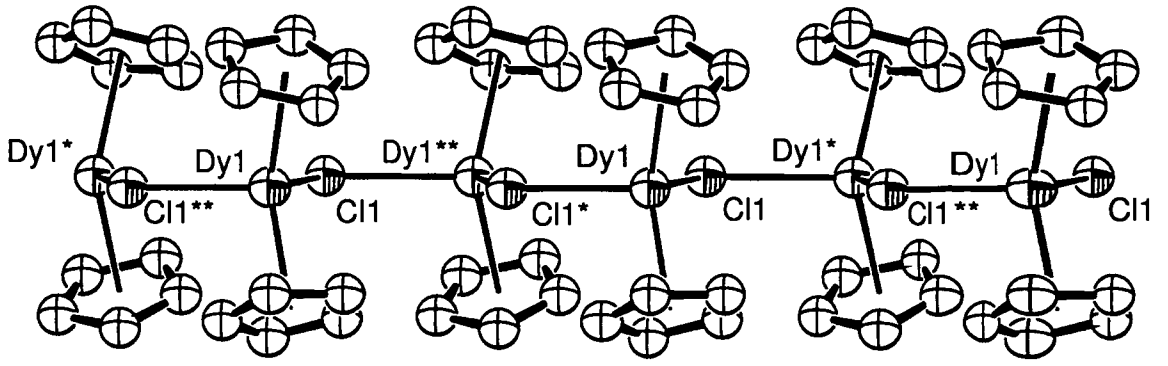

Figure 16. Single crystal X-ray structure of $[(\eta^5\text{-}C_5H_5)_2DyCl]_n$, **(LII)**,[52] X-ray crystal structure reproduced from the CCDC database.[22,23] Thermal ellipsoids are shown with arbitrary radii, hydrogens have been removed for clarity.

While the cyclopentadienyl system proved a useful ligand in the expanding chemistry of the lanthanides, it was not until 1980 that the sterically demanding pentamethylcyclopentadienyl system was introduced into lanthanide chemistry.[55-57] The increased size of the pentamethylcyclopentadienyl system in comparison to that of the cyclopentadienyl group has allowed for increased solubility of complexes largely as a result of decreased aggregation states of the complexes. An example of this increased solubility was the isolation of the first organosamarium(II) complex **(LIII)** in 1981 by Evans *et al.*[58] In comparison, the analogous bis(cyclopentadienyl) complex, reported by Watt and Gillow in 1969,[59] showed limited solubility and therefore its chemistry was limited. The solubility of **(LIII)** allowed for the reduction chemistry of samarium(II) in an organometallic environment to be investigated thoroughly. Even the unsolvated bis(pentamethylcyclopentadienyl)samarium complex was isolated and well characterised and is highly soluble in non-polar solvents.[60,61]

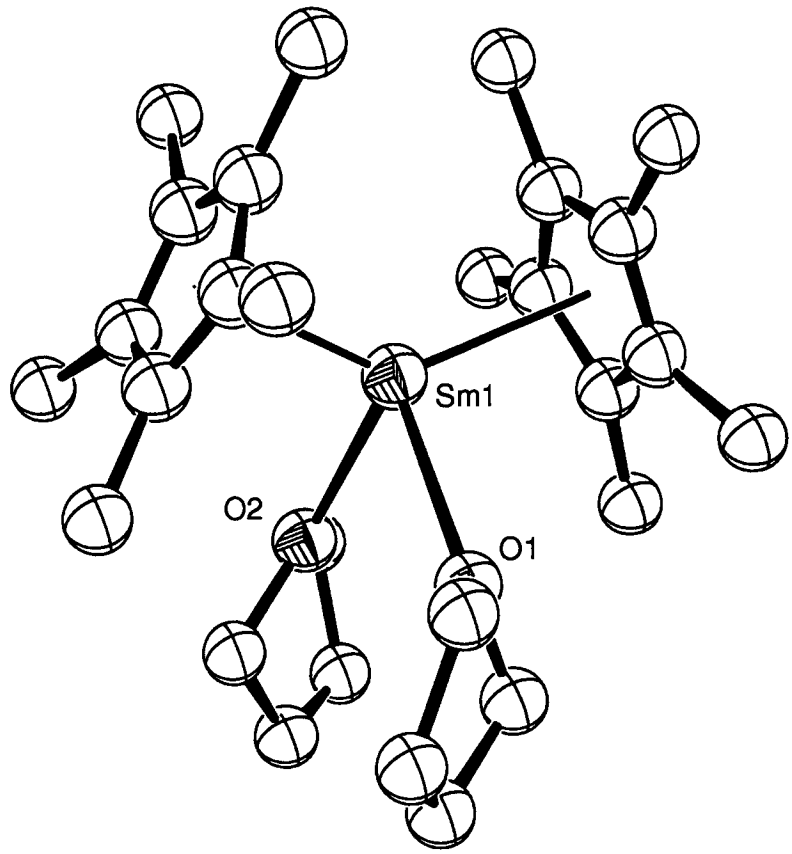

Figure 17. Single crystal X-ray structure of $[(\eta^5\text{-}C_5H_5)_2Sm(THF)_2]$, **(LIII)**,[58] X-ray crystal structure reproduced from the CCDC database.[22,23] Thermal ellipsoids are shown with arbitrary radii.

The depth of lanthanocene chemistry is not limited to the use of the cyclopentadienyl anion and its substituted derivatives. Mixed lanthanocenes containing indenyl and fluorenyl ligands with cyclopentadienyl anions are also known, for example **(LIV)**. In 2003 Carpentier and co-workers reported the synthesis of lanthocenes containing fluorenyl ligands, **(LIV)** and **(LV)**.[62] Both complexes shown in Figure 18 were synthesised *via* salt metathesis reactions where the solvated lanthanide halide was reacted with the dilithium cyclopentadienide – fluorenide precursor.

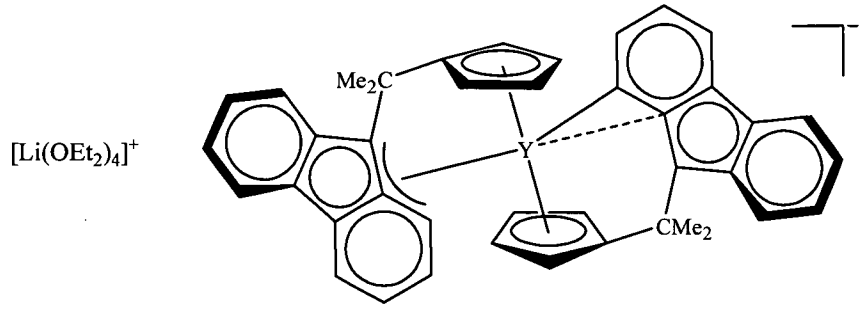

(LIV)

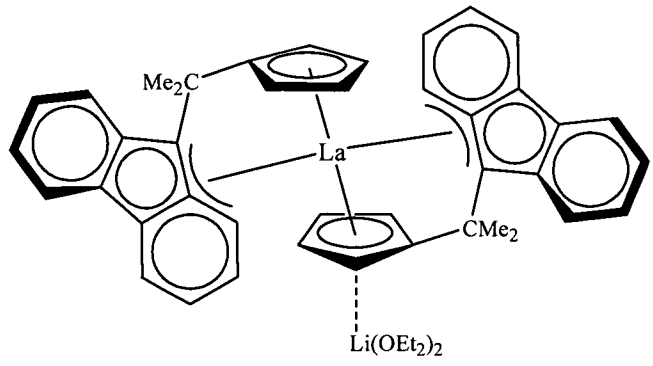

(LIV)

Figure 18. Metal ligand binding modes in indenyl based lanthanocenes

These complexes differ to those reported some four years earlier by Qian *et al.*, who reported the synthesis of complexes of the type $[Li(THF)_4][(\eta^5{:}\eta^5\text{-}C_5H_4\text{-}CPh_2\text{-}C_{13}H_8)LnCl_2]$, [62] in that they contain two *ansa*-metallocene type units per metal centre. The determined X-ray crystal structure of complexes **(LIV)** and **(LV)** showed that each cyclopentadienyl and fluorenyl anion is bonded to the lanthanide centre, however the fluorenyl moieties showed non symmetrical binding modes. In complex **(LIV)** the yttrium coordinates to the two ligand units in a distorted tetrahedral geometry. The yttrium centre is shown to coordinate with each cyclopentadienyl anion *via* η^5 interactions whilst it coordinates with one of the fluorenyl anions *via* an exocyclic η^3 binding mode and *via* an η^1 interaction to the other. In comparison the lanthanum centre in **(LV)** has a distorted tetrahedral geometry with both fluorenyl units coordinating to the lanthanum *via* exocyclic η^3- bonding modes. Carpentier and colleagues also reported the synthesis and structure of *ansa*-lanthanocenes featuring indenyl ligands such as complex **(LVI)**.[62] The synthesis of **(LVI)** was related to that for **(LIV)** and **(LV)**.

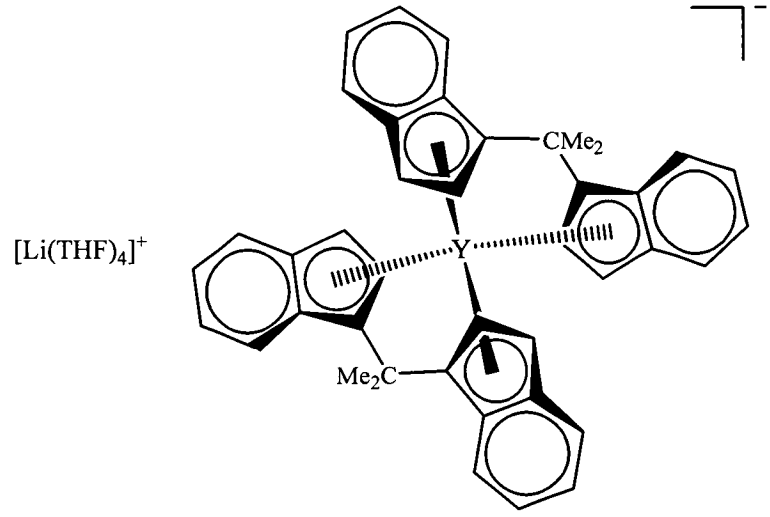

(LVI)

1.4 BRIEF OVERVIEW OF METALLOCENES IN ALKENE POLYMERISATION CATALYSIS

The potential for a ligand in an organometallic complex to interconvert between different binding modes, such as the η^5 to η^3 shift observed in the indenyl complex [(η^5-C_9H_7)Rh], **(LVII)** during olefin hydroboration catalytic cycle,[63] is seen as an important property for application in catalytic cycles.[23,63] One of the earliest known metallocene precatalysts was titanocene dichloride, reported in 1957, which in the presence of alkyl aluminium chlorides was shown to catalyse the polymerisation of ethene in a homogenous environment. The early metallocene catalysts based on this particular system, however, exhibited low activity in the polymerisation of ethene and did not homopolymerise 1-olefins well.[64] Later, in 1976, the group of Sinn and Kaminsky reported the successful polymerisation of 1-propene and some cyclic alkenes catalysed by Group 4 metallocenes in the presence of the co-catalyst methylalumoxane, MAO.[65] While this class of catalyst and co-catalyst showed excellent activity towards alkene polymerisation the process did not result in the production of stereoregular polymers. A simplified outline of the catalytic cycle is shown in Scheme 11.[65]

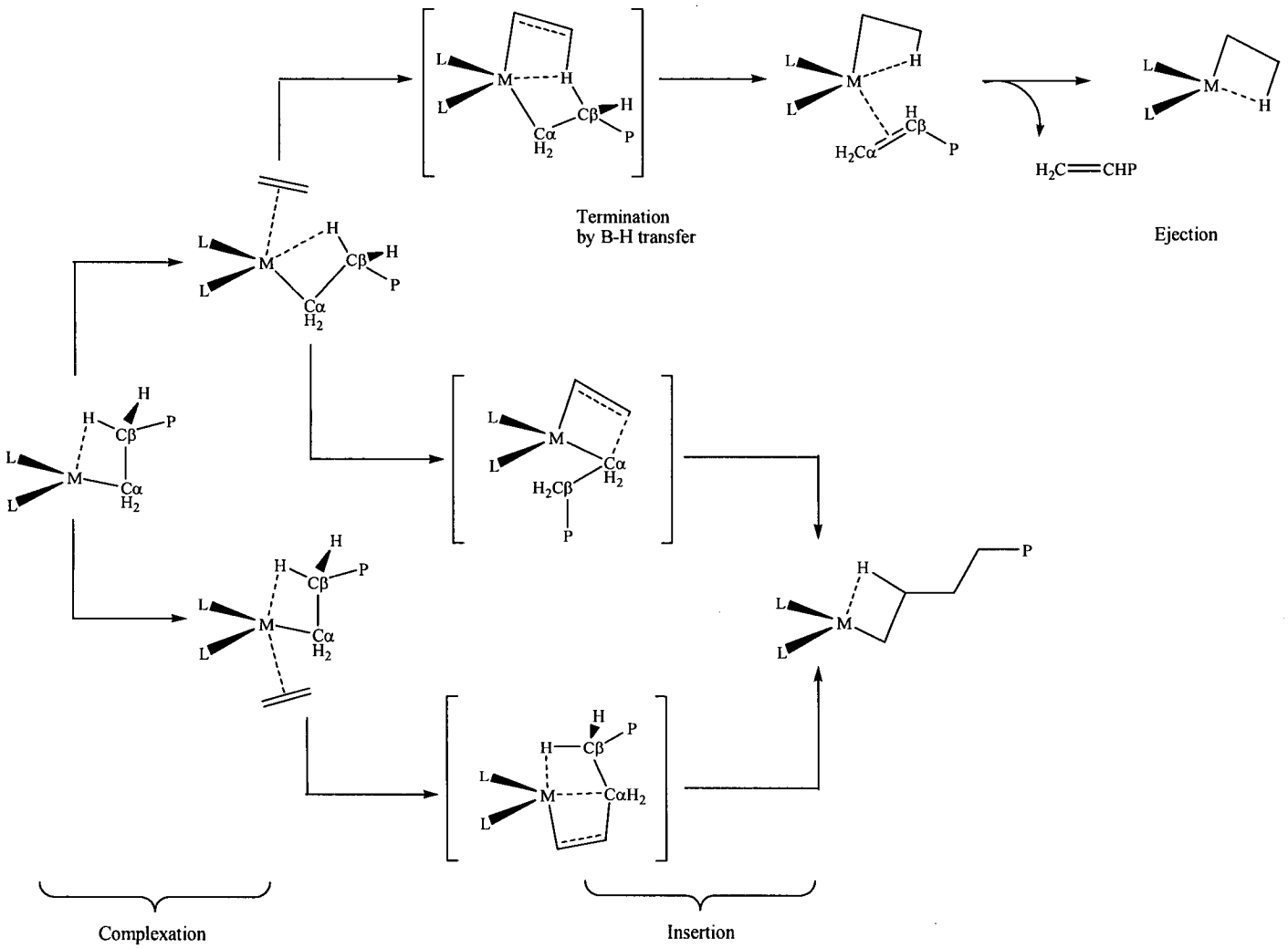

Scheme 11. Catalytic cycle of the polymerisation of 1-olefins

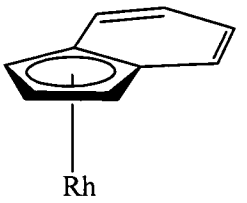

(LVII)

In order to overcome the lack of stereoselectivity experienced by the Sinn - Kaminsky system, research into factors which influence the growth of the polymer chain were investigated in the 1980s. During this time it was discovered that several key factors were responsible in influencing the performance of the metallocene catalysts and stereoregularity of the polymer. The first of these concerns the effect of substitutions made to the cyclopentadienyl ligand of the metallocene. The early work done in this particular area was carried out by the groups of Ewan and Giannetti.[64] The incorporation of alkyl substituents on the cyclopentadienyl or the extension of the cyclopentadienyl system was found to increase the stereospecificity of the polymerisation.

The second factor found to influence the production of stereospecific polymers was the development of stereorigid metallocene catalysts, some of which were also chiral metallocene complexes. Investigations into these constrained metallocene catalysts was initially carried out by the groups of Britzinger and Ewan who found that the constrained nature of these catalysts was found to induce enantioselectivity in the olefin insertion process during polymerisation.[66,67] These particular metallocenes have been shown to be isospecific due to their symmetry and produce isotactic polymers which have a narrow molecular weight distribution. The application of this knowledge has led to the greater control of polymerisation reactions and reaction production such that very high selectivity for both isotactic and syndiotactic polypropylene are possible with various C2 and Cs symmetric *ansa*-metallocenes, Scheme 12.

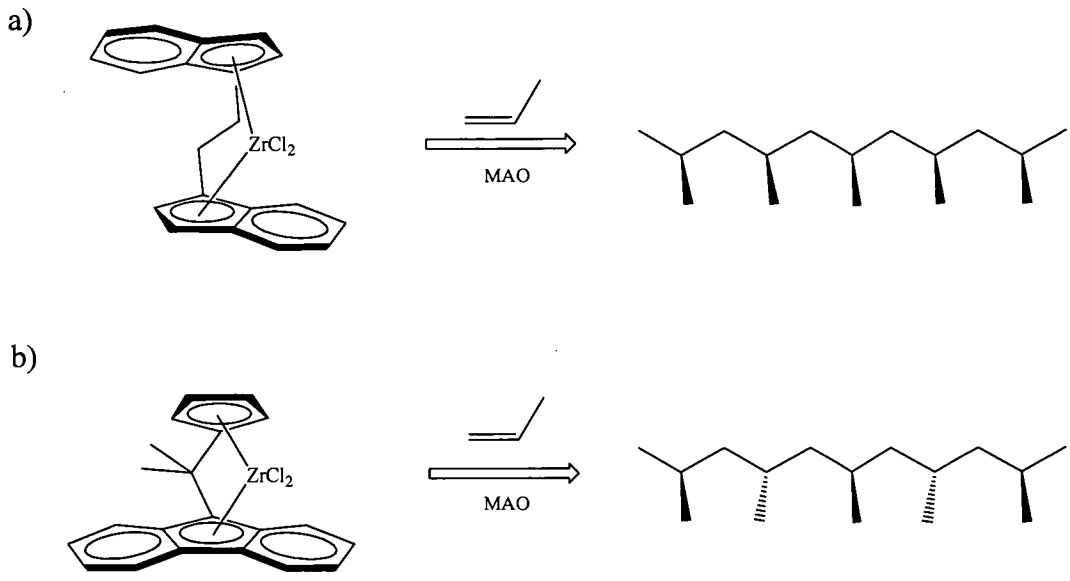

Scheme 12. Catalysts for enantioselective polymerisation of olefins
a) C_2-symmetric catalyst giving isotactic polymer
b) C_s-symmetry catalyst giving syndiotactic polymer

The highly selective and active metallocene catalysts have not been limited to those which contain Group 4 metal centres, lanthanide based analogues have also been shown to polymerise alkenes. The development of the chemistry of the cyclopentadienyl system to include substituted cyclopentadienyl anions greatly aided the development of lanthanide based polymerisation of alkenes. The increased steric bulk of the cyclopentadienyl ligands gave the lanthanide complexes greater stability. In 1978 the first successful polymerisation by a lanthanide metallocene was reported by Ballard and co-workers who used an alkyl metallocene complex of erbium, **(LVIII)**, to polymerise ethylene at 100 °C.[68] This particular catalyst, along with other alkyl metallocene catalysts, were shown to have moderate catalytic activity in the polymerisation of alkenes.[69] Later work carried out by Schumann, Marks and colleagues on lanthanide complexes of the type shown in Figure 19 were found to have high activities, 146 400 g $mmol^{-1}$ h^{-1} bar^{-1}, however it should be noted that these catalytic reactions were only carried out for a very short time.[70-72]

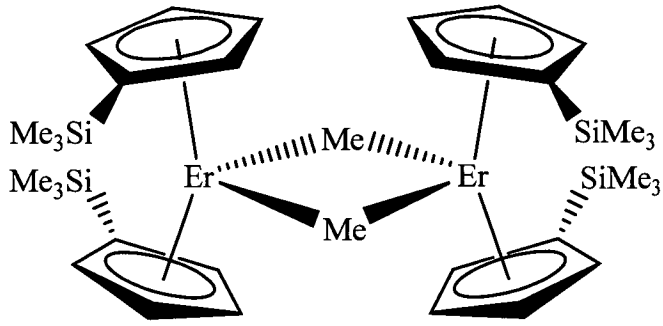

(LVIII)

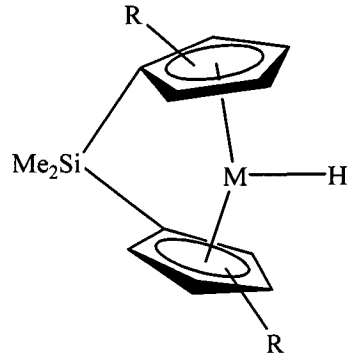

R = Me_4, $(SiMe_3)_2$
M = Nd, Sm, Lu

Figure 19. Lanthanide catalysts shown to have high olefin polymerisation activity.

In order to gain a greater understanding of the steps which occur during the polymerisation process, in particular alkyl/hydride migration onto alkenes, researchers have utilised various theoretical methods. In 1991 Morokuma and Koga reviewed the current literature on *ab initio* molecular orbital (MO) studies with regard to catalytic reaction mechanisms for transition metal complexes, concluding; "The insertion of an olefin into a metal – hydrogen bond is an essential step for conversion of olefin to alkyl in a catalytic cycle." (Morokuma and Koga 1991).[73] The review indicated that the results obtained by *ab initio* MO calculations resulted in greater quantitative information allowing for the determination of the catalytic reaction pathway.

Various theoretical studies have been undertaken to investigate this important step in the polymerisation of alkenes in order to understand and determine the

geometry of the transition state species. In 1989 Jolly and Marynick investigated alkene insertion into $[Ti(C_5H_5)_2CH_3]^+$, **(LIX)**, using *ab initio* MO theory, applying the restricted Hartree-Fock (RHF) level of theory and second order Møller-Plesset perturbation theory[74,75] (MP2).[76] The calculated structures indicated that the insertion step has a low activation barrier, however, due to the eclipsed conformation of the C-H bonds of the propyl group the transition state geometry found was improbable. The aforementioned review carried out by Morokuma and Koga indicated that the use of *ab initio* MO studies on such catalytic systems provided a valuable insight into the mechanisms, geometries and transition structures which occur during catalytic reactions and catalytic cycles.

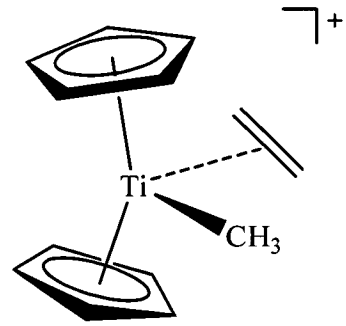

(LIX)

In 1999 Ziegler *et al.* investigated the "general aspects of ethylene polymerisation by d^0 and d^0f^n transition metals" using density functional theory (DFT) methods.[77] Their work encompassed looking at a variety of metal centres as well as a range of ligand systems within the bis(cyclopentadienyl) metallocene-type systems and their effect on three reaction steps in the polymerisation process. The three steps which they investigated were alkene uptake, insertion and termination. Their work indicated that the formation of the π interaction between the alkene and the catalyst is subtly influenced by steric influences of the non-participative cyclopentadienyl ligands. They found that the geometry of the π complex was largely determined by the nature of the metal ion centre itself. That is, the formation of a "front side" over a "back side" π complex, Figure 19, increases on moving down the group and going from Group 3 to Group 4 metal complexes.

The studies by Ziegler *et al.* indicated that the olefin insertion barriers for all d^0 complexes were found to be low. This was explained in terms of there being a lack of d metal electrons: "d^0 and d^0f^n transition metal alkyl complexes intrinsically have a low barrier for ethylene insertion into the M-Cα bond due to the absence of an alkyl-olefin antibonding interaction." (Ziegler *et al.* 1999).[77] Their studies also indicated that by changing the metal in the system the insertion barrier could be increased or decreased. They found that the increase in this barrier energy occurred on going down a group, for example the insertion barrier was found to increase according to Sc < Y < La.[77] Finally, they were able to show that the activation barrier for the preferred β-hydrogen transfer in chain termination is weakly dependent on the nature of the metal centre but the steric bulkiness of the ligand can dramatically alter the barrier. The β-hydrogen elimination process was found to always be higher in energy than that of the β-hydrogen transfer termination and found to be very sensitive to the steric bulk around the metal centre as well as the size of the metal centre.

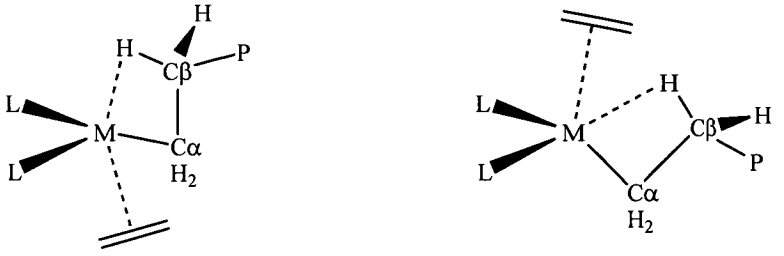

Figure 20. π complex formation, distinguishing front and back side.

Theoretical studies of metallocene complexes in the alkene insertion processes have been reported for a wide range of complexes. It has been possible in some cases to compare these results with those which have been determined experimentally. One such study was reported by Bercaw and colleagues in 2003, where they monitored the insertion of ethylene into the metal hydride bonds of *ansa*-metallocenes *via* dynamic NMR methods, in particular niobocene and tantalocene.[32] Their DFT calculations determined the barriers for hydrogen exchange after intramolecular ethylene insertion of unbridged, singly and doubly bridged metallocenes which correlated well with their determined experimental results. They were able to also

show the insertion barrier for the niobocene complexes, **(LX - LXII)**, is effected by the number of bridges between the two cyclopentadienyl anions present. They found that the overall activation energy was lowest for the singly bridged niobocene complex, **(LXI)**, whilst the activation energy for the unbridged and doubly bridged complexes are similar in energy.

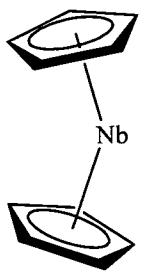

unbridged
(LX)

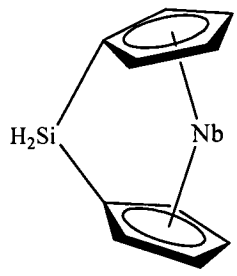

singly
(LXI)

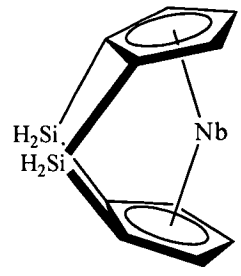

doubly
(LXII)

In Bercaw's study it was shown that the introduction of a single bridge decreased the insertion barrier in comparison to that of the unbridged species. The introduction of a second bridge did little to lower the insertion barrier in comparison to the unbridged species. The differences in insertion barrier between the unbridged and doubly bridged complexes to the singly bridged complex indicate that the electron population shift from the ground state to the transition state is more favourable for the singly bridged complex, leading to the faster hydrogen exchange rate which was observed in the NMR studies.

1.5 AIMS AND THESIS OVERVIEW

The primary objective of this project was to investigate the chemistry and the potential of the 4-azapentalenyl anion as a ligand for Group 1, Group 3 and lanthanide metal complexes. The synthetic component of this work involved the synthesis of the parent compound, 3*H*-pyrrolizine, and benzoannulated derivatives of the 3*H*-pyrrolizine, along with the preparation and characterisation of a number of novel potassium complexes. The theoretical aspect of this project covered a range of 4-azapentalenyl complexes; Group 1, Group 3 and lanthanide metal complexes, as well as the benzoannulated derivatives. The thesis can be divided into three distinct areas; synthesis and structural characteristics of Group 1 complexes; theoretical investigations into the properties of 4-azapentalenyl complexes and theoretical investigations of catalytically relevant complexes.

The work outlined in Chapter 2 concentrates on the synthesis and characterisation of the benzoannulated compounds; 5*H*-pyrrolo[2,1-a]isoindole, **(LXIII)**, 6*H*-isoindolo[2,1-a]indole, **(LXIV)**, 5-methyl-5*H*-pyrrolo[2,1-a]isoindole, **(LXV)**, and 9*H*-pyrrolo[1,2-a]indole, **(LXVI)**, as well as the synthesis of 3*H*-pyrrolizine. The benzoannulated systems were shown to have greater stability at elevated temperatures in comparison to 3*H*-pyrrolizine which decomposes at moderate temperatures. It was also hoped that hoped these benzoannulated systems would overcome the problem of high pK_a values observed for 4-azapentalenyl anion. Chapter 3 concentrates on the synthesis and characterisation of novel, highly air and moisture sensitive potassium complexes of 5*H*-pyrrolo[2,1-a]isoindolenyl, **(LXVII)**, and 6*H*-isoindolo[2,1-a]indolenyl, **(LXVIII)**. This Chapter also discusses possible reasons as to why reduction of the anion during the isolation of some of these complexes occurs to give the parent heterocycle or in some cases the reductively coupled product **(LXIX)**.

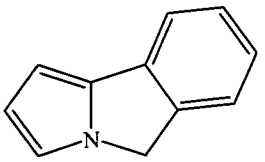

(LXIII)

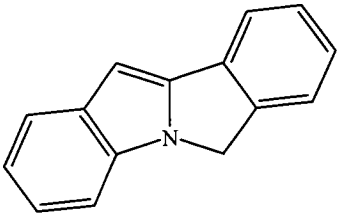

(LXIV)

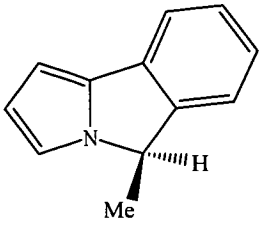

(LXV)

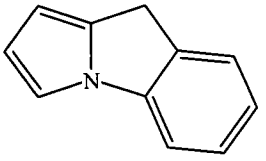

(LXVI)

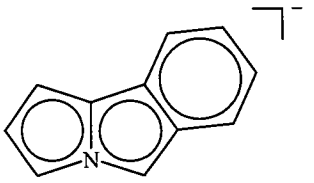

(LXVII)

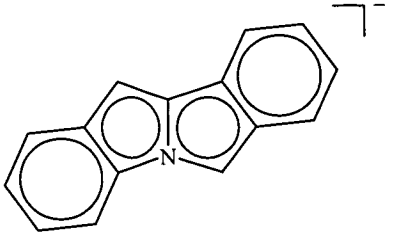

(LXVIII)

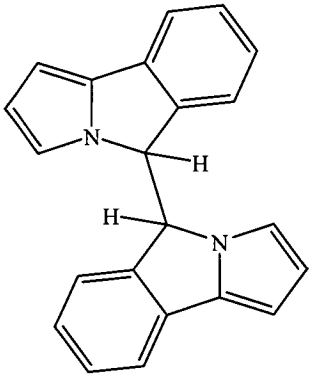

(LXIX)

Chapters 4 through to 6 apply DFT using appropriate basis sets to calculate the geometries and various properties, as well as catalytic potential of various Group 1, Group 3 and lanthanide metal complexes based on the 4-azapentalenyl anion. Chapter 4 discusses the results of the investigation into the geometries and the subsequent energies of the unsolvated complexes of Group 1, 3 and 4 4-azapentalenyl and benzoannulated complexes.

The potential of metallocene type complexes containing the 4-azapentalenyl anion as alkene polymerisation catalysts is discussed in Chapter 5. Here the geometries along with energies and subsequent insertion barrier were calculated, as well as the determination of transition states and intermediates in the polymerisation pathway. The fluxtionality of binding modes between the metal and ligand within the

catalytic pathway is seen as a highly desirable feature when designing a catalyst. The influence the approaching ethylene has on the geometry of the 4-azapentalenyl anion and therefore any changes in the metal – ligand interaction are also described in this Chapter.

The final chapter, Chapter 6, investigates the reduction pathway for the 3*H*-pyrrolizine and the benzoannulated compounds, **(LXIII)** and **(LXVI)**. This Chapter contains both synthetic and theoretical studies into the stability and subsequent reactivity of these compounds. The synthetic study involved the forced reduction of a potassium 5*H*-pyrrolo[2,1-a]isoindolenyl complex to give a neutral reduced, coupled product which was identified using NMR spectroscopies and mass spectrometry. The energy required to couple two 4-azapentalenyl anions or two 5*H*-pyrrolo[2,1-a]isoindolenyl anions for this particular reductive pathway was determined using DFT with the application of appropriate basis sets. The stability of the above compounds was investigated using DFT to calculate the respective pK_a values.

1.6 REFERENCES

(1) Wilkinson, G., Ed. *Comprehensive Coordination Chemistry. The Synthesis, Reactions, Properties and Applications of Coordination Compounds*; 1st Edition ed.; Pergamon Press Ltd.: Oxford, 1987; Vol. 1.

(2) Pauson, P. L.; Kealy, T. J. *Nature* **1951**, *168*, 1039 - 1040.

(3) Wilkinson, G.; Rosenblum, M.; Whiting, M. C.; Woodward, R. B. *J. Am. Chem. Soc.* **1952**, *74*, 2125 - 2126.

(4) King, R. B. *Transition-Metal Organometallic Chemistry An Introduction.*; Academic Press Ltd.: New York, 1969.

(5) Dunitz, J.; Orgel, L. E.; Rich, A. *Acta Cryst.* **1956**, *9*, 373 - 375.

(6) Cotton, F. A.; Wilkinson, G. *Advanced Inorganic Chemistry*; Fifth ed.; John Wiley & Sons, Inc.: New York, 1988.

(7) O'Connor, J. M.; Casey, C. P. *Chem. Rev.* **1987**, *87*, 307-318.

(8) Jutzi, P.; Burford, N. *Chem. Rev.* **1999**, *99*, 969-990.

(9) Cotton, F. A. *J. Am. Chem. Soc.* **1968**, *90*, 6230 - 6232.

(10) Piper, T. S.; Wilkinson, G. *J. Inorg. Nucl. Chem.* **1956**, *2*, 38 - 45.

(11) Wilkinson, G.; Cotton, F. A. *Prog. Inorg. Chem.* **1959**, *1*, 1 - 124.

(12) Huttner, G.; Brintzinger, H. H.; Beller, L. G.; Friedrich, P.; Bejenke, V.; Neugebauer, D. *J .Organomet. Chem.* **1978**, *145*, 329 - 333.

(13) Ustynyuk, Y. A.; Voevodskaya, T. I.; Zharikova, N. A.; Ustynyuk, N. A. *Dokl. Acad. Nauk SSSR* **1968**, 640 - 643.

(14) Tsutsui, M.; Hancock, M.; Ariyoshi, J.; Levy, M. N. *J. Am. Chem. Soc.* **1969**, *91*, 5233 - 5236.

(15) Cross, J. R.; Wardle, R. J. *J. Chem. Soc. A* **1971**, 2000 - 2007.

(16) Cotton, F. A.; Rusholme, G. A. *J. Am. Chem. Soc.* **1972**, *94*, 402 - 406.

(17) Kita, W. G.; Lloyd, M. K.; McCleverty, J. A. *J. Chem. Soc., Chem. Commun.* **1971**, 420 - 421.

(18) Hunt, M. M.; Kita, W. G.; Mann, B. E.; McCleverty, J. A. *J. Chem. Soc., Dalton Trans.* **1978**, 467 - 474.

(19) Werner, H.; Kraus, H.-J. *Angew. Chem., Int. Ed. Engl.* **1979**, *18*, 948 - 949.

(20) Rogers, R. D.; Bynum, R. V.; Atwood, J. L. *J. Am. Chem. Soc.* **1978**, *100*, 5238 - 5239.

(21) Werner, H.; Kuehn, A.; Burschka, C. *Chem. Ber.* **1980**, *113*, 2291 - 2307.

(22) Rerek, M. E.; Ji, L.-N.; Basolo, F.
J. Chem. Soc., Chem. Commun. **1983**, 1208 - 1209.

(23) Calhorda, M. J.; Romão, C. C.; Veiros, L. F.
Chem. Eur. J. **2002**, *8*, 868 - 875.

(24) Hart-Davis, A. J.; Mawbay, R. *J. Chem. Soc. A* **1969**, 2403 - 2407.

(25) Crichton, O.; Rest, A. J.; Taylor, D. J.
J. Chem. Soc., Dalton Trans. **1980**, 167 - 173.

(26) Frenking, G.; Fröhlich, N. *Chem. Rev.* **2000**, *100*, 717 - 774.

(27) Katz, T. J.; Rosenberger, M. *J. Am. Chem. Soc.* **1963**, 2030-2031.

(28) Katz, T. J.; Acton, N. *J. Am. Chem. Soc.* **1972**, *94*, 3281-3283.

(29) Cloke, F. G. N.; Kuchta, M., C.; Harker, R. M.; Hitchcock, P. B.; Parry, J. S.
Organometallics **2000**, *19*, 5795-5798.

(30) Jonas, K.; Kolb, P.; Kollbach, G.; Gabor, B.; Mynott, R.; Angermund, K.; Heinemann, O.; Krüger, C.
Angew. Chem., Int. Ed. Engl. **1997**, *36*, 1714-1718.

(31) Jonas, K.; Gabor, B.; Mynott, R.; Angermund, K.; Heinemann, O.; Krüger, C.
Angew. Chem., Int. Ed. Engl. **1997**, *36*, 1712-1714.

(32) Ackerman, L. J.; Green, M. L. H.; Green, J. C.; Bercaw, J. E.
Organometallics **2003**, *22*, 188 -194.

(33) Bruno, I. J.; Cole, J. C.; Edgington, P. R.; Kessler, M.; Macrae, C. F.; McCabe, P.; Pearson, J.; Taylor, R. *Acta Crystallogr.* **2002**, *B58*, 389-397.

(34) Cloke, F. G. N.; Hitchcock, P. B. *J. Am. Chem. Soc.* **1997**, *119*, 7899 - 7900.

(35) Cloke, F. G. N.; Green, J. C.; Jardine, C. N.
Organometallics **1999**, *18*, 1080 - 1086.

(36) Cloke, F. G. N.; Hitchcock, P. B. *J. Am. Chem. Soc.* **2002**, *124*, 9352-9353.

(37) Sadimenko, A. P.; Garnovskii, A. D.; Retta, N.
Coord. Chem. Rev. **1993**, *126*, 237 - 318.

(38) Nief, F. *Eur. J. Inorg. Chem.* **2001**, 891 - 904.

(39) Bordwell, F. G.; Druker, G. E.; Fried, H. E.
J. Org. Chem. **1981**, *46*, 632 - 635.

(40) King, R. B.; Bisnette, M. B. *Inorg. Chem.* **1964**, *3*, 796 - 800.

(41) Joshi, K. K.; Pauson, P. L. *Proc. Chem. Soc.* **1962**, 326.

(42) Kuhn, N.; Kockerling, M.; Stubenrauch, S.; Blaser, D.; Boese, R.

J. Chem. Soc., Chem. Commun. **1991**, 1368 - 1370.

(43) Kuhn, N.; Jendral, K.; Boese, R.; Blaser, D. *Chem. Ber.* **1991**, *124*, 89 - 91.

(44) Kuhn, N.; Henkel, G.; Kreutzberg, J.; Stubenrauch, S.; Janiak, C. *J. Organomet. Chem.* **1993**, *456*, 97 - 106.

(45) Schumann, H.; Gottfriedsen, J.; Demtschuk, J. *Chem. Commun.* **1999**, 2091 - 2092.

(46) Kuhn, N.; Henkel, G.; Stubenrauch, S. *J. Chem. Soc., Chem. Commun.* **1992**, 760 - 761.

(47) Kuhn, N.; Henkel, G.; Stubenrauch, S. *Angew. Chem., Int. Ed. Engl.* **1992**, *31*, 778 - 779.

(48) Okamura, W. H.; Katz, T. J. *Tetrahedron* **1967**, *23*, 2941 - 2957.

(49) Kissounko, D. A.; Kissounko, N. S.; Krutko, D. P.; Brusova, G. P.; Lemenovskii, D. A.; Boag, N. M. *J. Organomet. Chem.* **1998**, *556*, 145 - 149.

(50) Birmingham, J. M.; Wilkinson, G. *J. Am. Chem. Soc.* **1956**, *78*, 42 - 44.

(51) Wilkinson, G.; Birmingham, J. M. *J. Am. Chem. Soc.* **1954**, *76*, 6210 - 6210.

(52) Schumann, H.; Meese-Marktscheffel, J. A.; Esser, L. *Chem. Rev.* **1995**, *95*, 865 - 986.

(53) Eggers, S. H.; Schultze, H.; Kopf, J.; Fischer, R. D. *Angew. Chem., Int. Ed. Engl.* **1986**, *25*, 656 - 657.

(54) Smith, K. D.; Atwood, J. L. *J. Chem. Soc., Chem. Commun.* **1972**, 593b - 594.

(55) Evans, W. J.; Wayda, A. L. *Inorg. Chem.* **1980**, *19*, 2190 - 2191.

(56) Watson, P. L. *J. Chem. Soc., Chem. Commun.* **1980**, 652 - 653.

(57) Tilley, T. D.; Andersen, R. A.; Spencer, B.; Ruben, H.; Zalkin, A.; Templeton, D. H. *Inorg. Chem.* **1980**, *19*, 2999 - 3003.

(58) Evans, W. J.; Bloom, I.; Hunter, W. E.; Atwood, J. L. *J. Am. Chem. Soc.* **1981**, *103*, 6507 -6508.

(59) Watt, G. W.; Gillow, E. W. *J. Am. Chem. Soc.* **1969**, *91*, 775 - 776.

(60) Evans, W. J.; Hughes, L. A.; Hanusa, T. P. *J. Am. Chem. Soc.* **1984**, *106*, 4270 - 4272.

(61) Evans, W. J.; Davies, B. L. *Chem. Rev.* **2002**, *102*, 2119 - 2136.

(62) Kirillov, E.; Toupet, L.; Lehmann, C. W.; Razavi, A.; Kahlal, S.; Saillard, J.-Y.; Carpentier, J.-F. *Organometallics* **2003**, *22*, 4038 - 4046.

(63) Garrett, C. E.; Fu, G. C. *J. Org. Chem.* **1998**, *63*, 1370 - 1371.

(64) Resconi, L.; Cavallo, L.; Fait, A.; Piemontesi, F.
Chem. Rev. **2000**, *100*, 1253 - 1345.

(65) Andresen, A. A.; Cordes, H. G.; Herwig, J.; Kaminsky, W.; Merck, A.; Mottweiler, R.; Pein, J.; Sinn, H.; Vollmer, H.J.
Angew. Chem., Int. Ed. Engl. **1976**, *15*, 630 - 632.

(66) Ewen, J. A. *J. Am. Chem. Soc.* **1984**, *106*, 8330-8330.

(67) Kaminsky, W.; Külper, K.; Brintzinger, H. H.; Wild, F.
Angew. Chem., Int. Ed. Engl. **1985**, *24*, 507 - 508.

(68) Ballard, D. G. H.; Courtis, A.; Holton, J.; McMeeking, J.; Pearce, R.
J. Chem. Soc., Chem. Commun. **1978**, *22*, 994 - 995.

(69) Britovsek, G. J. P.; Gibson, V. C.; Wass, D. F.
Angew. Chem, Int. Ed. **1999**, *38*, 428 - 447.

(70) Jeske, G.; Schock, L. E.; Swepston, P. N.; Schumann, H.; Marks, T. J.
J. Am. Chem. Soc. **1985**, *107*, 8103 - 8110.

(71) Jeske, G.; Lauke, H.; Mauermann, H.; Swepston, P. N.; Schaumannn, H.; Marks, T. J. *J. Am. Chem. Soc.* **1985**, *107*, 8091 - 8103.

(72) D., S.; Sabat, M.; Marks, T. J. *J. Am. Chem. Soc.* **1990**, *112*, 9558 - 9575.

(73) Koga, N.; Morokuma, K. *Chem. Rev.* 1991, 91, 823 - 842.

(74) Möller, C.; Plesset, M. S. *Phys. Rev.* **1934**, 46, 618 - 622.

(75) Binkley, J. S.; Pople, J. A. *Int. J. Quantum Chem.* **1975**, 9, 229 - 236.

(76) Jolly, C. A.; Marynick, D. S. *J. Am. Chem. Soc.* **1989**, *111*, 7968 - 1974.

(77) Margl, P.; Deng, L.; Ziegler, T. *Topics in Catalysis* **1999**, *7*, 187 - 208.

CHAPTER 2

SYNTHESIS OF 3*H*-PYRROLIZINE SYSTEMS

2.1 INTRODUCTION

The first reported synthesis of 3*H*-pyrrolo[1,2-a]pyrrole, more commonly and here on referred to as 3*H*-pyrrolizine, **(I)**, was reported in 1964 by Schweizer and Light.[1] The cascade synthesis utilised a Michael addition reaction between a carboxaldehyde substituted sodium pyrrolide and a vinyl phosphonium bromide that underwent a subsequent cyclisation *via* a Wittig reaction to give the nitrogen bridgehead bicyclic 3*H*-pyrrolizine system in 87 % yield,[1] as shown in Equation 1.

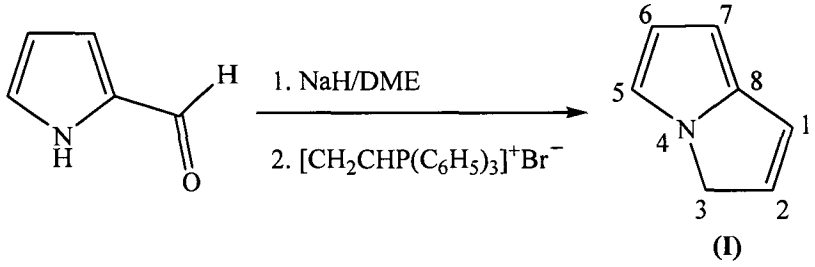

(I)

Equation 1: Synthesis of 3*H*-pyrrolizine **(I)**.

In 1967 the first complexes of the 3*H*-pyrrolizine were reported by Okamura and Katz who prepared Group 1 metal complexes of the deprotonated 3*H*-pyrrolizine.[2] The chemistry of the system remained relatively dormant until 1998 when Kissounko *et al.* synthesised a methyl substituted lithium salt, a thallium salt as well as tin and silicon substituted derivatives of 3*H*-pyrrolizine.[3] Studies and further development of the system's chemistry had been focussed on the chemistry of the mitomycins, a family of unsaturated edge fused 5:5 bridgehead *N*-heterocycles of which 3*H*-pyrrolizine is a member. This system has been extensively studied, in particular the pyrrolo[1,2-a]indole ring system, **(II)**, has been of most interest, due to their importance as intermediates in organic synthesis and the presence of this structural motif in many natural products.[4-9] The mitomycins, which have the basic structure of **(III)**,[4] are one such class of compound which exhibits anti-tumour and antibacterial activity. In light of this, few reviews cover the narrow field of chemistry of 3*H*-pyrrolizine and its benzoannulated derivatives; instead reviews have tended to

concentrate on the wider pyrrolizine family, their biosynthesis and their biological importance.[8-13]

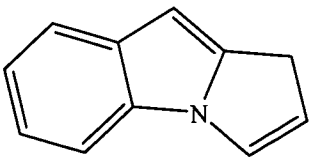

(II)

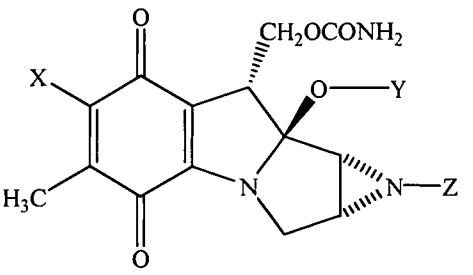

$X = OCH_3, NH_2$
$Y = CH_3, H$
$Z = CH_3, H$

(III)

The range of synthetic routes to 3*H*-pyrrolizines has been classified according to the numbering system for 3*H*-pyrrolizine, **(I)**, as described by Mosby,[14] and the position where the new bond or bonds are formed. The range of synthetic routes in which pyrrolizine systems have been able to be synthesised are given in Scheme 1.[15] Many target compounds of interest have been synthesised using pyrrole or indole as starting templates. This template may be built upon allowing for ring modifications and various substitutions which affect the chemistry of the system.

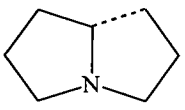

1,8-bond formation

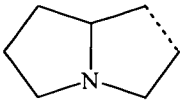

1,2-bond formation

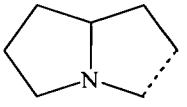

2,3-bond formation

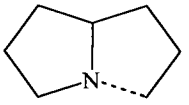

3,4-bond formation

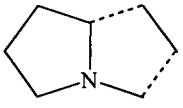

1,8:2,3-bond formation

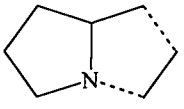

1,2:3,4-bond formation

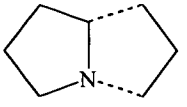

1,8:3,4-bond formation

Scheme 1: Classification of pyrrolizine synthetic routes, where the dash bonds (---) represent the position of the final ring closure step.

The synthesis of 3*H*-pyrrolizine published by Schweizer and Light[1] utilises the 1,2:3,4-bond formation approach. The 1,2-bond is formed during the Michael addition reaction, where the vinyl phosphonium salt is attacked by the nucleophilic

nitrogen centre of the *N*-deprotonated pyrrolide salt to form a phosphorane. The phosphorane then undergoes reaction with the aldehyde functionality to form the 3,4 linkage *via* the Wittig reaction. The mechanistic reaction sequence for the synthesis of 3*H*-pyrrolizine by this method is shown in Scheme 2. This reaction has since been developed[16,17] into a widely used method for the cyclisation of related compounds and the vinylphosphonium salt, known as Schweizer's salt, is commercially available.

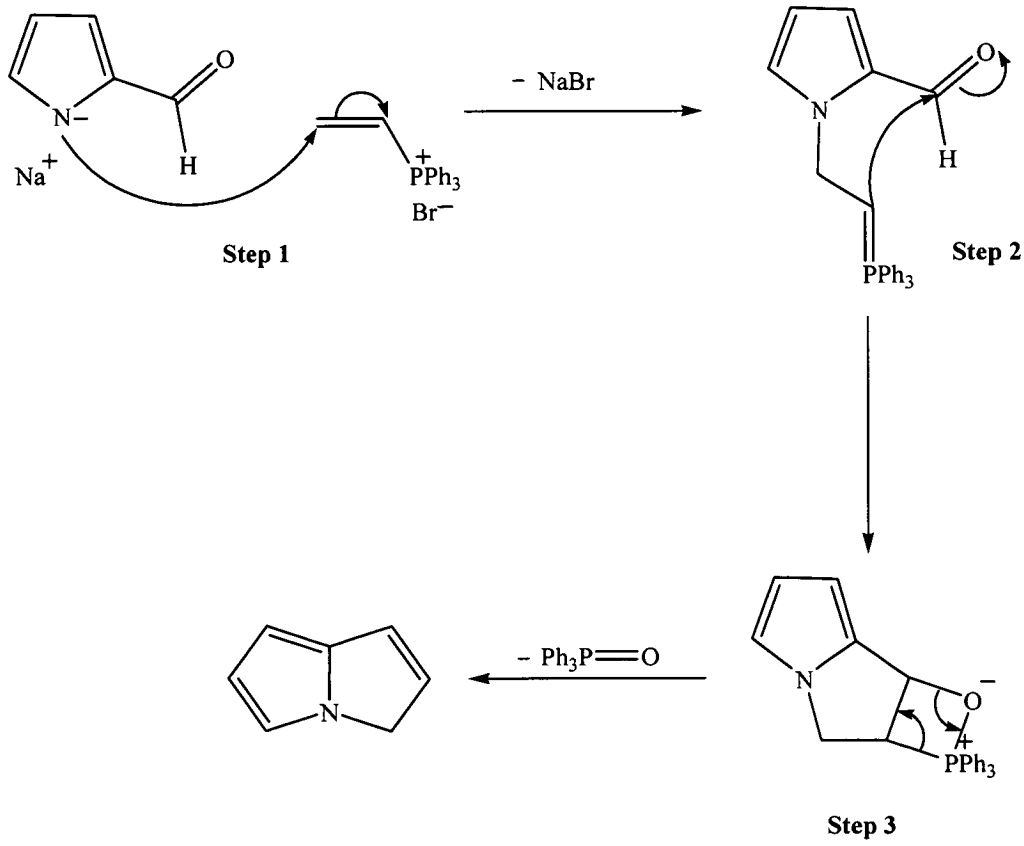

Scheme 2: Reaction mechanism for the synthesis of 3*H*-pyrrolizine. Step 1. Michael addition, Steps 2 and 3 intramolecular cyclisation *via* the Wittig reaction.

The synthetic procedure developed by Schweizer and Light has been modified *via* the use of various substituted vinylphosphonium salts in order to obtain 3*H*-pyrrolizine derivatives. These include, 3*H*-pyrrolo[1,2-a]indole, **(IV)**, dihydro-3*H*-pyrrolo[1,2-a]indole, **(V)**, and 1-methyl-3*H*-pyrrolizine, **(VI)**.[15,18] The phosphorous substituents of the vinylphosphonium salts, **(VII)**, were found to influence the cyclisation and, hence, the final yield of the pyrrolizine.[15] Cyclisation was shown to

be highest yielding when the electrophilicity of the phosphonium moiety was increased, for example, with triphenylphosphine as the phosphonium moiety, yields were much higher in comparison to the PPh_2Me analogue, as shown in Table 1.[15]

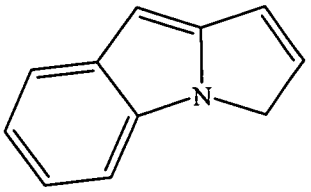

(IV)

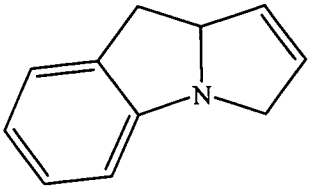

(V)

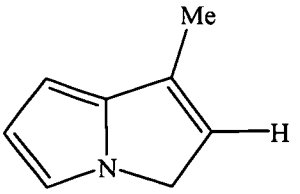

(VI)

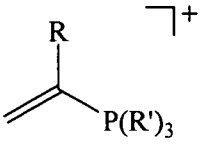

(VII)

Table 1: Yields of 3*H*-pyrrolizine with variations in the vinylphosphonium salts.[14]

Structure **(VII)**	R	$P(R')_3$	Product Yield (all isomers) (%)
a	H	PPh_3	87
b	Me	PPh_3	67
c	Me	PPh_2Me	25
d	Ph	PPh_3	0
e	Ph	$-POPh_2$	82
f	Ph	$-PO(OMe)_2$	45
g	CO_2Et	$-PO(OMe)_2$	66
h	$PhSO_2$	$-PO(OMe)_2$	85, 77

Whilst the formation of only one product from the cyclisation step is observed in the synthesis of 3*H*-pyrrolizine, quite often multiple isomers can be observed, as is the case for the product synthesised from the phosphonium salt **(VIIh)** in Table 1.

This formation of multiple isomers can be attributed to the occurrence of tautomeric shifts of the protons from the 3- to the 5-position of the system. For example in the synthesis of 2-formyl-5-methylpyrrole three isomers, **(VIII a-c)**, were observed as a 45:10:45 mixture, respectively, after the cyclisation.[15,19] The control of the product distribution during cyclisation, so the formation of one isomer over the other(s) is favoured, is possible by reacting the appropriately substituted vinylphosphonium salt with sodium 2-pyrrolide carboxaldehyde. Such an example of this is reaction of sodium 2-pyrrolide carboxaldehyde and vinylphosphane oxide **(VIIe)**, to form only the one isomer of phenylpyrrolizine in good yield.

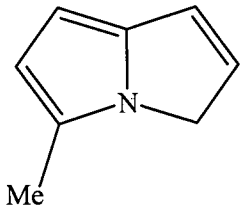

(VIIIa)

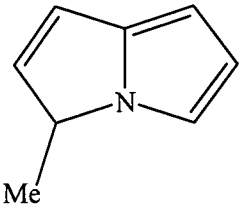

(VIIIb)

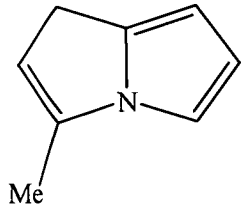

(VIIIc)

A convenient method for the synthesis of the pyrrolizine system is *via* cycloaddition reactions of the corresponding bases of Vilsmeier salts of pyrroles, known as the Vilsmeier-Haack reaction. The Vilsmeier-Haack reaction has shown to be a general method which is used for the synthesis of aldehydes and ketones of reactive aromatic compounds such as pyrroles, thiophenes and furans.[20] It is a highly selective reaction, preferentially formylating at the C-2 position of the heterocycle. The reaction has been shown to be a most effective method in the synthesis of pyrrole-2-carboxaldehydes which are intermediate compounds required for the synthesis of porphyrins[21] and, in the case of interest here, in the synthesis of 3*H*-pyrrolizines. The Vilsmeier-Haack reaction uses a combination of phosphorus oxychloride, *N*,*N*-dimethyl formamide followed by a hydrolytic workup in order to formylate the system, Scheme 3.

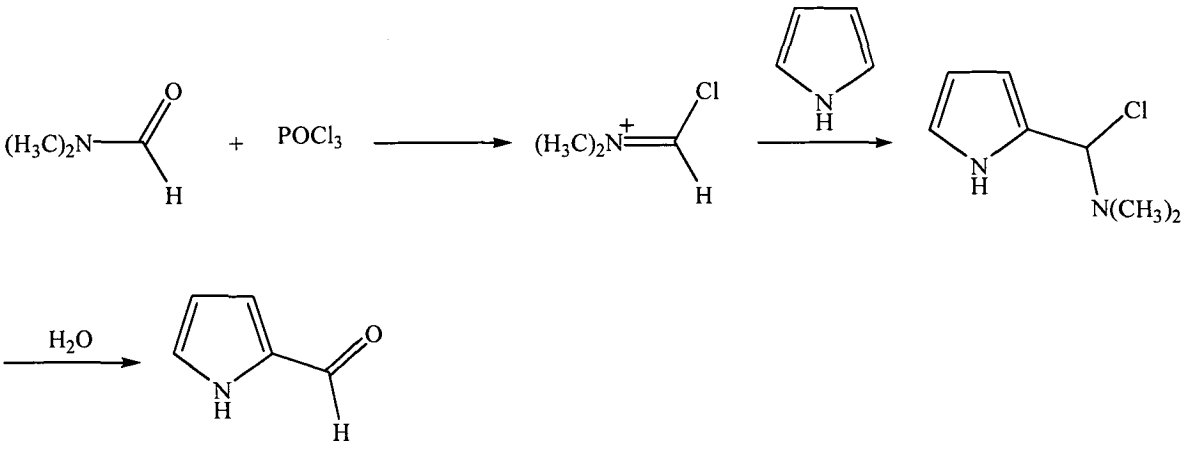

Scheme 3: Vilsmeier-Haack Reaction.

Whilst the 1,2:3,4-bond formation is the most convenient synthetic route of choice for the formation of the parent heterocycle 3*H*-pyrrolizine, the heterocyclic chemistry of the system has further been explored. Numerous compounds based on this system have been successfully synthesised *via* the application of other bond formation methods, as outlined in Scheme 1. The 1,8-bond formation approach has allowed synthesis of benzannulated derivatives of the 3*H*-pyrrolizine system. In this particular bond formation intramolecular acylation of pyrrole and indole carboxylic acids are employed frequently, as in the case of the Houben-Hoesch cyclisation of 1-β-cyanoethylpyrrole to 1-oxo-2,3-dihydropyrrolizine, Scheme 4.[15]

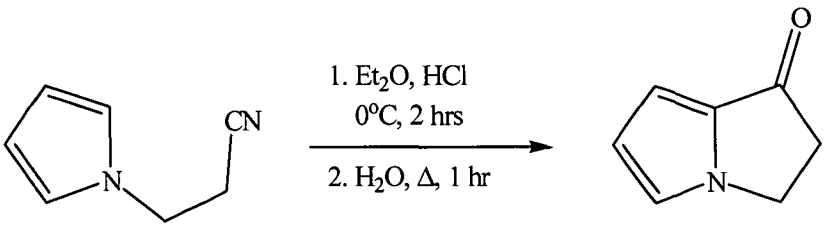

Scheme 4: Houben-Hoesch cyclisation.

9*H*-Pyrrolo[1,2-a]indol-9-one, **(IX)**, was first reported in 1955 by Shirley, Gross and Roussel who formed **(IX)** as yellow oil by-product from the reaction of 1-phenylpyrrole with *n*-butyllithium.[22] Five years later in 1960, Laschtuvka and Huisgen[23] reported the synthesis of **(IX)**, which they gave the name fluorazone, as well as synthesising a series of substituted compounds of **(IX)**. Seven years after the first report of **(IX)**, Joesy and Jenner reported a more convenient route, the formation

of the heterocyclic system *via* a 1,8-bond formation, a Friedel-Crafts cyclisation, in 32% yield using hot phosphoric acid as the catalyst.[24] This yield was subsequently improved by Mazzola and colleagues in 1967 who synthesised **(IX)** in 88% yield.[5] Their approach involved the Friedel-Crafts cyclisation of 2-(1-pyrrolyl)benzoic acid using phosphorus trichloride to form the acid chloride, which is cyclised in the presence of tin(IV) chloride to give 9*H*-pyrrolo[1,2-a]indol-9-one. The initial step in this three part synthesis involves a Clauson-Kaas reaction first reported in 1952 by Clauson-Kaas and Tyle, Scheme 5, step 1.[25] This particular reaction allows for the preparation of *N*-substituted pyrroles in good yields *via* a reaction between 2,5-dialkoxytetrahydrofurans and primary amines. By placing various substituents on either the cyclic acetal or the aromatic primary amine it is possible to synthesise a wide variety of substituted *N*-heterocyclic compounds.

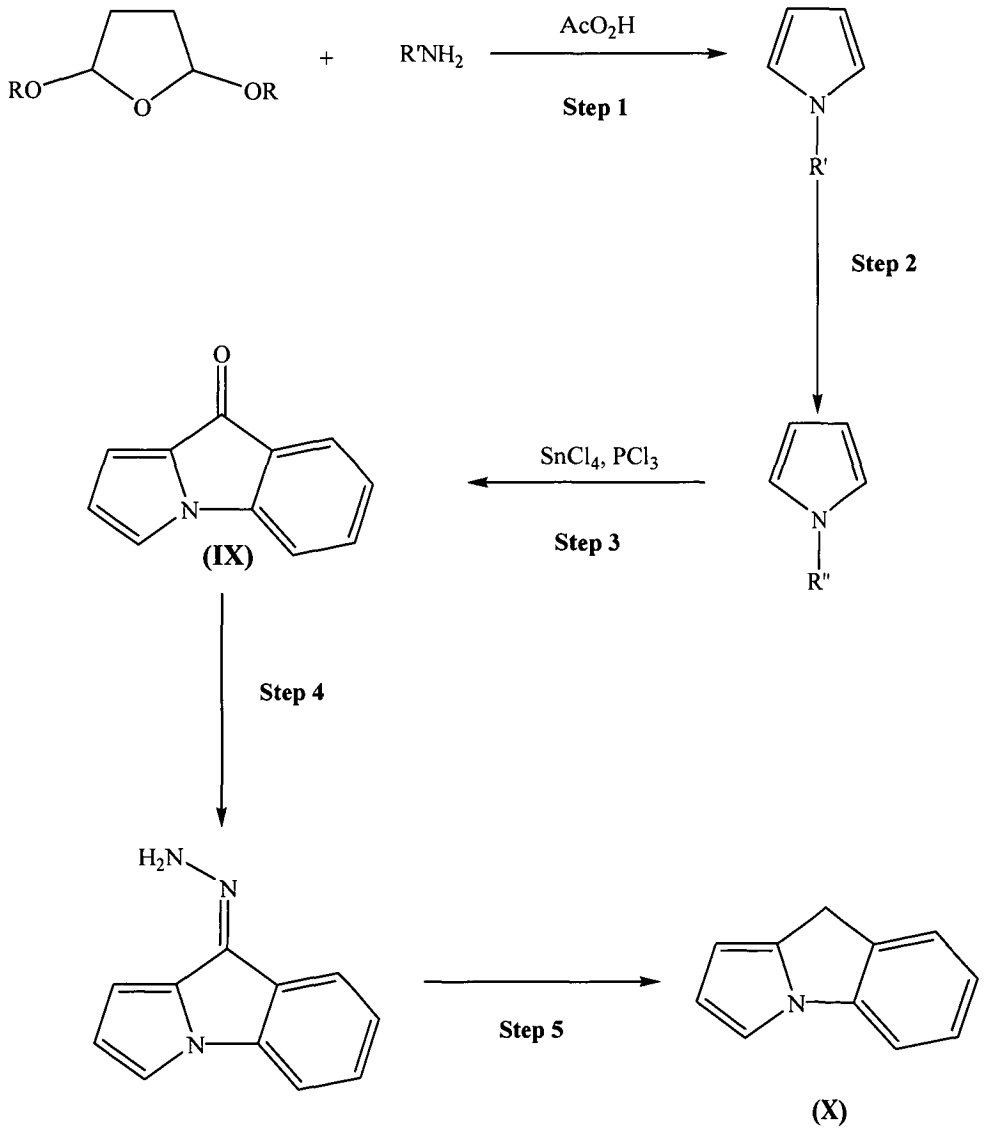

Scheme 5: Synthesis of 9*H*-pyrrolo[1,2-a]indole **(X)**, Step 1. Clauson-Kaas reaction and Steps 4 and 5 Wolff Kishner reduction.

Step 1, Scheme 5, in the synthesis of 9*H*-pyrrolo[1,2-a]indole **(X)** was the formation of the *N*-substituted pyrrole *via* the condensation of 2,5-diethoxytetrahyrofuran with methyl anthranilate which proceeds in good yield, 80%.[24] The methyl ester undergoes hydrolysis to give the corresponding acid, step 2. The 2-(1-pyrrolyl)benzoic acid is converted to 9*H*-pyrrolo[1,2-a]indol-9-one following the synthetic procedure of Mazzola, step 3.[5] The tin(IV) phosphorus system utilised in this step is more commonly used due to the increased yields obtained from the cyclisation process.[5] The ketone functionality of **(IX)** can be reduced *via* Wolf Kishner reduction of the semicarbazone of the ketone to yield the desired 9*H*-pyrrolo[1,2-a]indole, steps 4 and 5.

Substitution of the 3*H*-pyrrolizine heterocyclic system has enabled the chemistry of this system to be greatly diversified. Substituents are able to be incorporated early in the synthetic procedure, usually before the 2nd ring closure. This early incorporation in some cases allows the specific formation of one particular isomer, such an example is the cyclisation of 3-methyl-1*H*-pyrrole-1-propanenitrile. Here the 3-methyl substituent influences the intramolecular electrophilic substitution by selectively activating the C-2 position so that only one isomer is formed, as shown in Scheme 6.[15]

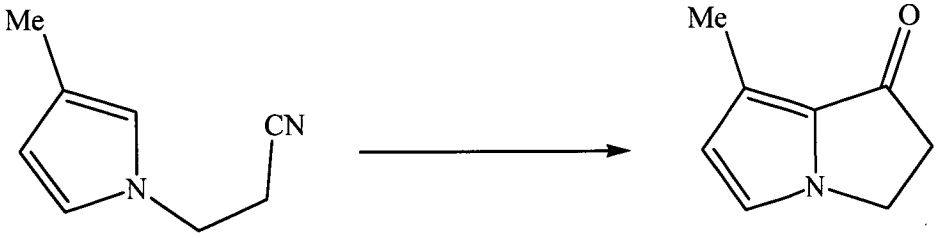

Scheme 6: The cyclisation of 3-methyl-1*H*-pyrrole-1-propanenitrile.

The 1,8-bond formation approach to 3*H*-pyrrolizine synthesis should allow for further derivatives based on the 3*H*-pyrrolizine system, such as 5*H*-pyrrolo[2,1-a]isoindole, **(XI)**, to be synthesised. The previously mentioned synthesis of 9*H*-pyrrolo[1,2-a]indol-9-one, **(IX)**, involved the intramolecular acylation of an indole carboxylic acid leading to the formation of the precursor ketone containing heterocycle, that required subsequent reduction. In comparison, the structure of the

isomeric 5*H*-pyrrolo[2,1-a]isoindole, **(XI)**, allows alternative synthetic approaches, such as *via* an intramolecular Heck reaction of a *N*-(2-bromobenzyl)pyrrole, see Section 2.2.2.1 for a detailed description of the synthetic procedure. In similar fashion, the chemistry could be extended to 6*H*-isoindolo[2,1-a]indole, **(XII)**, as shown in Scheme 7. This was the synthetic approach used to prepare 5*H*-pyrrolo[2,1-a]isoindole, **(XI)**, and 6*H*-isoindolo[2,1-a]indole, **(XII)**, in this project, whilst 3*H*-pyrrolizine, **(I)**, was synthesised using the literature preparation of Schweizer and Light discussed earlier in this introduction.

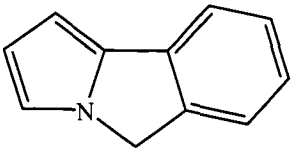

(XI)

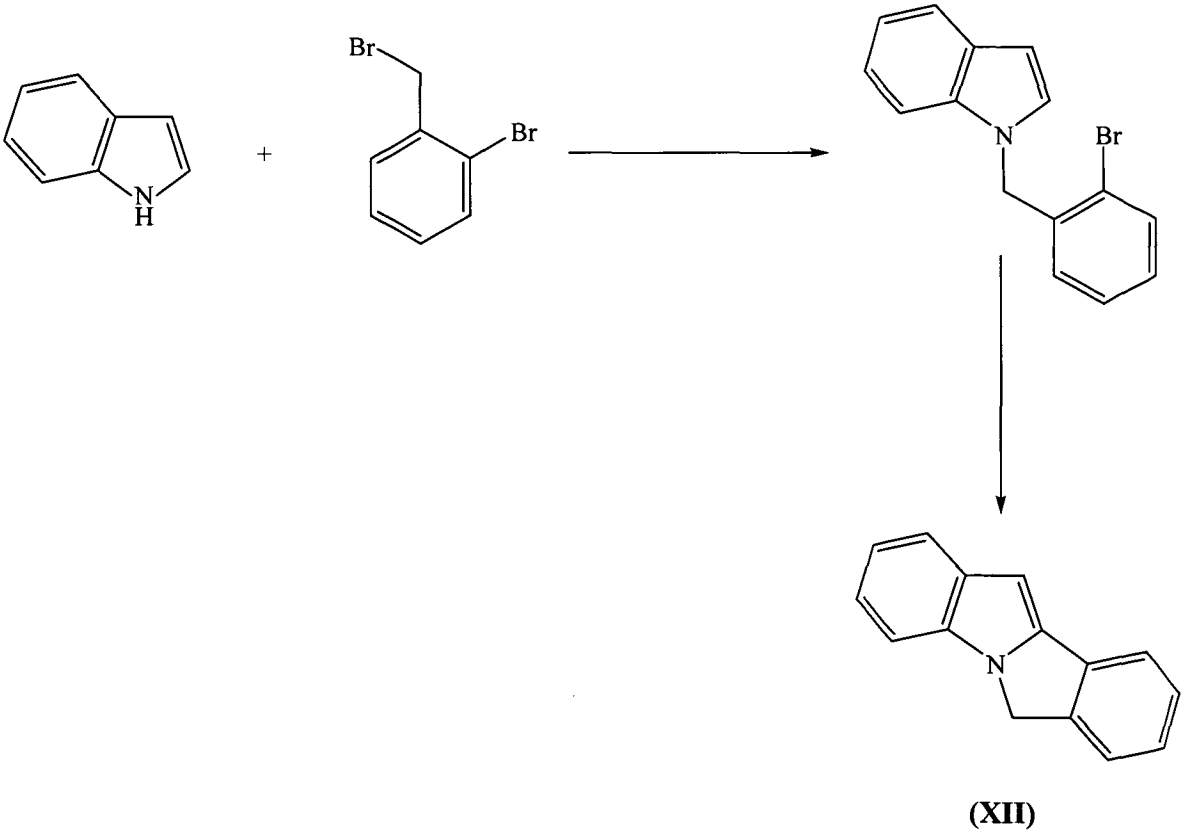

(XII)

Scheme 7: Synthesis of 6*H*-isoindolo[2,1-a]indole **(XII)**.

2.2 RESULTS AND DISCUSSION

2.2.1.1 Synthesis of 3*H*-pyrrolizine, (5)

The synthesis of 3*H*-pyrrolizine, **(5)**, was carried out following the procedure reported by Schweizer and Light,[1] in accordance with Scheme 8.

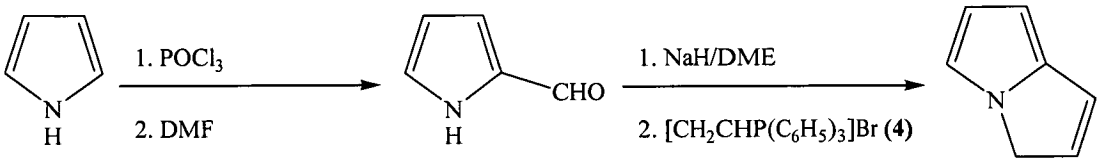

(1) (5)

Scheme 8: Synthesis of 3*H*-pyrrolizine, **(5)**.

The exothermic reaction of N,N-dimethyl formamide and phosphorous oxychloride affords a phosphorous oxychloride-N,N-dimethyl formamide complex,[26,27] which in turn reacts with pyrrole to give 2-pyrrolecarboxaldehyde, **(1)**, as a crude oil. The 2-pyrrolecarboxaldehyde is purified *via* fractional distillation (88 °C, 1.5 x 10^{-1} mbar) giving a colourless oil, which upon cooling crystallises to give the aldehyde **(1)**, in 47% yield. Deprotonation of 2-pyrrolecarboxaldehyde, **(1)**, by NaH in 1,2-dimethoxyethane (DME) gives the intermediate carboxaldehyde substituted sodium pyrrolide, which then undergoes a Michael addition with vinyltriphenylphosphonium bromide, **(4)**. Subsequent cyclisation *via* a Wittig reaction yields the desired 3*H*-pyrrolizine, **(5)**, as a crude oil. 3*H*-pyrrolizine, **(5)**, is purified *via* fractional distillation *in vacuo* (70 °C, 20 mbar). The temperature of the distillation must be carefully monitored as the compound is thermally unstable and decomposes at temperatures greater than 85 °C. The thermal instability of 3*H*-pyrrolizine and the need for fractional distillation for product purification lead to a decreased yield of 21%, which is considerably lower than that reported by Schweizer and Light (87%).[1] Numerous syntheses were conducted however the best yield obtained was 21%

Compounds **(1)**, **(4)**, and **(5)** were characterised by ^{1}H and $^{13}C\{^{1}H\}$ NMR spectroscopy. Further details of the NMR characterisation of **(5)** are given in Section 2.2.3.

The thermal instability of 3*H*-pyrrolizine, **(5)**, lead to the investigation and development of substituted 3*H*-pyrrolizine syntheses, which exhibit greater thermal stabilities. 5*H*-pyrrolo[2,1-a]isoindole, **(9)**, 6*H*-isoindolo[2,1-a]indole, **(11)**, 9*H*-pyrrolo[1,2-a]indole, **(XIV)**, and 5-methyl-5*H*-pyrrolo[2,1-a]isoindole, **(XVI)**, were chosen and their synthesis and subsequent reactivity will be discussed later.

2.2.2 Synthesis of substituted 3*H*-pyrrolizines

2.2.2.1 Synthesis of 5*H*-pyrrolo[2,1-a]isoindole, (9)

The synthesis of 5*H*-pyrrolo[2,1-a]isoindole, **(9)**, was carried out according to Scheme 9, which involved a palladium catalysed Heck reaction as the key cyclisation methodology.

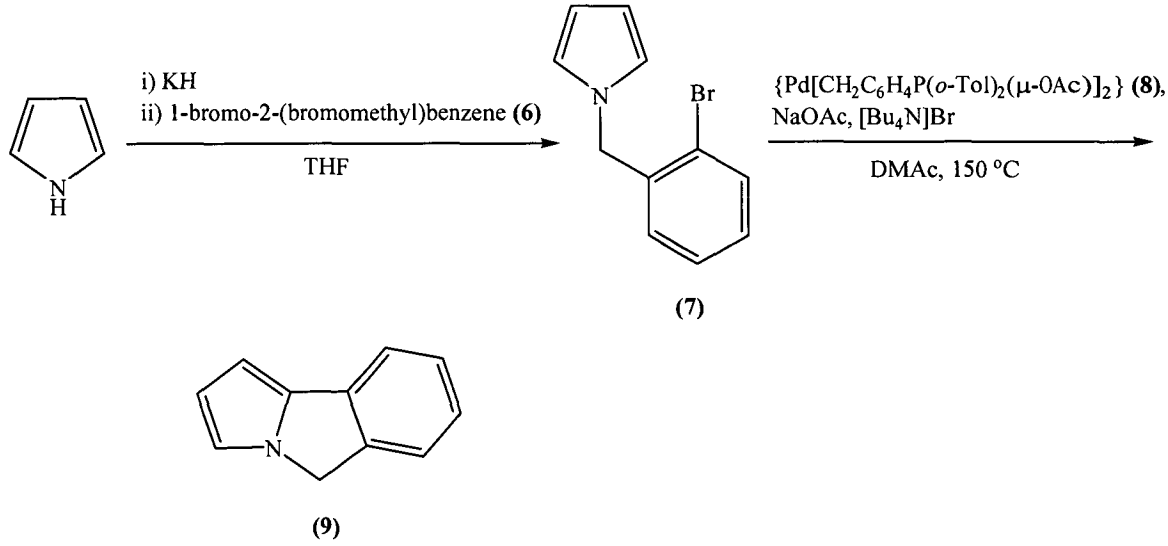

Scheme 9: Synthesis of 5*H*-pyrrolo[2,1-a]isoindole, **(9)**.

Pyrrole was deprotonated at the nitrogen centre with one molar equivalent of KH in THF at 0 °C. This intermediate was *N*-alkylated with 1-bromo-2-(bromomethyl)benzene, **(6)**, at 0 °C leading to the formation of *N*-(2-

bromobenzyl)pyrrole, **(7)**, in 99% yield as a crude oil, which was purified *via* fractional distillation *in vacuo* (100 °C, 6.4 x 10^{-2} mbar) yielding **(7)** as a colourless oil in 88% yield. Intramolecular cyclisation of *N*-(2-bromobenzyl)pyrrole was achieved by a Heck reaction using [{Pd[$CH_2C_6H_4P$(*o*-Tol]$_2$(μ-OAc)]$_2$}], **(8)**, as the catalyst, sodium acetate as the base and [Bu_4N]Br as a salt additive in *N*,*N*-dimethyl acetamide (DMAc) at 150 °C affording 5*H*-pyrrolo[2,1-a]isoindole, **(9)**, as a pale yellow solid in 40% yield. The crude material was sublimed (80 °C, 2.6 x 10^{-2} mbar) to give the purified product, **(9)**, as a colourless crystalline solid in 33% yield, which often takes on a yellow appearance.

Milder conditions that were necessary for the synthesis of 3*H*-pyrrolizine[1] were not required in the synthesis of 5*H*-pyrrolo[2,1-a]isoindole, **(9)**, due to its increased thermal stability allowing for the forcing reaction conditions required by the Heck reaction, the use of higher temperatures and the presence of base. The yield of 5*H*-pyrrolo[2,1-a]isoindole, **(9)**, however, is lower than the reported yield for 3*H*-pyrrolizine, **(5)**, 87%.[1] The intramolecular Heck reaction for the synthesis of **(9)** was also attempted using tetrakis(triphenylphosphine)palladium(0) as the catalyst, resulting in a poorer yield than that found with Herrmann's catalyst.

Compounds **(7)** and **(9)** were characterised by ^{1}H and ^{13}C{^{1}H} NMR spectroscopy and, in the case of **(9)**, an X-ray crystal structure determination was performed, the results of which are discussed in Section 2.2.4. Further details of the NMR studies of **(9)** are found in Section 2.2.3.

2.2.2.2 Synthesis of 6*H*-isoindolo[2,1-a]indole, (11)

The synthesis of 6*H*-isoindolo[2,1-a]isoindole, **(11)**, was adapted from the previously described procedure to 5*H*-pyrrolo[2,1-a]isoindole, **(9)**, utilising indole as the starting *N*-heterocyclic reagent and a palladium catalysed Heck reaction, as shown in Scheme 10.

Indole was deprotonated at the nitrogen centre with one molar equivalent of KH in the presence of THF at 0 °C. The intermediate was *N*-alkylated with 2-bromo

o-tolylbromide, **(6)**, at 0 °C leading to the formation of *N*-(2-bromobenzyl)indole, **(10)**, in 31% yield as a pink solid. Intramolecular cyclisation of *N*-(2-bromobenzyl)pyrrole was achieved by a Heck reaction using [{Pd[$CH_2C_6H_4P$(*o*-Tol]$_2$(μ-OAc)]$_2$}] (Herrmann's catalyst), **(8)**, sodium acetate and [Bu_4N]Br in DMAc affording 6*H*-isoindolo[2,1-a]indole, **(11)**, as a tan solid in 63% yield. The crude material was recrystallised from DCM to give the purified product, **(11)**, as a pale tan crystalline solid in 58% yield.

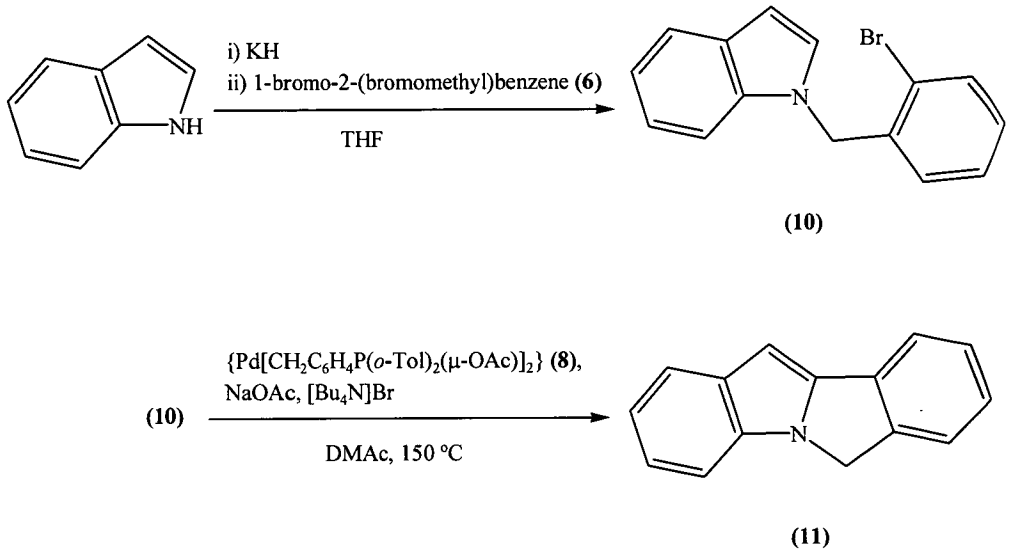

Scheme 10: Synthesis of 6*H*-isoindolo[2,1-a]indole, **(11)**.

Like 5*H*-pyrrolo[2,1-a]isoindole, **(9)**, 6*H*-isoindolo[2,1-a]indole, **(11)**, exhibits improved thermal stability relative to 3*H*-pyrrolizine. The yield of 6*H*-isoindolo[2,1-a]indole, **(11)**, was also lower than the yield reported for 3*H*-pyrrolizine, **(5)**, though improved on 5*H*-pyrrolo[2,1-a]isoindole, **(9)**. 6*H*-Isoindolo[2,1-a]indole, **(11)**, exhibits decreased solubility in all solvents in comparison to 5*H*-pyrrolo[2,1-a]isoindole, **(9)**. 6*H*-isoindolo[2,1-a]indole, **(11)**, exhibits poor solubility in acetone (at room temperature, moderate when heated), hexane and chloroform but had an increased solubility in THF, hence subsequent NMR studies were carried out in THF-d_8. The decreased solubility of **(11)** proved to be convenient during the isolation procedure, as **(11)** was found to be less volatile than **(9)**.

Compounds **(10)** and **(11)** were characterised by ^{1}H and ^{13}C{^{1}H} NMR spectroscopy, with the solid state structure of **(11)** being determined by single

crystal X-ray diffraction studies. Further details of the NMR studies of **(11)** are found in Section 2.2.3.

2.2.2.3 Attempted synthesis of 5-methyl-5*H*-pyrrolo[2,1-a]isoindole, (XIII)

The synthesis of 5-methyl-5*H*-pyrrolo[2,1-a]isoindole, **(XIII)** was attempted according to Scheme 11. 5-Methyl-5*H*-pyrrolo[2,1-a]isoindole, **(XIII)**, was prepared *via* an intramolecular Heck reaction, as outlined previously for the synthesis of **(9)** and **(11)**.

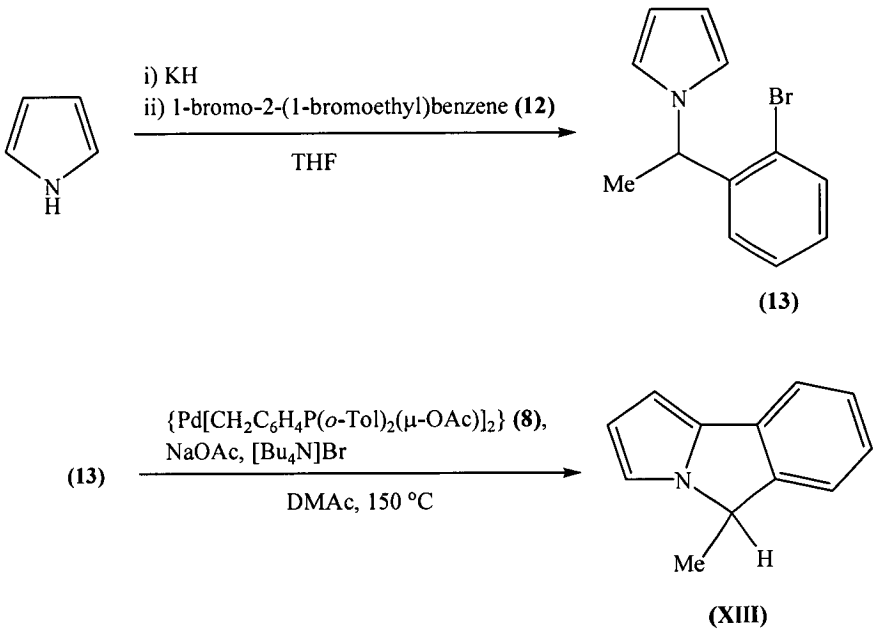

Scheme 11: Synthesis of 5-methyl-5*H*-pyrrolo[2,1-a]isoindole, **(XIII)**.

N-(2-Bromo-1-ethylbenzyl)pyrrole, **(13)**, was formed in 80% yield as a crude oil via the reaction of 1-bromo-2-(1-bromoethyl)-benzene, **(12)**, with potassium pyrrolide at 0 °C. Compound **(13)** was purified *via* fractional distillation *in vacuo* (81 °C, 3.2 x 10^{-2} mbar) yielding **(13)** as a colourless oil in 59% yield. Intramolecular cyclisation of *N*-(2-bromo-1-ethylbenzyl)pyrrole, **(13)**, was achieved by a Heck reaction using [{Pd[$CH_2C_6H_4P(o\text{-Tol})_2(\mu\text{-OAc})]_2$}], **(8)**, with the formation of **(XIII)** confirmed by ^{1}H NMR spectroscopy of the crude reaction mixtures, where the CH-Me signal was observed to occur at δ 1.64 ppm. Sublimation and flash column chromatography of the crude material was unsuccessful in separating the desired

compound from *N*-(2-bromo-1-ethylbenzyl)pyrrole, **(13)**. Compounds **(12)** and **(13)** were characterised by ^{1}H and ^{13}C NMR spectroscopies.

2.2.2.4 Attempted synthesis of 9*H*-pyrrolo[1,2-a]indole, (XV)

The synthesis 9*H*-pyrrolo[1,2-a]indol-9-one, **(16)**, was carried out in accordance with Scheme 12.

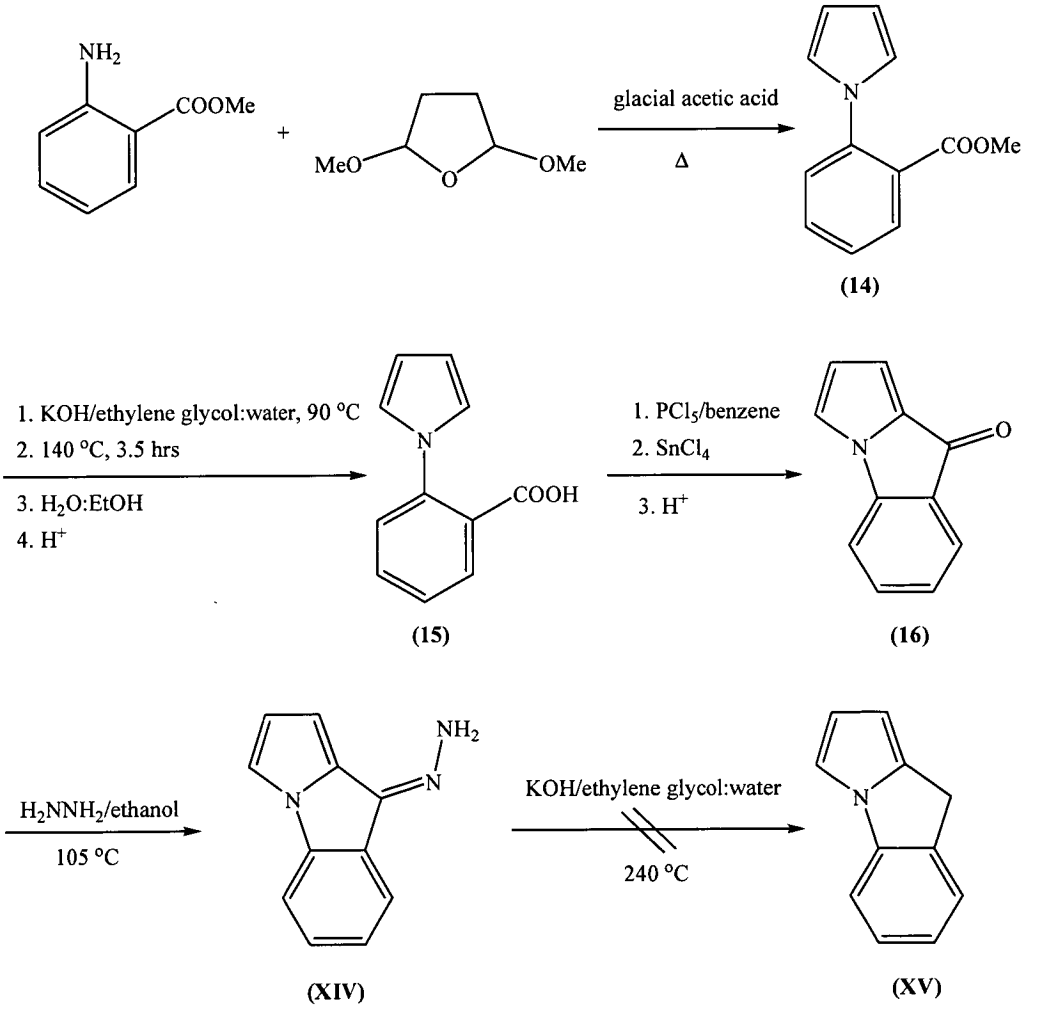

Scheme 12: Attempted synthesis of 9*H*-pyrrolo[1,2-a]indol-9-one, **(16)**.

2,5-Dimethoxytetrahydrofuran was condensed with methyl anthranilate to give 2-(1*H*-pyrrol-1-yl)-benzoic acid methyl ester, **(14)**, in 80% yield. Hydrolysis of the ester **(14)** in the presence of potassium hydroxide in an ethylene glycol/water (10:2) mixture followed by acidification lead to the formation of 2-(1*H*-pyrrol-1-yl)-benzoic

acid, **(15)**, in 86% yield. The Friedel-Crafts cyclisation of **(15)** was achieved using a 1.6 molar excess of phosphorous pentachloride in benzene, in the presence of a 1.6 molar excess of tin(IV) chloride as a Lewis acid catalyst, leading to the formation of 9*H*-pyrrolo[1,2-a]indol-9-one, **(16)**, in 23% yield. Attempts to synthesise 9*H*-pyrrolo[1,2-a]indole, **(XV)**, involving Wolff Kishner reduction were unsuccessful. ^{1}H NMR spectroscopy indicated that the conversion of **(16)** to **(XV)** had been unsuccessful, with the hydrazone intermediate **(XIV)** being isolated. Further attempts to reduce the ketone functionality of **(16)** to give 9*H*-pyrrolo[1,2-a]indole using

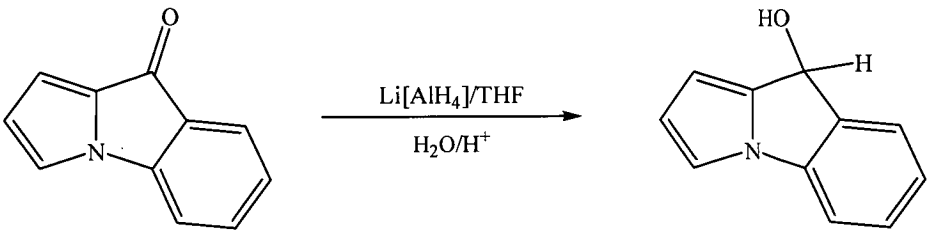

(16) **(XVI)**

Scheme 13: Synthesis of 9*H*-pyrrolo[1,2-a]indol-9-ol **(XVI)**.

$Li[AlH_4]$ were also unsuccessful, yielding the alcohol **(XVI)** as a partially reduced intermediate, Scheme 13, on the basis of GC-MS analysis with a compound of two higher mass units than the ketone being detected. Compounds **(14)**, **(15)**, **(16)** and **(XIV)** were characterised by ^{1}H NMR spectroscopy.

2.2.3 NMR spectroscopy of pyrrolizines

The ^{1}H NMR spectral data of compounds **(5)**, **(9)** and **(11)**, including the full assignment of the proton resonances for **(5)** and **(9)**, are listed in Table 2. The aromatic protons of the unsaturated five membered ring cores in the compounds have chemical shifts in the range δ = 5.55 – 6.93 ppm, while the remaining aromatic protons resonate at between δ = 6.99 – 7.71 ppm. The methylene protons have chemical shifts in the range δ = 3.60 – 5.10 ppm.

Complete proton resonance assignment for compounds **(5)** and **(9)** were based on two dimensional NMR spectroscopic studies, gCOSY, and gNOESY spectra. Chemical shift differences for **(5)** and **(9)** are highlighted in Figure 1. The greatly

decreased solubility of compound **(11)** at room temperature meant that gCOSY NMR spectroscopy was not feasible to allow full assignment of the phenylene proton resonances.

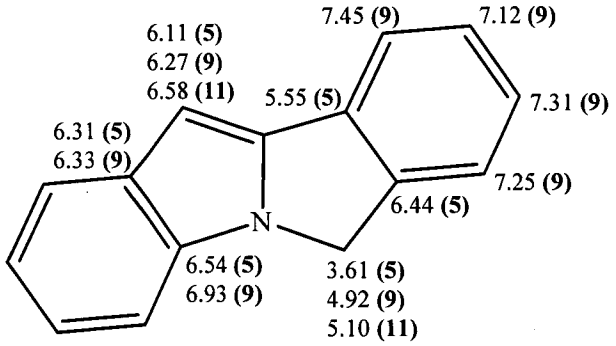

Figure 1: ^{1}H NMR spectral data assignments for compounds **(5)**, **(9)** and **(11)**, partial data only for **(11)**, (C_6D_6 for **(5)**, $CDCl_3$ for **(9)**, THF-d^8 for **(11)**, 299.90 MHz, 298 K, ppm).

The methylene resonances in compounds **(9)** and **(11)** (4.92 and 5.10 ppm, respectively) experience a large downfield shift relative to the methylene group in compound **(5)**, 3.61 ppm, see Table 2. This shift can be attributed to the shielding effect of the phenylene functionality present in the former two heterocyclic compounds. A downfield shift is also seen in the resonances related to the positions 2 and 4 of the unsaturated five membered rings of compound **(9)** in comparison to compound **(5)**, which is again attributed to the shielding effects of the phenylene functionality of **(9)**. Likewise, a further downfield shift is observed for position 4 in compound **(11)**, indicating that the substitution of a second phenylene group further shields the proton in this position.

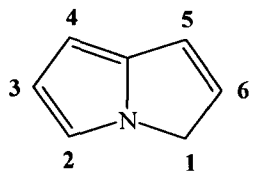

(5)

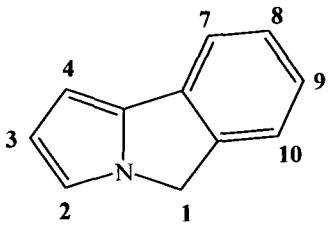

(9)

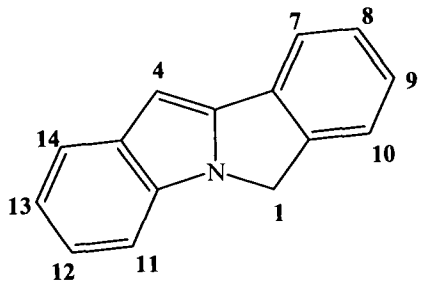

(11)

Table 2: ^{1}H NMR spectral data for compounds **(5)**, **(9)** and **(11)** (C_6D_6 for **(5)**, $CDCl_3$ for **(9)**, THF-d_8 for **(11)**, 299.90 MHz, 298 K, ppm).

	CH_2	CH (unsaturated 5 membered ring)					CH (phenylene)							
	1	2	3	4	5	6	7	8	9	10	11	12	13	14
C_7H_7N **(5)**	3.61	6.54	6.31	6.11	5.55	6.44	-	-	-	-	-	-	-	-
$C_{11}H_9N$ **(9)**	4.92	6.93	6.33	6.27	-	-	7.45	7.12	7.31	7.25	-	-	-	-
$C_{15}H_{11}N$ **(11)**	5.10	-	-	6.58	-	-	6.99, 7.09, 7.29, 7.37 (x2), 7.51, 7.55, 7.71							

The appearance of the phenylene proton resonances in the ^{1}H NMR spectra of compound **(9)** were as expected in the aromatic region between δ = 7.12 - 7.45 ppm. An AA'BB' spin system is observed for compound **(9)** with the following characteristic resonances in the aromatic region: 7.12 ppm (pseudo triplet); 7.25 ppm (doublet); 7.31 ppm (pseudo triplet) and 7.45 ppm (doublet), as shown in Figure 2. The coupling constants range from 7.42 – 7.56 Hz, which falls within the expected values. The range of coupling constants for the unsaturated proton resonances on the five membered rings was 2.59 – 3.50 Hz. This is a somewhat larger range than that observed for the aromatic region yet is similar to the coupling constant range observed for pyrrole reported by Fukui *et al.* in 1970, 1.37 – 3.63 ppm.[28] The multiplicity observed for the protons of the unsaturated five membered rings are as follows: 6.27 ppm (doublet); 6.33 ppm (pseudo triplet) and 6.93 (doublet).

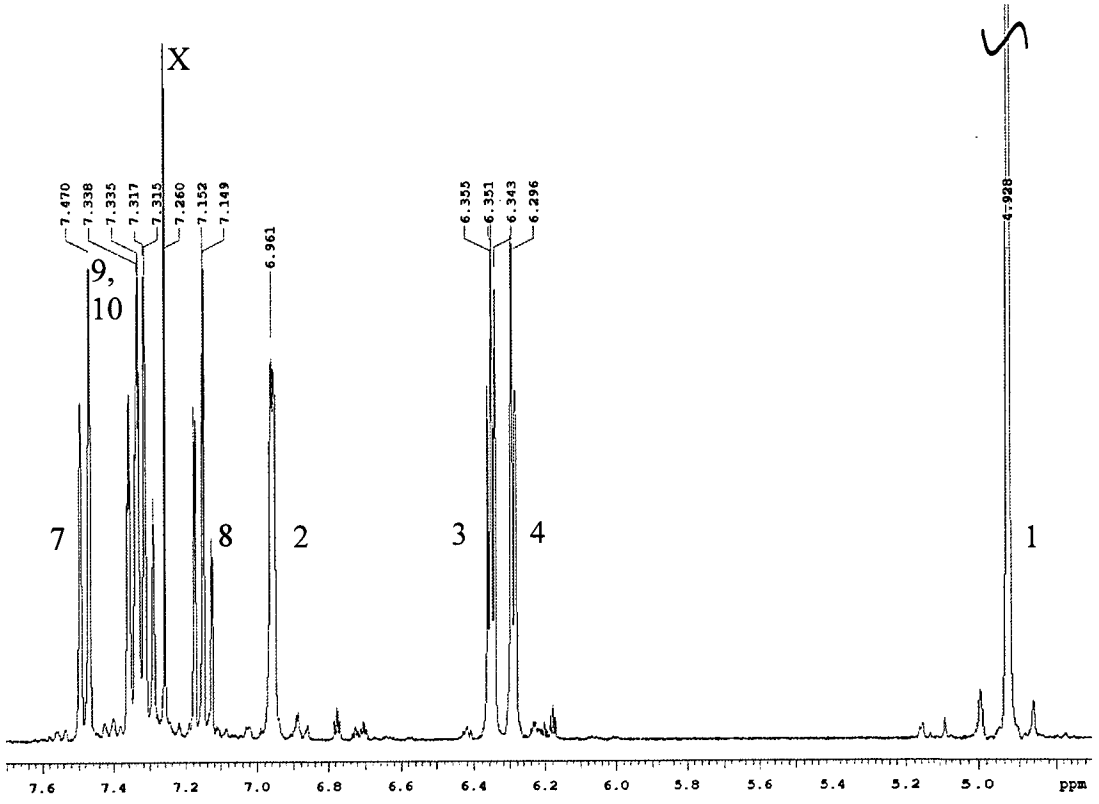

Figure 2: ^{1}H NMR spectrum of 5*H*-pyrrolo[2,1-a]isoindole, **(9)**, ($CDCl_3$, 299.90 MHz, 298 ppm). X=solvent

In contrast to the well resolved aromatic resonances of compound **(9)**, the resonances in the aromatic region for the tetracyclic compound **(11)** exhibit some overlap with the phenylene proton resonances occurring between δ = 6.99 – 7.71 ppm. The observed resonances are characteristic for the tetracyclic compound **(11)**, however an X-ray crystal structure determination was performed to provide complete confirmation of correct product formation as cyclisation onto the 7-position of the indole to give **(XVII)**, Figure 3, may have occurred. The ^{1}H NMR spectrum of compound **(11)** exhibits two singlets and 2 x AA'BB' spin systems for the phenylene protons. The following phenylene resonances were observed in the ^{1}H NMR spectra: 6.99 ppm (pseudo triplet); 7.09 ppm (pseudo triplet); 7.29 ppm (pseudo triplet); 7.37 ppm (multiplet); 7.51 ppm (doublet); 7.55 ppm (doublet) and 7.71 ppm (doublet), Figure 4. The coupling constants observed for the phenylene resonances in **(11)** are similar to those observed in compound **(9)**, with the range being 7.41 – 8.00 Hz. A singlet resonance observed at 6.58 ppm corresponds to the proton at position 4 of the unsaturated five membered ring. The singlet resonance is characteristic of compound **(11)** and aids in the identification of the correct cyclisation product as this proton would not resonate as a singlet if the cyclisation had occurred at the 7-position of the indole giving the isomer **(XVII)**.

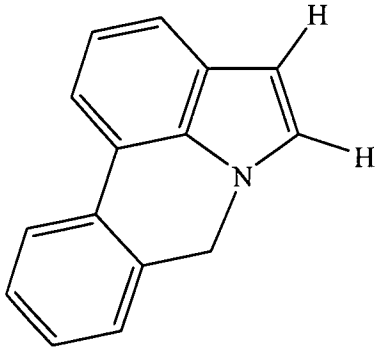

Figure 3. Possible product of cyclisation, compound **(XVII)**.

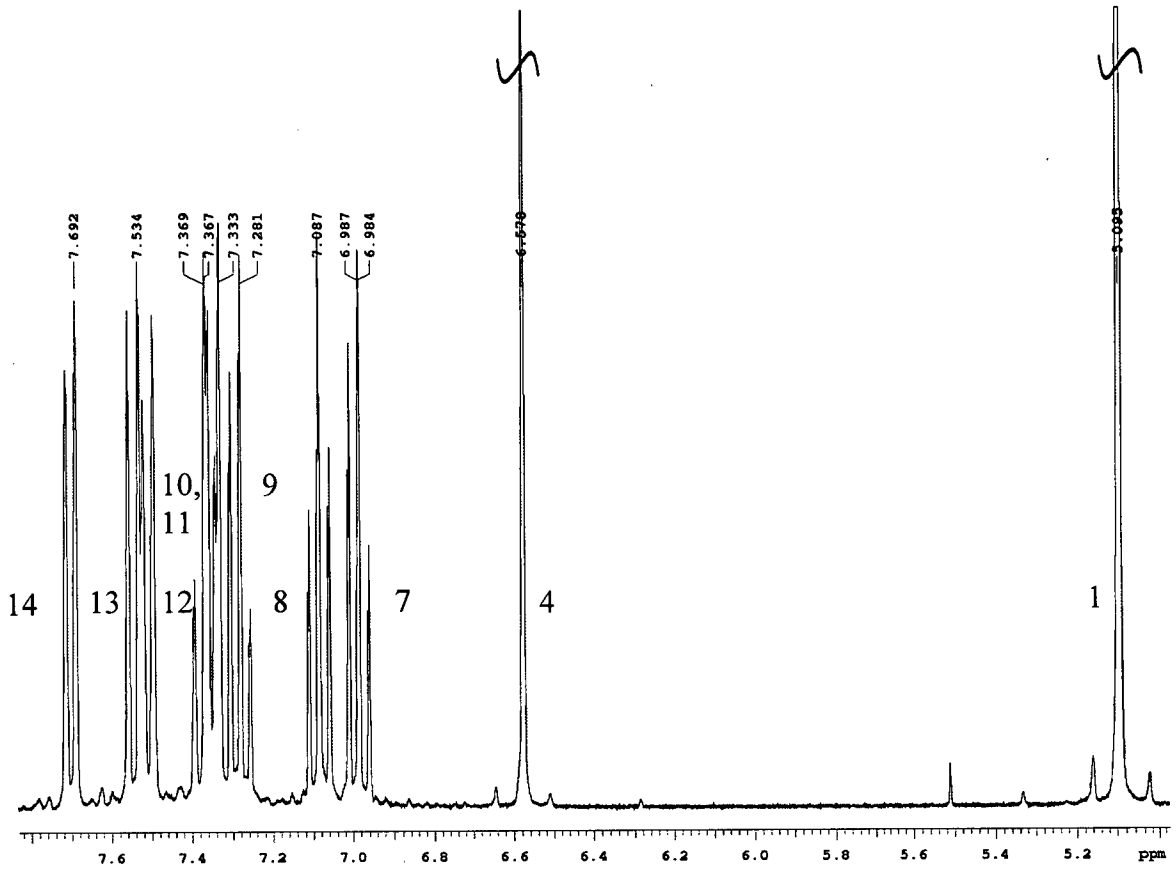

Figure 4: ^{1}H NMR spectrum of 6*H*-isoindolo[2,1-a]indole, **(11)**, (THF-d_8, 299.90 MHz, 298 K, ppm).

The $^{13}C\{^{1}H\}$ NMR spectral data of compounds **(5)**, **(9)** and **(11)** are listed in Table 3. The carbons of the unsaturated five membered ring cores in the three compounds occur in the range δ = 91.8 – 127.0 ppm, while the phenylene carbons resonate at between δ = 120.1 – 144.6 ppm. The methylene carbon resonances occur between δ = 49.0 – 51.5 ppm. The complete assignment of the $^{13}C\{^{1}H\}$ NMR spectrum for compound **(9)** was possible from the analysis of two dimensional gHMBC and gHMQC spectra obtained, shown in Table 3. As mentioned in discussion of the proton NMR assignments for compound **(11)**, complete carbon assignment was not possible for **(11)** due to its poorer solubility in solution at room temperature.

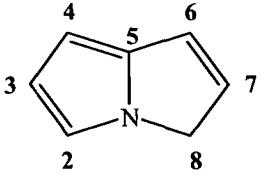

(5)

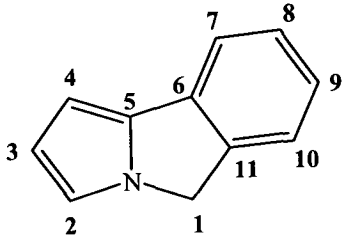

(9)

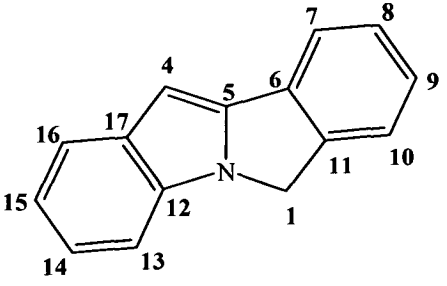

(11)

Table 3: $^{13}C\{^{1}H\}$ NMR spectral data for compounds **(5)**, **(9)** and **(11)** (C_6D_6 for **(5)**, $CDCl_3$ for **(9)**, THF-d_8 for **(11)**, 75.4 MHz, 298 K, ppm).

	CH_2	CH (unsaturated five membered ring)				CH (phenylene)					
	1	2	3	4	5	6	7	8	9	10	11
C_7H_7N **(5)**	50.2	97.8, 141.1.6	112.5,	116.8,	124.0,	127.0,					
$C_{11}H_9N$ **(9)**	51.5	116.7	112.9	98.2	138.7	140.4	118.8	125.0	128.1	123.2	134.0
$C_{15}H_{11}N$ **(11)**	49.0	98.1, 109.9				120.1, 128.8,	121.4, 133.9,	122.0, 134.0,	122.2, 135.0,	124.5, 143.3,	127.7, 144.6

2.2.4 Crystal Structures of Pyrrolizines

2.2.4.1 5*H*-pyrrolo[2,1-a]isoindole, (9)

Colourless crystals of 5*H*-pyrrolo[2,1-a]isoindole, **(9)**, suitable for X-ray structure determination were obtained by sublimation (80 °C, 2.6 x 10^{-2} mbar). The crystals of **(9)** belong to the monoclinic space group $P2_1/n$ (No. 14), a = 10.1227(7), b = 5.6528(4), c = 14.1174(9) Å, β = 97.300(2) °. The asymmetric unit contains one molecule of **(9)**, and the unit cell consists of four molecules of **(9)**. The molecular structure of **(9)** is shown in Figure 5.

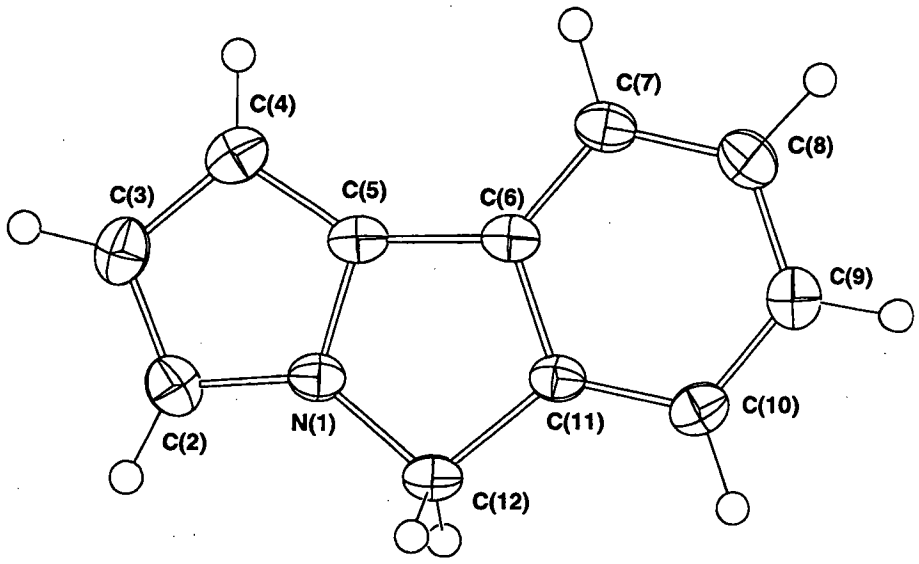

Figure 5: Molecular structure of 5*H*-pyrrolo[2,1-a]isoindole, **(9)**, with thermal ellipsoids are drawn at the level of 50% probability.

Figure 6 is a representation of the unit cell contents of compound **(9)**.

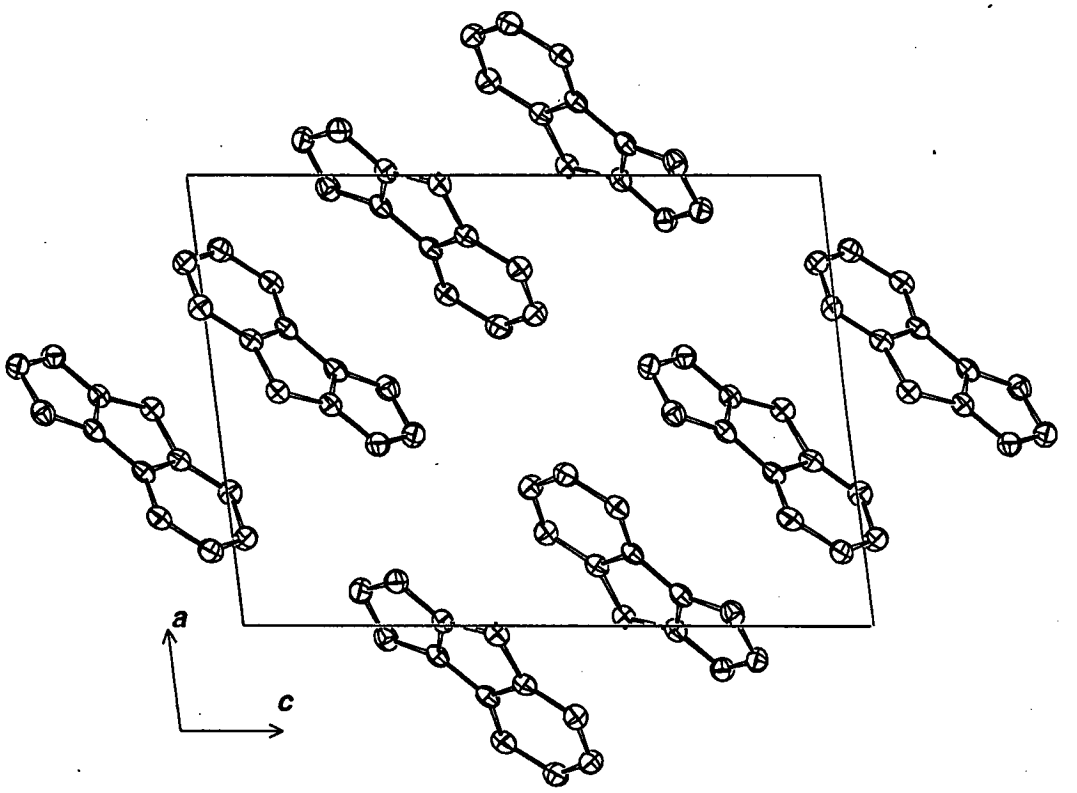

Figure 6: Unit cell packing diagram of 5*H*-pyrrolo[2,1-a]isoindole, **(9)**, thermal ellipsoids are drawn at the level of 50% probability, with protons removed for clarity.

Compound **(9)** adopts a planar 5:5:6 ring structure, with the methylene carbon exhibiting little deviation from the least squares plane, defined by the molecule. This is similar to the crystal structure of compound **(11)**. Compound **(11)** also adopts a planar 6:5:5:6 ring structure. However, unlike **(9)** a crystallographic disorder in the solid state structure exists. A 50% occupational disorder of the central C and the bridgehead C and N positions, as well as the and sp^2 and the sp^3 positions adjacent to these was reported by Frey.[29]

The bond lengths reported for compound **(9)** do not show any notable deviations form the typical bond lengths for known compounds of similar structure.[30,31] The C–N bonds between the bridgehead N(1) and carbons C(2) and C(5) are 1.363(2) and 1.379(1) Å, respectively, and the C–N bond between N(1) and the methylene carbon C(12) measures slightly longer at 1.464(1) Å. The difference

observed in the C–N bond lengths is not unexpected, with C–N bonds in aromatic heterocyclic compounds being shorter, 1.382(5) Å, than single C–N bonds, 1.472(5) Å.[32] No significant variations in the aromatic C–C bond lengths are observed, likewise no large deviation from the expected C–C single bond length is observed, 1.514(2) Å, C(11) – C(12). The bond angles which include the angle of bridgehead nitrogen of the fused five membered unsaturated rings with the adjacent carbon atoms are given in Table 4.

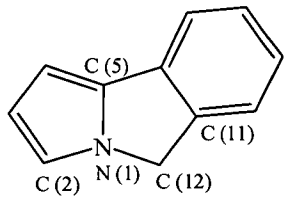

(9)

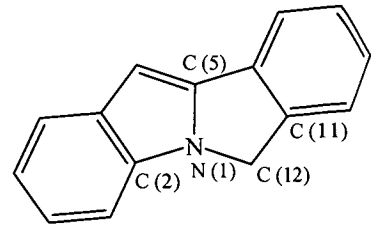

(11)

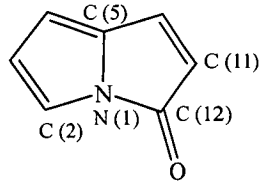

(XVIII)

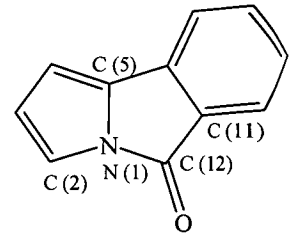

(XIX)

Table 4: Selected bond lengths and angles for nitrogen containing heterocycles **(9)**, **(11)**, **(XVIII)** and **(XIX)**.

		Bond Length (Å)		
	(9)	**(11)**[29]	**(XVIII)**[30]	**(XIX)**[31]
C(2)-N(1)	1.363(2)	1.430(19)	1.384(2)	1.386(2)
N(1)-C(5)	1.379(1)	1.364(2)	1.381(2)	1.386(2)
N(1)-C(12)	1.464(1)	1.418(17)	1.408(2)	1.403(2)
C(11)-C(12)	1.514(2)	1.478(19)	1.489(2)	1.484 (2)
		Bond Angle (°)		
	(9)	**(11)**[29]	**(XVIII)**[30]	**(XIX)**[31]
C(2)-N(1)-C(5)	110.24(9)	108.31(13)	110.03(10)	110.06(11)
C(2)-N(1)-C(12)	136.20(1)	138.31(13)	138.07(11)	137.22(11)
C(5)-N(1)-C(12)	113.47(9)	113.01(14)	111.12(11)	112.70(11)

The C(2)-N(1) and the N(1)-C(5) bond lengths observed for **(9)** compare well with those of compounds **(XVIII)** and **(XIX)**, however differences are observed for the bond lengths corresponding to C(11)-C(12) and in particular N(1)-C(12). The noticeable shortening of the N(1)-C(12) bond length in compounds **(XVIII)** and **(XIX)** in comparison to **(9)** occurs in both compounds due to C(12) in being a sp^2 type carbon. The differences in the lengths observed between compounds **(9)** and **(11)** can be accounted for by the fact that C(12) and C(5) along with N(1) were found to have 50% occupational disorder in the solid state structure of **(11)**.[29]

2.3 EXPERIMENTAL

2.3.1 3*H*-pyrrolizine

Synthesis of 2-pyrrole carboxaldehyde, **(1)**.

2-Pyrrole carboxaldehyde, **(1)**, was prepared by the following modified literature method.[26] To *N*,*N*-dimethylformamide (75.35 g, 1031 mmol) at 0 °C, phosphorous oxychloride (128.31 g, 837 mmol) was added over 5 minutes. After 15 minutes dichloromethane (135 mL) and pyrrole (50.79 g, 757 mmol) were alternately added to the mixture at 0 °C over one hour. The reaction mixture was refluxed for 15 minutes. Upon cooling of the reaction a sodium acetate solution (740 mL, 5.6 M) was added, dropwise for the first 30 mL and then added quickly. The mixture was refluxed for a further 15 minutes after which the cooled organic layer was separated and the aqueous layer washed with diethyl ether (2 x 50 mL). The organic layers were combined, washed with a saturated sodium carbonate solution and separated. The extracted organic layer was then dried over anhydrous magnesium sulfate and the solvent removed under reduced pressure with the crude material being purified *via* fractional distillation *in vacuo* (88 °C, 1.5 x 10^{-1} mbar). Upon cooling a colourless crystalline solid formed (44.47 g, 62%). Compound **(1)** was recrystallised from 40-60 °C petroleum spirits (33.81 g, 47%).

^{1}H NMR ($CDCl_3$, 299.90 MHz, 298 K, ppm): δ 6.33 (m, 1H, CH, pyr), 6.99 (m, 1H, CH, pyr), 7.16 (m, 1H, CH, pyr), 9.49 (s, 1H, O=CH), 10.49 (broad, s, 1H, NH).

^{13}C{^{1}H} NMR ($CDCl_3$, 75.4 MHz, 298 K, ppm): δ 111.6 (CH), 122.1 (CH), 127.2 (CH), 133.0 (CR), 179.9 (O=CH).

Synthesis of β-bromophenetole, **(2)**.

β-Bromophenetole, **(2)**, was prepared by the following modified literature method.[33] To phenol (38.38 g, 408 mmol) in water (200 mL) 1,2-dibromoethane (44 mL, 510 mmol) was added. The mixture was then heated to boiling, upon which sodium hydroxide (18.05 g, 449 mmol) in water (100 mL) was added over 30 minutes and the reaction was refluxed for 12 hours. Upon cooling the organic layer was separated and compound **(2)** was obtained as a colourless oil *via* fractional distillation (72 °C, 45 mbar) (65.85 g, 80%).

^{1}H NMR ($CDCl_3$, 199.98 MHz, 298 K, ppm): δ 3.67 (t, $^3J_{H\text{-}H}$ = 6.24 Hz, 2H, CH_2), 4.32 (t, $^3J_{H\text{-}H}$ = 6.20 Hz, 2H, CH_2), 7.01 (m 3H, CH, arom), 7.36 (m, 2H, CH, arom).

Synthesis of phenoxyethyltriphenylphosphonium bromide, **(3)**.

Phenoxyethyltriphenylphosphonium bromide, **(3)**, was prepared by the following modified literature method. Triphenylphosphine (65.43 g, 249 mmol), β-bromophenetole, **(2)**, (49.56 g, 249 mmol) and phenol (225.61 g, 2390 mmol) were refluxed for 48 hours, the condenser was fitted with a calcium chloride drying tube. The reaction mixture was cooled to ambient temperature and added dropwise into 500 mL of rapidly stirred diethyl ether over 2 hours. The white precipitate which formed was collected and placed in another 500 mL of diethyl ether, which was stirred vigorously for 15 minutes. The white precipitate was collected and washed with diethyl ether (2 x 100 mL) and dried by vacuum filtration to give compound **(3)**

as a white solid with an unknown number of phenols of crystallisation present in the final compound (135.01 g, 120%).

^{1}H NMR ($CDCl_3$, 299.90 MHz, 298 K, ppm): δ 4.25 (m, 2H, CH_2), 4.41 (d t $^3J_{H\text{-}H}$ = 5.69 Hz, $^2J_{H\text{-}H}$ = 22.49, Hz, 2H, CH_2), 6.40 (pseudo d, $^3J_{H\text{-}H}$ = 7.79 Hz 1H, CH, arom), 6.80 (pseudo t, $^3J_{H\text{-}H}$ = 7.20 Hz, 1H, CH, arom), 6.93 (pseudo d, $^3J_{H\text{-}H}$ = 7.50 Hz, 1H, CH, arom), 7.12 (pseudo t, $^3J_{H\text{-}H}$ = 7.50 Hz, 1H, CH, arom), 7.61 (m, 6H, CH, arom), 7.74 (m, 9H, CH, arom).

Synthesis of vinyltriphenylphosphonium bromide, **(4)**.

Vinyltriphenylphosphonium bromide **(4)** was prepared by the following modified literature method.[34] Phenoxyethyltriphenylphosphonium bromide, **(3)** (10.14 g, 219 mmol) in ethyl acetate (400 mL) was refluxed for 12 hours giving a solid. The solution was cooled to room temperature and the ethyl acetate decanted from the solid. To the solid material fresh ethyl acetate (400 mL) was added and refluxed for a further 12 hours. The process was repeated once more before the white solid was collected and washed with ethyl acetate (2 x 50 mL) followed by diethyl ether (2 x 50 mL). The product was thoroughly dried *in vacuo* to yield compound **(4)** as a white solid (5.14 g, 64%).

^{1}H NMR ($CDCl_3$, 199.98 MHz, 298 K, ppm): δ 6.13 (m, CH), 7.21 (broad m, 1H, CH), 7.76 (m, 15H, CH, arom), 8.30 (m, 5H, CH, arom), 8.55 (m, 1H, CH,).

Synthesis of 3*H*-pyrrolizine, **(5)**.

Note all glassware used in this synthesis was wrapped in foil as this compound is known to be light sensitive.

3*H*-Pyrrolizine, **(5)**, was prepared by the following modified literature method.[18] To a solution of sodium hydride (1.47 g, 61.28 mmol) in dry ethylene glycol dimethyl ether (150 mL) at 0 °C 2-pyrrole carboxaldehyde, **(1)**, (5.92 g, 62.23

mmol) was added portionwise over a period of 5 minutes. The reaction was warmed to ambient temperature and stirred for 30 minutes, after which the reaction was cooled to 0 °C and vinyltriphenylphosphonium bromide, **(4)**, (22.46 g, 60.08 mmol) was added over a period of 10 minutes. The reaction was sealed under argon and allowed to stir at ambient temperature for 12 hours, during which solid sodium bromide precipitated from solution. The yellow coloured liquor was filtered from the solid and concentrated *in vacuo* to *ca.* 10 mL. The product was purified *via* fractional distillation (70 °C, 20 mbar) to yield **(5)** as a yellow oil (1.347 g, 21%).

^{1}H NMR (C_6D_6, 299.90 MHz, 298 K, ppm): δ 3.60 (s, 2H, CH_2), 5.55 (d, $^3J_{H\text{-}H}$ = 2.17 Hz, 1H, pyr), 6.11(d, $^3J_{H\text{-}H}$ = 3.28 Hz, 1H, pyr), 6.31 (t, $^3J_{H\text{-}H}$ = 2.12 Hz, 1H, pyr), 6.44 (t, $^3J_{H\text{-}H}$ = 3.29 Hz, 1H, pyr), 6.67 (s, 1H, pyr).
$^{13}C\{^1H\}$ NMR (C_6D_6, 75.4 MHz, 298 K, ppm): δ 51.5 (CH_2), 97.8 (CH), 112.5 (CH), 116.8 (CH), 124.0 (CH), 127.0 (CH), 141.6 (C).

2.3.2 Synthesis of modified 3*H*-pyrrolizines

Synthesis of 2-bromobenzyl bromide, **(6)**.

2-Bromobenzyl bromide **(6)** was prepared by the following modified literature method.[35] To 2-bromotoluene (51.2 g, 299 mmol) in carbon tetrachloride (100 mL), *N*-bromosuccinimide (52.3 g, 294 mmol) was added and the system purged with nitrogen for 5 minutes. Benzoyl peroxide (0.12 g, 0.49 mmol) was added to the stirred mixture and the reaction refluxed for 2 hours. Upon cooling the solid succinimide was removed *via* filtration and washed with carbon tetrachloride, (2 x 50 mL) and the washings added to the filtrate. The carbon tetrachloride was removed from the combined solution under reduced pressure to yield a crude oil, which was purified *via* fractional distillation *in vacuo* (72 °C, 1.8 mbar) to yield **(6)** as a clear colourless oil (60.75 g, 83%).

^{1}H NMR ($CDCl_3$, 299.90 MHz, 298 K, ppm): δ 4.74 (s, 2H, CH_2), 7.30 (t, $^3J_{H-H}$ = 7.66 Hz, 1H, CH, arom), 7.43 (t, $^3J_{H-H}$ = 7.57, 1H, CH, arom), 7.59 (d, $^3J_{H-H}$ = 8.12 Hz, 1H, CH, arom), 7.72 (d, $^3J_{H-H}$ = 8.00 Hz, 1H, CH, arom).

^{13}C{^{1}H} NMR ($CDCl_3$, 75.4 MHz, 298 K, ppm): δ 33.7 (CH_2), 128.1 (CBr), 130.2 (CH), 131.2 (CH), 131.4 (CH), 133.4 (CH), 137.1 (C).

Synthesis of *N*-(2-bromobenzyl)pyrrole, **(7)**.

N-(2-Bromobenzyl)pyrrole, **(7)**, was prepared by the following modified literature method.[29] To a solution of potassium hydride (4.55 g, 114 mmol) in tetrahydrofuran (100 mL) at 0 °C, pyrrole (7.60 g, 113 mmol) was added dropwise over a period of 5 minutes. The reaction was warmed to ambient temperature and stirred for 3 hours. The solution was then cooled to 0 °C and 2-bromobenzyl bromide, **(6)**, (28.33 g, 113 mmol) added dropwise over 10 minutes. The reaction was then stirred at ambient temperature for 12 hours, after which time the reaction was quenched with water (75 mL) and the organic layer separated. The aqueous layer was extracted into diethyl ether (2 x 50 mL), the organic layers combined and dried over anhydrous magnesium sulfate. The solvent was removed *in vacuo* to yield the crude product as a brown oil, which was purified *via* fractional distillation *in vacuo* (100 °C, 6.4 x 10^{-2} mbar) yielding **(7)** as a clear, colourless oil (23.50 g, 88%).

^{1}H NMR ($CDCl_3$, 199.978 MHz, 298 K, ppm): δ 5.15 (s, 2H, CH_2), 6.23 (t, $^3J_{H-H}$ = 3.34 Hz, 2H, CH, pyr), 6.73 (d, $^3J_{H-H}$ = 2.06 Hz, 2H, CH, pyr), 7.14 (pseudo t, $^3J_{H-H}$ = 7.64 Hz, CH, arom), 7.24 (m, 2H, CH, arom), 7.56 (d, $^3J_{H-H}$ = 7.72 Hz, 1H, CH, arom).

Synthesis of *trans*-di(μ-acetato)-bis[*o*-(di-*o*-tolylphosphino)benzyl]dipalladium(II), **(8)**, Herrmann's catalyst.

Trans-di(μ-acetato)-bis[*o*-(di-*o*-tolylphosphino)benzyl]dipalladium, **(8)**, was prepared by the following modified literature method.[36,37] A solution containing tri-*o*-tolylphosphine (0.54 g, 1.77 mmol), and palladium chloride (0.28 g, 1.26 mmol) in

toluene (25 mL) was heated for 10 minutes at 60 °C where a change in colour from deep orange to yellow was observed, after which time the reaction was cooled rapidly in an ice bath to 0 °C. The reaction was then stirred for 45 minutes at 0 °C before concentrating *in vacuo* to *ca.* 10 mL upon which a yellow crystalline solid began to form. The solid was collected after 5 minutes and washed with cold hexane before drying *in vacuo* to yield **(8)** as a yellow crystalline solid (0.55 g, 93%), which was stored under an atmosphere of argon.

Synthesis of 5*H*-pyrrolo[2,1-a]isoindole, **(9)**.

This synthesis was carried out under standard Schlenk conditions with dry solvents under an inert atmosphere of argon.

To sodium acetate (5.21 g, 63 mmol), tetrabutylammonium bromide (6.82 g, 21 mmol), *trans*-di(μ-acetato)-bis[*o*-(di-*o*-tolylphosphino)benzyl]dipalladium, **(8)**, (0.45 g, 0.48 mmol, 2 mol%) and *N*-(2-bromobenzyl)pyrrole, **(7)**, (12.04 g, 50 mmol), *N,N*-dimethylacetamide (150 mL) was added. The reaction was heated at 150 °C for 12 hours, after which the reaction was quenched with water (75 mL) and the organic layer separated. The aqueous layer was washed with diethyl ether (2 x 75 mL), the organic extracts combined and dried over anhydrous magnesium sulfate. The solvent was then removed *in vacuo* to yield a thick, brown oil, which upon sublimation *in vacuo* (80 °C, 2.6 x 10^{-2} mbar) yielded a bright yellow crystalline solid. The crystalline material was washed with chilled hexane to afford **(9)** as an off white crystalline solid (2.95 g, 38%).

^{1}H NMR ($CDCl_3$, 299.90 MHz, 298 K, ppm): δ 4.92 (s, 2H, **H5**), 6.27 (pseudo d, $^3J_{H\text{-}H}$ = 3.50 Hz, 1H, **H4**), 6.33 (pseudo t, $^3J_{H\text{-}H}$ = 2.59 Hz, 1H, **H3**), 6.93 (p, 1H, **H2**), 7.12 (pseudo t, $^3J_{H\text{-}H}$ = 7.53 Hz, 1H, **H8**), 7.29 (d, $^3J_{H\text{-}H}$ = 7.52 Hz, 1H, **H6**), 7.31 (pseudo t, $^3J_{H\text{-}H}$ = 7.42 Hz, 1H, **H7**), 7.45 (d, $^3J_{H\text{-}H}$ = 7.56 Hz, 1H, **H9**).

^{13}C{^{1}H} NMR ($CDCl_3$, 75.4 MHz, 298 K, ppm): δ 50.5 (**C5**), 98.2 (**C4**) 112.9 (**C3**), 116.7 (**C2**), 118.8 (**C9**), 123.2 (**C6**), 125.0 (**C8**), 128.1 (**C7**), 134.0 (**C5a**), 138.7 (**C4a**), 140.4 (**C9a**).

Synthesis of *N*-(2-bromobenzyl)indole, **(10)**.

To a solution of potassium hydride (4.66 g, 116 mmol) in tetrahydrofuran at 0 °C (150 mL) indole (12.04 g, 103 mmol) was added over 5 minutes. The reaction was warmed to ambient temperature and stirred for 3 hours. The solution was cooled to 0 °C and 2-bromobenzyl bromide, **(6)**, (28.34 g, 113 mmol) was added dropwise over 10 minutes. The reaction was warmed to ambient temperature and stirred for 12 hours, after which time it was quenched with water (75 mL) and the organic layer separated. The aqueous layer was washed with diethyl ether (2 x 30 mL) and the organic layers combined and dried over anhydrous magnesium sulfate. The solvent was removed *in vacuo* to yield a crude red oil, which on standing crystallised to give a bright red/pink crystalline solid. The solid was collected by vacuum filtration and washed with chilled hexane to yield **(10)** as a pale pink crystalline solid (9.17 g, 31%).

^{1}H NMR ($CDCl_3$, 299.90 MHz, 298 K, ppm): δ 5.37 (s, 2H, CH_2), 6.50 (pseudo t, $^3J_{H\text{-}H}$ = 4.49 Hz 1H, CH pyr), 6.58 (d, $^3J_{H\text{-}H}$ = 2.99 Hz, 1H, pyr), 7.16 (m, 6H, CH, arom), 7.58 (pseudo t, $^3J_{H\text{-}H}$ = 6.30 Hz, 1H, CH, arom), 7.66 (d, $^3J_{H\text{-}H}$ = 8.39 Hz, 1H, CH, arom).

^{13}C{^{1}H} NMR ($CDCl_3$, 75.4 MHz, 298 K, ppm): δ 50.4 (CH_2), 102.3 (CH), 109.9 (CH), 119.9 (CH), 121.2 (CH), 122.1 (CH), 122.3 (CH), 128.0 (CH), 128.2 (CH), 128.6 (CH), 128.8 (CH), 129.2 (CH), 132.9 (C), 136.4 (C), 136.8 (C).

Synthesis of 6*H*-isoindolo[2,1-a]indole, **(11)**.

This synthesis was carried out under standard Schlenk conditions with dry solvents under an inert atmosphere of argon. 6*H*-Isoindolo[2,1-a]indole, **(11)**, was prepared by the following modified literature method.[29]

To sodium acetate (3.33 g, 41 mmol), tetrabutylammonium bromide (4.25 g, 13 mmol), *trans*-di(μ-acetato)-bis[*o*-(di-*o*-tolylphosphino)benzyl]dipalladium(II), **(8)**,

(0.3 g, 32 mmol, 2 mol%) and *N*-(2-bromobenzyl)indole, **(10)**, (9.19 g, 32 mmol), *N,N*-dimethylacetamide (150 mL) was added. The reaction was then heated at 120 °C for 12 hours (monitored by thin layer chromatography, silica, 40 – 60° petroleum spirits : dichloromethane, ratio of 7:3), during which time a tan precipitate formed. Upon cooling to ambient temperature the solid was collected (first crop) and dried *in vacuo*. Water (75 mL) was added to the filtrate and the organic layer separated. The aqueous layer was washed with dichloromethane (2 x 75 mL), the organic layers combined, dried over anhydrous magnesium sulfate and the solvent concentrated to *ca.* 20 mL. Upon cooling to 4 °C for 12 hours a second crop of the tan crystalline solid formed, this was collected by vacuum filtration and washed with chilled hexane to yield **(11)** as a tan crystalline solid (combined yield of 3.74 g, 58%).

^{1}H NMR (THF-d_8, 299.90 MHz, 298 K, ppm): δ 5.10 (s, 2H, CH_2), 6.58 (s, 1H, CH, pyr), 6.99 (pseudo t, $^3J_{H\text{-}H}$ = 7.55 Hz, 1H, CH, arom), 7.09 (pseudo t, $^3J_{H\text{-}H}$ = 7.55 Hz, 1H, CH, arom), 7.29 (pseudo t, $^3J_{H\text{-}H}$ = 7.49 Hz, 1H, CH, arom), 7.37 (m, $^3J_{H\text{-}H}$ = 8.00 Hz, 2H, CH, arom), 7.51 (d, $^3J_{H\text{-}H}$ = 7.42 Hz, 1H, CH, arom), 7.55 (d, $^3J_{H\text{-}H}$ = 7.95 Hz, 1H, CH, arom), 7.71 (d, $^3J_{H\text{-}H}$ = 7.41 Hz, 1H, CH, arom).

^{13}C{^{1}H} NMR (THF-d_8, 75.4 MHz, 298 K, ppm): δ 49.0 (CH_2), 91.8 (C), 109.9 (C), 120.1 (C), 121.4 (C), 122.0 (C), 122.2 (C), 124.5 (C), 127.7 (C), 128.8 (C), 133.9 (C), 134.0 (C), 135.0 (C), 143.3 (C), 144.6 (C).

Synthesis of 1-bromo-2-(1-bromoethyl)-benzene, **(12)**.

1-Bromo-2-(1-bromoethyl)-benzene, **(12)**, was prepared by the following modified literature method.[38] To a solution of 1-bromo-2-ethyl-benzene (9.2 g, 35 mmol) in carbon tetrachloride (110 mL) *N*-bromosuccinimde (8.80 g, 270 mmol) was added. The system was flushed with nitrogen for 5 minutes upon which benzoyl peroxide (0.38 g) was added and the reaction mixture refluxed under a lamp (100W, 240V globe) for 3.5 hours. The solid succinimide was removed by filtration upon cooling and washed with carbon tetrachloride (2 x 50 mL). The combined carbon tetrachloride solutions were washed with dilute sodium hydroxide solution (0.5 M, 50 mL) and the organic layer separated. The aqueous layer was washed with carbon

tetrachloride (2 x 50 mL), the organic layers combined and dried over anhydrous magnesium sulfate. The carbon tetrachloride was removed under reduced pressure (11 mbar) to yield a crude oil which was purified *via* fractional distillation *in vacuo* (72 °C, 1.5 x 10^{-1} mbar) to yield **(12)** as a clear colourless oil (7.35 g, 56%).

^{1}H NMR ($CDCl_3$, 299.90 MHz, 298 K, ppm): δ 2.04 (d, $^3J_{H-H}$ = 6.93 Hz, 3H, CH_3), 5.60 (q, $^3J_{H-H}$ = 7.00 Hz, 1H, CH), 7.14 (pseudo t, $^3J_{H-H}$ = 7.71 Hz, 1H, CH, arom), 7.35 (pseudo t, $^3J_{H-H}$ = 7.66 Hz, 1H, CH, arom), 7.53 (d, $^3J_{H-H}$ = 7.96 Hz, 1H, CH, arom), 7.66 (d, $^3J_{H-H}$ = 7.87 Hz, 1H, CH, arom).
^{13}C{^{1}H} NMR ($CDCl_3$, 75.4 MHz, 298 K, ppm): δ 26.2 (CH_3), 47.7 (CHBr), 123.3 (C-Br), 128.3 (CH), 128.4 (CH), 129.9 (CH), 133.2 (CH), 142.0 (C).

Synthesis of *N*-(2-bromo-1-ethylbenzyl)pyrrole, **(13)**.

To a solution of potassium hydride (0.77 g, 19 mmol) in tetrahydrofuran (50 mL) at 0 °C, pyrrole (1.29 g, 19 mmol) was added dropwise over a period of 5 minutes. The reaction mixture was warmed to ambient temperature and stirred for 2 hours. The mixture was then cooled to 0 °C and 1-bromo-2-(1-bromoethyl)-benzene, **(12)**, (5.0 g, 19.0 mmol) was added dropwise over a 10 minute period, after which it was warmed to ambient temperature and stirred for 12 hours. The reaction was quenched with water (50 mL), the organic layer was separated and the aqueous layer washed with diethyl ether (3 x 80 mL). The combined organic layers dried over anhydrous magnesium sulfate. The solvent was removed *in vacuo* to yield the crude product as a brown coloured oil, which was purified *via* fractional distillation *in vacuo* (81 °C, 3.2 x 10^{-2} mbar) to yield **(13)** a clear colourless oil (2.83 g, 59%).

^{1}H NMR ($CDCl_3$, 299.898 MHz, 298 K, ppm): δ 1.83 (d, $^3J_{H-H}$ = 7.04 Hz, 3H, CH_3), 5.70 (q, $^3J_{H-H}$ = 7.06 Hz, 1H, CH), 6.23 (m, 2H, pyr), 6.83 (m 2H, pyr), 6.86 (pseudo d, $^3J_{H-H}$ = 7.73 Hz, 1H, CH, arom), 7.11 (pseudo t, $^3J_{H-H}$ = 7.42 Hz, 1H, CH, arom), 7.23 (pseudo t, $^3J_{H-H}$ = 7.54 Hz, 1H, CH, arom), 7.57 (pseudo d, $^3J_{H-H}$ = 7.91 Hz, 1H, CH, arom).

Attempted synthesis of 5-methyl-5*H*-pyrrolo[2,1-a]isoindole, **(XV)**.

To sodium acetate (1.1 g, 13.3 mmol), tetrabutylammonium bromide (1.66 g, 5.12 mmol), *trans*-di(μ-acetato)-bis[*o*-(di-*o*-tolylphosphino)benzyl]dipalladium, **(8)**, (0.096 g, 10 mmol, 2 mol%) and *N*-(2-bromo-1-ethylbenzyl)pyrrole, **(13)**, (2.56 g, 9.6 mmol), *N,N*-dimethylacetamide (150 mL) was added. The reaction was heated at 150 °C for 8 hours, during which the reaction was monitored *via* thin layer chromatography (silica, dichloromethane/40 - 60 °C petroleum spirits (3:7)). The reaction was cooled to ambient temperature and water (50mL) added and the organic layer was separated. The aqueous layer washed with diethyl ether (2 x 75 mL) and the organic extracts combined and dried over anhydrous magnesium sulfate. The solvent was removed *in vacuo* to yield a thick brown oily substance. An attempt to purify the desired compound **(XV)** *via* sublimation *in vacuo* (140 °C, 4.5 x 10^{-2} mbar) was unsuccessful with the brown liquor that sublimed containing a mixture of starting material and the desired product, as identified *via* ^{1}H NMR spectroscopy; δ 5.04 ppm (q, $^3J_{H\text{-}H}$ = 6.81 Hz, -CH) and δ 1.64 ppm (d, $^3J_{H\text{-}H}$ = 6.80 Hz, $-CH_3$). Further attempts to obtain the product *via* flash column chromatography were also unsuccessful.

Synthesis of 2-(1*H*-pyrrol-1-yl)-benzoic acid methyl ester, **(14)**.

2-(1*H*-pyrrol-1-yl)-benzoic acid methyl ester, **(14)**, was prepared following the literature method.[24] A solution of 2,5-dimethoxytetrahydrofuran (24.89 g, 248 mmol) and methyl anthranilate (37.56 g, 248 mmol) in glacial acetic acid (200 mL) was refluxed for 1 hour. The reaction was cooled to ambient temperature and the acetic acid removed *in vacuo* to yield the crude product. The pure product, a colourless oil, was purified by fractional distillation *in vacuo* (110 °C, 2.6 x 10^{-1} mbar) (39.9 g, 80%).

^{1}H NMR ($CDCl_3$, 199.99 MHz, 298 K, ppm): δ 3.74 (s, 3H, CH_3), 6.36 (t, $^3J_{H\text{-}H}$ = 2.14 Hz, 2H, pyr), 6.85 (t, $^3J_{H\text{-}H}$ = 2.10 Hz, 2H, pyr), 7.41 (t, $^3J_{H\text{-}H}$ = 2H, CH, arom), 7.54 (d, 1H, CH, arom), 7.84 (d, 1H, CH, arom).

Synthesis of 2-(1*H*-pyrrol-1-yl)-benzoic acid, **(15)**.

2-(1*H*-pyrrol-1-yl)-benzoic acid, **(15)**, was prepared by the following modified literature method.[24] A solution of potassium hydroxide (7.53 g, 134 mol) in a mixture of ethylene glycol : water (75 mL, 10:2) was heated at 90 °C with shaking to obtain an emulsion. 2-(1H-pyrrol-1-yl)-benzoic acid methyl ester, **(14)**, (17.15 g, 85 mmol) was added to the emulsion and the mixture heated for 3.5 hours at 135 – 140 °C. The reaction was cooled to ambient temperature, after which time it was poured into a stirred mixture of water : 95% ethanol (250 mL, 6:4). The mixture was acidified to a pH of 1 with concentrated hydrochloric acid and stood at ambient temperature for an hour, during which time a pale pink precipitate formed. The precipitate was collected and dried *via* vacuum filtration to yield **(15)** as a pale pink solid (19.06 g, 86%).

^{1}H NMR ($CDCl_3$, 199.98 MHz, 298 K, ppm): δ 4.15 (broad, s, 1H, OH), 6.33 (t, $^3J_{H\text{-}H}$ = 2.18 Hz, 2H, pyr), 6.85 (t, $^3J_{H\text{-}H}$ = 2.22 Hz, 2H, pyr), 7.42 (m, 2H, CH, arom), 7.61 (pseudo t, $^3J_{H\text{-}H}$ = 7.64 Hz, 1H, CH, arom), 7.94 (d, $^3J_{H\text{-}H}$ = 7.38 Hz, 1H, CH, arom).

Synthesis of 9*H*-pyrrolo[1,2-a]indol-9-one, **(16)**.

9*H*-Pyrrolo[1,2-a]indol-9-one, **(16)**, was prepared by the following modified literature method.[5] To 2-(1*H*-pyrrol-1-yl)-benzoic acid, **(15)**, (8.8 g, 47 mmol) in benzene (50 mL), phosphorus pentachloride (10.4 g, 50 mmol) was added and the mixture stirred for one hour. The solution was cooled to 0 °C, upon which tin tetrachloride (25.7 g, 12.0 mmol), used as a catalyst, was added. The reaction was stirred at ambient temperature for 45 minutes after which time a mixture of 2M hydrochloric acid (300 mL) and ice (300 g) was added to the reaction mixture which was then allowed to stir at ambient temperature for one hour. The tin salt was removed *via* filtration and the organic layer separated. The aqueous layer was washed with chloroform (3 x 75 mL), the organic layers combined and dried over anhydrous magnesium sulfate. The solvent was then removed under reduced pressure to yield **(16)** as a crude brown coloured oil. The product was purified using flash

column chromatography; silica, eluent mixture of 40 – 60 °C petroleum spirits and diethyl ether in the ratio of 60:40 (1.21 g, 23%).

^{1}H NMR ($CDCl_3$, 199.98 MHz, 298 K, ppm): δ 6.32 (pseudo t, $^3J_{H\text{-}H}$ = 3.75 Hz, 1H, CH, pyr), 6.79 (pseudo d, $^3J_{H\text{-}H}$ = 3.81 Hz, 1H, CH, pyr), 7.09 (m, 2H, CH), 7.12 (d, $^3J_{H\text{-}H}$ = 7.64 Hz, 1H, CH, arom), 7.70 (pseudo t, $^3J_{H\text{-}H}$ = 7.74 Hz, 1H, CH, arom), 7.61 (d, $^3J_{H\text{-}H}$ = 7.40 Hz, 1H, CH, arom).

Attempted synthesis of 9*H*-pyrrolo[1,2-a]indole, **(XV)**.

Method A:

To hydrazine hydrochloride (3.69 g, 33 mmol) in ethanol (50 mL) 9*H*-pyrrolo[1,2-a]indol-9-one, **(16)**, (1.0 g, 5.9 mmol) was added. The reaction was heated for 6 hours at 105 °C after which time the reaction mixture was cooled to ambient temperature and the unreacted hydrazine hydrochloride was filtered from the mixture. Water (25 mL) was added to the filtrate which lead to the formation of a dark yellow precipitate when the solution was cooled to 4 °C, this was collected and dried *via* vacuum filtration (1.37 g, 102 %). The solid was identified by NMR as the hydrazine compound.

Method B:

A solution of lithium aluminium hydride (0.12 g, 3.1 mmol) in tetrahydrofuran (70 mL) was stirred for 30 minutes after which time the solution was filtered from any undissolved lithium aluminium hydride. The solution was cooled to 0 °C upon which 9*H*-pyrrolo[1,2-a]indol-9-one, **(16)**, (0.35 g, 2.07 mmol) was added over a five minute period. The reaction was warmed to room temperature and left to stir for 16 hours after which time the reaction was cooled to 0 °C and quenched with ethanol (15 mL) and water (25 mL). The solution was then filtered to remove the red solid which had formed on the addition of the water. To the reaction solution ethanol (60 mL) and 40 – 60 °C petroleum spirits (80 mL) and the organic layer was separated. The aqueous layer washed with 40 – 60 °C petroleum spirits (2 x 80 mL), the organic layers combined and dried over anhydrous magnesium sulfate. The solvent was removed under reduced pressure to yield 9*H*-pyrrolo[1,2-a]indol-9-ol, **(XVI)**, as an

orange solid in 66% yield (0.21 g, 1.23 mmol). The product, 9*H*-pyrrolo[1,2-a]indol-9-ol, was identified by GC-MS were a compound two mass units higher in mass than 9*H*-pyrrolo[1,2-a]indol-9-one, **(16)**, was observed.

2.4 REFERENCES

(1) Schweizer, E. E.; Light, K. K. *J. Am. Chem. Soc.* **1964**, *86*, 2963-2963.

(2) Okamura, W. H.; Katz, T. J. *Tetrahedron* **1967**, *23*, 2941-2957.

(3) Kissounko, D. A.; Kissounko, N. S.; Krutko, D. P.; Brusova, G. P.; Lemenovskii, D. A.; Boag, N. M. *J. Organomet. Chem.* **1998**, *556*, 145-149.

(4) Crump, D. R.; Franck, R. W.; Gruska, R.; Ozorio, A. A.; Pagnotta, M.; Sluta, G. J.; White, J. G. *J. Org. Chem.* **1997**, *42*, 105-108.

(5) Mazzola, V. J.; Bernady, K. F.; Frank, R. W. *J. Org. Chem.* **1967**, *32*, 486-489.

(6) Cartoon, M. E. K.; Cheeseman, G. W. *J .Organomet. Chem.* **1981**, *212*, 1-9.

(7) Laudree, D.; El Kashef, H.; Robba, M. *Heterocycles* **1984**, *22*, 299-305.

(8) Suita, G. J.; Franck, R. W.; Kempton, R. J. *J. Org. Chem.* **1974**, *39*, 3739-3744.

(9) Barluenga, J.; Miguel, T.; Koutznetsov, V.; Suarez-Sobrino, A.; Rubio, E. *J. Org. Chem.* **1996**, *61*, 2185-2190.

(10) Coleman, R. S.; Wei, C. *Org. Lett.* **2001**, *3*, 1141-1144.

(11) Varoglu, M.; Mao, Y.; Sherman, D. H. *J. Am. Chem. Soc.* **2001**, *123*, 6712-6713.

(12) Wang, Z.; Jimenez, L. S. *J. Am. Chem. Soc.* **1994**, *116*, 4977-4978.

(13) Lee, J.; Ha, J. D.; Cha, J. K. *J. Am. Chem. Soc.* **1997**, *119*, 8127-8128.

(14) Mosby, W. L. *Heterocyclic Systems with Bridgehead Nitrogen Atoms, Part one*; Interscience Publishers, Ltd.: New York, 1961; Vol. 15.

(15) Flitsch, W.; Jones, G. In *Advances in Heterocyclic Chemistry*; Academic Press inc., 1984; Vol. 37, pp 2-65.

(16) Zbiral, E. *Synthesis* **1974**, 775-797.

(17) Becker, K. B. *Tetrahedron* **1980**, 1717-1745.

(18) Schweizer, E. E.; Light, K. K. *J. Org. Chem.* **1966**, *31*, 870-872.

(19) Johnson, D.; Jones, G. *J. Chem. Soc., Perkins I* **1972**, 2517-2521.

(20) Davies, D. T. *Aromatic Heterocyclic Chemistry*; Oxford University Press: Oxford, 1992; Vol. 2.

(21) Gilchrist, T. L. *Heterocyclic Chemistry*; Longman Scientific and Technical: Harlow, 1985.

(22) Shirley, D. A.; Gross, B. H.; Roussel, P. A. *J. Org. Chem.* **1955**, *20*, 225-231.

(23) Laschtuvka, E.; Huisgen, R. *Chem. Ber.* **1960**, *93*, 81-88.

(24) Joesy, A. D.; Jenner, E. L. *J. Org. Chem.* **1962**, *27*, 2466-2470.

(25) Clauson-Kaas, N.; Tyle, Z. *Acta Chem. Scand.* **1952**, *6*, 667-670.

(26) Silverstein, R. M.; Ryskiewicz, E. E.; Willard, C. *Organic Syntheses* **1956**, *36*, 74-77.

(27) Silverstein, R. M.; Ryskiewicz, E. E.; Chaikin, S. W. *J. Am. Chem. Soc.* **1954**, *76*, 4485-4486.

(28) Fukui, H.; Shimukawa, S.; Sohma, J. *Mol. Phys.* **1970**, *18*, 217-223.

(29) Frey, A. S. P. In *School of Chemistry*; University of Sydney: Sydney, 2000, p 51.

(30) Blockhuys, F.; Hinchley, S. L.; Robertson, H. E.; Blake, A. J.; McNab, H.; Despinoy, X. L. M.; Harris, S. G.; Rankin, D. W. H. *J. Chem. Soc., Perkins Trans. 2* **2001**, *11*, 2195-2201.

(31) McNab, H.; Parsons, S.; Stevenson, E. *J. Chem. Soc., Perkins Trans. 1* **1999**, *15*, 2047-2048.

(32) Mitchell, A. D.; Sommerfield, A. E.; Cross, L. C. *Tables of Interatomic Distances and Configuration in Molecules and Ions, Supplement 1956 - 1959*; The Chemical Society: London, 1965.

(33) Marvel, C. S.; Tanenbaum, A. L. *Organic Syntheses* **1929**, *9*, 423-426.

(34) Schweizer, E. E.; Bach, R. D. *Organic Syntheses* **1964**, *29*, 1746-1751.

(35) Fuson, R. C.; Bernard, F. *J. Org. Chem.* **1958**, *23*, 1161-1166.

(36) Herrmann, W. A.; Böhm, V. P. W.; Reisinger, C.-P. *J. Chem. Ed.* **2000**, *77*, 92-95.

(37) Herrmann, W. A.; Brossmer, C.; Oefele, K.; Reisinger, C.-P.; Priermeier, T.; Beller, M.; Fischer, H. *Angew. Chem. Int. Ed.* **1995**, *34*, 1844-1847.

(38) Halpern, Y.; Meidar, D. *Organic Preparations and Procedures International* **1976**, *8*, 299-302.

CHAPTER 3

GROUP 1 METAL MODIFIED

4-AZAPENTALENYL COMPLEXES

3.1 INTRODUCTION

The first Group 1 metal complexes of 3*H*-pyrrolizine, **(I)**, were synthesised by Okamura and Katz in 1967.[1] This was achieved by deprotonation of 3*H*-pyrrolizine at the 3 – position using a Group 1 metallating reagent giving the 4-azapentalenyl anion, **(II)**. The 4-azapentalenyl anion is a simple nitrogen containing heterocycle that is isoelectric with that of the pentalenyl dianion, **(III)**. These types of systems can be seen as an extension of the cyclopentadienyl anion. The organometallic chemistry of the pentalenyl dianion and the cyclopentadienyl anion, $(C_5H_5)^-$ **(IV)**, along with the pentamethylcyclopentadienyl anion, (C_5Me_5) have been extensively studied, whereas in comparison little is known about the chemistry of the 4-azapentalenyl anion.

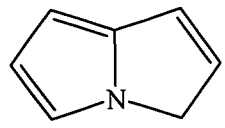

(I)

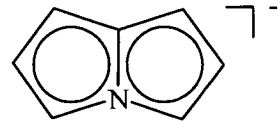

(II)

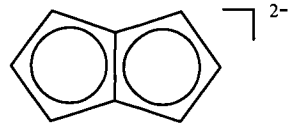

(III)

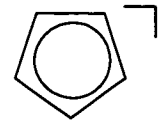

(IV)

The cyclopentadienyl anion has proven to be a most useful and versatile system in the organometallic chemistry of transition metals, lanthanides and actinides. The first Group 1 metal complexes of cyclopentadienyl were reported in 1901[2]. It was not until 1951 that Kealy and Paulson reported the synthesis of the first transition metal cyclopentadienyl complex, bis(cyclopentadienyl)iron (III), **(V)**, more commonly

known as ferrocene,[3] which has became widely utilised. This initial discovery of ferrocene lead to the rapid expansion of the chemistry of the cyclopentadienyl anion to include complexes of other transition metals leading to the synthesis of a vast array of new bis(cyclopentadienyl) metal complexes. These bis(cyclopentadienyl) complexes are generally known as metallocenes or sandwich complexes.[4] The metallocene structure of ferrocene in Figure 1 shows the iron cation interacting with two cyclopentadienyl anions in an η^5 fashion. [5,6,7,8]

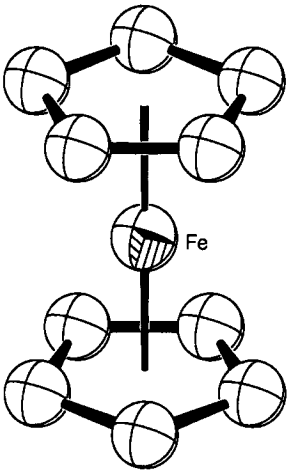

Figure 1. X-ray structure of ferrocene, **(V)**, X-ray crystal structure reproduced from the CCDC database. Arbitrary isotropic thermal ellipsoids, hydrogens have been removed for clarity.

Mononuclear cyclopentadienyl transition metal complexes are able to be divided into three general categories: **(VI)** those with a sandwich like structure often referred to as "metallocenes", **(VII)** those which exhibit a "bent metallocene" structure where the number of unidentate ligands varies from one to three and **(VIII)** those that have a half sandwich structure where the number of ligands now varies from one to four, where L is a unidentate ligand such as carbon monoxide.[9]

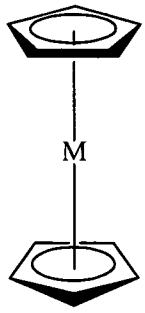

(VI)

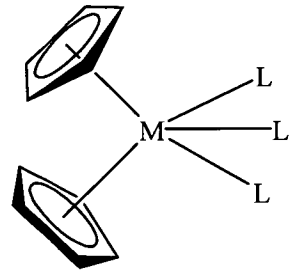

(VII)

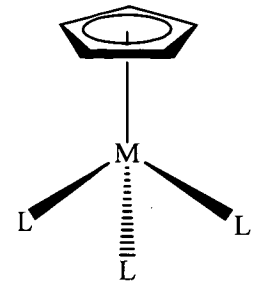

(VIII)

The chemistry of the cyclopentadienyl system rapidly expanded after the first report of ferrocene. Transition metal complexes with the $(C_5H_5)^-$ system and halide ligands were prepared soon after the report of ferrocene, with most containing the bis(cyclopentadienyl) system, these include: $(C_5H_5)_2TiCl_2$; $(C_5H_5)_2ZrF_2$ and $(C_5H_5)_2MoCl_2$. The chemistry of the metallocenes and the bent metallocenes expanded more rapidly than that of the monocyclopentadienyl half sandwich systems, even though complexes containing low oxidation state carbonyl derivatives had been developed. In the early 1960s the first monocyclopentadienyl halide complexes were prepared including $(C_5H_5)TiCl_2$, $(C_5H_5)TiCl_3$ and $(C_5H_5)CrCl_2$.[10]

Interest in the cyclopentadienyl ligand stemmed from the range of possible interactions between the metal centre and the anion. The system can act as a six-electron π donor with the properties of the complexes formed dependent on the number of valence electrons. The number of valence electrons involved is mainly dependent on the electronegativity of the metal.[9] If the metal is electropositive in nature than the interaction between the metal centre and the cyclopentadienyl anion is mainly ionic, which is true for many Group 1 metal cyclopentadienyl complexes. In contrast, for those of lower electropositivity the interaction between the metal centre and the cyclopentadienyl ligand is described as one of a highly covalent nature, this holds true for *p* block metal complexes.[11]

The cyclopentadienyl anion has been observed to exhibit a variety of binding modes between itself and the metal centre, these included η^5, η^3 and η^1 interactions, as shown in Figure 2.[12] This versatility is apparent in complexes of the main group elements where both ionic and covalent interactions may be observed.

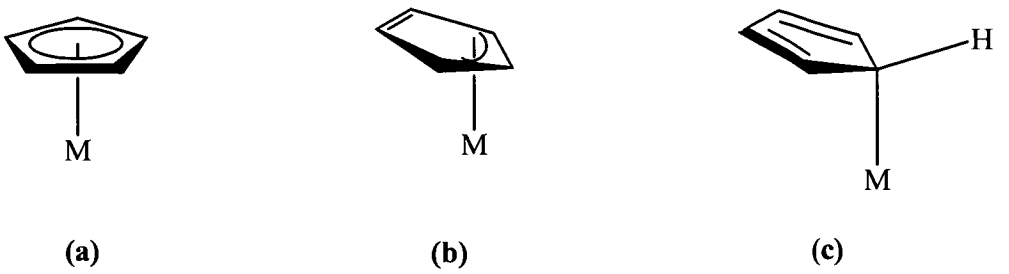

Figure 2. Possible binding modes for the cyclopentadienyl ligand system, **a)** η^5, **b)** η^3, **c)** η^1.

The first Group 1 metal complex of the cyclopentadienyl anion was reported in 1901 by Thiele, who prepared potassium cyclopentadienide by reacting potassium metal with cyclopentadiene in benzene.[13] Current preparations of Group 1 metal Cp complexes involve the deprotonation of cyclopentadiene with a Group 1 metal as shown in Scheme 1 in THF, diethyl ether or benzene and in some cases in liquid ammonia, Scheme 1.

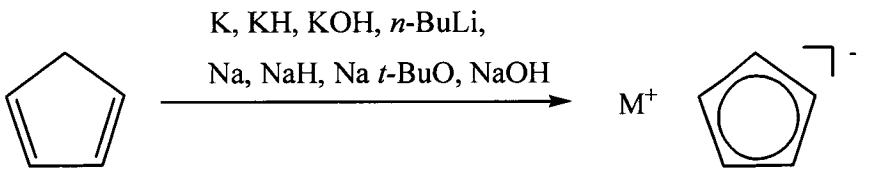

M = Na, K, Li

Scheme 1. Synthesis of Group 1 metal cyclopentadienide complexes.

In 2003 Roesky and his colleagues reported an improved synthesis of sodium and potassium cyclopentadienyl complexes.[13] This new procedure involved a one pot synthesis where the Group 1 metal was directly reacted with dicyclopentadiene at high temperatures in the absence of any solvent to give the desired complex, Scheme 2. This procedure provided a more direct route to the desired complex in much higher yields than previously reported. No similar synthesis is used to date to form lithiated cyclopentadiene, the synthetic method still used today involves the reaction of an alkyl lithium with cyclopentadiene.

Group 1 metal cyclopentadienyl complexes exhibit very limited solubility in non-donating solvents[14,15] and in the case of the lithium complex it was shown to be insoluble in most non-coordinating solvents making it difficult to obtain crystals suitable for solid state structure determination. Due to the difficulty in crystallising these complexes, most syntheses with unsubstituted cyclopentadiene involve the addition of a chelating Lewis base, such as *N,N,N',N'*-tetramethylethylenediamine (TMEDA), to increase the solubility of the complexes. Many Lewis base adducts of alkali metal complexes have been achieved and a rich structural chemistry identified through systematic studies into the coordination and structure of metal complexes where the Lewis base was varied.

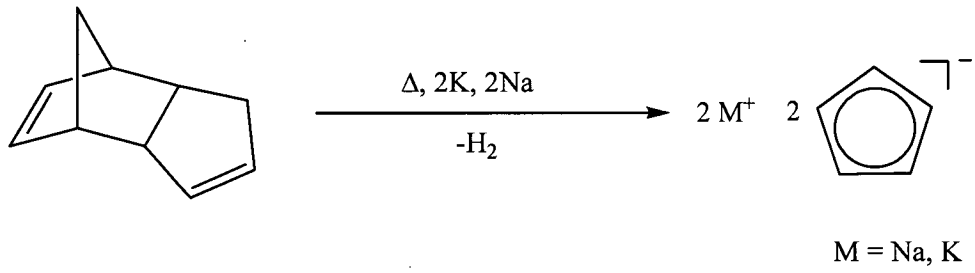

Scheme 2. New synthetic scheme for synthesis of sodium and potassium cyclopentadienide complexes.

The effect of varying the Lewis base in cyclopentadienylsodium complexes was investigated in 1979 Aoyagi and his collegues.[16] He reported that some Lewis bases such as THF and diethyl ether coordinated weakly, while other bases such as TMEDA and pyridine are more strongly coordinating. By determining the X-ray crystal structure of the TMEDA adduct, Aoyagi illustrated the importance that the size of the metal has on the coordination of the TMEDA, that is, whether it is observed to form a bridge between two metal centres or chelates the metal centre, as is the case observed in $[\{(C_5H_5)Na(TMEDA)\}]_n$ **(IX)**. Figure 3 shows the TMEDA chelating the sodium centre, which is η^5 coordinated to the cyclopentadienyl ring. **(IX)** forms a 1-dimensional polymeric chain in its solid state structure, Figure 3. Similar structures have been observed such as the diethyl ether adduct of (cyclopentadienyl)potassium, which also has a polymeric chain structure where the diethyl ether coordinates to the potassium *via* the oxygen.[7,8,16,17]

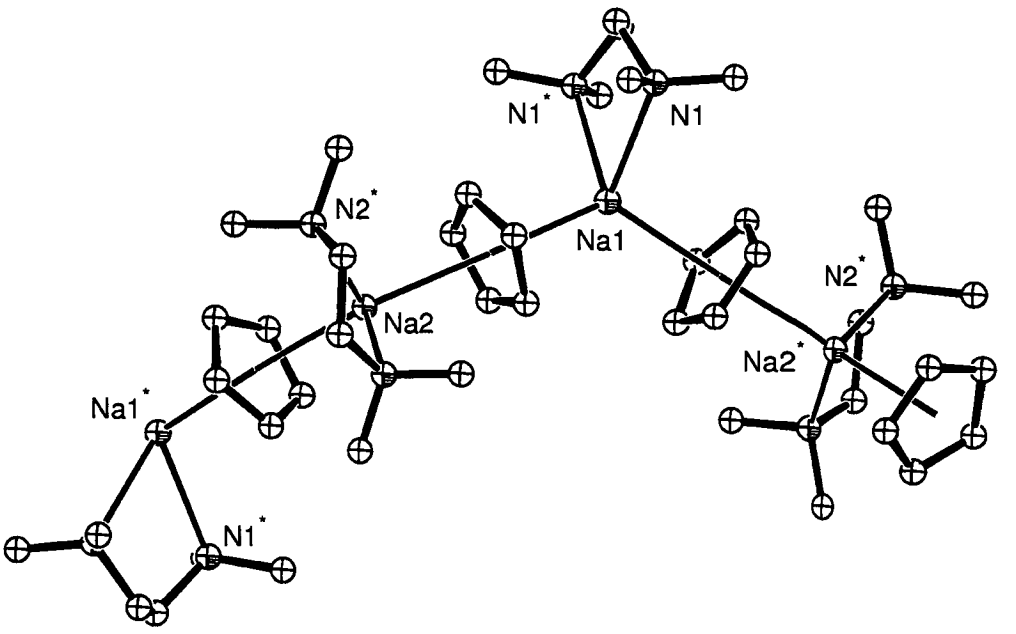

Figure 3. X-ray structure of $[\{(\eta^5\text{-}C_5H_5)Na(TMEDA)\}_n]$, **(IX)**, X-ray crystal structure reproduced from the CCDC database. Thermal ellipsoids are shown with arbitrary radii, hydrogens have been removed for clarity.

Whilst the synthesis of these Group 1 complexes has been known for over one hundred years, their low solubility has remained a problem. The associated problem of insolubility leads to the fact that a single crystal X-ray diffraction structure is still unknown for the unsolvated Group 1 metal complexes. The structure of these unsolvated Group 1 metal complexes was determined in 1997 by Olbrich and co-workers using powder diffraction methods using high resolution synchrotron radiation powder diffraction.[18] It was found that cyclopentadienylsodium and cyclopentadienyllithium, **(X)**, exhibit very similar solid state structures consisting of a multidecker structure with the metal centres coordinated in η^5 interactions with two cyclopentadienyl anions which builds up into a polymeric strand, Figure 4. There is a slight bend observed between the metal centre and the cyclopentadienyl centroid of the polymeric strand, 176.4° (Li) and 177.7° (Na), with little variation of the metal out of the plane, the M----M----M angle for both complexes being close to 180°. [7,8,18]

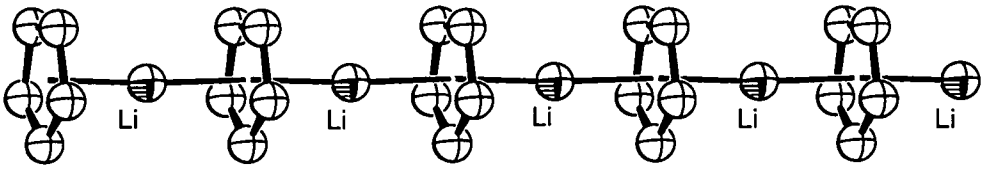

Figure 4. Solid state structure of cyclopentadienyl lithium, **(X)**, X-ray crystal structure reproduced from the CCDC database. Thermal ellipsoids are shown with arbitrary radii, hydrogens have been removed for

In comparison to the lithium and sodium cyclopentadienide complexes, the solid state structure of the potassium complex, **(XI)**, is quite different, Figure 5. Whilst the potassium cyclopentadienide structure exhibits the same multidecker structure seen in the other Group 1 complexes, the angle between the metal and anion is much greater now, 174.6 °. Not only does the metal – anion angle increase but a greater bend in the K----K----K angle is observed, 138 °, compared to the larger angle observed for the lithium and sodium analogues, 180 ° and 177.7 °, respectively.[18] The increase of the angle for potassium now exposes a side of the potassium which has the potential to interact and coordinate with Lewis bases. However, in this unsolvated $(C_5H_5)K$ species an additional cyclopentadienyl ring from an adjacent polymeric chain forms η^2 interactions with the exposed potassium faces.[7,8,18]

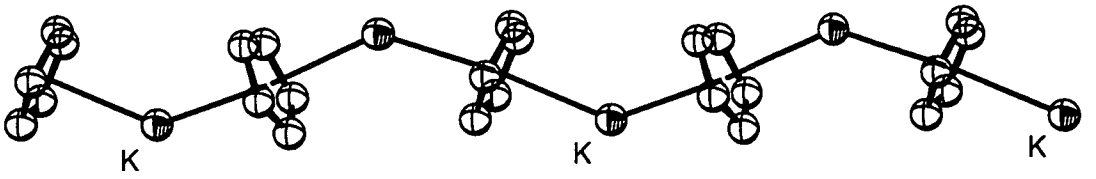

Figure 5a. Solid state structure of $[(\eta^5\text{-}C_5H_5)(\eta^2\text{-}C_5H_5)K]$, **(XI)**, showing the η^5 interactions only, X-ray crystal structure reproduced from the CCDC database. Thermal ellipsoids are shown with arbitrary radii, hydrogens have been removed for clarity.

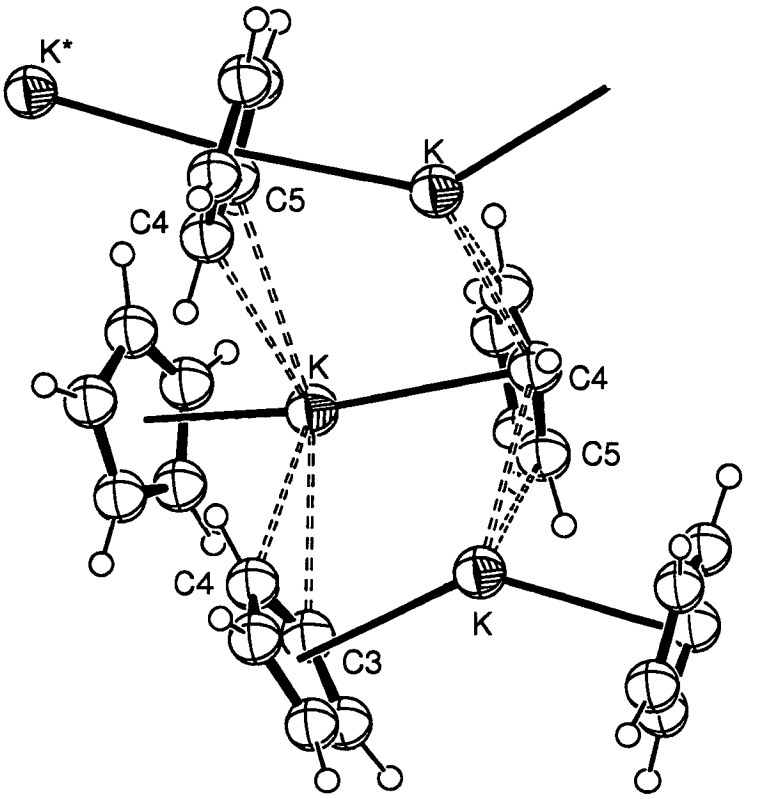

Figure 5b. Solid state packing of $[(\eta^5\text{-}C_5H_5)(\eta^2\text{-}C_5H_5)K]$, **(XI)**, showing eta-2 interactions, X-ray crystal structure reproduced from the CCDC database. Thermal ellipsoids are shown with arbitray radii.[18]

Whilst the cyclopentadienyl ligand system played an important role in the development of metallocene chemistry, the instability of some of its complexes during isolation under ordinary conditions proved to be a problem in addition to the aforementioned solubility issues. To overcome this problem substituted cyclopentadienyl anions were investigated as an alternative to cyclopentadienyl itself. The stability of the cyclopentadienyl complexes is greatly improved by the inclusion of bulky substituents in the system. The most successful and widely used of these substituted derivatives is the pentamethylcyclopentadienyl anion **(XII)**. The electron donating capability of the methyl groups increases the electron density of the cyclopentadienyl and this in turn generally strengthens the bond between the metal centre and the anion.

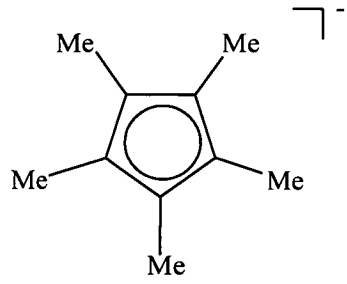

(XII)

The first reported organometallic complex utilising the pentamethylcylcopentadienyl anion was in 1962 when Rohl and his colleagues synthesised pentamethylcyclopentadienyltitanium trichloride.[19,20] The transition metal complexes of pentamethylcyclopentadienyl show an increase in stability as well as exhibiting increased solubility and crystallinity.[20] However, the development of the chemistry of pentamethylcyclopentadienyl was somewhat inhibited to begin with as there was no simple procedure for the large scale synthesis of pentamethylcyclopentadiene available until 1977.[21] The development of this synthetic route lead to progress in the field of pentamethylcyclopentadienyl chemistry with the synthesis of many new main group element complexes as well as complexes of transition and lanthanide metals.

The pentamethylcyclopentadienyl anion, like its unsubstituted analogue, exhibits a variety in binding nature, from being ionic to covalent, and also shows a range of multihaptic binding modes, with all possibilities in the range from η^1 to η^5 having been observed, Figure 6.[22] Like the cyclopentadienyl system, the ionic character of the bond between the metal and the ring system depends on the electronegativity of the metal itself; for example, alkali metal complexes with pentamethylcyclopentadienyl anion are highly ionic species, whereas in comparison pentamethylcylcopentadienide complexes of the *p* block elements form predominantly covalent compounds.[22] Pentamethylcyclopentadienide complexes show greater kinetic stability in comparison to the highly reactive cyclopentadienide analogues.[22] This kinetic stabilisation of the pentamethylcyclopentadienide complexes has been shown to be the result of the greater steric requirements of the σ or π bound pentamethylcyclopentadienyl anion.[22]

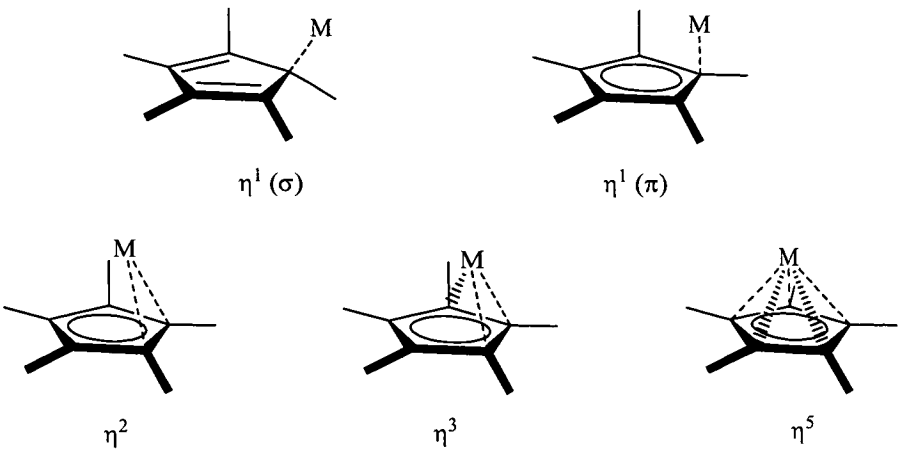

Figure 6. Possible binding modes for the pentamethylcyclopentadienyl anion.

Group 1 metal pentamethylcyclopentadienide complexes have been of great importance as starting materials for the synthesis and subsequent studies of main group, transition and rare earth metal complexes.[23] The Group 1 complexes are often synthesised in THF or in similar solvents and then reacted with the desired main group, transition or rare earth metal precursors (often halides) without isolation of the Group 1 metal complex. For this particular reason, along with the difficulty associated with isolating such highly air sensitive complexes, studies of these Group 1 metal complexes were rarely undertaken. The solid state structures have been determined for unsolvated pentamethylcyclopentadienidyllithium and -sodium[24,25] *via* X-ray powder diffraction studies, however no structure has been elucidated for the analogous potassium complex.

Various pentamethylcyclopentadienyl Group 1 metal complexes have been isolated as Lewis base adducts owing to their increased solubility and crystallinity, which has allowed for the determination of their solid state structures. The least solvated solid state structure of a pentamethylcyclopentadienide potassium complex determined is the THF adduct, **(XIII)**, Figure 7.[26] **(XIII)** is a one dimensional polymer featuring alternating potassium cations and pentamethylcyclopentadienyl anions, with each potassium forming η^5 interactions with two (C_5Me_5) anions as well as being coordinated to a THF moiety through the oxygen atom. Like the unsolvated cyclopentadienylpotassium structure, Figure 5, a bent polymeric strand is observed with a K---K---K angle of 141.06°, in comparison to the relatively linear M---M---M angle observed for the polymeric unsolvated lithium and sodium complexes. [7,8,24,25,26]

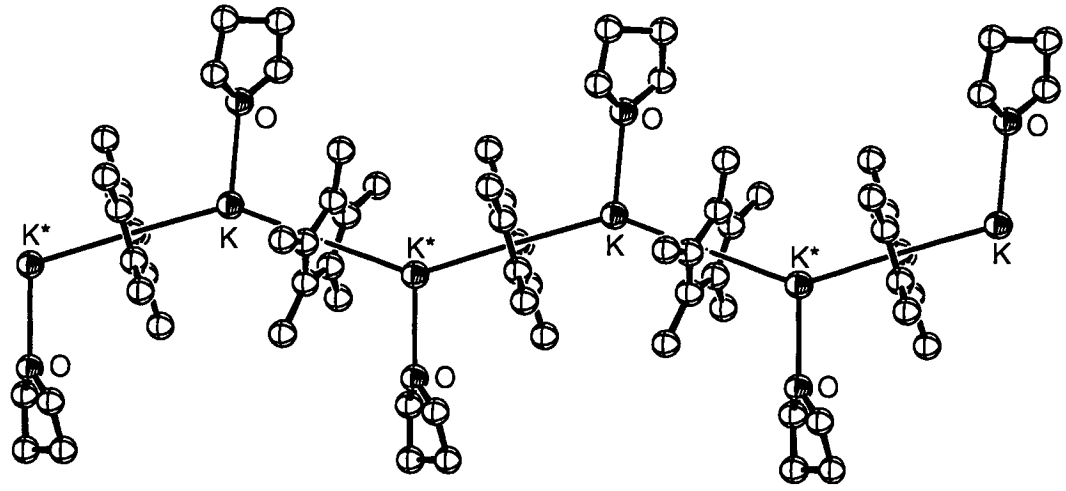

Figure 7. X-ray structure of [(η^5-C_5Me_5)K(THF)], **(XIII)**. X-ray crystal structure reproduced from the CCDC database. Thermal ellipsoids are shown with arbitrary radii, hydrogens have been removed for clarity.[26]

The incorporation of different Lewis bases into pentamethylcyclopentadienylpotassium complexes was found to alter their solid state structures. In the extreme, the polymeric strand of **(XIII)** in Figure 7 could be broken down into a monomeric structure, as was the case for the 18-crown-6 adduct **(XIV)**, Figure 8.[23] Like the THF analogue, the potassium centre forms an η^5 interaction with the pentamethylcyclopentadienyl anion. However the potassium is now encapsulated within the cavity of a 18-crown-6 molecule and is unable for interactions with another anion. A THF molecule is also incorporated into the solid state structure. Due to this the potassium is not situated in the middle of the cavity but instead is closer to the pentamethylcyclopentadienyl anion, the K-O (THF) bond length is 2.743 Å. Monomeric structures are also reported for the analogous caesium and rubidium 18-crown-6 complexes.[27] No structures containing lithium or sodium with the inclusion of 18-crown-6 have been reported, however a sodium analogue with pyridine is known which also exists as a monomer in the solid state. [7,8,23,28]

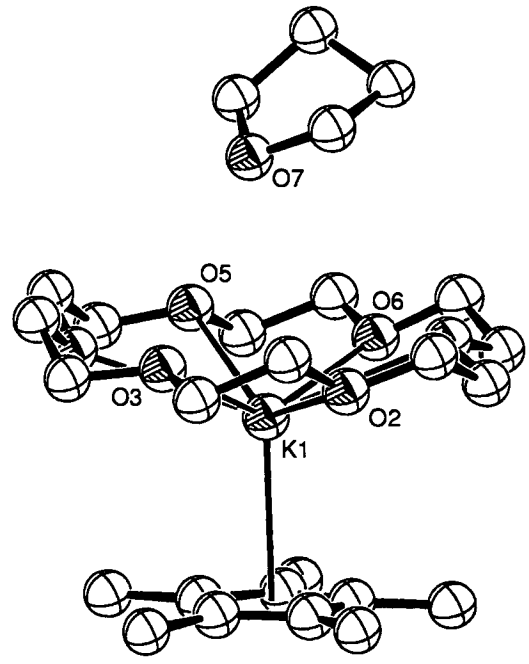

Figure 8. X-Ray Structure of $[(\eta^5\text{-}C_5Me_5)K(18\text{-crown-}6)]$, **(XIV)**. X-ray crystal structure reproduced from the CCDC database. Thermal ellipsoids are shown with arbitraty radii, hydrogens have been removed for clarity.[23]

The success of the cyclopentadienyl and pentamethylcyclopentadienyl anions in transition and main group chemistry led to the study of benzannulated systems, such as the edge fused indenyl and fluorenyl anions, **(XV)** and **(XVI)**, respectively. These systems are isoelectric and isostructural with the cyclopentadienyl and pentamethylcyclopentadienyl anions as they all bear a monoanionic charge. The extension of the π systems in **(XV)** and **(XVI)** gives rise to a phenomenon known as "ring slippage". This particular phenomenon leads to stable complexes where η^1, η^2 and η^3 as well as η^5 interactions between the metal and anion are more commonly observed.

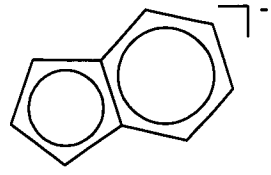

(XV)

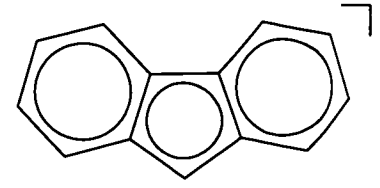

(XVI)

The indenyl anion is a bicyclic system which is comprised of a fused five and six membered ring. Not long after ferrocene was reported in *Nature* in 1951[3] Wilkinson and Pauson reported the preparation of the bis(indenyl) complexes of iron(II) and cobalt(II), **(XVII)** and **(XVIII)**.[29] Complex **(XVII)** was prepared by the reaction of indenyl lithium and iron(II) chloride. The analogous cobalt complex was prepared *via* the reaction of cobalt(III) acetylacetonate with a solution of indenylmagnesium bromide, which upon decomposition under acidic conditions led to the formation of the bis(indenyl) cobalt complex. Subsequent crystallographic studies of complexes **(XVII)** and **(XVIII)** indicated that the indenyl moieties interacted with the metal centre *via* η^5 type interactions.[30,31]

Whilst the indenyl anion has a variety of plausible binding modes, $\eta^1 - \eta^6$ the most common interactions which are observed and have been reported are the η^5 and η^3 interactions. There are two types of η^5 interaction which may occur in indenyl – metal complexes, a true η^5 interaction between the five membered ring and the metal centre and what has been termed as a "*3+2*" type interaction. It is however the η^5 and η^3 type interactions which have been of greatest interest and most extensively investigated due to their importance in a process known as the "indenyl effect". This particular effect involves the shift from an η^5 to an η^3 interaction, known also as "ring slippage" or "ring folding" processes.[32]

The η^5 to η^3 rearrangement was first observed by Hart-Davis and Mawby in 1969 who studied the reaction of $(\eta^5\text{-}C_9H_7)Mo(CO)_3CH_3$, **(XIX)**, with triphenylphosphine which gave $(\eta^5\text{-}C_9H_7)Mo(CO)_2(PPh_3)(COCH_3)$, **(XX)**, Scheme 3.[33] They proposed that the reaction goes *via* an η^3-indenyl intermediate, $(\eta^3\text{-}C_9H_7)Mo(CO)_3(PPh_3)(CH_3)$, **(XXI)**. This was confirmed a year later by Hart-Davis and Mawby along with White who observed increased rate constants for the reaction of $(\eta^5\text{-}C_9H_7)Mo(CO)_3X$ (where X was Cl, Br or I) with phosphine ligands in comparison to the corresponding $\eta^5\text{-}C_5H_5$ complexes. This increase in the rate constant was explained by the slippage of the indenyl ring from an η^5 to an η^3 complex during the association and dissociation of the halide and phosphine during the reaction.

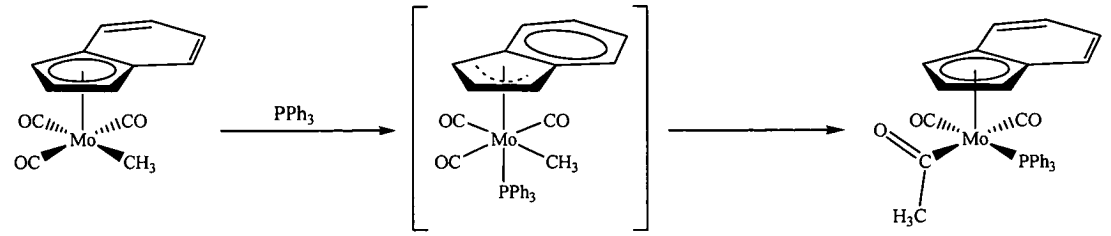

(XIX) (XXI) (XX)

Scheme 3.

The stability of η^5-indenyl complexes allowed for their isolation and structural characterisation, however it was not until 1979 that Struchkov and his colleagues successfully isolated and characterised the η^3-indenyl metal complex, $(\eta^5\text{-}C_9H_7)(\eta^3\text{-}C_9H_7)W(CO)_2$, **(XXII)**.[34] They noted that the indenyl anion that interacted *via* an η^3 binding mode with the tungsten centre was bent (folded), at an angle of 26 °, in comparison to the planar η^5 interaction of the second indenyl anion. Subsequent ^1H NMR spectroscopic studies by the group indicated rapid interconversions between the η^5 and η^3 binding modes in the complex. In 1986 Merola *et al.* reported the synthesis and structural characterisation of an η^3-indenyl iridium complex, $(\eta^3\text{-}C_9H_7)Ir(PMe_3)_3$, **(XXIII)**,where the η^3-indenyl anion was found to be bent at a similar angle, 28.5 °, to that of **(XXII)**.[35]

Recent studies on indenyl complexes have focussed on the use of density functional theory (DFT) to explore and explain the interconversions between the η^5 and η^3 binding modes, known as the indenyl effect. The group of Verios in Portugal has extensively investigated the indenyl effect by using *ab initio* molecular orbital (MO) and DFT calculations to determine the electronic factors which influence this effect. In 2002 they reported that the folding associated with the indenyl effect of a free cyclopentadienyl or indenyl anion was directly related to the metal anion bond strength.[32] They compared the energies for the η^3 and η^5 indenyl complexes with the analogous cyclopentadienyl anion complexes. The results from their calculations indicated that the $(\eta^5\text{-}C_5H_5)$-M, interaction, is stronger than that of $(\eta^5\text{-}C_9H_7)$-M however they found the reverse is true for the η^3 interactions with the indenyl – metal interaction being stronger than for cyclopentadienyl – metal.

A further extension of the cyclopentadiene system is the tricyclic 6:5:6 fused ring system, fluorene, **(XXIV)**. The fluorenyl anion, like the indenyl anion, has the potential to interact with a metal centre *via* several binding modes. The type of interaction between the metal and fluorenyl within the complex can be influenced by the presence or absence of a solvent molecule, or Lewis base, in the solid state. The incorporation of a solvent/Lewis base moiety into some of these complexes has also been shown to alter the aggregation state of the complex, that is whether the complex exists as a monomer or a polymer in the solid state.

One of the earliest reports of a Group 1 metal fluorenyl complex was the reported synthesis of sodium fluorenide by Weissgerber in 1909 who synthesised the title compound by reacting fluorene with sodium metal at 180 – 200 °C.[36] Weissgerber presumed that the sodium metal interacted with the fluorenyl anion *via* an η^1 interaction with the central carbon of the five membered ring.

In 1998 Johnels and his colleagues reported the synthesis, crystal structure and computational study of $[Li(C_{13}H_9)(Et_2O)_2]$, **(XXV)**.[37] In the crystal structure the lithium cation interacts with the fluorenyl anion *via* an η^2 interaction with the central five membered ring. The coordination sphere of the lithium is completed by two diethyl ether molecules, which coordinate to the lithium *via* the oxygen of the ether, resulting in the distorted tetrahedral geometry which is observed. The average lithium carbon distances were found to be shorter than those of other lithium fluorenyl complexes reported where η^3 and η^5 bonding was observed.[38-41] The crystal structure of the dilithium bisfluorenyl complex was to have each lithium cation interacting with the six membered ring of both fluorenyl anions *via* an η^6 interaction.[42]

While a significant number of η^3 indenyl complexes have now been characterised and reported, the number of η^3 fluorenyl complexes reported is fewer, with the majority of characterised complexes having either η^1 or η^5 interactions between the metal and anion. In 1999 Calhorda and Verios *et al.* reported the synthesis of the heteroleptic molybdenum complex, $[(\eta^5\text{-}C_9H_7)Mo(\eta^3\text{-}C_{13}H_9)(CO)_2]$,

[43] Single crystal X-ray studies indicated an exocyclic η^3 interaction between the fluorenyl anion and the molybdenum centre. In the same report they also showed that for this particular complex the η^3 exocyclic interaction between the fluorenyl and the molybdenum centre is preferred over the endocyclic η^3 interaction and an η^5 interaction using DFT calculations.

Extension of the cyclopentadienyl anion was not limited to the benzannulated anions of indenyl and fluorenyl but has included the fused 5:5 dihydropentalene. The first pentalendiyl dianion complex was synthesised in 1962 by Katz and Rosenberger, who reported dilithium pentalendiyl by treating dihydropentalene in tetrahydrofuran with 2 mole equivalents of *n*-butyl lithium in *n*-heptane to give a white crystalline solid, Scheme 3.[44] Katz and Rosenberger saw the dianion system as "a natural entry into the elusive pentalene series".[44] A year after the report of the first organometallic complex of the pentalendiyl system, Katz and Rosenberger synthesised a "ferrocene" type pentalendiyl derivative, (dihydro-1,1'-bipentalendiyl)iron(II), **(XXVI)** as per Figure 9,[45] which featured the unexpected coupling of the two ligand.[7,8,23,46]

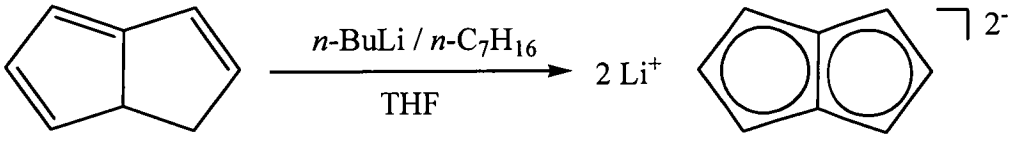

Scheme 4. Synthesis of the first pentalendiyl dianion complex.

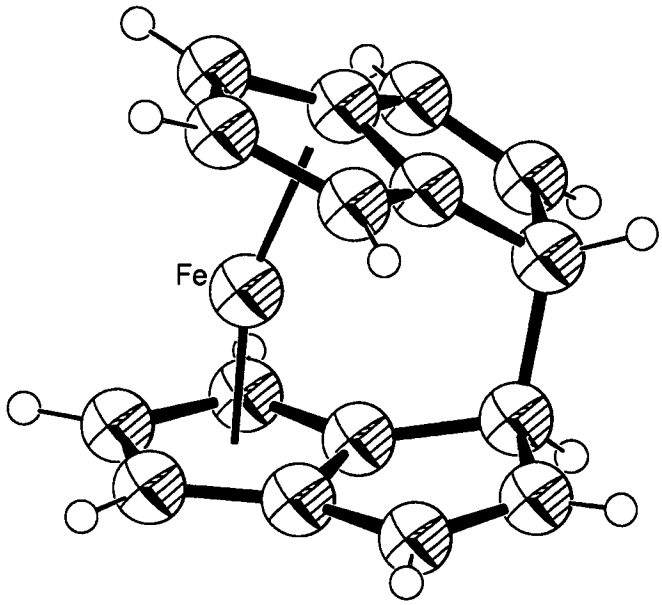

Figure 9. X-Ray Structure of (dihydro-1,1'-bipentalendiyl)iron, **(XXVI)**, X-ray crystal structure reproduced from the CCDC database. Thermal ellipsoids are shown with arbitrary radii.[45]

The chemistry of the pentalendiyl anion continued to expand slowly due to the difficult synthetic routes for the dihydropentalene system and its instability which prevents isolation. The pentalendiyl anion is prepared *via* the flash vacuum pyrrolysis of either diisohydrocylopentadiene or cyclooctatetraene in a nitrogen stream at 22 mmHg.[44] Depending on which compound is used as the starting material, the tautomeric form of the product varies. Either 1,3-dihydropentalene or a mixture of dihydropentalene isomers are formed, Scheme 5. The dihydropentalene, whether it be the one isomer or the mixture of isomers, can then be doubly deprotonated according to Scheme 3 to yield the desired pentalendiyl dianion. Only one other method is currently used in the synthesis of the tautomers of dihydropentalene, based on a procedure involving ring expansion of cycloheptatriene.[47]

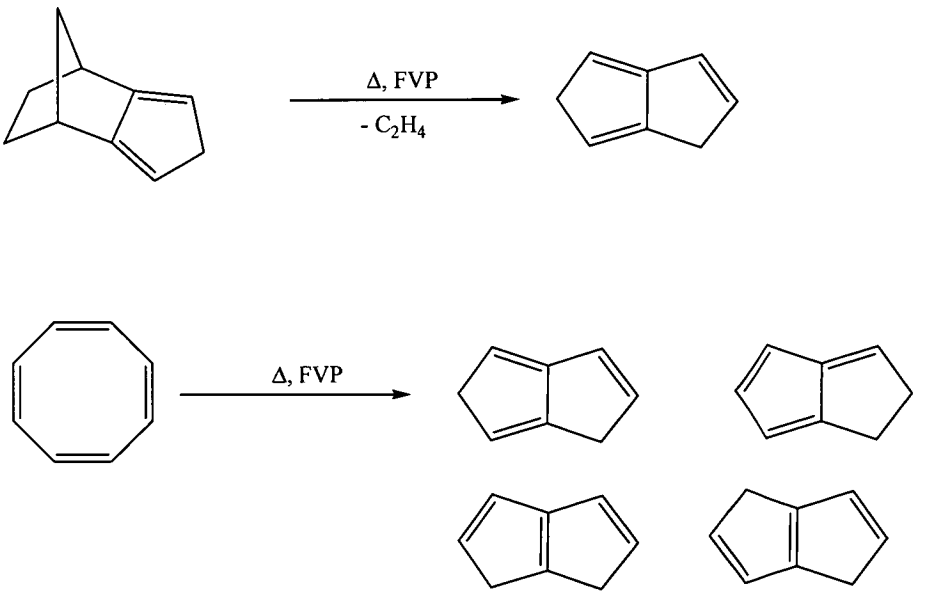

Scheme 5. Synthesis of tautomers of 1,3-dihydropentalenes.

Ten years after they reported the first metal complex of the pentalendiyl dianion, Katz and Acton reported the synthesis of a pure pentalendiyl sandwich compound, bis{(pentalendiyl)nickel}, **(XXVII)**.[48] Like the cyclopentadienyl anion and its analogues, the 10 π electron pentalendiyl dianion has the potential to interact with a metal centre *via* a variety of different binding modes ranging from η^1 through to η^8. Some transition metal complexes interact with the dianion in an η^3 allyl like fashion.[49]

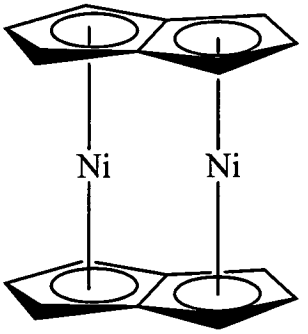

(XXVII)

The structure of complexes of the pentalendiyl anion can be altered by the inclusion of various bulky alkyl silyl groups. In 2000 Cloke *et al.* successfully synthesised trialkylsilyl substituted pentalendiyl anions *via* the reaction of a dilithium pentalendiyl dimethoxyethane (DME) complex, **(XXVIII)**, with the appropriate

trialkylsilyl compound, Scheme 6.[50] The substituted pentalenes were subsequently deprotonated to give the trialkylsilyl substituted potassium, **(XXIX)** or lithium **(XXX)** complexes. Complex **(XXX)** was further treated with chlorotrimethylsilane to obtain the tetrakis(trimethylsilyl)pentalene compound **(XXXI)**. Cloke showed that Group 1 complexes of the trimethylsilyl or triisopropylsilyl substituted pentalene formed an η^8 interaction between the metal centre and the substituted anion.[50] This was in comparison with the smaller dimethoxyethane adduct of the Group 1 metal lithium complex without silyl substituents which interacts with the pentalendiyl anion in an η^5 binding mode, Figure 10.

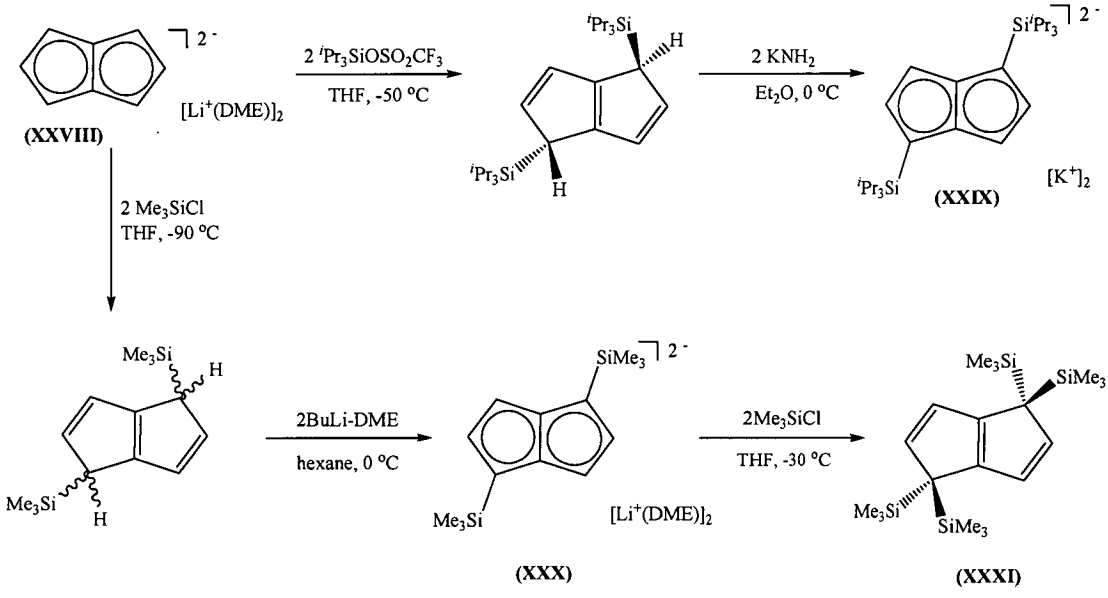

Scheme 6. Synthetic methodology for silyl substituted pentalendiyl systems.

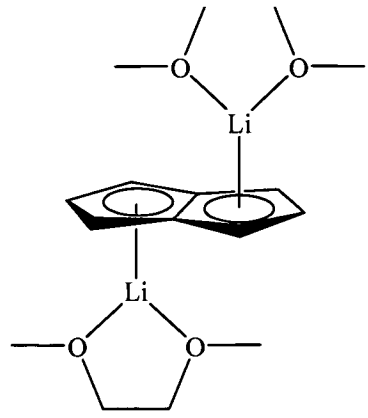

Figure 10: Pentalendiyl dilithium dimethoxyethane complex **(XIV)**.

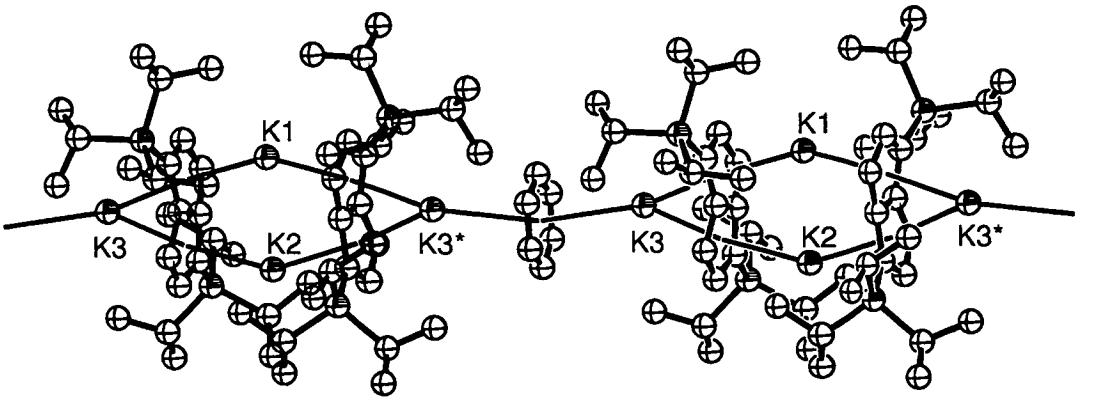

Figure 11. Crystal structure of 1,4-bis(triisopropylsilyl)pentalendiylpotassium complex as a benzene solvate **(XVIII)**. X-ray crystal structure reproduced from the CCDC database. Thermal ellipsoids are shown with arbitrary radii.[50]

The incorporation of these bulky silyl substituents not only showed a change in the observed binding mode of the pentalendiyl complexes but also lead to greater thermal stability of the silyl substituted dihydropentalene precursor. This compound remained unchanged after many days at room temperature in comparison to the unsubstituted dihydropentalene, which under went rapid isomerisation at the same temperature.[50] In 1997 Cloke and Jonas reported solid state crystal structures for transition metal complexes where the above η^8 binding mode was also observed. Both groups also noted that for the first time two pentalendiyl ligands were coordinated to a single metal centre.[50,51] Cloke used alkyl\silyl substituted pentalendiyls to investigate their effect on the metal – dianion interaction. In 2000 Cloke reported the synthesis and crystal structure of a dipotassium 1,4-bis(triisopropylsilyl)pentalendiyl complex **(XVIII)**, Figure 11, which was prepared from a potassium amide and 1,4-bis(triisopropylsilyl)pentalene.[50] The chemistry of the silyl substituted dianion has been extended to now include actinide metal complexes.[7,8,50,52,53]

The pentalendiyl complexes reported by Cloke were mainly restricted to homoleptic silyl\alkyl substituted complexes, whereas Jonas investigated the chemistry heteroleptic systems, in particular the mixed system of the pentalendiyl dianion and the cyclopentalendiyl anion and halides, Figure 12. The pentalendiyl complexes were synthesised from the reaction of a heteroleptic halide containing pentalendiyl complex and dilithium pentalendiyl or by reacting a metal cyclopentadienyl halide with dilithium pentalendiyl.[54] The heteroleptic systems were synthesised *via* the reaction of dilithium pentalendiyl with the desired metal cyclopentadienide, metal indenide or metal pentamethylcyclopentadienide.[55] The metal forms an η^5 interaction with the cyclopentadienyl based anions and an η^8 interaction with the pentalendiyl dianion, which exhibits a bent or folded structure, Figure 13. The folding of the dianions towards the metal centre is comparable to the dinickel dipentalendiyl complex, **(XV)** (seen earlier), where the dianions are planar.

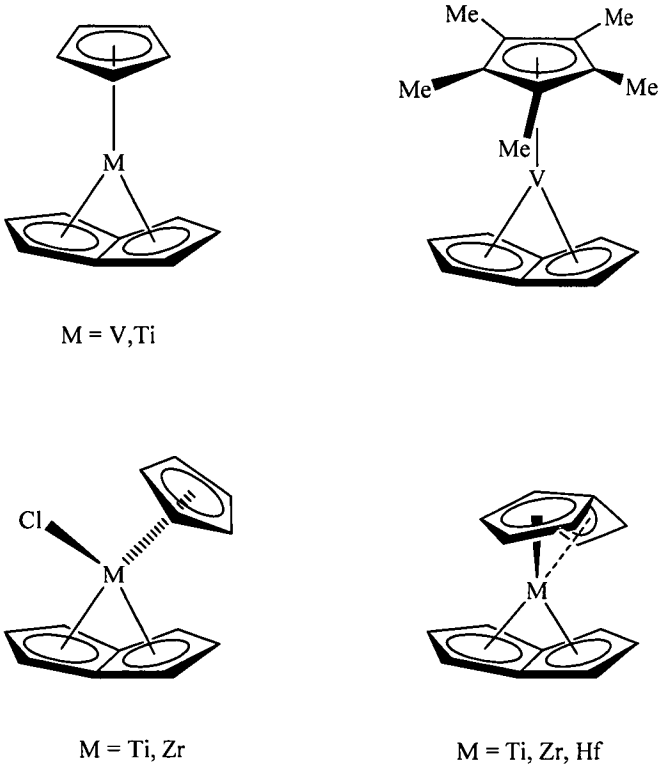

Figure 12. Transition metal complexes of the pentalendiyl dianion.

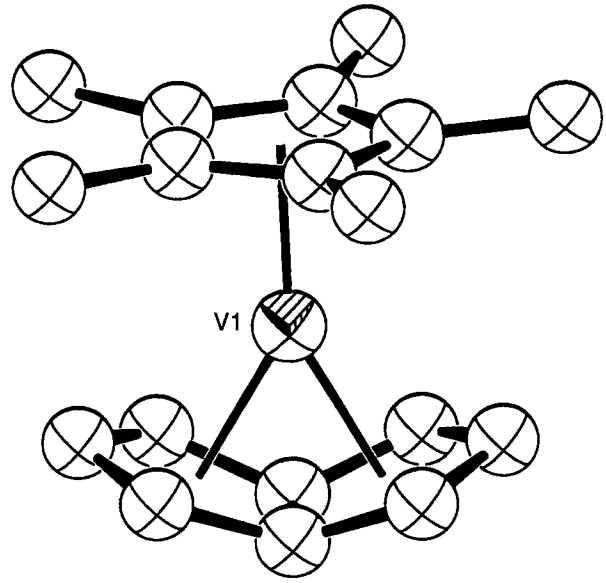

Figure 13. X-ray structure of $[(\eta^5\text{-}C_5Me_5)(\eta^8\text{-}C_8H_6)V]$. **(XXI)** X-ray crystal structure reproduced from the CCDC database. Thermal ellipsoids are shown with arbitrary radii, hydrogens have been removed for clarity.[55]

The chemistry of the cyclopentadienyl, substituted cyclopentadienyl and benzannulated cyclopentadienyl anions, such as indenyl, as well as the pentalendiyl dianion have indicated that a variety binding modes between the metal and anion/dianion are possible, as shown from the X-ray structures discussed here. A system which also has the potential to have a variety of different interactions between the metal and the anion is that of the earlier mentioned 4-azapentalenyl system, whose monoanionic charge makes it suitable for use in the chemistry of large, low valent metals, such as the lanthanides. The first complexes of the 4-azapentalenyl anion were reported in 1967 by Okamura and Katz, who not only reported the synthesis of the lithium, sodium and potassium Group 1 metal 4-azapentalenyl complexes but also described some of the properties of the anion.[1] The properties examined included further reactions of the complexes, NMR and UV spectral properties and the acidity of the parent heterocycle; this particular property will be discussed in greater detail in Chapter 6. No solid state structure determinations were made and these still remain undetermined to date.

The chemistry of this particular anion system remained relatively unstudied until 1998 when Kissounko and his colleagues reported silicon, tin and thallium complexes of the 4-azapentalenyl anion, Scheme 7.[49] The thallium salt of the complex, **(XXII)**, was reported to be quite stable to air and moisture and to have limited solubility, with **(XXII)** only being soluble in THF. **(XXII)** is unstable in solution. This instability in solution made NMR spectroscopic studies unsuitable for characterising the complex and characterisation was limited to mass spectroscopic identification.[49] In the same report, Kissounko and his co-workers also reported various lithiated analogues of the parent 4-azapentalenyl anion, as well as silyl and stannyl substituted, Scheme 8.[49]

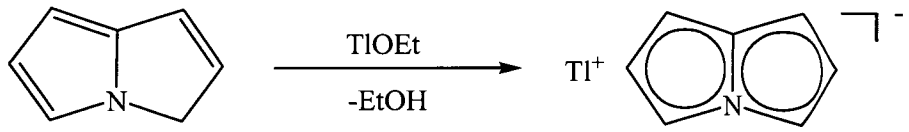

(XXII)

Scheme 7. Synthesis of 4-azapentalenylthallium **(XXII)**.

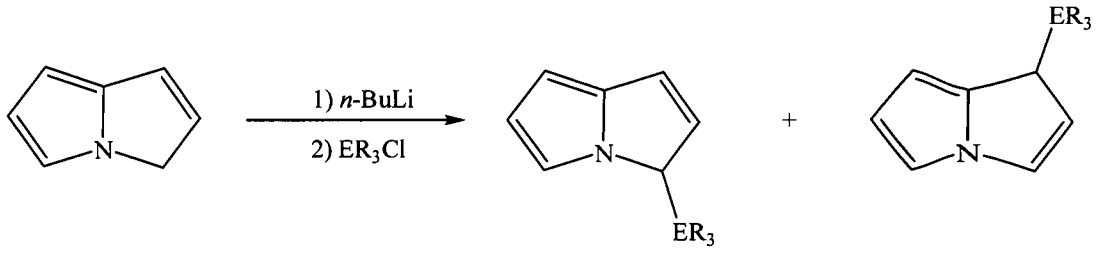

R = Me, Ph.
E = Si, Sn.

(XXIIIa) **(XXIIIb)**

Scheme 8. Synthesis of silyl and stannyl substituted pyrrolizines.

Apart from the early study on the 4-azapentalenyl system by Okamura and Katz and that in the late 1990s by Kissounko, the chemistry of this system remains relatively unknown with metal – anion solid state interactions of the complexes still to be determined. The more stable benzannulated pyrrolizine systems introduced in Chapter 2, Figure 14, became our focus in the investigation of Group 1 metal complexes of these extended 4-azapentalenyl systems. The complexes were

synthesised with a range of Lewis bases to investigate the effect on the metal anion interactions allowing for the first reports of the solid state structures of the 4-azapentalenyl based system.

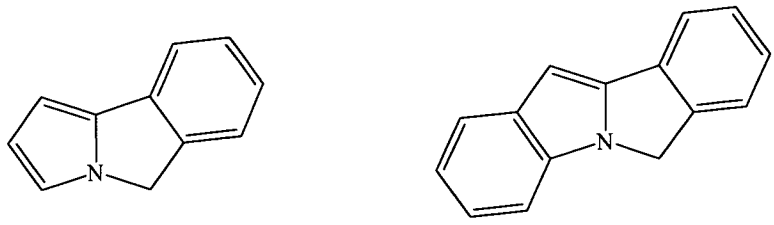

Figure 14. Benzannulated derivatives of the 3*H*-pyrrolizine.

3.2 RESULTS AND DISCUSSION

3.2.1 Group 1 metal complexes of the 4-azapentalenyl anion and derivatives

The synthesis of 4-azapentalenyl complexes of the Group 1 metals lithium and potassium were carried out, using *n*-butyllithium and potassium metal in the presence of THF as the solvent, as outlined in Scheme 8.

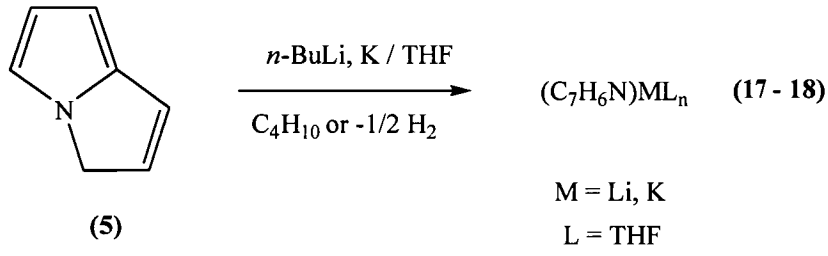

Scheme 8. Synthesis of Group 1 metal 4-azapentalenide complexes.

The general molecular formula given to the Group 1 complexes derived from **(5)** is $(C_7H_6N)ML_n$, where 'M' is used as the general symbol for the Group 1 metals Li or K and 'L_n' the general symbol for the coordinated Lewis base. Each monoanionic heterocycle, C_7H_6N, is countered by one monovalent Group 1 metal cation in the complex. Thus, the complexes are more closely related to the Group 1

metal cyclopentadienyl complexes than the pentalendiyl system, where each dianionic heterocycle, $(C_8H_6)^{2-}$, is countered by two alkali metal cations.

The K and Li species, **(17)** and **(18)**, were prepared by the method of Okamura and Katz, 1968.[1] The Group 1 metal complexes of the 4-azapentalenyl system exhibit similar properties to those seen in many alkali metal organometallic complexes in being very air and moisture sensitive. The complexes synthesised here were unable to be isolated as crystalline solids, but were obtained as solids and only characterised by ^1H and $^{13}C\{^1H\}$ NMR spectroscopy, which compared well with the data given in the literature. Symmetrising of both rings is the most characteristic change in the NMR spectra of the heterocycle upon metallation.

Group 1 metal derivatives of metallated 5*H*-pyrrolo[2,1-a]isoindole, **(9)**, were synthesised for the alkali metals lithium, sodium and potassium in the presence of THF as the solvent and a Lewis base, either N,N,N',N'-tetramethylethylenediamine (TMEDA), N,N,N',N",N" pentamethyldiethylenetriamine (PMDETA), 18-crown-6 or dibenzo-18-crown-6, Scheme 9.

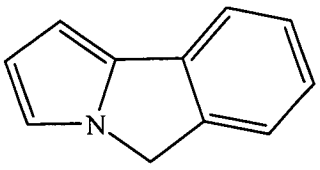

(9)

n-BuLi, NaH, K/ THF

C_4H_{10} or H_2 or -1/2 H_2

$(C_{11}H_8N)ML_n$ **(19 - 24)**

M = Li, Na, K

L = THF, TMEDA
PMDETA, 18-crown-6,
dibenzo-18-crown-6

Scheme 9. Synthesis of Group 1 metal complexes of 5*H*-pyrrolo[2,1-a]isoindole, **(9)**.

5*H*-Pyrrolo[2,1-a]isoindole, **(9)**, when reacted with the Group 1 metal reagents potassium metal and sodium hydride yielded a range of the desired Group 1 complexes which were characterised by distinctive changes to the ^1H NMR spectrum of the heterocycle, see Section 3.2.2. Crystalline solids were able to be isolated for all the potassium complexes, with the exception of complex **(23)**, see Table 1. Complex **(23)** was isolated as a red solid and characterised by NMR spectroscopy

studies and elemental analysis. Complexes **(19)**, **(20)**, **(21)** and **(21)** were characterised by ^{1}H and $^{13}C\{^{1}H\}$ NMR spectra, elemental analysis and X-ray structure determinations, see Sections 3.2.2 and 3.2.3, respectively. The use of lithium and sodium provided quantitative metallation in THF solution, but the products were unstable once deprotonated and reprotonation occurred when attempts were made to isolate the crystalline product.

Table 1. Synthesised potassium 5*H*-pyrrolo[2,1-a]isoindolenyl complexes.

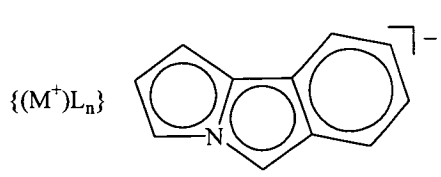

Complex	M	L	n
19	K	THF	½
20	K	TMEDA	1
21	K	PMDETA	1
22	K	18-crown-6, THF†	1
23	K	Dibenzo-18-crown-6	1

† THF may have been lost *in vacuo* during preparation of microanalysis sample.

The potassium complex $[(C_{11}H_8N)K(THF)_{1/2}]$, **(19)**, was synthesised from the reaction between 5*H*-pyrrolo[2,1-a]isoindole, **(9)**, and potassium metal in the presence of THF. An excess of potassium metal was added to ensure that the reaction could reach completion and the mixture was allowed to stir at ambient temperature for a period of 12 hours. Removal of the excess potassium metal by filtration and concentration of the reaction mixture *via* the removal of THF *in vacuo* gave an oil. Subsequent standing at ambient temperature for two weeks resulted in the formation of the red crystalline product **(19)**, which was isolated in 93% yield.

Complexes **(20) – (23)** were synthesised in a similar manner to that of complex **(19)**, however different Lewis bases were added as neutral coordinating species to the reaction mixture once the metallation had taken place. The use of such Lewis bases was to explore the structural variations that are possible between the metal and the anionic heterocycle. Structural variations ranging from a monomeric species to linear and three-dimensional polymers were envisaged based on established cyclopentadienyl chemistry which could be employed in further transition and early

lanthanide metal chemistry of the heterocyclic anions. The synthesis of each complex began with the formation of the anion by the reaction of the protonated heterocycle with potassium metal in THF at ambient temperature. In the case of the synthesis of $[(C_{11}H_8N)K(TMEDA)]_n$, **(20)**, and $[(C_{11}H_8N)K(PMDETA)]_n$, **(21)**, 46 and 14 molar equivalents of TMEDA and PMDETA respectively were added to the dried compound **(19)**. This was concentrated to half the volume and cooled to – 4 °C from ambient temperature; the red crystalline products **(20)** and **(21)** formed, respectively, and were isolated in 92% and 51 % yields, respectively. Both complexes **(20)** and **(21)** form linear polymeric chains in the solid state which will be discussed later in more detail, see Section 3.2.3. $[(C_{11}H_8N)K(18\text{-crown-}6)(THF)]$, **(22)**, was obtained from the addition of a THF solution of 18-crown-6 to a concentrated THF solution of **(19)** which was left to stir at ambient temperature for 12 hours. On concentrating the solution a crystalline material began to form which was redissolved with gentle heating and upon slow cooling to room temperature red crystalline prisms formed which were collected in 50 % yield.

The final complex in this series, $[(C_{11}H_8N)K(\text{dibenzo-}18\text{-crown-}6)]$, **(23)**, was unable to be isolated as a crystalline solid even though numerous attempts were made including liquid phase diffusion methods. The synthesis of complex **(23)** is similar to that described previously for complex **(22)**. The solubility of both dibenzo-18-crown-6 and complex **(23)** proved to be problematic. The dibenzo-18-crown-6 was marginally soluble in THF at ambient temperature and did not improve with heating. Complex **(23)** was isolated as an insoluble red solid at – 4 °C which was analysed *via* ^1H and $^{13}C\{^1H\}$ NMR spectroscopy and elemental analysis. Complex **(23)** was insoluble in THF, toluene and petroleum spirits, which prevented recrystallisation, and hence no X-ray structure determination was able to be performed.

The synthesis of the sodium complex $[(C_{11}H_8N)Na(THF)_n]$, **(24)**, proved to be more challenging and lead to subsequent investigations computationally into the stability of the anionic heterocycle. This aspect of the chemistry will be discussed in detail in Chapter 6. Sodium hydride reacted with 5*H*-pyrrolo[2,1-a]isoindole, **(9)**, in the presence of THF at ambient temperature over a period of days giving **(24)**. The isolated product, although crystalline, was found to be the protonated heterocycle **(9)** from ^1H NMR spectra. It appeared that the complex had decomposed in solution to

give the protonated 5*H*-pyrrolo[2,1-a]isoindole, **(9)**. Similar outcomes were noted when the reaction was carried out at reflux for a period of 48 hours at 70 °C. Pure crystalline solids were not able to be isolated. However NMR scale reactions and their subsequent ^{1}H and $^{13}C\{^{1}H\}$ NMR spectra studies confirmed the synthesis of $[(C_{11}H_8N)Na(THF)_n]$, **(24)**, in quantitative yield. Attempts to isolate the complex as a solid from the dark claret coloured solutions were always unsuccessful, with ^{1}H NMR spectra indicating the presence of two species, the protonated heterocycle and the sodium complex **(24)**.

The Group 1 metal complexes **(25)** – **(27)** derived from metallation of 6*H*-isoindolo[2,1-a]indole, **(11)**, were synthesised as outlined in Scheme 10. The reactions between 6*H*-isoindolo[2,1-a]indole, **(11)**, and the alkali metal reagents did not reach completion after 3 days at 85 °C giving a mixture of two products, the protonated heterocycle and the metallated complex. The reactions could be forced to completion by refluxing the reaction mixture for 24 hours at 70 °C after which time the colour of the reaction mixture was a deep purple. On isolating the complexes from THF the heterocycle **(11)** was identified by the ^{1}H NMR spectra. The decomposition of the complex to the heterocycle **(11)** observed here was not due to the presence of air or moisture in the reaction mixture but from the monoanionic heterocycle attacking the solvent molecule allowing reprotonation at the formerly sp^3 carbon site, **(XXIV)**. From theoretical studies done on the heterocyclic system one influencing factor for this attack may be linked to the high pK_a for 6*H*-isoindolo[2,1-a]indole, **(11)**, indicating an unstabilised anion upon metallation, see Chapter 6. NMR scale reactions, including reflux at 70 °C for 24 hours, followed by ^{1}H and $^{13}C\{^{1}H\}$ NMR spectral studies indicated complete reaction and formation of the complex species.

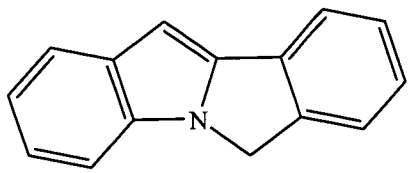

(11)

n-BuLi, NaH, K / THF

C_4H_{10} or H_2 or -1/2H_2

$(C_{11}H_8N)ML_n$ **(25 - 26)**

M = Li, Na, K

L = THF

Scheme 10. Synthesis of Group 1 metal complexes of 6*H*-isoindolo[2,1-a]indole, **(11)**.

3.2.1.1 Attempted synthesis of a lanthanide metal modified 4-azapentalenyl complexes

The synthesis of heteroleptic lanthanide complexes from the reaction of the potassium salt of 5*H*-pyrrolo[2,1-a]isoindole and various lanthanide halides was attempted. In particular the synthesis of a samarium complex was attempted, Scheme 11, utilising a metathetical exchange reaction between the potassium salt and $(C_5Me_5)_2SmCl(THF)$. This attempt was unsuccessful yielding the reductively coupled product of the anion $(C_{11}H_8N)_2$. This is linked with the poor acidity of the heterocycle and its redox chemistry which leads to the reductively couple product. The poor acidity of the heterocycles will be discussed in terms of their high pK_a values determined by density functional theory in Chapter 6.

$$2\ [(C_{11}H_8N)\ K(THF)_{1/2}] + 2\ SmCp^*_2Cl(THF) \longrightarrow (C_{11}H_8N)_2 + 2\ Cp^*_2Sm + 2\ KCl$$

Scheme 11. Attempted synthesis of a samarium complex of 5*H*-pyrrolo[2,1-a]isoindolyl anion.

A second attempt at synthesising a lanthanide complex involved a direct metallation of 3*H*-pyrrolizine with a highly reactive $Y(CH_2SiMe_3)_3(THF)_2$. These particular type of compounds are known to be excellent reagents for deprotonation. The reaction was performed on a NMR scale, indicating the formation of a new complex. Unfortunately, complex could not be isolated and spectroscopic evidence did not allow for further speculation on the identity of the complex.

3.2.2 NMR Spectroscopic Characterisation

3.2.2.1 Group 1 metal 4-azapentalenyl complexes

The ^{1}H NMR spectral data of the Group 1 metal complexes featuring the heterocyclic system **(5)** are listed in Table 2, ^{13}C NMR data are given in Table. The ^{1}H NMR spectral data of the pyrrolizine system **(5)** is included for comparison with the reported complexes, however the resonances of the coordinating Lewis bases have not been included. The absence of the methylene resonance in the ^{1}H NMR spectra of complexes **(17)** – **(18)** is a clear indication that deprotonation of the parent heterocycle has occurred.

The potassium and lithium complexes of the 4-azapentalenyl anion exhibit similar spectroscopic characteristics and resonances with little variation shown in the chemical shifts between the two complexes, Table 2. The small variation observed here in the chemical shifts was also noted by Okamura and Katz, who in 1967, reported the synthesis and ^{1}H NMR characterisation of the first Group 1 metal complexes of the 4-azapentalenyl anion.[1] The resonances reported here for the potassium and lithium complexes are not dissimilar to those reported by Okamura and Katz for the corresponding Group 1 complexes.

Table 2. ^{1}H NMR spectral data for compounds **(5)**, **(17)** and **(18)**.*

	CH_2	CH – arom			
C_7H_7N **(5)**	3.61	6.54	6.31	6.11	5.55	6.44
$(C_7H_6N)K$ **(17)**	-	4.78		6.07		6.38
$(C_7H_6N)Li$ **(18)**	-	4.77		6.06		6.47

* C_6D_6 for **(5)** (299.90 MHz, 298 K, ppm).
THF-d_8 for **(17)** (299.898 MHz, 298 K, ppm) and **(18)** (399.782 MHz, 298 K, ppm).

The ^{1}H NMR spectra of the Group 1 metal complexes are comprised of three distinct multiplets of equal intensity. These multiplets arise from the three different kinds of protons present in the azapentalenyl complex in comparison to the five resonances which are observed in the parent compound **(5)**, see Section 2.2.3 for discussion of **(5)**. Similar changes are apparent in the ^{13}C NMR spectra, Table 3.

Table 3. $^{13}C\{^{1}H\}$ NMR spectral data for compounds **(5)**, **(17)** and **(18)**.*

	CH_2	Carbons of unsaturated five membered rings				
C_7H_7N **(5)**	50.2	97.8	112.5	116.8	124.0	127.0
$(C_7H_6N)K$ **(17)**	-	74.8	74.4	112.0	139.4	
$(C_7H_6N)Li$ **(18)**	-	72.1	85.9	110.4	141.2	

* C_6D_6 for **(5)** (75.4 MHz, 298 K, ppm).
THF-d_8 for **(17)** (75.4 MHz, 298 K, ppm) and **(18)** 100.5MHz, 298 K, ppm).

3.2.2.2 Group 1 metal 5*H*-pyrrolo[2,1-a]isoindenyl complexes

The proton resonances in the ^{1}H NMR spectra for the benzannulated 4-azapentalenyl Group 1 complexes **(19)** – **(24)** with various Lewis bases occur as multiplets in the chemical shift range 5.86 – 8.00 ppm, some of these multiplets are well resolved while in some cases an overlap is observed to occur, Table 4. The

expected chemical shifts for the coordinated THF for both complex **(19)** and **(24)** are masked by the resonances of the deuterated THF and are therefore not seen in the ^{1}H NMR spectra of either complex. The aromatic resonances of complexes **(19)** – **(24)** display an up field shift in comparison to the chemical shifts of the protonated parent heterocycle **(9)**. The absence of the methylene singlet at 4.92 ppm for complexes **(19)** – **(24)** is a clear indication that deprotonation of the molecule had occurred successfully at the 5*H* position.

The full assignment of the proton and the carbon resonances was possible for complex **(19)** by gCOSY, NOESY, gHMQC and gHMBC spectroscopies. Complex **(19)** was chosen for this spectroscopic investigation due to the clearly defined resonances observed in its ^{1}H and $^{13}C\{^{1}H\}$ spectra. A detailed discussion of the results from these experiments follows the discussion of the ^{1}H and $^{13}C\{^{1}H\}$ NMR of complexes **(19)** – **(24)**.

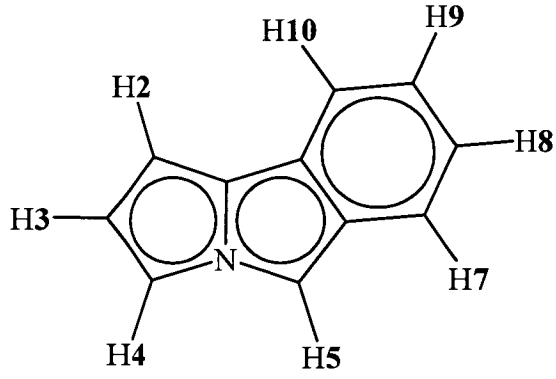

Figure 15. Assignment of protons in ^{1}H NMR spectrum of complex **(19)**.

Table 4. ^{1}H NMR spectral data for compounds **(9), (19) – (24).**[†‡]

	1	2	3	4	5	7	8	9	10
$C_{11}H_9N$ **(9)**		4.92	6.27	6.33	6.93	7.12	7.25	7.31	7.45
$[(C_{11}H_8N)K(THF)_{1/2}]$ **(19)**		5.85	6.21	6.71	6.76	7.35	6.58	5.97	6.81
$[(C_{11}H_8N)K(TMEDA)]_n$ **(20)**		6.56	6.93		7.44 (2H)	8.00	7.16	6.62	7.46
$[(C_{11}H_8N)K(PMDETA)]_n$ **(21)**		5.88	6.17	6.55		7.36	6.30	5.98	7.44 (2H)
$[(C_{11}H_8N)K(18\text{-crown-6})(THF)]$ **(22)**		5.88	6.54 (2H)	6.76	6.79	7.39 (2H)		6.26	
$[(C_{11}H_8N)Na(THF)_n]$**(24)**		5.87	6.27	6.76		7.36	6.57	5.96	6.81 (2H)

† $CDCl_3$ for **(9)** (299.90 MHz, 298 K, ppm).

THF-d_8 for **(19)**, **(22)**, **(24)**, (299.90 MHz, 298 K, ppm) **(21)**, (199.975 MHz, 298 K, ppm).

pyr-d_5 for **(20)** (300.13 MHz, 300 K, ppm).

‡ The chemical shifts of the protons assigned for the Lewis bases are typical (ppm): THF δ: 1.84 (CH_2) and 3.73 (CH_2) ; TMEDA δ: 2.16 (CH_3) and 2.35 (CH_2); PMDETA δ: 2.15 (CH_3), 2.26 (CH_3) and 2.36 (CH_2); 18-crown-6 δ: 3.35, (CH_2) and dibenzo-18-crown-6 δ: 4.04 (CH_2), 4.16 (CH_2) and 6.83 (CHarom).

The proton chemical shifts of the potassium and sodium complexes, **(19)** and **(24)**, show only slight differences in their ^{1}H NMR spectra from each other. This similarity in chemical shift indicates a similarity in the solution state structure of these two complexes which maybe due to either the ionic interactions between the metal and anion or the rapid fluxionality which can occur in these type of complexes. In contrast to the other complexes vary considerably and this maybe linked to changes which are occurring in the solution state of the complex.

As mentioned in Section 3.1 the benzannulated 4-azapentalenyl anion has various potential binding modes of η^1 through to η^8, representing many fluxional processes that may be operative. This variety in modes is confirmed *via* the solid state X-ray crystal structure studies with different binding modes being observed between the metal and anion, to be discussed in more depth in Section 3.2.3.1.

^{1}H NMR spectra of the benzannulated 4-azapentalenyl complexes **(19)** – **(24)** are shown in Figure 16 and have the typical following multiplicities that allow for easy characterisation. The example of multiplicities given here is for complex **(19)**: (ppm) δ; 5.85 – doublet; 5.97 – well-resolved pseudo triplet; 6.27 – multiplet; 6.58 – well-resolved triplet; 6.71 – singlet; 6.76 – singlet, 6.81 – well resolved doublet and 7.35 – well resolved doublet. In Figure 16(b) the resolved pseudo doublets of 10, 6.81 ppm, and 7, 7.35 ppm along with the pseudo triplets of 8, 6.58 ppm, and 9, 5.97 ppm, are characteristic of the aromatic hydrogens of the six membered ring present in the anion (see Figure 15, for the assignments based on gCOSY, NOESY, gHMQC and gHMBC spectroscopic experiments). The singlet 5 at 6.76 ppm corresponds to the 5*H* position of the heterocycle, H5 in Figure 15. The multiplets 5.85, 2, and 6.27 ppm, 3, are characteristic for the protons associated with the terminal five membered ring of the anion. The multiplet at 5.85 ppm was determined to be that of the proton H2 in Figure 15, whilst the other multiplet at 6.27 ppm was assigned to H3; see discussion on two dimensional experiments for more detail in determination of assignments. The final multiple resonance at 6.71 ppm was assigned to H4 of the heterocyclic anion, which was determined from the gCOSY, NOESY, gHMQC and gHMBC spectroscopic studies.

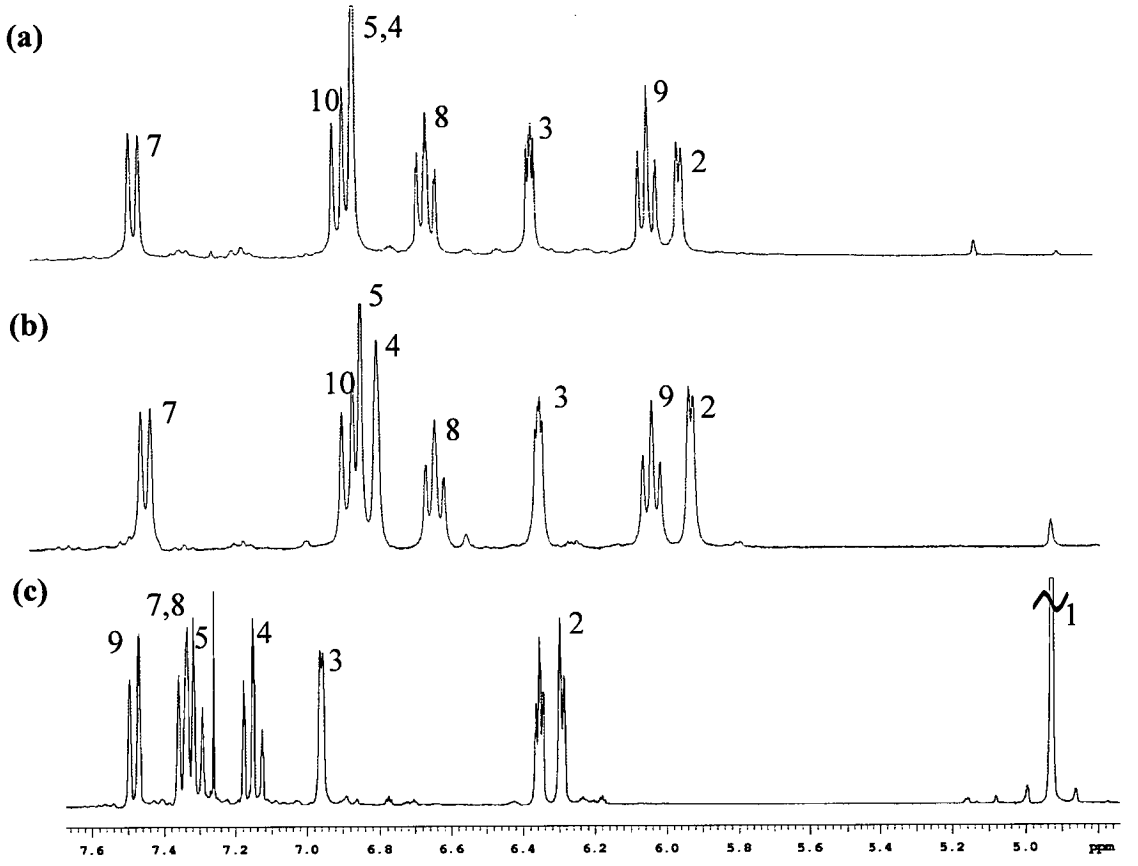

Figure 16. ^{1}H NMR spectra of complexes **(24)** (a), **(19)** (b), compound **(9)** (c). $CDCl_3$ for **(9)** (299.90 MHz, 298 K, ppm), THF-d_8 for **(19)** and **(24)**, (299.90 MHz, 298 K, ppm).

The carbon resonances observed in the ^{13}C NMR spectra for the Lewis base adducts of the benzannulated 4-azapentalenyl Group 1 metal complexes **(19)** – **(24)** fall in the range 81.9 – 132.1 ppm (d_5-pyridine and THF-d_8), as summarised in Table 5. Absence of the methylene carbon resonance at 51.5 ppm in the spectra of complexes **(19)** – **(24)**, along with the absence of the methylene proton resonance in the ^{1}H NMR spectra, confirms that the deprotonation occurred. Complete assignment of the eleven carbon resonances in the ^{13}C{^{1}H} NMR spectra of complex **(19)** was achieved *via* gCOSY, NOESY, gHMQC and gHMBC spectra, with assignment of the carbon resonances for the other complexes based on these results; this will be discussed later in this section.

Table 5. ^{13}C $\{^1H\}$ NMR spectral data for compounds **(9)**, **(19)** – **(24)**.†‡

	1	2	3	4	5	6	7	8	9	10	11
$C_{11}H_9N$ **(9)**	138.7	98.2	112.9	116.7	51.5	134.0	123.2	128.1	125.0	140.4	118.8
$[(C_{11}H_8N)K(THF)_{1/2}]$ **(19)**	106.2	83.9	109.6	98.1	83.3	132.2	118.9	120.5	105.0	111.2	131.5
$[(C_{11}H_8N)K(TMEDA)]_n$ **(20)**	110.2	85.0	109.9	99.0	84.3	132.0	119.4	120.6	105.1	111.4	131.5
$[(C_{11}H_8N)K(18\text{-crown-6})(THF)]$ **(22)**	106.8	82.0	108.7	95.9	81.9	130.1	117.8	???	101.8	116.8	129.9
$[(C_{11}H_8N)Na(THF)_n]$ **(24)**	108.8	83.2	109.9	98.4	82.9	132.1	118.5	120.1	104.6	110.6	131.5

† $CDCl_3$ for **(9)** (299.90 MHz, 298 K, ppm).
THF-d^8 for **(19)**, **(22)**, **(24)**, (299.90 MHz, 298 K, ppm)
pyr-d_5 for **(20)** (300.13 MHz, 300 K, ppm).

‡ The chemical shifts of the carbons assigned to the Lewis bases are typical (ppm): TMEDA δ: 46.0 (CH_3) and 58.2 (CH_2); PMDETA δ: 42.9 (NCH_3), 45.9 (NCH_3), 56.2 (CH_2) and 57.5 (CH_2); 18-crown-6 δ: 70.7 (CH_2) ppm and dibenzo-18-crown-6 δ: 69.2 (CH_2), 70.1 (CH_2), 114.29 (CHarom), 121.5 (CHarom), 149.1 (=C).

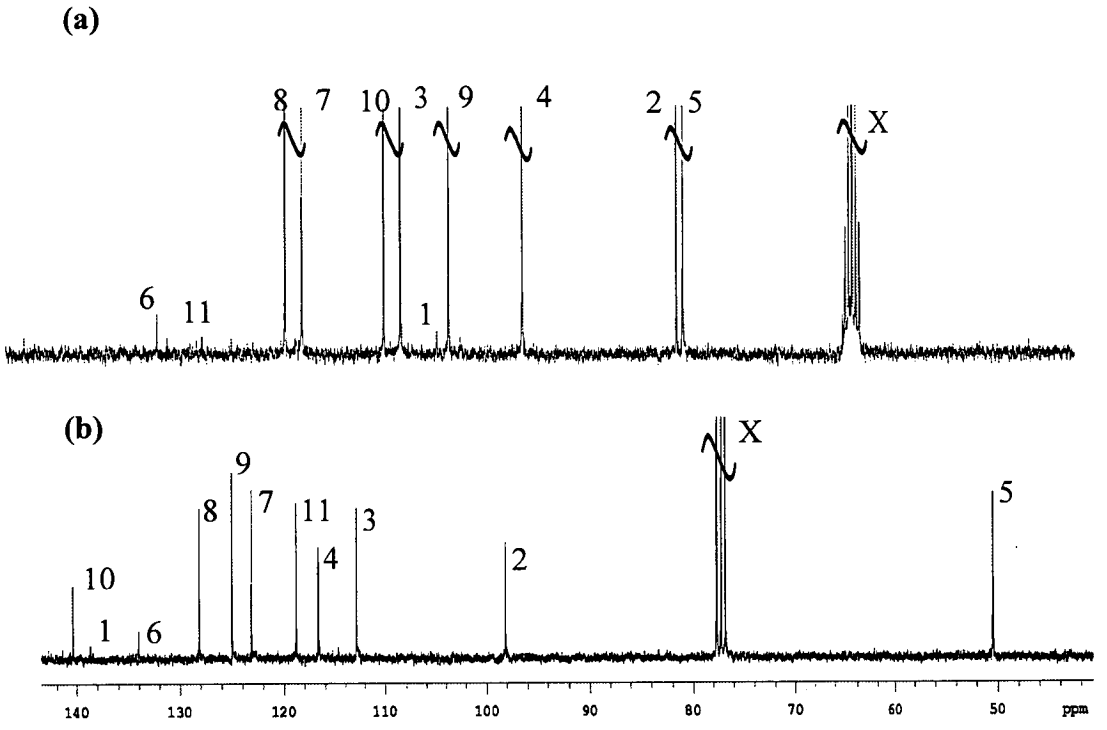

Figure 17. $^{13}C\{^{1}H\}$ NMR spectra of compound **(9)**, (b), and complex **(19)**, (a), where X = solvent. $CDCl_3$ for **(9)** (299.90 MHz, 298 K, ppm), THF-d_8 for **(19)** (299.90 MHz, 298 K, ppm).

The comparison of the spectrum of complex **(19)**, Figure 17 (a), with that of the parent heterocycle, Figure 17 (b), indicates a shift upfield in comparison to the carbon resonances of **(9)**. The observed shift upfield of the resonances and the subsequent intensities of the resonances indicate a substantial build up of charge on the aromatic CH carbon centres. The quaternary carbon resonances occur at δ = 106.2, 131.5 and 132.2 ppm. These resonances are relatively weak resonances in comparison to the other carbon resonances present in the $^{13}C\{1H\}$ NMR spectrum of complex **(19)**.

Complete assignment of the resonances observed in the ^{1}H and $^{13}C\{^{1}H\}$ NMR spectra of complex **(19)** was achieved *via* gCOSY, NOESY, gHMQC and gHMBC studies. Two dimensional studies were only carried out on complex **(19)** due to the unstable nature of the complexes, this particular complex was relatively more stable than the others over a longer period of time in solution. Table 6 summarises the assignments of both the proton and carbon resonances in their respective spectra for complex **(19)**.

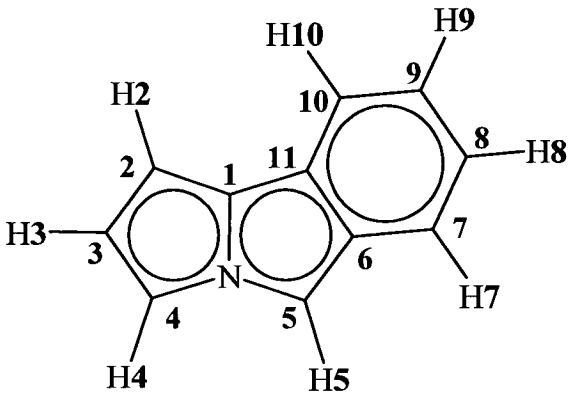

Table 6. Chemical shift assignments for the ^{1}H and $^{13}C\{^{1}H\}$ NMR resonances of $[(C_{11}H_8N)K(THF)_{1/2}]$ **(19).**†

	1	2	3	4	5	6	7	8	9	10	11
δ H (ppm)		5.85	6.27	6.71	6.76		7.35	6.58	5.97	6.81	
δ C (ppm)	106.2	83.9	109.6	98.1	83.3	132.2	118.9	120.5	105.0	111.2	131.5

† The following NMR experiments were done in THF-d_8 at 298 K to determine the given solution structure: ^{1}H NMR (299.90 MHz); $^{13}C\{^{1}H\}$ NMR (75.4 MHz); gCOSY; gNOESY; gHMQC and gHMBC.

The gCOSY NMR spectrum of complex **(19)**, Figure 18, allowed for assignment of the proton at the 5*H* position of **(19)**. No correlation is observed between this aromatic resonance at δ = 6.76 ppm and any of the other resonances present in this spectrum. Correlation between the four aromatic protons of the six membered ring is observed for the following resonances in the gCOSY spectrum: the resonance at δ = 5.97 ppm (triplet) correlates with the triplet at δ = 6.58 ppm and the doublet at δ = 7.35 ppm. A correlation is also observed between the aromatic resonance at δ = 6.58 ppm (a triplet) and the resonance at δ = 6.81 ppm.

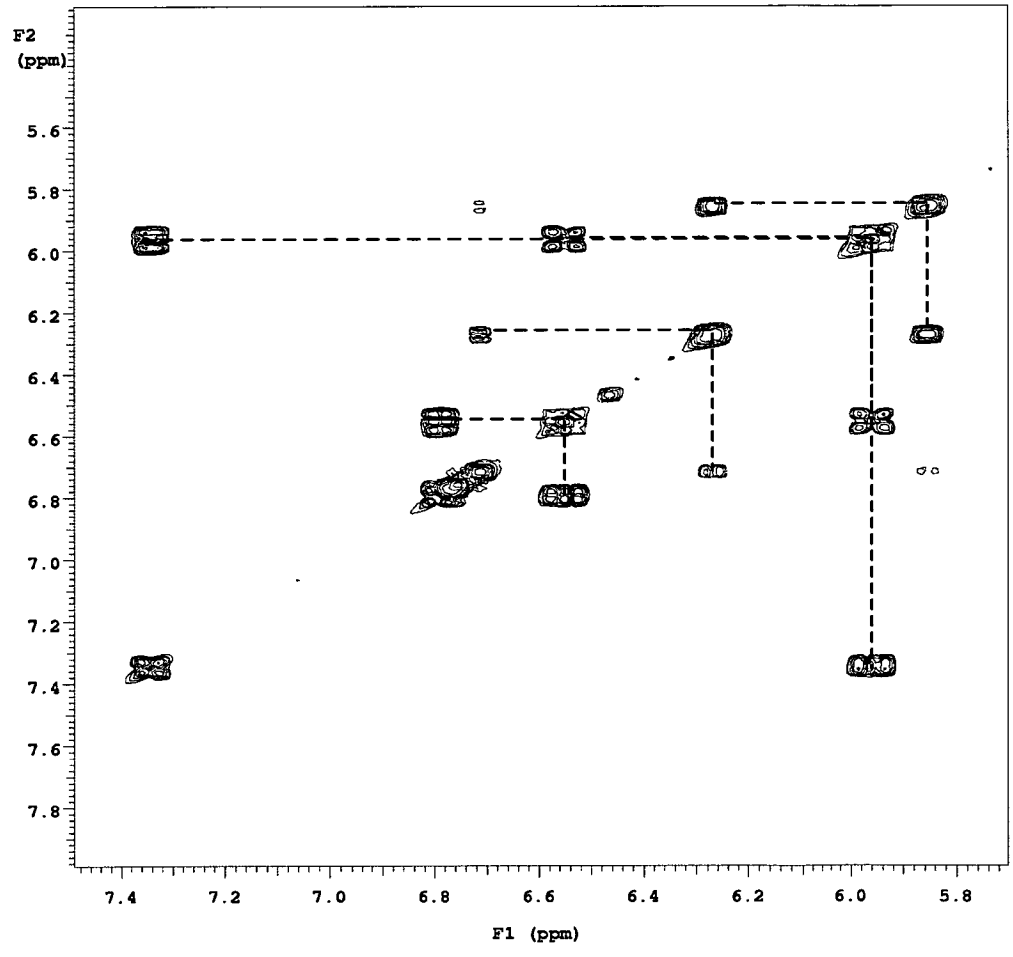

Figure 8. gCOSY NMR spectrum of **(19)**, THF-d^8 (299.90 MHz, 298 K, ppm).

As discussed in the ^{1}H NMR section for the Group 1 metal complexes the resonances at δ = 5.85 and 6.27 ppm are observed as multiplets, they can not be clearly defined as doublets or triplets. These multiplets arise from the pyrrolide

protons of the benzannulated 4-azapentalenyl anion. Correlation is observed in the gCOSY of complex **(19)** for the following pyrrolide protons: the first is between δ = 5.85 and 6.27 ppm and the second between δ = 6.27 and 6.71 ppm.

The assignment of the nonquaternary carbon resonances to their proton resonance was possible *via* the analysis of the gHMQC spectrum of complex **(19)**, as shown in Figure 19. Carbon resonances at δ = 83.3 and 83.9 ppm correlated to the pyrrolide proton resonances at δ = 6.27 and 5.85 ppm, respectively. These resonances correspond to the carbons at positions 13 and 2 of the benzannulated 4-azapentalenyl anion, respectively. The carbon resonance at δ = 98.1 ppm exhibited a correlation with the pyrrolide proton resonance at δ = 6.71 ppm. The resonance at δ = 83.3 ppm observed in the $^{13}C\{^{1}H\}$ NMR spectrum correlates to the proton H5 at 6.76 ppm.

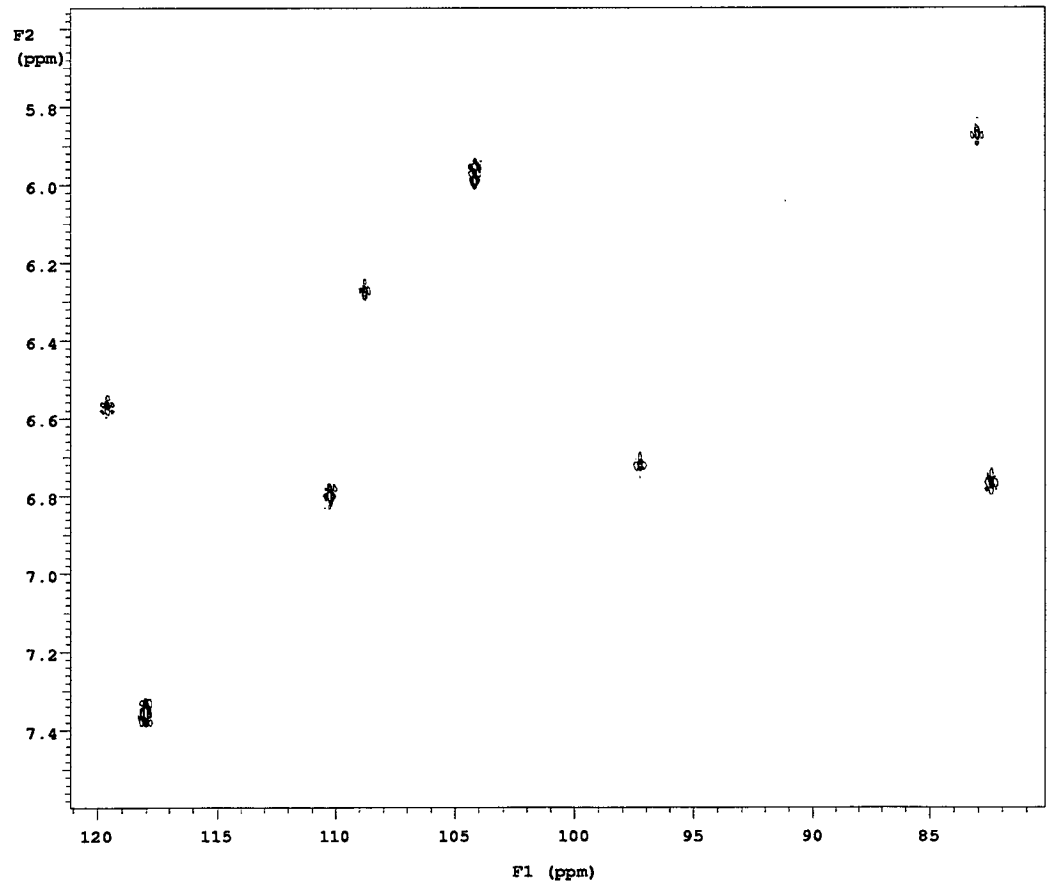

Figure 17. gHMQC of complex **(19)**, THF-d^8 (299.90 MHz, 298 K, ppm).

The connectivity of the aromatic carbon – protons of the six membered ring were confirmed *via* the following correlations observed in the gHMQC spectrum: the carbon resonance at 105.0 ppm is correlated to the proton resonance at 5.97 ppm; the resonance at 120.5 ppm in the $^{13}C\{^{1}H\}$ NMR correlates to the proton resonance at 6.58 ppm; the carbon resonance at 111.2 ppm correlates to the resonance at 6.81 ppm in the ^{1}H NMR and the carbon resonance at 118.9 ppm correlates to the observed doublet resonance at 7.35 ppm in the ^{1}H NMR spectrum.

In order to fully assign the remaining carbons and proton resonances the gHMBC spectrum of complex **(19)** was analysed, Figure 20. Correlation between the carbon resonance at 132.2 ppm and the aromatic proton resonances at 6.78 ppm and 7.35 ppm allow for the correct assignment of the quaternary carbon at position 6 in Figure 21. The correlation mentioned here also allows for the assignment of the carbon resonance at δ = 118.9 ppm and its related proton at 7.35 ppm at position 7. A correlation between the carbon resonance at δ = 118.9 ppm and the proton resonance at 6.58 ppm is observed from the gHMBC. This is reciprocated with the carbon directly connected to the proton at 6.58 ppm showing a correlation between its carbon resonance at 120.5 ppm and the proton resonance at 7.35 ppm (which in turn is connected to the carbon whose resonance is at 118.9 ppm). This allows for the assignment of the carbon resonance at 120.5 ppm and its associated proton resonance to position 7, Figure 20.

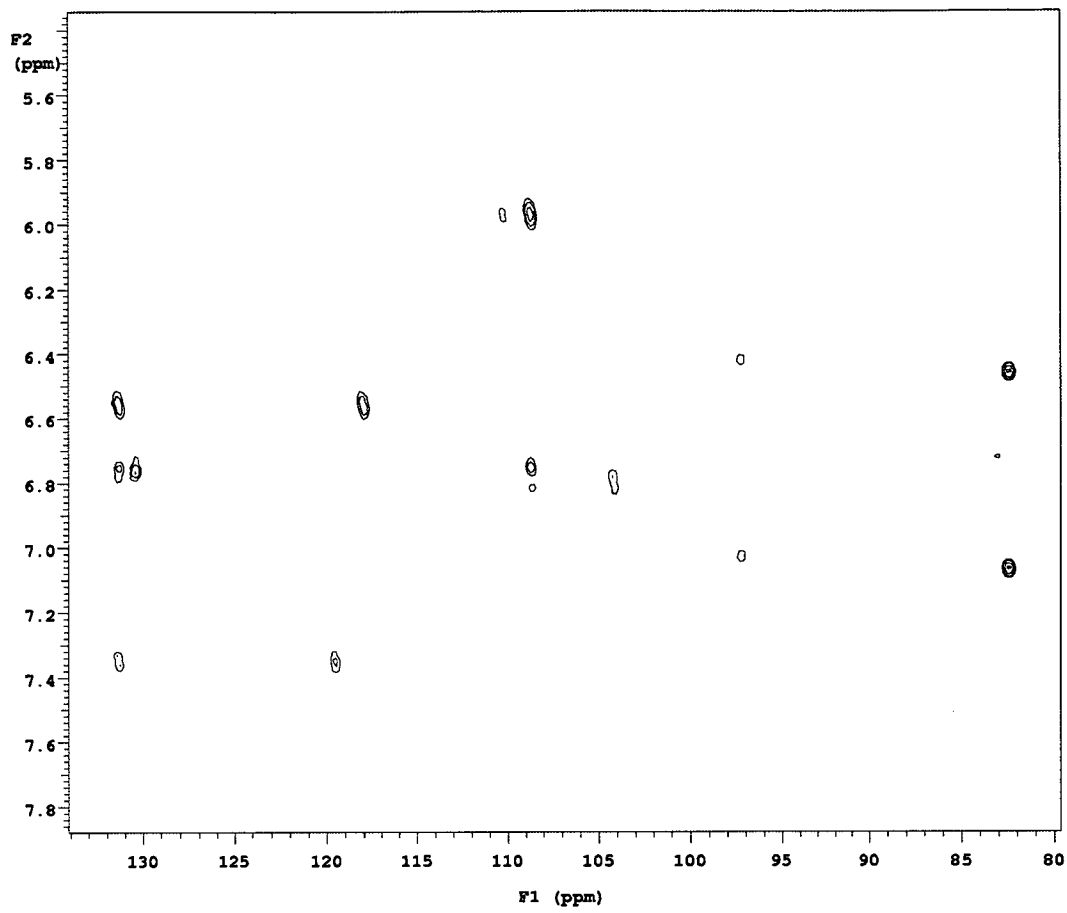

Figure20. gHMBC NMR spectrum of complex **(19),** THF-d^8 (299.90 MHz, 298 K, ppm).

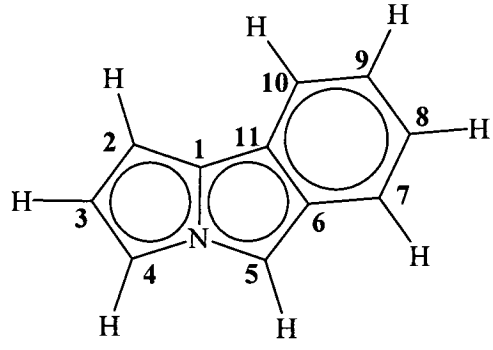

Figure 21.

From the assignment of positions 5, 6, 7 and 8 in Figure 21 it then becomes possible to fully assign the final two positions of the six membered ring of the heterocyclic anion. The carbon resonance at δ = 111.2 ppm correlates to the proton

resonance at 5.97 ppm. From this information and the multiplicity of the resonance at δ = 5.97 ppm, a triplet, seen in the ^{1}H NMR of complex **(19)** the following positions in Figure 21 were able to be determined: the carbon resonance at δ = 111.2 ppm and its connected proton, resonance of 6.81 ppm, are at position 10; and the carbon resonance at 105.0 ppm and it associated proton resonance are at position 9.

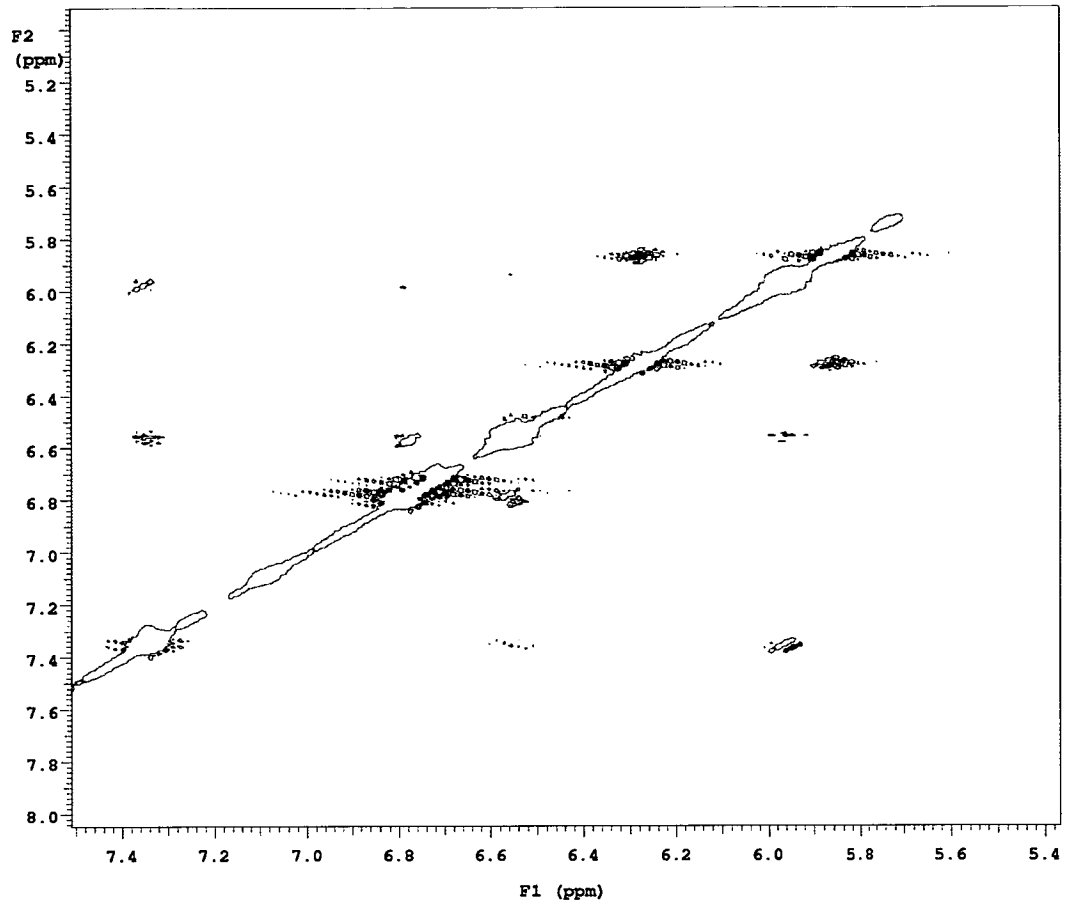

Figure 22. NOESY of complex **(19)**, THF-d^8 (299.90 MHz, 298 K, ppm).

The final assignment of the proton and carbon resonances is concerned with positions 2 and 4 of the pyrrolide section of the benzannulated 4-azapentalenyl potassium complex. The carbon resonance at 83.3 ppm is correlated with the proton resonance 6.71 ppm as seen in the gHMBC spectrum for complex **(19)**. This assignment of the proton resonance at 6.71 ppm and its respective carbon resonance to position 4 of Figure 21 was confirmed *via* the analysis of the ^{1}H – ^{1}H NOESY spectrum of complex **(19)**, Figure 22. The spectrum showed nOe enhancements between the proton resonances of the proton at δ = 6.76 ppm in position 5 and the

proton at 6.71 ppm, thus confirming the assignment for the resonance at 6.71 ppm mentioned above. This means that the carbon resonance at 83.9 ppm and its proton resonance at 5.85 ppm are at position 2. Further nOe enhancements in the spectra confirm the connectivity of previously assigned resonances which are summarised in Figure 23.

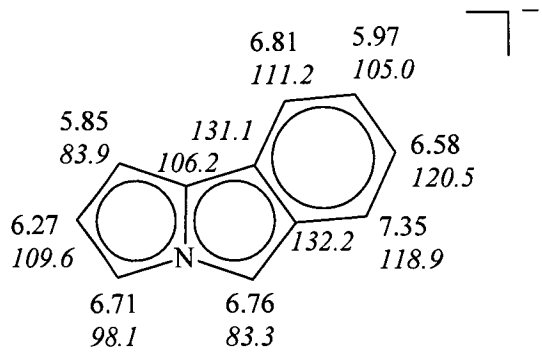

Figure 23. Full ^{1}H and ^{13}C NMR assignments for complex **(19)**, chemical shifts in ppm, ^{13}C NMR shifts in italics.

3.2.2.3 Group 1 metal 6*H*-isoindolo[2,1-a]indenyl complexes

The proton resonances in the ^{1}H NMR spectra for the benzannulated 4-azapentalenyl Group 1 complexes **(25)** and **(26)** with THF as the coordinated Lewis base occur as well resolved multiplets in the chemical shift range 6.05 – 7.56 ppm, Table 7. The expected chemical shifts for the coordinated THF for both complex **(25)** and **(26)** are masked by the resonances of the deuterated THF and are therefore not seen in the ^{1}H NMR spectra of either complex. The aromatic resonances of complexes **(25)** and **(26)** display an up field shift in comparison to the chemical shifts of the protonated parent heterocycle **(11)**. The absence of the methylene singlet at 5.10 ppm in the ^{1}H NMR for both complexes is a clear indication that deprotonation of the molecule had occurred.

Table 7. ^{1}H NMR spectral data for compounds **(11)**, **(25)** and **(26)**.†‡

	CH_2						CH – arom
	1	2	3	4	6	6	
$C_{15}H_{11}N$**(11)**	5.10			6.58			6.99, 7.09, 7.29, 7.37 (x2), 7.51, 7.55, 7.71
$[(C_{15}H_{10}N)K(THF)]$ **(25)**	-	6.05	6.10	6.55	6.68	6.84	6.99, 7.14, 7.38, 7.56
$[(C_{15}H_{10}N)Na(THF)]$ **(26)**	-	6.00	6.05	6.48	6.62	6.78	6.96, 7.09, 7.33, 7.50, 7.89

† THF-d_8 for **(11)** (299.90 MHz, 298 K, ppm), **(25)** and **(26)** (199.98 MHz, 298 K, ppm).

‡ The chemical shifts of the protons assigned for the Lewis base is typical (ppm): THF δ: 1.84 (CH_2) and 3.73 (CH_2)

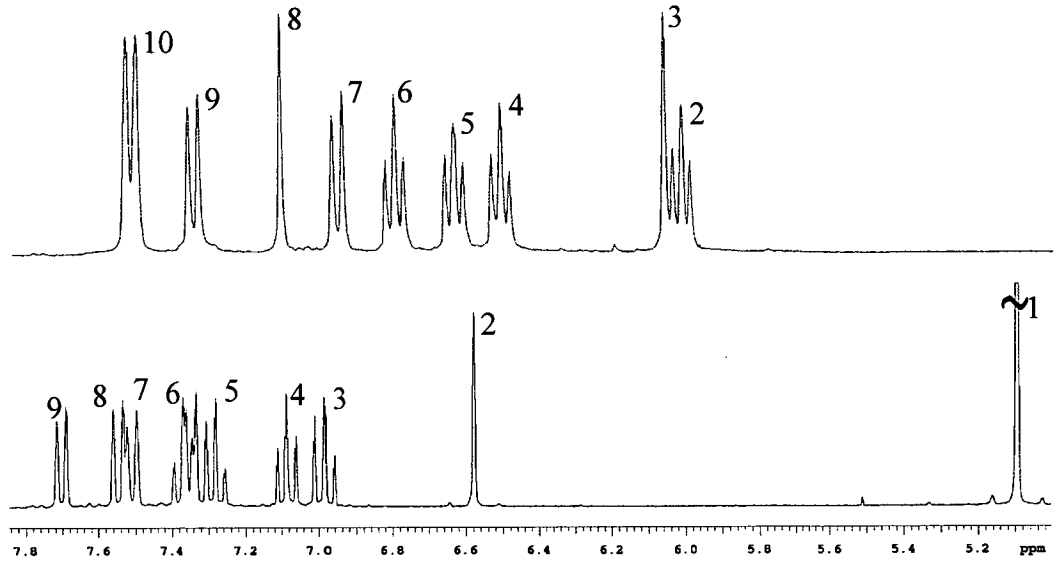

Figure 24. ^{1}H NMR spectra of complex **(25)** (a) and compound **(11)** (b), THF-d_8 for **(11)** (299.90 MHz, 298 K, ppm) and **(25)** (199.98 MHz, 298 K, ppm).

The proton chemical shifts of the potassium and sodium complexes, **(25)** and **(26)**, show only minor differences in their ^{1}H NMR spectra from each other. This similarity in chemical shift indicates a similarity in the solution state structure of these two complexes which may be due to either the ionic interactions between the metal and anion or the rapid fluxionality which can occur in these type of complexes.

Table 8. ^{13}C $\{^1H\}$ NMR spectral data for compounds **(11)**, **(25)** and **(26)**.*

	CH_2												
$C_{15}H_{11}N$ **(11)**	49.0	98.1	109.9	120.1	121.4	122.0	124.5	127.7	128.8	133.9	135.0	143.3	144.6
			113.0							134.0			
$[(C_{15}H_{10}N)K(THF)]$ **(25)**		75.7	82.7	105.8	107.6	110.1	110.5	113.3	117.7	121.6	124.0	132.3	137.0
									118.3	122.1	131.8		
$[(C_{15}H_{10}N)Na(THF)]$ **(26)**		73.5	82.4	105.4	109.3	110.4	113.2	117.3	117.8	121.7	126.1	132.0	132.3
									121.5	125.8	130.0		

* THF-d_8 for **(11)** (299.90 MHz, 298 K, ppm), **(25)** and **(26)** (199.98 MHz, 298 K, ppm).

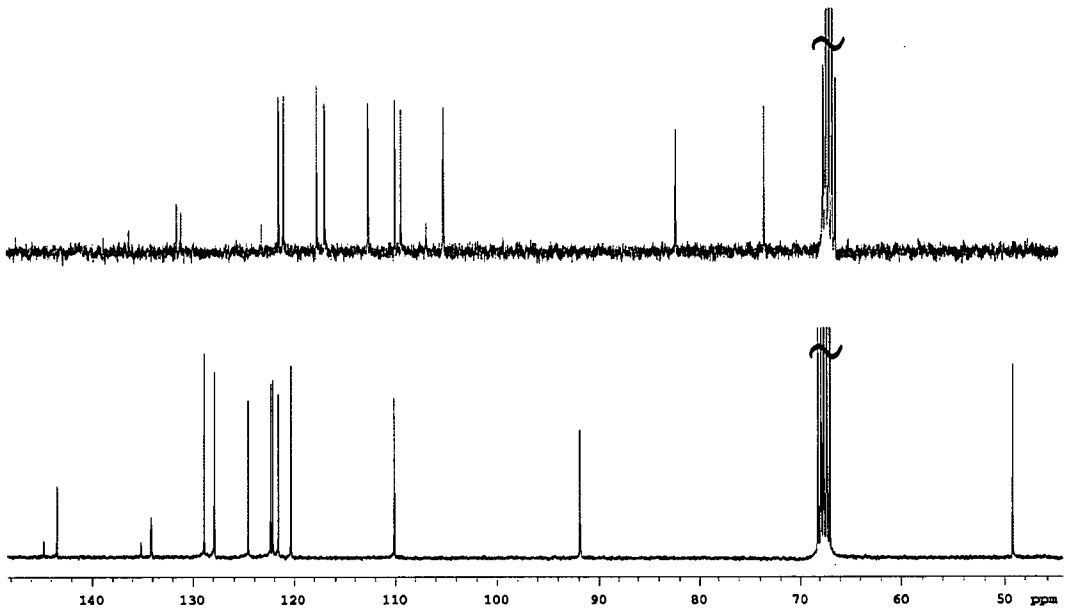

Figure 25. ^{13}C NMR spectra of complex **(25)** (a) and compound **(11)** (b)

3.2.3 Molecular Structures

3.2.3.1 Molecular structure of $[(C_{11}H_8N)K(THF)_{1/2}]$, (19)

The complex $[(C_{11}H_8N)K(THF)_{1/2}]$, **(19)**, crystallises as red prisms from a concentrated THF at ambient temperature over two weeks in the monoclinic space group *C2/c*. Complex **(19)** has 8 molecules in the unit cell with the asymmetric unit being comprised of 2 independent halves of molecules. The complex comprises two K cations which are bridged by a THF molecule, each potassium coordinates to three anions ($C_{11}H_8N$), Figure 26 a = 17.6808(2), b = 10.2199(2), c = 12.4844(4) Å, β = 102.1350(10) °. The crystals were isolated and mounted in sealed thin-walled glass capillaries under an argon atmosphere. The diffraction data was collected by Gary Fallon at the Department of Chemistry, Monash University and the structure solution and refinement carried out by Dr Michael Gardiner.

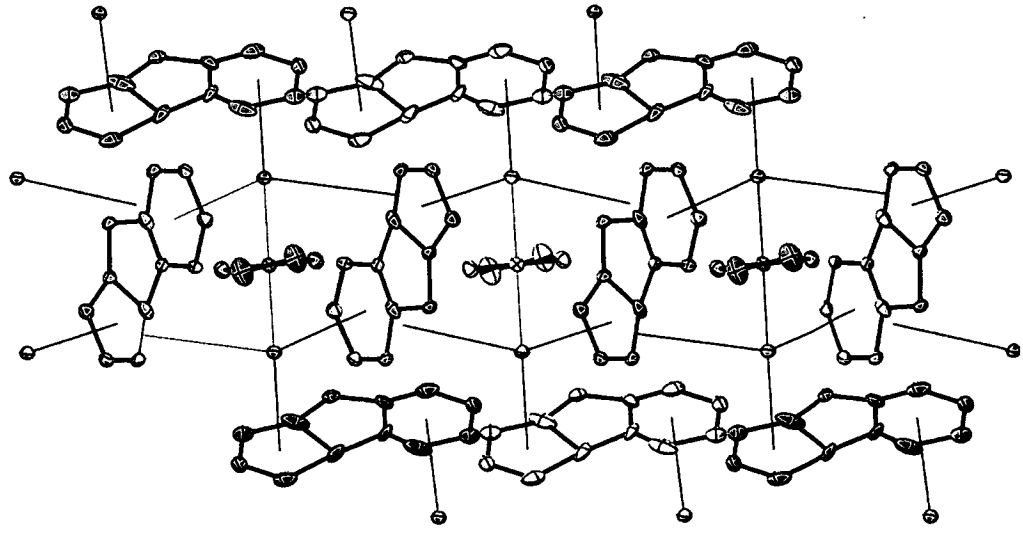

Figure 26. Molecular structure of $[(C_{11}H_8N)K(THF)_{1/2}]_n$, **(19)**, thermal ellipsoids are drawn at the level of 50% probability, hydrogens have been removed for clarity.

Compound **(19)** adopts a complex 3-dimensional polymeric lattice network in the solid state. This complex structure can be broken down in order to understand and outline the important features. A central core strand is identified as a cationic

linear polymer with one anion alternating with two potassium cations. In this projection the two potassiums are bridged *via* the oxygen of a single THF molecule, Figure 26. Complex **(19)** exhibits the multihaptic nature of the modified azapentalenyl system with numerous binding modes featuring within in the complex. The two bridged potassiums bind to two anions in the linear polymer, each potassium features η^6 – binding to the terminal six membered ring of one anion and an η^2 interaction with the terminal five membered ring of the other anion. The binding mentioned occurs on one face of the anion, different binding modes are present on the other face of the anion. The back face features an η^5 interaction between one potassium on the terminal five membered ring and an allylic interaction of the terminal six membered ring and the other potassium cation.

The cationic linear polymer features potassium cations that are exposed on the edges. This exposure of the potassium centres allows for binding interactions between adjacent anions in η^5 and η^6 fashion thus giving complex **(19)** an overall neutral charge. Due to the badly disordered structure only quantitative aspects of this work will be discussed in regards to this particular structure.

3.2.3.2 Molecular structure of $\{(C_{11}H_8N)K(TMEDA)\}_n$, (20)

The complex $\{(C_{11}H_8N)K(TMEDA)\}_n$, **(20)**, crystallised as red prisms from TMEDA at – 4 °C over two days in the triclinic space group Pī (No. 2). Complex **(20)** has a polymeric structure with eight molecules in the unit cell and the asymmetric unit comprising of four molecules, as shown in Figure 27. The complex consists of two crystallographically independent, though similar, linear zigzag polymeric strands where planar heterocyclic anions alternate with TMEDA coordinated potassium cations, (a = 10.1459(2), b = 17.4901(4), c = 20.997(5) Å, α = 77.0870(10), β = 82.899(2), γ = 82.0080(10) °). The crystals were isolated and mounted in a sealed thin-walled glass capillary under an argon atmosphere and the data collected at –100 °C. The diffraction data was collected by Dr. P. B. Hitchcock at the School of Chemistry, University of Sussex, United Kingdom.

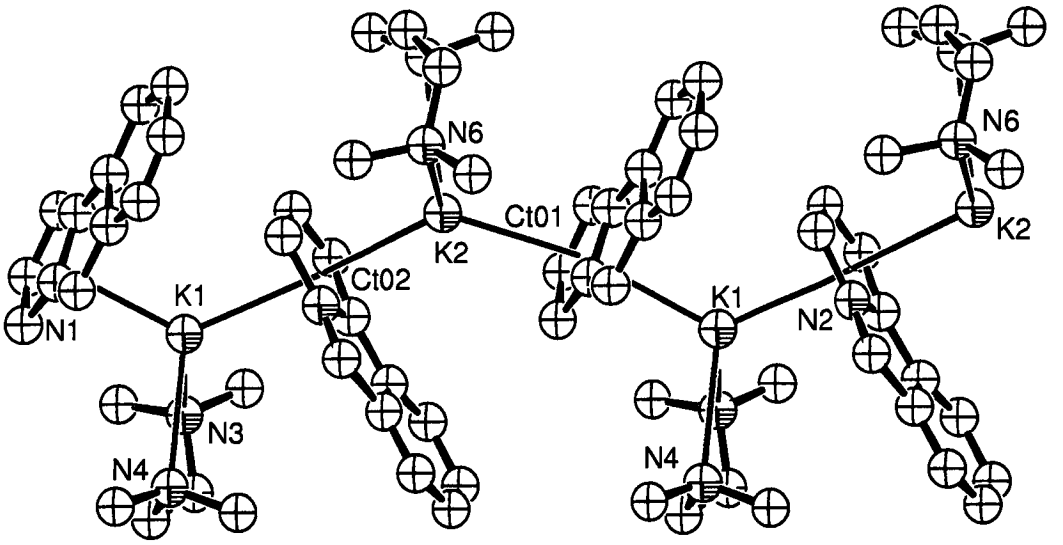

Figure 27: Molecular structure of $[(C_{11}H_8N)K(TMEDA)]_n$, **(20)**, thermal ellipsoids are drawn at the level of 50% probability, hydrogens have been removed for clarity.

Complex **(20)** adopts a polymeric structure in the solid state with the centroid-potassium-centroid angles ranging from 122.9 – 126.8 °, Figure 27. The potassium cation resides between two benzannulated 4-azapentalenyl anions, with the two

anions being at an angle of 123.4 ° to each other. The complex exhibits a slipped η^5-interaction between the potassium cation and one face of the terminal five membered ring of the anion. The chelating TMEDA molecule completes the pseudo-tetrahedral geometry of the potassium cation, with the bite angle of TMEDA (N-K-N) ranging from 64.54(9) – 65.31(10) °, these are typical angles measured for potassium complexes see Table 9.

The structure of complex **(20)** is similar to those solid-state structures that have been reported for Group 1 metal cyclopentadienyl derivative complexes, Table 11. Complexes **(20)**, **(XXV)** **(XXVI)** and **(XXVII)** all form a polymer in the solid state with the potassium cation being located between two anions, the coordination sphere of the potassium or sodium is completed *via* the chelation of a single TMEDA molecule in **(20)**, **(XXVI)** and **(XXVII)** or in the case of complex **(XV)** two pyridine molecules chelate to the potassium centre. From Table 11 it can been seen that there is very little difference in the metal-metal-metal angle when comparing the larger potassium metal centres to the smaller sodium cation with the K···K···K angle ranging from 121.8 – 126.9 °; this will be discussed in more detail later in the Chapter. No comparison has been made here with the smaller lithium cation as no analogous polymeric lithium complexes chelated by TMEDA are known, however there are reported structures for monomeric chelated lithium compounds.

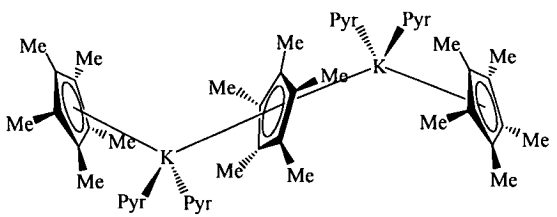

(XXV)

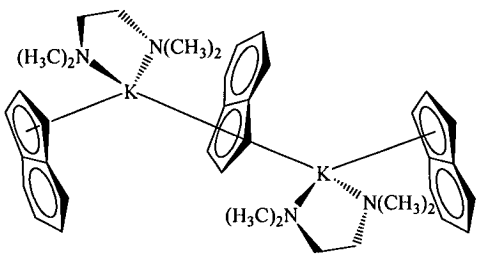

(XXVI)

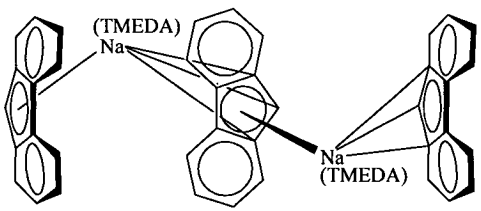

(XXVII)

Table 9.

	(20)	(XXV)[28]	(XXVI)[17]	(XXVII)[56]
M-$N_{(base)}$ (Å)	2.836(3) – 2.852(3)	2.878 – 2.975	2.865 – 2.914	2.487 – 2.535
M(4)-N(7) (Å)	3.106(4)			
M(3)-N(7) (Å)	2.868(4)			
M(4)-C(35-38) (Å)	2.994(4) – 3.151(5)	2.962 – 3.104	3.046 – 3.113	2.633 – 3.153 (η^3)
M(3)-C(35-38) (Å)	3.045(4) – 3.342(5)	2.959 – 3.104	2.952 – 3.192	2.773 – 3.162
K(4)-C(35-38) mean (Å)	3.078	3.030	3.0760	2.968 (η^3)
K(3)-C(35-38) mean (Å)	3.186	3.040	3.0760	2.979
N-K-N (°)	65.31(10)	84.270	64.013	73.94
M···M···M (°)	126.9	121.8	124.1	123.6

These linear polymeric chains of the complexes listed in Table 4 show crystallographic similarities to the unsolvated Group 1 metal cyclopentadienyl complexes. While the complexes being discussed here all have a zigzag linear polymer structure with a significant M···M···M angle the same is not true for the smaller lithium and sodium cyclopentadienyl complexes. These smaller Group 1 complexes exhibit a very linear M···M···M angle with little deviation from 180 °; 180 ° and 177.7 ° for lithium and sodium respectively.[18] In contrast to the smaller metal centres the larger potassium cyclopentadienyl complex shows a marked increase in this angle with the M···M···M angle now reported to be 138 °, Figure 28.[7,8,18]

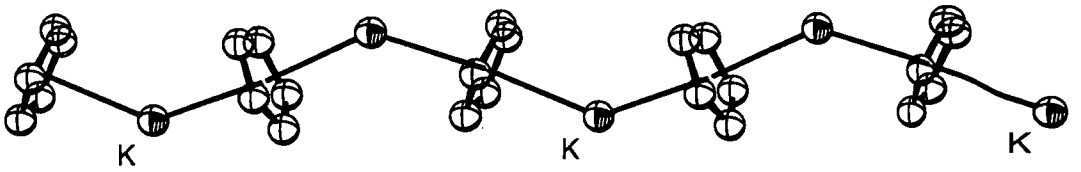

Figure 28. Molecular structure of cyclopentadienyl potassium from CCDC database. Thermal ellipsoids are are shown with arbitrary radii, hydrogens have been removed for clarity.[18]

The introduction of a chelating nitrogen Lewis base into the cyclopentadienyl complexes of Table 9 shows a change in the M···M···M angle relative to the unsolvated complexes. Little difference is observed in this angle for the larger potassium cation and the smaller sodium TMEDA containing complexes, 123.6 – 127.9 °. The TMEDA chelates to the metal cation center *via* the nitrogens leading to a pseudo tetrahedral geometry. The differences in the M – N(TMEDA) lengths seen for the potassium and sodium complexes can be attributed to the difference in the bite angles, which is directly influenced by the size of the metal centre. Whilst complex **(XXV)** has similar K – N bond lengths the bite angle N···K···N is much greater, 84.27 ° compared to 65.31(10) ° for complex **(20)**. Here the size of the Lewis base not only influences the size of the bite angle but also the M···M···M angle on the linear polymer which is now 121.8 °.

The complexes listed in Table 9 consist of only π interactions between the metal cation and the respective anions, with no σ bonds present in the complexes except those interactions between the metal cation and the chelating Lewis bases. Anions of the type shown in Table 4 all have the potential to interact with the cation *via* either face. In all complexes discussed here this potential is seen through the existence of a polymeric chain in the solid state, with each face of the anion interacting with a metal cation. In the case of complex **(20)**, the η^5 interaction between the metal and anion is with the terminal five membered ring of the tricyclic heterocycle, like wise complexes **(XXVI)** and **(XXVII)** interact with the metal cation in an η^5 fashion *via* the five membered ring only.

In comparison to the benzannulated 4-azapentalenyl potassium complex and the cyclopentadienyl potassium complex discussed above, complex **(XXVII)**, a sodium complex, differs in that now there are two types of interactions occurring between the metal cation and the fluorenyl anion, Figure 29. In this particular compound, one face of the fluorenyl anion interacts with the sodium cation through an η^5 binding mode, while in contrast the other face forms an allyl bond with another sodium cation, Figure 29. This differs to the other mentioned complexes where both faces of the anions interact with the metal centre in an η^5 binding mode. [7,8,56]

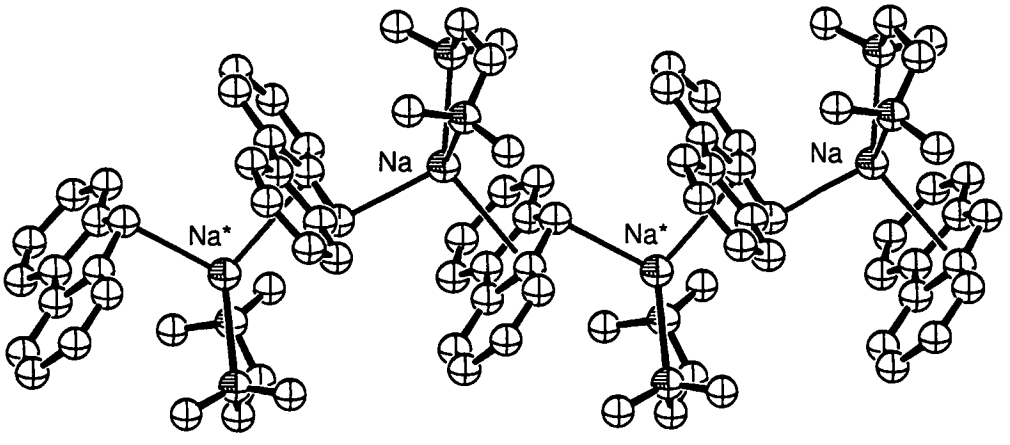

Figure 29. Molecular structure of 9*H*-fluorenyl, sodium (TMEDA) complex **(XXVII)**, X-ray crystal structure reproduced from the CCDC database. from the CCDC database. Thermal ellipsoids are shown with arbitrary radii, hydrogens have been removed for clarity.[56]

The potassium – anion distances for complex **(20)** compare closely with the other potassium cyclopentadienyl type complexes listed in Table 9 The greatest variation of bond lengths within the M – C distances in each of these structures is most noticeable for compound **(XXVII)** where the Na – C bond length varies from 2.773 – 3.162 Å for the η^5 interaction, with an even greater variation noted for the allyl bond interaction, the bond length varying 2.633 – 3.153 Å between the sodium cation and the anion. In comparison, little variation in the lengths is noted for the potassium complexes. What is noticeable, though, is the significant difference in the bond lengths of K – C and K – N for complex **(20)**. This difference in length causes a slippage of the η^5 – interactions towards the nitrogen centres, which in turn influences the K – centroid – K angle that is approaching linearity. Variation is also seen within the K – N distances with these varying from 2.868(4) – 3.016(4) Å. These varying distances are influenced by the previously mentioned ring slippage which occurs in complex **(20)**. The slippage of the ring forces the potassium centre towards the heteroatom of only one of the faces of the anion, this is where the shorter interactions are seen.

3.2.3.3 Molecular structure of [($C_{11}H_8N$)K(PMDETA)], (21)

Red needle shaped crystals of [($C_{11}H_8N$)K(PMDETA)], **(21)**, suitable for X-ray structure determination were grown from a heated PMDETA solution cooled slowly to ambient temperature over 2 days. The crystals were isolated and mounted in a sealed thin-walled glass capillary under an argon atmosphere. The crystals belong to the orthorhombic $P2_12_12_1$ space group, a = 10.3397(16), b = 11.4447(17), c = 17.755(3) Å, with four molecules in the unit cell, the asymmetric unit consisting of one molecule of [($C_{11}H_8N$)K(PMDETA)], **(21)**, as shown in Figure 30.

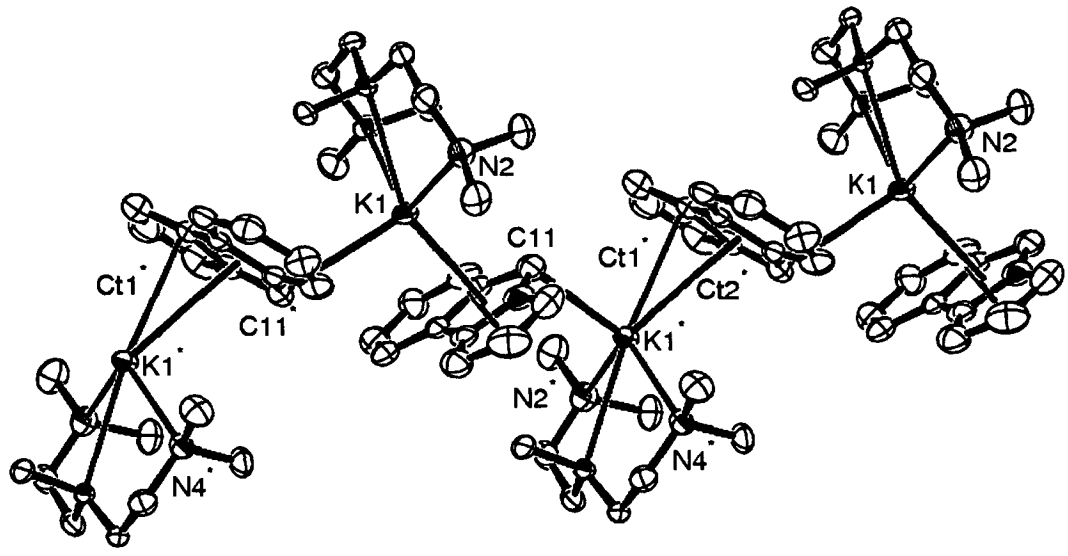

Figure 30: Molecular structure of $[(C_{11}H_8N)K(PMDETA)]_n$, **(21)**, thermal ellipsoids are drawn at the level of 50% probability, hydrogens have been removed for clarity.

Complex **(21)** exhibits a polymeric structure in the solid state similar to that of complex **(20)** discussed in Section 3.2.3.2. The solid state structure of **(21)** is comprised of the 5*H*-pyrrolo[2,1-a]isoindole anion with the charge being counter balanced by a potassium cation. This same potassium cation then interacts with another like anion to give rise to the polymeric strand which is observed. The coordination sphere of the potassium is completed *via* its chelation to a single PMEDTA molecule through coordination with the three nitrogen atoms present. The K···K···K angle in complex **(21)** is more acute than that observed and reported earlier for complex **(20)**, with the angle decreasing from 126.9 ° to 119.7 °. The K···K···K angle observed for complex **(21)** is quite different to that seen in the analogous potassium indenyl complex **(XXVIII)** whose angle was reported to be 125.1°.[17] Both these complexes exist as polymers in the solid state, which is comprised of a cation interacting with two anions, the cation anion ratio however is still 1:1, with the coordination sphere of the potassium completed through the chelation of a single PMDETA entity; this can be seen in Figure 30 for complex **(21)**.

Both complexes exhibit similar potassium nitrogen (PMDETA nitrogens) bond lengths with these varying between 2.874 and 2.954 Å, however this is not true for the potassium carbon bond lengths where some slight variation is seen. This may

be due to the different types of metal anion interaction present in each of these complexes; both exhibit two different binding modes between the anion and the potassium cation in the solid state structures. The anion of 5*H*-pyrrolo[2,1-a]isoindole interacts with a potassium cation *via* both of its faces, in this particular case each face exhibits a different binding mode with a metal cation, either an η^8 or an η^1 interaction is observed. The observed η^8 interaction is between the five membered rings of the heterocyclic anion and the potassium centre whilst the second interaction seen for the same anion, however on its opposing face, is that of an η^1 nature between the formerly sp^2 carbon of the central five membered ring and a second potassium centre. The centroid bond lengths between each five membered ring in the system and the potassium centre show a small variation with the internal five membered ring being slightly longer than that between the terminal five membered ring and the potassium centre and longer than the average potassium carbon bond length.. The η^1 bond length in this complex (3.103 Å) is only marginally shorter in comparison to the average of the metal centroid distances (3.108 Å). This may explain why very minimal to no folding is experienced in this particular complex, the dihedral angle between the azapentalenyl section of the benzannulated derivative was found to be 0.9 °.

In comparison to complex **(21)** the reported indenyl analogue **(XXVIII)** appears quite similar with minimal folding observed in the dihedral angle between the five and six membered rings, 0.27 °; this leads to the planar anion seen in this complex.[17] Like **(21)** the potassium indenyl complex consists of two different types of binding modes, this time however η^5 and η^3 interactions between a single indenyl anion and two different potassium centres are observed in the polymer. The difference observed in **(21)** regarding the bond lengths for each interaction between the potassium and the anion is also observed in **(XXVIII)** however in the case of **(XXVIII)** the η^5 interaction and η^3 interaction differ markedly (3.120 and 3.253 Å, respectively) when compared to the difference in average bond length observed for complex **(21)**, see Table 10. Both these complexes exist as a bent polymer in the solid state with complex **(21)** exhibiting a slightly more bent polymer than **(XXVIII)**.

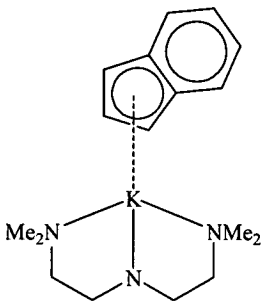

(XXVIII)
(polymer)

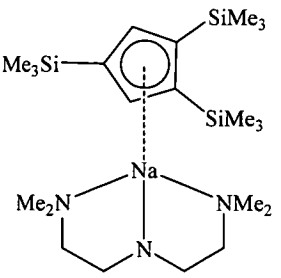

(XXIX)

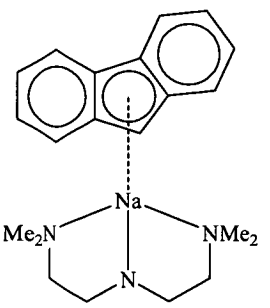

(XXX)

Table 10.

	(21)	(XXVIII)[17]	(XXIX)[57]	(XXX)[56]
M-N distance (Å)	2.874 – 2.898	2.871 – 2.954	2.530 – 2.648	2.442 – 2.457
M-C distance (Å)	3.096 – 3.119	3.195 – 3.298 (η^3)	2.711 – 2.859	2.620 – 3.043
	3.103 (η^1)	3.093 – 3.156		
M-C mean (Å)	3.108	3.253 (η^3)	2.782	2.831
		3.120		
M'-M-M" (°)	119.66	125.09	monomer	monomer

In comparison to the polymeric complexes **(21)** and **(XXVIII)**, compounds **(XXIX)** and **(XXX)** have monomeric solid state structures. As well as being monomeric, these complexes only exhibit one binding mode between the metal centre and the anion, in both these cases this is an η^5 interaction. These η^5 interactions have a shortened carbon – metal bond distance in comparison to the η^5 interactions which are observed in the polymeric complexes. Whilst the interaction between the anion and metal are slightly different, what does remain constant is the geometry of the heterocyclic anion. Complex **(XXX)** exhibits a flat geometry with minimal folding of the fluorenyl like those previously discussed for complexes **(21)** and **(XXVIII)**; 1.49 ° and 0.69 ° between the six membered rings and the five membered ring of the fluorenyl, respectively.

3.2.3.4 Molecular structure of $[(C_{11}H_8N)K(18\text{-crown-6})]$ (22)

Red crystals of $[(C_{11}H_8N)K(18\text{-crown-6})]$, **(22)**, suitable for X-ray structure determination were grown by storing a THF solution at –4 °C for two days. The crystals were isolated and mounted in a sealed thin-walled glass capillary under an argon atmosphere. Preliminary refinement has revealed a monomeric complex in which the potassium centre binds above the C-N bridgehead atoms. The potassium centre is bound by the 18-crown-6 and an additional weak THF interaction. The complex is severely disordered and full data has not been released by Professor Allan White, University of Western Australia.

Table 11 gives selected structural data for a range of related 18-crown-6 cyclopentadienyl type potassium complexes which have been isolated as monomeric species. Complex **(23)** is similar in structure to these Group 1 metal cyclopentadienyl complexes where the multidentate Lewis bases are observed to break up the polymers giving the monomer.

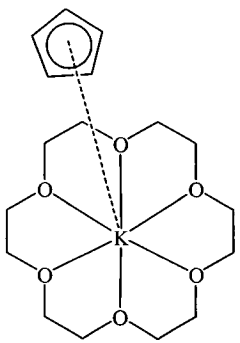

(XXXI)

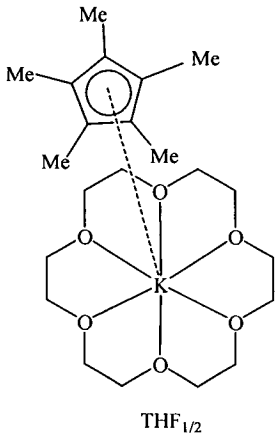

(XXXII)

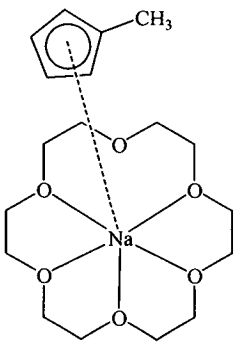

(XXXIII)

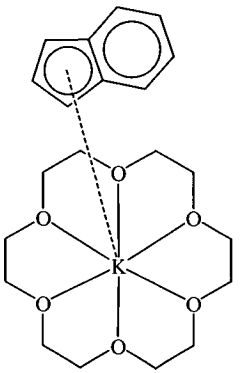

(XXXIV)

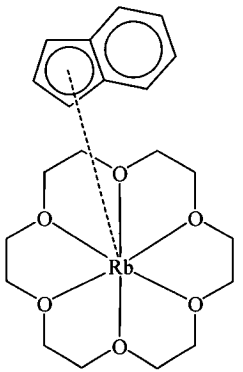

(XXXV)

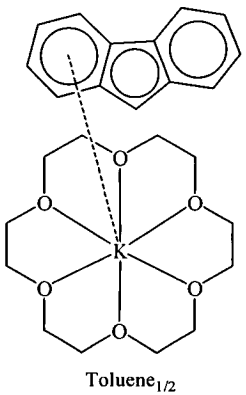

(XXXVI)

Table 11.

	(22)	(XXXI)[23]	(XXXII)[23]	(XXXIII)[15]	(XXXIV)[23]	(XXXV)[27]	(XXXVI)[23]
K-O distance (Å)		2.787 – 2.946	2.853 – 3.056	2.712 – 2.932	2.792 – 2.957	2.843 –3.033	2.785 – 2.959
K-O mean (Å)		2.901	2.967	2.823	2.880	2.940	2.847
K-C distance (Å)		2.970 – 3.130	3.066 – 3.124	2.602 – 3.037	3.065 – 3.153	3.178 – 3.209	3.239 – 3.371
K-C mean (Å)		3.058	3.093	2.806	3.104	3.193	3.354
O-K-O (°)		57.07 – 59.02	55.34 – 56.77		57.32 – 59.46	56.75 – 58.93	57.37 – 60.15
O-K-O mean (°)		58.04	56.34		58.45	57.63	59.04

3.3 EXPERIMENTAL

3.3.1 Group 1 metal 4-azapentalenyl complexes

Synthesis of $(C_7H_6N)K$, **(17)**

To a stirred solution of 3*H*-pyrrolizine, **(5)**, (1.20 g, 11.41 mmol) in dry tetrahydrofuran (20 mL) potassium metal (0.5 g, 12.9 mmol) was added along with 1,2-dimethoxyethane (50 mL). The reaction was sealed under argon and left to stir for 12 hours at ambient temperature. The colour of the reaction changed during the course of the reaction through yellow, to orange, red, a deeper red, purple, brown and finally green. The reaction mixture was filtered from the unreacted potassium metal and the solution was then concentrated *in vacuo* to *ca.* 10 mL and stored at –30 °C overnight, however no crystalline solid was isolated. The remaining solvent was removed to yield a green solid (380 mg, 16 %).

^{1}H NMR (THF-d_8, 299.90 MHz, 298 K, ppm): δ 4.78 (m, 2H, CH), 6.07 (s, 2H, CH), 6.38 (s, 2H, CH).
^{13}C{^{1}H} NMR (THF-d_8, 75.4 MHz, 298 K, ppm): δ 74.8 (CH), 94.4 (CH), 112.0 (CH), 139.4(C).

Synthesis of $(C_7H_6N)Li$, **(18)**

To a stirred solution of 3*H*-pyrrolizine, **(5)**, (322 mg, 3.07 mmol) in hexane (15 mL) *n*-butyl lithium (2.5 g, 24.5 mL, 39 mmol, 1.6M in hexanes) was added dropwise. The solution was stirred at ambient temperature for 3 hours during which time a precipitate formed and the solution became blue in colour. The reaction mixture was then centrifuged and the pale, green solution separated from the bright blue solid. The solid was dissolved in tetrahydrofuran (5 mL) to give a dark blue-green solution. This solution was concentrated *in vacuo* to *ca.* 4 mL and cooled to –4 °C overnight during which time a blue-green crystalline solid formed. An attempt to isolate the crystalline solid for X-ray structure determination lead to the decomposition of the complex to a powder.

^{1}H NMR (THF-d_8, 399.78 MHz, 298 K, ppm): δ 4.77 (s, 2H, CH), 6.06 (s, 2H, CH), 6.47 (s, 2H, CH).

^{13}C{^{1}H} NMR (THF-d_8, 100.5 MHz, 298 K, ppm): δ 72.1 (CH), 95.9 (CH), 110.4 (CH), 141.2 (C).

3.3.2 Group 1 metal 4-azapentalenyl modified complexes

Synthesis of [$(C_{11}H_8N)K(THF)_{1/2}$], **(19)**

To a stirred solution of 5*H*-pyrrolo[2,1-a]isoindole, **(9)**, (1.00 g, 6.44 mmol) in tetrahydrofuran (50 mL) potassium metal (500 mg, 12.8 mmol) was added. The colour of the reaction solution changed from a clear colourless solution to a bright red solution. The reaction was sealed under argon and stirred at ambient temperature for 12 hours, after which time the colour of the solution had become a deep blood red colour. The solvent was concentrated *in vacuo* to *ca.* 10 mL. Upon cooling to –4 °C overnight red crystals suitable for X-ray structure determination formed (1.36 g, 93%).

^{1}H NMR (THF-d_8, 299.90 MHz, 298 K, ppm): δ 5.85 (d, $^3J_{H\text{-}H}$ = 3.13 Hz, **H2**), 5.97 (t, $^3J_{H\text{-}H}$ = 7.11 Hz, **H9**), 6.27 (m, b, **H3**), 6.58 (t, $^3J_{H\text{-}H}$ = 7.55 Hz, **H8**), 6.71 (s, **H4**), 6.76 (s, **H5**), 6.81 (d, $^3J_{H\text{-}H}$ = 8.41 Hz, **H10**), 7.35 (d, $^3J_{H\text{-}H}$ = 7.78 Hz, **H7**).

^{13}C{^{1}H} NMR (THF-d_8, 75.4 MHz, 298 K, ppm): δ 83.3 (**C5**), 83.9 (**C2**), 98.1 (**C4**), 105.0 (**C9**), 106.2 (**C1**), 109.6 (**C3**), 111.2 (**C10**), 118.9 (**C7**), 120.5 (**C8**), 131.3 (**C11**), 132.2 (**C6**).

Anal. Calcd.: C, 67.71; H, 5.25; N, 6.08 ($C_{13}H_{12}KNO_{1/2}$, MW 261.36).
Found: C, 67.68; H, 5.29; N, 6.08.

Synthesis of [$(C_{11}H_8N)K(TMEDA)$], **(20)**.

To a stirred solution of 5*H*-pyrrolo[2,1-a]isoindole, **(9)**, (517 mg, 3.33 mmol) in tetrahydrofuran (50 mL), potassium metal (250 mg, 6.39 mmol) was added. The

colour of the reaction solution changed from a clear colourless solution to a bright red solution. The reaction was sealed under argon and stirred at ambient temperature for 12 hours, after which time the colour of the reaction solution had gone a deep blood red colour. The solvent was removed *in vacuo* to give an oily red residue which was dissolved in *N,N,N',N'*-tetramethylethylenediamine (20 mL, 153 mmol). The solution was stirred at ambient temperature for 2 hours, after which time the solution was filtered from the undissolved solid. The reaction solution was concentrated to 15mL *in vacuo*. Upon cooling to –4 °C overnight red crystals suitable for X-ray structure determination were obtained (0.95g, 92%).

^{1}H NMR (pyr-d_5, 300.13 MHz, 300K, ppm): δ 2.16 (s, 12H, CH_3), 2.35 (s, 4H, CH_2), 6.56 (pt, $^3J_{H\text{-}H}$ = 8.0 Hz, 1H, CH), 6.62 (m, 1H, CH), 6.93 (m, 1H, CH), 7.16 (pt, $^3J_{H\text{-}H}$ = 8.2Hz, 1H, CH), 7.44 (m, 2H, CH), 7.46 (m, 1H, CH), 8.00 (d, $^3J_{H\text{-}H}$ = 8.2 Hz, 1H, CH).

^{13}C{^{1}H} NMR (pyr-d_5, 75.4 MHz, 300K, ppm): δ 46.0 (CH_3), 58.2 (CH_2), 84.32 (CH), 85.0 (CH), 99.0 (CH), 105.1 (CH), 109.9 (CH), 110.2 (=CR), 111.4 (CH), 119.4 (CH), 120.6 (CH), 131.5 (=CR), 132.0 (=CR)

Anal. Calcd.; C, 65.97; H, 7.82; N, 13.58 ($C_{17}H_{24}KN_3$, MW 309.49).
Found; C, 66.08; H, 7.58; N,13.24

Synthesis of [($C_{11}H_8N$)K(PMDETA)], **(21)**

To a stirred solution of 5*H*-pyrrolo[2,1-a]isoindole, **(9)**, (1.00 mg, 6.43 mmol) in tetrahydrofuran (25 mL), potassium metal (500 mg, 12.8 mmol) was added. A colour change was noted from a clear colourless reaction solution to a bright red solution. The reaction was sealed under argon and stirred at ambient temperature for 12 hours, after which time the reaction mixture was concentrated *in vacuo* to yield a red oily residue. The residue was dissolved in a mixture of *N,N,N',N',N''*-pentamethyldiethylenetriamine (20 mL, 95 mmol) and tetrahydrofuran (5 mL). The reaction solution was then filtered from any undissolved residue before concentrating to *ca.* 15 mL *in vacuo* during which red needle shaped crystals formed at ambient temperature. The crystals were redissolved with gentle heating and cooled slowly to ambient temperature upon which crystals suitable for X-ray structure determination were obtained (1.2 g, 51%).

^{1}H NMR (THF-d_8 , 199.98 MHz, 298 K, ppm): δ): δ 2.15 (s, 12H, CH_3), 2.25 (s, 8H, CH_2), 2.36 (s, 3H, CH_3), 5.88, 5.98 , 6.17, 6.30, 6.55, 7.36, 7.44 (2H).

Anal. Calcd.; C, 65.53; H, 8.52; N, 15.28 ($C_{20}H_{31}KN_4$, MW 366.59).
Found; C, 65.61; H, 8.62; N, 15.13

Synthesis of [($C_{11}H_8N$)K(18-crown-6)], **(22)**

To a stirred solution of 5*H*-pyrrolo[2,1-a]isoindole, **(9)**, (1.03 g, 6.64 mmol) in tetrahydrofuran (50 mL), potassium metal (500 mg, 12.8 mmol) was added. A colour change in the reaction mixture was noted from a clear colourless solution to a bright red solution. The reaction was sealed under argon and stirred at ambient temperature for 12 hours after which time the solution was concentrated *in vacuo* to 15 mL. A tetrahydrofuran solution (15 mL) of dried 18-crown-6[23] (360 mg, 1.36 mmol) was added. The solution was stirred for 24 hours at ambient temperature after which time the reaction mixture was concentrated to *ca.* 10 mL *in vacuo*. Red prism shaped crystals formed at ambient temperature, which were redissolved with gentle heating and cooled slowly to ambient temperature during which time crystals suitable for X-Ray structure determination were obtained (1.49 mg, 50 %).

^{1}H NMR (THF-d_8 , 299.90 MHz, 298 K, ppm): δ 3.35 (s, 24H, CH_2), 5.88 (d, $^3J_{H\text{-}H}$ = 3.59 Hz, 1H), 6.26 (t, $^3J_{H\text{-}H}$ = 7.17 Hz, 1H), 6.54 (m, 1H), 6.76 (m, 2H), 6.79 (s, 1H), 7.36 (m, 2H).

^{13}C{^{1}H} NMR (THF-d_8 , 75.4 MHz, 298 K, ppm): δ 38.9 (O-CH_2), 81.9 (C), 82.0 (C), 95.9 (C), 101.8 (C), 106.8 (C), 108.7 (C), 116.8 (C), 117.8 (C), 129.9 (C), 130.1 (C).

Anal. Calcd.; C, 60.86; H, 7.66; N, 2.96 ($C_{23}H_{32}KNO_6$, MW 457.60).
Found; C, 60.90; H, 7.59; N, 2.89.

Synthesis of [($C_{11}H_8N$)K(dibenzo-18-crown-6)], **(23)**.

To a stirred solution of 5*H*-pyrrolo[2,1-a]isoindole, **(9)**, (510 mg, 3.29 mmol) in tetrahydrofuran (50 mL), potassium metal (250 mg, 6.39 mmol) was added. A colour change in the reaction mixture was noted from a clear colourless solution to a bright

red solution. The reaction was sealed under argon and stirred at ambient temperature for 12 hours after which time the solution was filtered from the unreacted potassium metal. A stirred solution of dried dibenzo-18-crown-6 (1.07 g, 2.97 mmol) in tetrahydrofuran (25 mL) was added to the reaction mixture. The solution was stirred for an hour after which time the reaction mixture was concentrated *in vacuo* to *ca.* 35 mL. No crystalline solid was isolated upon cooling to –4 °C, however a red solid was isolated (720 mg, 45%).

Anal. Calcd.; C, 67.25; H, 5.83; N, 2.53 ($C_{31}H_{32}KNO_6$, MW 553.69).
Found; C, 67.31; H, 5.86; N, 2.49.

Synthesis of $[(C_{11}H_8N)Na(THF)_n]$, **(24)**

To a stirred suspension of sodium hydride (180 mg, 7.50 mmol) in tetrahydrofuran (25 mL), a solution of 5*H*-pyrrolo[2,1-a]isoindole, **(9)**, (1.10 g, 7.08 mmol) in tetrahydrofuran (20 mL) was added. The reaction mixture was heated at 90 °C under argon for 72 hours after which time the colour of the reaction solution changed from a colourless solution to a deep red colour. The reaction mixture was filtered from any unreacted sodium hydride and the solvent concentrated *in vacuo* to *ca.* 15 mL. No crystalline material was isolated upon cooling to –4 °C. Any solid that was obtained contained a mixture of complex **(24)** and the parent heterocycle **(9)**. The NMR results were obtained by repeating the experiment on an NMR scale in THF-d_8.

^{1}H NMR (THF-d_8, 299.90 MHz, 298 K, ppm): δ 5.87 (d, $^3J_{H\text{-}H}$ =3.69 Hz, CH,), 5.96 (t, $^3J_{H\text{-}H}$ = 6.73 Hz, CH), 6.27 (t, $^3J_{H\text{-}H}$ = 3.09 Hz, CH), 6.57 (t, $^3J_{H\text{-}H}$ = 7.73 Hz, CH), 6.76 (s, CH), 6.81 (m, CH), 7.36 (d, ^{3}J = 7.91 Hz, CH).

^{13}C{^{1}H} NMR (THF-d_8, 75.4 MHz, 298 K, ppm): δ 82.9, 83.2, 98.4, 104.6, 108.8, 109.9, 110.6, 118.5, 120.1, 131.5, 132.1.

Synthesis of $[(C_{15}H_{10}N)K(THF)]$, **(25)**

To a stirred solution of 6*H*-isoindolo[2,1-a]indole, **(11)**, (990 mg, 4.82 mmol) in tetrahydrofuran (50 mL) potassium metal (210 mg, 5.37 mmol) was added. The reaction was sealed under argon and stirred for 72 hours at 85 °C after which time the colour of the reaction mixture changed from colourless to a deep purple. The reaction mixture was filtered from the unreacted potassium metal. Decomposition of complex **(25)** occurred during the attempt to isolate a crystalline solid. The NMR results were obtained by repeating the experiment on an NMR scale in THF-d_8, however potassium hydride was used in place of potassium metal.

^{1}H NMR (THF-d_8, 199.99 MHz, 298 K, ppm): δ 6.05 (t, $^3J_{H\text{-}H}$ = 6.84 Hz), 6.10 (s), 6.55 (t, $^3J_{H\text{-}H}$ = 7.43 Hz), 6.68 (t, $^3J_{H\text{-}H}$ = 7.23 Hz), 6.84 (t, $^3J_{H\text{-}H}$ = 7.37 Hz), 6.99 (d, $^3J_{H\text{-}H}$ = 8.60 Hz), 7.14 (s), 7.38 (d, $^3J_{H\text{-}H}$ = 8.10 Hz), 7.56 (d, $^3J_{H\text{-}H}$ = 8.20 Hz).

^{13}C{^{1}H} NMR (THF-d_8, 75.4 MHz , 298 K, ppm): δ 75.7, 82.7, 105.8, 107.6, 110.1, 110.5, 113.3, 117.7, 118.3, 121.6, 122.1, 124.0, 131.8, 132.3, 137.0.

Synthesis of $[(C_{15}H_{10}N)Na(THF)]$, **(26)**

To a stirred suspension of sodium hydride (63 mg, 26 mmol) in tetrahydrofuran (10 mL) a solution of 6*H*-isoindolo[2,1-a]indole, **(11)**, (500 mg, 2.43 mmol) in tetrahydrofuran (15 mL) was added. The reaction mixture was heated at 85 °C under argon with stirring for 72 hours during which time the colour of the reaction solution changed from colourless to a deep purple colour. The reaction solution was filtered from any unreacted sodium hydride before removing the tetrahydrofuran *in vacuo* to give **(26)** as an oily residue. This residue did not give clear NMR spectra and for this reason the experiment was repeated on an NMR scale in THF-d_8.

^{1}H NMR (THF-d_8, 199.98 MHz, 298 K, ppm): δ 6.00 (t, $^3J_{H\text{-}H}$ = 7.39 Hz), 6.05 (s), 6.48 (t, $^3J_{H\text{-}H}$ = 7.27 Hz), 6.62 (t, $^3J_{H\text{-}H}$ = 7.58 Hz), 6.78 (t, $^3J_{H\text{-}H}$ = 7.46 Hz), 6.96 (d, $^3J_{H\text{-}H}$ = 8.54 Hz), 7.09 (s), 7.33 (d, $^3J_{H\text{-}H}$ = 7.96 Hz), 7.50 (d, $^3J_{H\text{-}H}$ = 7.89 Hz).

$^{13}C\{^{1}H\}$ NMR (THF-d_8, 75.4 MHz , 298 K, ppm): δ 73.5, 82.4, 105.4, 109.3, 110.4, 113.2, 117.3, 117.8, 121.5, 121.7, 125.8, 126.1, 130.0, 132.0, 132.3.

3.4 REFERENCES

(1) Okamura, W. H.; Katz, T. J. *Tetrahedron* **1967**, *23*, 2941-2957.

(2) Thiele, J. *Chem. Ber.* **1901**, *34*, 68-71.

(3) Kealy, T. J.; Paulson, P. L. *Nature (London)* **1951**, *168*, 1039-1040.

(4) Jutzi, P.; Burford, N. *Chem. Rev.* **1999**, *99*, 969-990.

(5) Eiland, P. F.; Pepinsky, R. *J. Am. Chem. Soc.* **1952**, *74*, 4971-4971.

(6) Brock, C. P.; Yigang, F.
Acta Crystallogr., Sect. B : Struct. Sci. **1997**, *53*, 928-938.

(7) Allen, F. H. *Acta Crystallogr.* **2002**, *B58*, 380-388.

(8) Bruno, I. J.; Cole, J. C.; Edgington, P. R.; Kessler, M.; Macrae, C. F.; McCabe, P.; Pearson, J.; Taylor, R. *Acta Crystallogr.* **2002**, *B58*, 389-397.

(9) Collman, J. P.; Hegedus, L. S.; Norton, J. R.; Finke, R. G. *Principles and Applications of Organotransition Chemistry*; University Science Books: Mill Valley, 1987.

(10) Poli, R. *Chem. Rev.* **1991**, *91*, 509-551.

(11) Jutzi, P. *J. Organomet. Chem.* **1990**, *400*, 1-17.

(12) O'Connor, J. M.; Casey, C. P. *Chem. Rev.* **1987**, *87*, 307-318.

(13) Panda, T. K.; Gamer, M. T.; Roesky, P. W.
Organometallics **2003**, *22*, 877-878.

(14) Harvey, M. J.; Hanusa, T. P.; Pink, M.
J. Chem. Soc., Dalton Trans. **2001**, 1128-1130.

(15) Cole, M. L.; Jones, C.; Junk, P. C.
J. Chem. Soc., Dalton Trans. **2002**, 896-905.

(16) Aoyagi, T.; Shearer, H. M. M.; Wade, K.; Whitehead, G.
J. Organomet. Chem. **1979**, *175*, 21-31.

(17) Jordan, V.; Behrens, U.; Olbrich, F.; Weiss, E.
J. Organomet. Chem. **1996**, *517*, 81-88.

(18) Dinnebier, R. E.; Behrens, U.; Olbrich, F.
Organometallics **1997**, *16*, 3855-3858.

(19) Röhl, H.; Lange, E.; Gossl, T.; Roth, G. *Angew. Chem.* **1962**, *74*, 155-155.

(20) King, R. B. *Coord. Chem. Rev.* **1976**, *20*, 155-169.

(21) Threlkel, R. S.; Bercaw, J. E. *J. Organomet. Chem.* **1977**, *136*, 1-5.

(22) Jutzi, P.; Reumann, G. *J. Chem. Soc., Dalton Trans.* **2000**, *14*, 2237-2244.

(23) Neander, S.; Tio, F. E.; Buschmann, R.; Behrens, U.; Olbrich, F. *J. Organomet. Chem.* **1999**, *582*, 58-65.

(24) Tedesco, C.; Dinnebier, R. E.; Olbrich, F.; van Smaalen, S. *Acta Crystallogr., Sect. B : Struct. Sci.* **2001**, *57*, 673-679.

(25) Dinnebier, R. E.; Schneider, M.; van Smaalen, S.; Olbrich, F.; Behrens, U. *Acta Crystallogr., Sect. B : Struct. Sci.* **1999**, *55*, 35-44.

(26) Evans, W. J.; Brady, J. C.; Fujimoto, C. H.; Giarikos, D. G.; Ziller, J. W. *J. Organomet. Chem.* **2002**, *649*, 252-257.

(27) Neander, S.; Behrens, U.; Olbrich, F. *J. Organomet. Chem.* **2000**, *604*, 59-67.

(28) Rabe, G.; Roesky, P. W.; Stalke, D.; Pauer, F.; Sheldrick, G. M. *J. Organomet. Chem.* **1991**, *403*, 11-19.

(29) Pauson, P. L.; Wilkinson, G. *J. Am. Chem. Soc.* **1954**, *76*, 2024-2026.

(30) Westcott, S. A.; Kakkar, A. K.; Stringer, G.; Taylor, N. J.; Marder, T. B. *J. Organomet. Chem.* **1990**, *394*, 777-794.

(31) Calhorda, M. J.; Gamelas, C. A.; Gonçalves, I. S.; Herdtweck, E.; Romão, C. C.; Veiros, L. F. *Organometallics* **1998**, *17*, 2597-2611.

(32) Calhorda, M. J.; Romão, C. C.; Veiros, L. F. *Chem. Eur. J.* **2002**, *8*, 868-875.

(33) Hart-Davis, A. J.; Mawby, R. J. *J. Chem. Soc.A* **1969**, 2403-2407.

(34) Nesmeyanov, A. N.; Ustynyuk, N. A.; Makarova, L. G.; Andrianov, V. G.; Struchkov, Y. T.; Andrae, S.; Ustynyuk, Y. A.; Malyugina, S. G. *J. Organomet. Chem.* **1979**, *159*, 189 - 199.

(35) Merola, J. S.; Kacmarick, R. T.; Van Engen, D. *J. Am. Chem. Soc.* **1986**, *108*, 329-331.

(36) Weissgerber, R. *Ber.* **1909**, *4*, 2913-2916.

(37) Håkansson, M.; Ottosson, C.-H.; Boman, A.; Johnels, D. *Organometallics* **1988**, *17*, 1208-1214.

(38) Brooks, J. J.; Rhine, W.; Stucky, G. D. *J. Am. Chem. Soc.* **1972**, *94*, 7339-7346.

(39) Buchholtz, S.; Harms, K.; Marsch, M.; Masse, W.; Boche, G. *Angew. Chem.* **1989**, *101*, 57-58.

(40) Becker, B.; Volker, E.; Müllen, K. *Angew. Chem.* **1989**, *101*, 501-503.

(41) Könemann, M.; Erker, G.; Fröhlich, R.; Würthwein, E.-U. *J. Am. Chem. Soc.* **1997**, *119*, 11155-11164.

(42) Ferdani, R.; Hu, J.; Leevy, W. M.; Pajewska, J.; Pajewski, R.; Villalobos, V.; Barbour, L.; Gokel, G. W. *Journal of Inclusion Phenomena and Macrocyclic Chemistry* **2001**, *41*, 7-12.

(43) Calhorda, M. J.; Gonçalves, I. S.; Herdtweck, E.; Romão, C. C.; Royo, B.; Veiros, L. F. *Organometallics* **1999**, *18*, 3956-3958.

(44) Katz, T. J.; Rosenberger, M. *J. Am. Chem. Soc.* **1962**, *84*, 865-866.

(45) Churchill, M. R.; Lin, K.-K. G. *Inorg. Chem.* **1973**, *12*, 2274-2279.

(46) Katz, T. J.; Rosenberger, M. *J. Am. Chem. Soc.* **1963**, 2030-2031.

(47) Abbasali, Q. A.; Cloke, F. G. N.; Hitchcock, P. B. *J. Chem. Soc., Chem. Commun.* **1997**, *119*, 1541-1542.

(48) Katz, T. J.; Acton, N. *J. Am. Chem. Soc.* **1972**, *94*, 3281-3283.

(49) Kissounko, D. A.; Kissounko, N. S.; Krutko, D. P.; Brusova, G. P.; Lemenovskii, D. A.; Boag, N. M. *J. Organomet. Chem.* **1998**, *556*, 145-149.

(50) Cloke, F. G. N.; Kuchta, M. C.; Harker, R. M.; Hitchcock, P. B.; Parry, J. S. *Organometallics* **2000**, *19*, 5795-5798.

(51) Gleiter, R.; Bethke, S.; Okubo, J.; Jonas, K. *Organometallics* **2001**, *20*, 4274-4278.

(52) Cloke, F. G. N.; Hitchcock, P. B. *J. Am. Chem. Soc.* **2002**, *124*, 9352-9353.

(53) Cloke, F. G. N.; Hitchcock, P. B. *J. Am. Chem. Soc.* **1997**, *119*, 7899-7900.

(54) Jonas, K.; Kolb, P.; Kollbach, G.; Gabor, B.; Mynott, R.; Angermund, K.; Heinemann, O.; Krüger, C. *Angew. Chem., Int. Ed. Engl.* **1997**, *36*, 1714-1718.

(55) Jonas, K.; Gabor, B.; Mynott, R.; Angermund, K.; Heinemann, O.; Krüger, C. *Angew. Chem., Int. Ed. Engl.* **1997**, *36*, 1712-1714.

(56) Corbelin, S.; Kopf, J.; Weiss, E. *Chem. Ber.* **1991**, *124*, 2417-2422.

(57) Edelman, M. A.; Hitchcock, P. B.; Lappert, M. F.; Lui, D.-S.; Tian, S. *J. Organomet. Chem.* **1998**, *550*, 397-408.

CHAPTER 4

DENSITY FUNCTIONAL STUDIES OF UNSOLVATED GROUP 1, 3 AND 4 METAL 4-AZAPENTALENYL COMPLEXES

4.1 INTRODUCTION

Since the report of the first metallocene complex ferrocene in 1951[1] the cyclopentadienyl anion has been of great importance to the field of organometallic chemistry. The synthesis, structure and chemistry of a variety of mono and bis cyclopentadienyl ($C_5H_5^-$) complexes and derivatives, such as the pentamethylcyclopentadienyl anion ($C_5Me_5^-$), have been widely reported and reviewed.[2-8] In order to gain further understanding of these systems, computational methods such as density functional theory (DFT) has become a widely utilised tool over the last two decades.[9] This has allowed information regarding the energetics, structure and bonding properties as well as thermodynamic parameters of various cyclopentadienyl and cyclopentadienyl derived structures to be determined. The application of computational calculations to bis- and mono- cyclopentadienyl complexes of alkali, alkaline earth, main group, transition and lanthanide metals have allowed for the prediction of the geometry of the complexes as well as the determination of various energies and reaction pathways.[10-19]

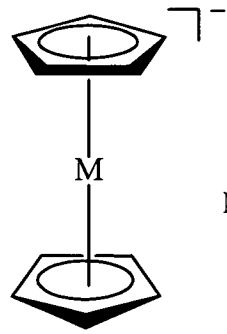

M = Li, Na, K, Rb

(I)

In 1997 Bridgeman reported the geometries of bis(cyclopentadienyl) complexes of the alkali and alkaline earth metals using DFT calculations.[17] The results of the optimised anionic structures of the bis(cyclopentadienyl) alkali metal complexes, $[M(C_5H_5)_2]^-$ **(I)** (M = Li, K, Na, Rb), indicated that the rings are staggered and coparallel in all of the complexes. The calculated geometries of the sodium and lithium complexes were shown to be in good agreement with the respective determined X-ray crystal structures.[20-22] A decrease in the dissociation energies was observed on going down the group, however no such trend was apparent in regards to the metal carbon bond order. The study of these complexes also indicated the type of bonding present in the system, with the metal charges indicating that the bonding in the lithium complex was predominately covalent whilst the potassium and rubidium complexes showed a decrease in ionic bonding in comparison to the analogous sodium complex.

The coparallel, staggered ring geometry observed for the optimised geometries of the bis(cyclopentadienyl) Group 1 complexes was only noted for $[(C_5H_5)_2Mg]$ **(II)** in the study of bis(cyclopentadienyl) Group 2 metal complexes. This calculated structure was found to be of a similar geometry to the crystal structure reported in 1975 by Bunder and Weiss.[23] The optimised geometries of the calcium and strontium complexes also had staggered rings, however the centroid-M-centroid angles were bent at angles of 150 and 145 °, respectively. This was reflected in the solid state X-ray crystal structure of $[(C_5H_5)_2Ca]$, **(III)**, reported in 1974 by Zerger and Stucky.[24]

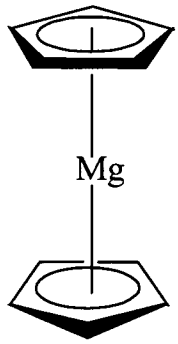

(II)

In the solid state **(III)** exists as a polymer where the calcium cation is surrounded by four cyclopentadienyl anions, of which three interact with the calcium in an η^5 fashion and one *via* an η^1 interaction. A similar trend to the dissociation energies of the Group 1 metal complexes was observed for the $[(C_5H_5)_2M]$ Group 2 metal complexes, with a decrease in energy again observed on going down the group. This, however, was only found to hold true for those Group 2 complexes whose dissociation occurred *via* the heterolytic process, $[(C_5H_5)_2M] \rightarrow M + 2(C_5H_5)$. If the dissociation occurred *via* a homolytic process, $[(C_5H_5)_2M] \rightarrow M^{2+} + 2(C_5H_5^-)$ then an increase in dissociation energy was observed on descending the group.

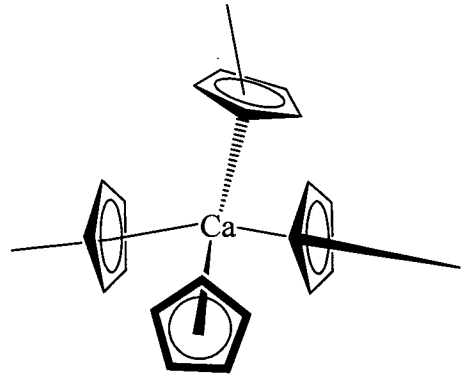

(III)

In 2002 Rayón and Frenking reported a similar study into the structure, bond energies and bonding of monocyclopentadienyl Group 1 metal complexes.[18] They restricted the geometries of the investigated complexes to C_{5v} symmetry, which was retained after the optimisation was carried out. The geometries of $[(C_5H_5)Na]$ and $[(C_5H_5)Li]$ exhibited similar bond lengths to those values previously determined from other accurate quantum chemical methods.[18] Data was also obtained for the analogous potassium, rubidium and caesium complexes. They reported the geometries, giving the first complete set of theoretically determined data for these complexes.

Rayón and Frenking made no comparisons between their theoretical results and data obtained from the known X-ray crystal structures of Group 1 metal cyclopentadienyl complexes as these structures are either polymeric and/or solvated

in the solid state. As expected, an increase in the M-C_5H_5 centroid distance is observed for the calculated structures on going down the group, from the smaller lithium centre through to the larger caesium. Their results showed a large difference in the dissociation energies between the lithium complex, which had a dissociation energy of -359.82 kJ/mol, and the other Group 1 metal complexes. There was little difference reported in the dissociation energies of the remaining Group 1 metal complexes studied with their dissociation energies within the range of -254.0 to -258.6 kJ/mol.[18] These dissociation energies indicate that the lithium cyclopentadienyl interaction is much stronger than those of the heavier Group 1 metal complexes, which have similar M-(C_5H_5) bond strengths.

Theoretical methods have also been applied to complexes of extended cyclopentadienyl systems such as indenyl $(C_9H_7)^-$, fluorenyl $(C_{13}H_9)^-$ and pentalendiyl $(C_8H_6)^{2-}$ complexes, Figure 1. These studies have focussed on the geometries, energies and metal-anion coordination modes of the complexes. These systems have been used as alternatives to the cyclopentadienyl anion in reactivity applications due to the range of possible binding modes that the ligands can adopt. For example, the indenyl anion has been studied extensively both synthetically and *via* computational methods due to its ability to change its mode of coordination to satisfy the electronic requirements of the metal centre.[25] The most common coordination shift observed and studied in indenyl complexes is that of η^5- to η^3- which has been shown to occur in processes where the complex undergoes reduction or by the addition of a donor ligand increasing the metal's valence electron count.[26]

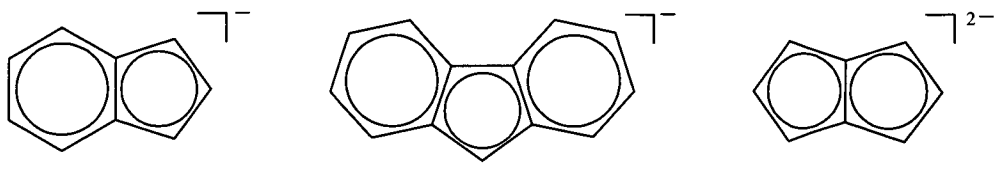

Figure 1. Extended cyclopentadienyl systems, left to right: indenyl $(C_9H_7)^-$; fluorenyl $(C_{13}H_9)^-$ and pentalendiyl $(C_8H_6)^{2-}$.

In 1998 Veiros and coworkers looked at the effect that Lewis base coordination had on the metal – indenyl coordination (ring slippage) in both neutral and cationic molybdenum indenyl complexes of the type $[(C_9H_{11})MoL_2(CO)_2]$ **(IV)**.[27] DFT calculations on the cationic η^5 coordinated indenyl complexes, Figure 2 **(IV)**, indicated that there was a preference for the six membered ring of the indenyl to be *trans* to the two carbonyl moieties in the complex. In comparison to the η^5- complex, the cationic η^3- coordinated indenyl complexes, Figure 2 **(V)**, showed that the six membered ring of the indenyl was preferentially *cis* to the carbonyl moieties, with the η^3- complexes being lower in energy than the η^5- complexes. The η^3- structures also exhibited a folding of the indenyl moiety of **(V)** the folding angle being calculated to be 31.5 ° which was found to be similar to the angle reported for the X-ray crystal structure of the tungsten analogues.[28] Veiros and coworkers further investigated the indenyl molybdenum system in 2001 looking at the changes in hapticity during a redox reaction.[29]

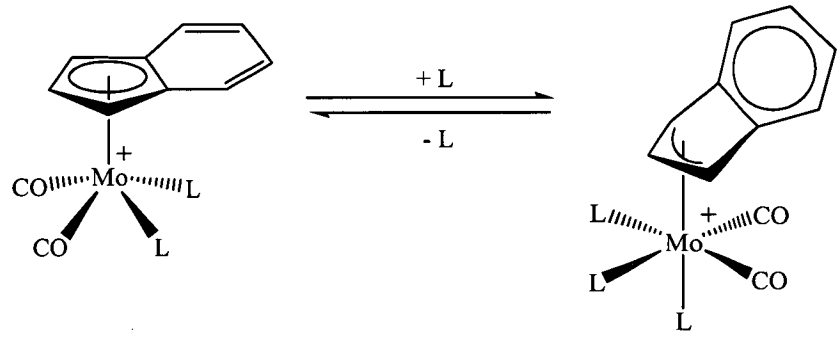

(IV) **(V)**

Figure 2.

Ring slippage is not only associated with indenyl complexes, but has also been noted to occur in fluorenyl complexes, $(C_{13}H_9^-)$, where η^1-, endocyclic and exocyclic η^3- and η^5- are all possible.[30] In some complexes there is sufficient distortion in the η^5 interaction that it is best described as an η^3 interaction.[31-34] In 1999 Veiros and his colleagues showed through their DFT calculations that, of the two η^3- coordination modes possible, Figure 3, the exocyclic mode was preferred over the endocyclic

mode. This was in agreement with the crystal structure of $[(\eta^5\text{-}C_9H_7)Mo(\eta^3\text{-}C_{13}H_9)(CO)_2]$, **(VI)**, reported in the same paper.[35] The DFT calculated distances between the metal centre and the fluorenyl, in particular those involved in the exocyclic interaction, were found to be similar to those of the reported crystal structure. Veiros and his colleagues concluded from their work that the electronic properties of the metal influenced the coordination mode present, and are not driven by steric properties.

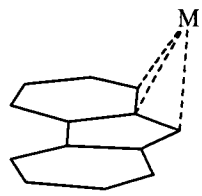

exocyclic (η^3-$C_{13}H_7^-$)

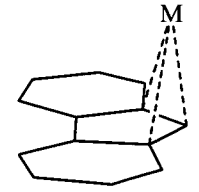

endocyclic (η^3-$C_{13}H_7^-$)

Figure 3.

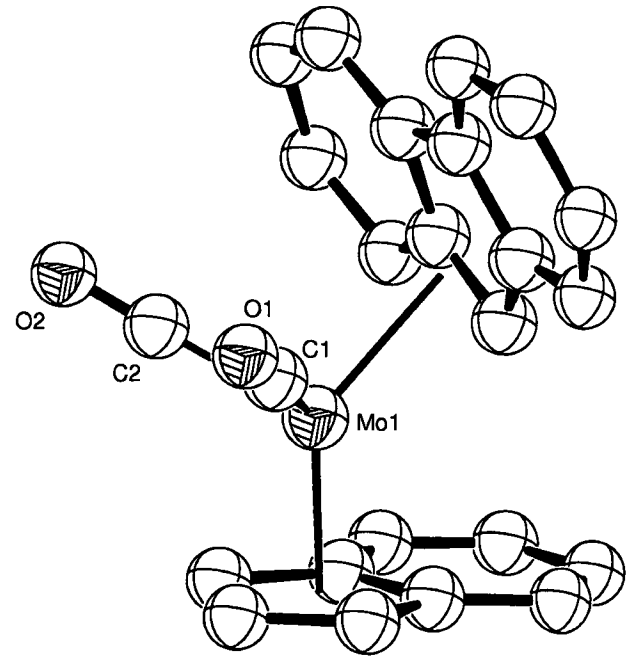

Figure 4. Single crystal X-ray structure of $[(\eta^5\text{-}C_9H_7)Mo(\eta^3\text{-}C_{13}H_9)(CO)_2]$ **(VI)**,[35] X-ray crystal structure reproduced from the CCDC database.[36,37] Thermal ellipsoids are shown with arbitrary radii, hydrogens have been removed for clarity.

Density functional calculations have also been carried out on cyclopentadienyl, indenyl and fluorenyl lanthanide complexes. In 2003 Carpentier and coworkers studied the unusual coordination modes of fluorenyl in *ansa* lanthanocenes, **(VII – X)**, which had been determined by single crystal X-ray diffraction studies.[38] The presence of an η^1- (η^2-) interaction between the metal centre and the fluorenyl anion was able to be confirmed by looking at the Y-C Mulliken overlap populations. From the calculations carried out, they were able to show that a stronger interaction was present between one of the carbons of the six membered rings and the yttrium in comparison to the interaction with the adjacent bridging carbon. The asymmetric η^3-allylic bond between the yttrium metal centre and the fluorenyl moiety was also able to be confirmed by the calculations.

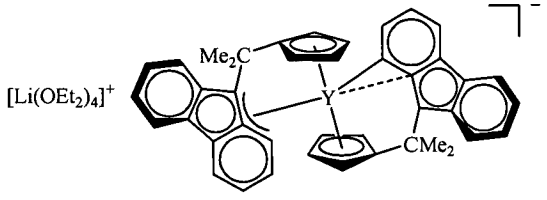

(VII)

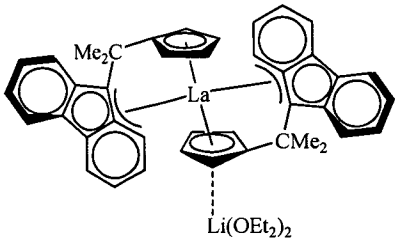

(VIII)

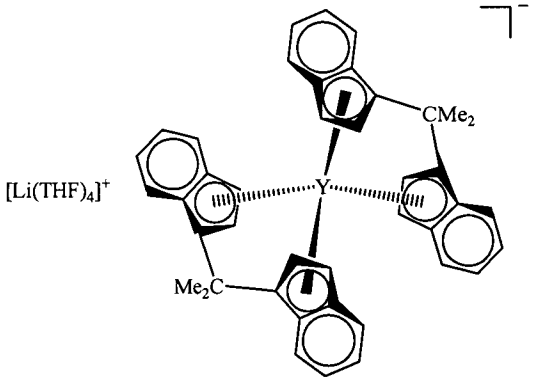

(IX)

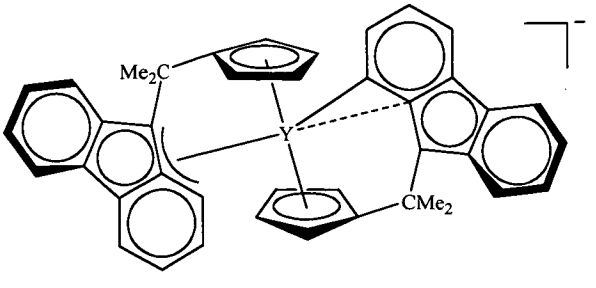

(X)

The final extended cyclopentadienyl systems to be discussed are pentalendiyl complexes, whose first metal complexes were synthesised in the early 1960s by Katz *et al.*[39,40] The proposed structures of these early complexes were those of a bimetallic bis(pentalendiyl) complex, an example of which is given in Figure 5, **(XI)**.[41,42] During the late 1990s theoretical work was undertaken by a number of groups to investigate complexes of the pentalendiyl system.[43,44]

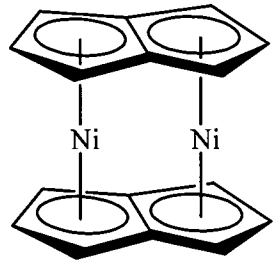

Figure 5. Bimetallic bis(pentalendiyl) complexes **(XI)**

The interest in studying these complexes stemmed from the lack of information regarding their solid state structure as the proposed structures for these bimetallic unsubstituted bis(pentalendiyl) complexes were yet to be confirmed by single crystal X-ray diffraction studies. Whilst no solid state structures are confirmed for complexes similar to that of **(XI)**, the solid state structure for $[Mo_2(C_8H_4(1,4\text{-}Si^iPr_3)_2)_2]$ **(XII)** was reported in 1998 by Cloke *et al.*[45] This was the first report to structurally characterise a bimetallic bis(pentalendiyl) sandwich complex by single crystal studies. The information gained from this study indicated that the pentalendiyl dianions were relatively planar and of an eclipsed geometry.

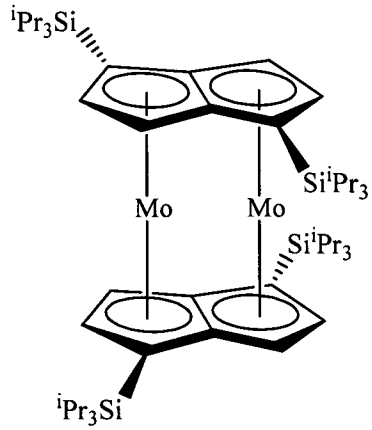

(XII)

In 1999 Green, in collaboration with the group of Cloke, undertook theoretical investigations into the bonding and geometry of unsubstituted bis(pentalendiyl)dimolybdenum $[Mo_2(C_8H_6)_2]$, **(XIII)**, as a model system for $[Mo_2(C_8H_4(1,4\text{-}Si^{i}Pr_3)_2)_2]$, **(XII)**.[43] The calculated geometry of the model system showed good correlation with the real system, **(XII)**. Green *et al.* in 1999 reported a similar geometry for the pentalendiyl dianion for **(XIII)** with a slight increase in the fold observed, 2.6 – 4.2 ° **(XIII)** in comparison to 1.73 – 3.03 ° for **(XII)**.[43]

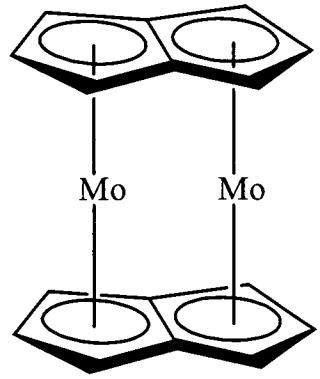

(XIII)

Whilst the bond lengths and angles of $[Mo_2(C_8H_6)_2]$, **(XIII)**, compared well with those of the real system, **(XII)**, a slight difference was observed in the symmetry between the two complexes. The final optimised geometry of **(XIII)** was found to have D_{2h} symmetry whilst the crystal structure of **(XII)** has D_2 symmetry. In order to explain the observed variation, Green constrained the model system during optimisation to D_2 symmetry with the pentalendiyl rings being twisted at 10 ° relative

to each other. The resulting energy of the model system, constrained to D_2 symmetry, was found to be 12.5 kJ/mol higher than that of the system with D_{2h} symmetry. From these results Green *et al.* concluded that the twisting observed in the crystal structure of **(XII)** may arise due to the presence of the bulky isopropyl silyl groups.[43]

Whilst Green and Cloke had looked at the bimetallic bis(pentalendiyl), complexes other groups were looking at monometallic, "metallocene type" complexes containing one or more pentalendiyl dianionic units. In 1998 DFT calculations carried out by Costuas and Saillard[44] confirmed the D_{2d} geometry of $[Ti(C_8H_6)_2]$, **(XIV)**, synthesised earlier by Jonas *et al.* in 1997.[46] The optimised geometry of **(XIV)** showed a folding of the pentalendiyl along the bridgehead carbon centres, with the bridgehead dihedral angle between the five membered rings calculated to be 149 °, Figure 6.

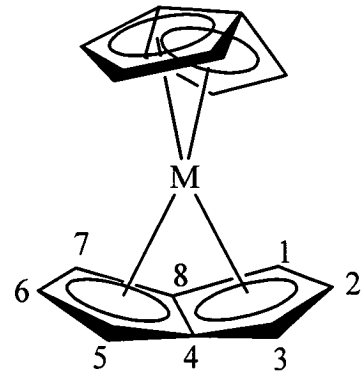

Figure 6. Bridgehead dihedral angles for pentalendiyl, atom numbers: 5-4-8-1 and 3-4-8-7.

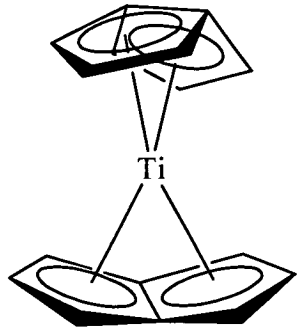

(XIV)

The calculated bridgehead dihedral angle in **(XIV)** was found to be larger, that is there was less folding of the dianion observed, than that which had been previously determined by the single crystal X-ray diffraction study of the complexes $[(\eta^8\text{-}C_8H_6)Ti(\eta^5\text{-}C_5H_5)]$ and $[(\eta^8\text{-}C_8H_6)V(\eta^5\text{-}C_5H_5)]$, 142 and 136 °, respectively, reported by Jonas *et al.*[46,47] The larger dihedral angle results in an increase of the metal - pentalendiyl carbon distances in comparison to that of the corresponding distances reported for the structurally known $[(\eta^5\text{-}C_5H_5)Ti(\eta^8\text{-}C_8H_6)]$ **(XV)**. In order to explore the electron count of these complexes, Costuas and Saillard studied the highest occupied molecular orbitals, HOMO, of the pentalendiyl in **(XIV)**. Their studies of the molecular orbitals showed **(XIV)** should have an 18 electron count when the symmetry of the complex is D_{2d}, with each pentalendiyl ligand acting as a nine electron donor and not a ten electron donor as was previously thought.[44]

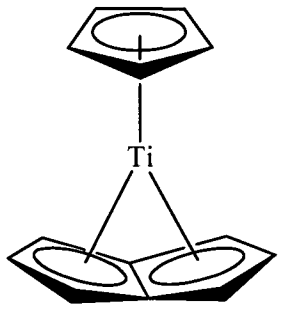

(XV)

Some three years after the report of Costuas and Saillard, Jonas and coworkers published their results regarding the optimised geometries of bis(pentalendiyl) complexes of the Group 4 metals: titanium; zirconium and hafnium: **(XIV)**, **(XVI)** and **(XVII)**, respectively.[48] Whilst Costuas and Saillard used DFT in their calculations, Jonas *et al.* utilised the restricted Hartree-Fock method, RHF. This particular method involves the Coulombic electron-electron repulsion being taken into account to give what is known as the self-consistent field approximation.[49] The RHF method is usually applied to molecules where there are no unpaired electrons and the same orbital spatial function may be used for the differing electron spins in each orbital pair. The energies that are calculated by this method are always greater than the exact energy in comparison to DFT calculations, which take into account some of the electron correlation.

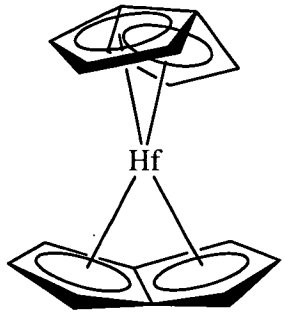

(XVI)

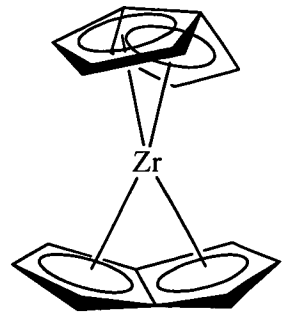

(XVII)

The optimisation of $[Hf(C_8H_6)_2]$, **(XVI)**, and $[Zr(C_8H_6)_2]$, **(XVII)**, gave geometries which displayed D_2 symmetry. The optimised geometry of **(XIV)**, however, did not give the expected D_2 symmetry, which had been predicted from ^1H and ^{13}C NMR spectroscopic studies of the synthetically prepared complex at – 80 °C. Instead, the RHF calculations performed by Jonas *et al.* predicted that the symmetry of the global minimum of **(XIV)** was C_1.[48] Earlier DFT *ab initio* calculations carried out by Costuas and Saillard predicted yet another different symmetry, D_{2d}, for **(XIV)**.[44] Jonas *et al.* calculated the energies of complexes **(XIV)**, **(XVI)** and **(XVII)**, freezing them at particular geometries finding that the C_1 geometry of **(XIV)** was 9.20 kJ/mol only lower in energy than the D_2 geometry. In comparison to the results obtained by Costuas and Saillard's which indicated that D_{2d} symmetry led to the global minimum, Jonas *et al.* found that the C_1 geometry **(XIV)** was 64.0 kJ/mol lower in energy than that of the D_{2d} geometry.[48]

Jonas and his colleagues noted that the symmetry of $[Ti(C_8H_6)_2]$, **(XIV)**, was not the only feature to differ when compared to $[Hf(C_8H_6)_2]$, **(XVI)**, and $[Zr(C_8H_6)_2]$, **(XVII)**, slight variations in bond lengths and bond angles were also present, Table 1. The pentalendiyl dianion in all three complexes had a folded geometry similar to that which was observed in the synthetically prepared and characterised monopentalendiyl complexes of Jonas *et al.*[46,47] Two different bridgehead dihedral angles were found to exist for the optimised geometry of **(XIV)**, Table 1. Jonas *et al.* showed *via* Mulliken population analysis that the pentalendiyl anion folds due an increase in the overlap between the metal and pentalene dianion orbitals. From this

analysis, and comparing the HOMO's for various geometries of differing symmetries, Jonas was able to confirm the symmetry of the complexes. This analysis showed that **(XVI)** and **(XVI)** preferred D_2 symmetry, whilst the molecular orbital studies of **(XIV)** indicated that D_{2d} symmetry was preferred.

Table 1. Structural parameters calculated for **(XIV)**, **(XVI)** and **(XVII)**.

	(XIV)	**(XVI)**	**(XVII)**
C-C (Å)	1.39 – 1.45	1.40 – 1.45	1.40 – 1.45
Dihedral angle (°) †	157, 149	152	151

† Bridgehead dihedral angle of the pentalendiyl dianion.

While the groups of Jonas and Saillard focussed on transition metal pentalendiyl complexes, the collaboration between Cloke and Green was now investigating the electronic structure of bis(pentalendiyl) actinide complexes, in particular thorium and uranium. As with their earlier study on the bis(pentalendiyl)dimolybdenum complex, Cloke and Green used a model system **(XVIII)** to compare with the known solid state structure of [Th{η^8-C_8H_4(1,4-Si^{i}Pr$_3$)$_3$}$_2$], **(XIX)**. A similar model was used for the analogous uranium species. In this particular study Cloke and Green determined the binding mode between the pentalendiyl dianion and the metal centre. Cloke and Green stated that "For η^8 bonding to a single metal, the wingtip carbons must interact with the metal. This necessitates a folding of the ligand toward the metal, ..." (Cloke, Green and Jardine 1999).[50] Cloke had already proposed in earlier synthetic reports on actinide bis(pentalendiyl) complexes that the size and exemption from the 18 electron rule made this class of metal complexes ideal for the presence of an η^8 interaction between metal and ligand.[50]

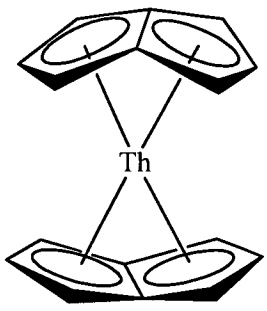

(XVIII)

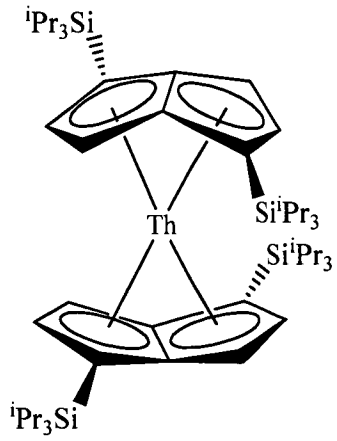

(XIX)

Green and Cloke constrained the geometry of both the thorium and uranium model systems to both D_2 and D_{2d} symmetries during the optimisation process to obtain the bond lengths and angles of the complexes as well as the energy of the various structures. They found that there was good agreement between the theoretical results for their model systems and the data obtained from known crystal structures of the real systems. The results from the optimisation of the thorium complex indicated that the D_{2d} structure of the thorium complex was found to be higher in energy than the structure with D_2 symmetry. This compares well with the experimentally found structure of **(XIX)** reported by Cloke in 1997 where the single crystal was found to have D_2 symmetry. It should be noted that both S_4 and D_2 symmetry was found in a single crystal, due to the presence of two isomers.[50]

4.2 RESULTS AND DISCUSSION

4.2.1 General computational methods

The geometries and relative binding energies of the complexes studied were carried out using B3LYP[51-53] density functional theory using Gaussian 03.[54] Possible starting geometries for the complexes to be studied were chosen and are illustrated in each of the forecoming sections of the results and discussion. The ligands in the

complexes investigated in this Chapter were optimised by applying the basis set 6-31+G(d);[55] for the appropriate basis set applied to the metal centre, see Table 2.

Table 2. Basis sets applied to metal centres during optimisation of geometries.

Metal	Basis Set	Reference
Group 1 Metals (Li – K)	6-31+G(d)	55
Sc	6-31+G(d)	55
Y, La	LANL2DZ	56,57
Group 4 metals (Ti – Hf)	LANL2DZ	56,57

Single point energy calculations for this Chapter were carried out by applying the basis set 6-311+G(d,p)[55] to ligands of the complexes. The appropriate basis set applied to the metal centre for these calculations are outlined in Table 3.

Table 3. Basis sets applied to metal centres for single point energy calculations.

Metal	Basis Set	Reference
Group 1 Metals (Li – K)	6-311+G(d,p)	55
Sc	6-311+G(d,p)	55
Y, La	SDD	58,59
Group 4 metals (Ti – Hf)	SDD	58,59

The relative dissociation energy of all complexes was calculated to be the difference between the calculated energy of the complex and the sum of individual calculated energies of the anion plus the metal centre/metal halide, Equation 1.

Dissociation Energy = Energy of complex - Σ(Energy of the individual components)

Equation 1. Calculation of Dissociation Energy of complexes.

4.2.2 DFT studies of Group 1 metal benzannulated 4-azapentalenyl complexes

4.2.2.1 Structural studies of 5*H*-pyrrolo[2,1-a]isoindolyl Group 1 metal complexes

The optimisation and single point calculations of three possible geometries of 5*H*-pyrrolo[2,1-a]isoindolyl Group 1 metal complexes, Figure 7, were carried out using DFT methods as outlined in 4.2.1. The final geometry after optimisation appeared dependent on the particular cation present in the complex. For example the optimisation of the three starting potassium geometries converged to give the single unique geometry d, whilst optimisation of the analogous lithium starting geometries gave the three unique geometries a – c, Figure 8.

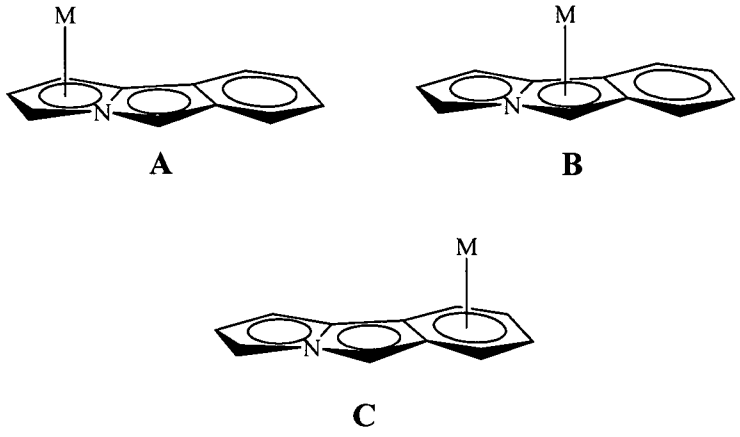

Figure 7. Starting geometries for 5*H*-pyrrolo[2,1-a]isoindolyl Group 1 metal complexes, M = Li, Na and K.

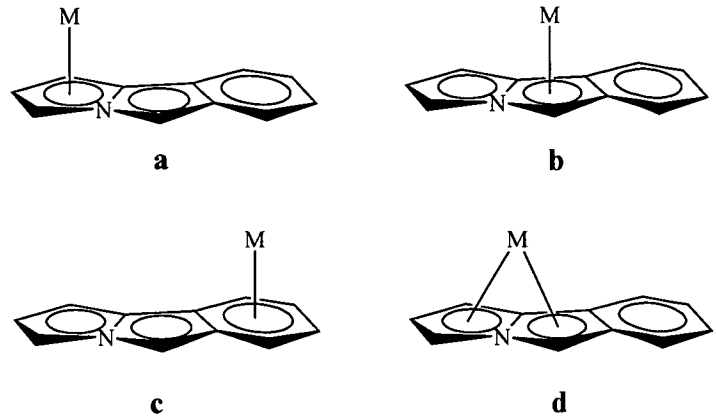

Figure 8. Optimised geometries for 5*H*-pyrrolo[2,1-a]isoindolyl Group 1 metal complexes, M = Li, Na and K

The dissociation energy of each complex was calculated using Equation 1, and are given in Table 4, (note that those entries not listed in Table 4 were not minima and have therefore been excluded). The lowest of the calculated dissociation energies is observed for the potassium complex **(XXIId)**, with the largest dissociation energies being observed for the lithium complexes **(XXa)** and **(XXb)**. The lowest binding energy for both the lithium and sodium complexes found was observed for structures **(XXc)** and **(XXIc)**, respectively. In these structures the cationic metal centre is observed to interact with the terminal six membered ring of the tricyclic anion.

Table 4. Dissociation energies Group 1 metal complexes of the type $M(NC_{11}H_8)$, where M = Li, Na or K.

	Dissociation Energy (kJ/mol)			
	a	**b**	**c**	**d**
Li (XX)	597.2	596.1	592.8	-
Na (XXI)	-	-	493.1	502.5
K (XXII)	-	-	-	456.9

The optimised geometries of the unsolvated lithiated complexes show minimal folding along the C/N bridgehead vector of the anion. The minimal folding which is observed occurs in order to satisfy the coordination sphere of the lithium without

greatly decreasing the aromaticity of the system. In each of the three geometries the anion is seen to preferentially interact with the lithium centre *via* the ring of the heterocyclic system over which the lithium cation is positioned, Figure 9a.

a)

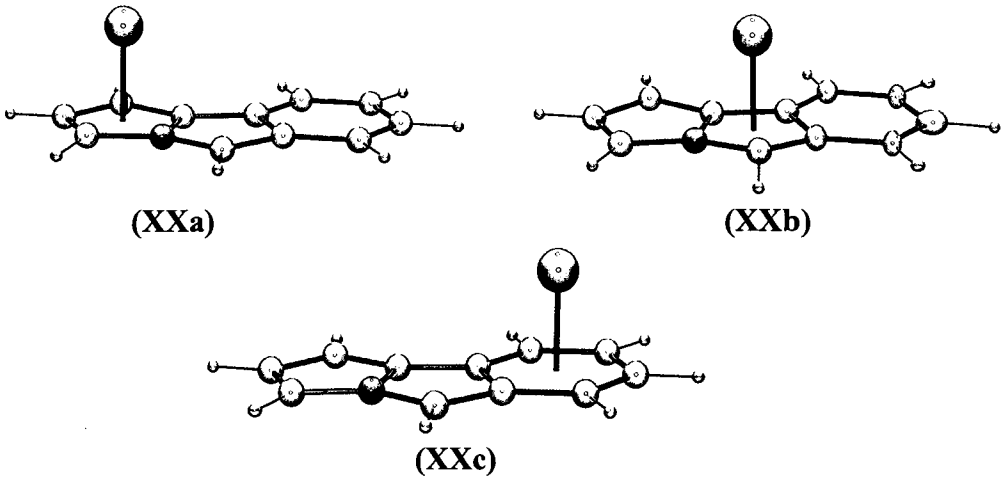

(XXa) **(XXb)**

(XXc)

b)

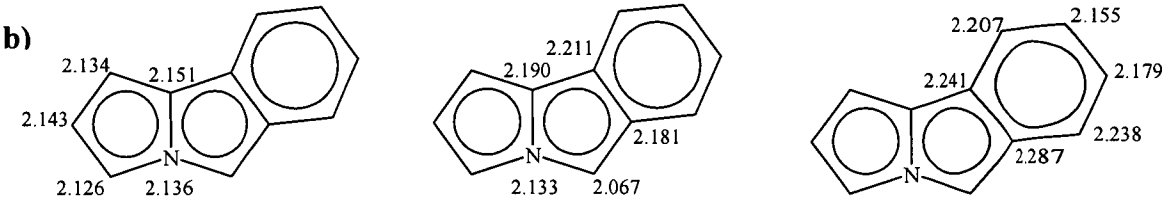

(XXa) **(XXb)** **(XXc)**

Figure 9. **a)** Optimised structures of the 5*H*-pyrrolo[2,1-a]isoindolyl lithium complexes, structure types a-c.

b) Individual lithium – carbon/nitrogen lengths for structures a-c of 5*H*-pyrrolo[2,1-a]isoindolyl lithium (all lengths in Å).

Variation in the anion - lithium lengths within and between each geometry is a clear indication slippage of the anion occurs, similar to that which has been observed and reported in indenyl complexes.[27] The slippage of the anion which occurs in all three optimised geometries gives rise to the differing Li-C/N bond lengths observed. Increased interaction between the lithium and the anion is observed to occur along the edge of the anion on which the nitrogen is located, thus resulting in the shorter bond lengths observed. Within this series of lithium geometries the coordination number is shown to increase from five, **(XXa)** and **(XXb)**, to six, **(XXc)**. This solely appears to be dependent on the position of the lithium cation, that is whether it is

positioned over the five or six membered ring of the 5*H*-pyrrolo[2,1-a]isoindolyl anion.

Variation in the lithium-anion centroid lengths for **(XXa)** – **(XXc)** were observed to occur, Table 5. The shortest of these lengths occurred in **(XXc)**, where the lithium interacts *via* an η^6 interaction with the six membered ring of the anion, Li-Ct_3 = 1.698 Å. Variation in the Li-Ct lengths between the three geometries arises from the different lithium anion interactions present, in turn this influences the degree of folding along the bridgehead nitrogen – carbon vector of the fused five membered rings. The structures **(XXa)** and **(XXb)** indicated that the lithium centre interacts with the anion *via* an η^5 bonding mode with the appropriate five membered ring.

Table 5. 5*H*-pyrrolo[2,1-a]isoindolyl lithium centroid lengths and bridgehead dihedral fold angle.

	(XXa)	**(XXb)**	**(XXc)**
M-Ct_1† (Å)	1.76_7	-	-
M-Ct_2† (Å)	-	1.78_0	-
M-Ct_3† (Å)	-	-	1.69_8
Fold angle* (°)	2.8	3.3	0.3

* Bridgehead nitrogen – carbon dihedral angle.

† Ct_1 – centroid of terminal five membered ring, Ct_2 – centroid of internal five membered ring, Ct_3 – centroid of six membered ring.

Optimisation of the sodium structures gave rise to two unique structures **(XXIc)** and **(XXId)**, Figure 10a. Those structures with the starting geometries type A and B converged during optimisation to give the single geometry of **(XXId)**. As expected the sodium anion bond lengths are longer than those reported for the previously discussed lithium structures of **(XXa)** – **(XXc)**. Likewise a lengthening of the determined sodium-anion centroids is observed when compared to the previous lithium structures, due to the increase in the size of the metal cation radii, Table 6.

a)

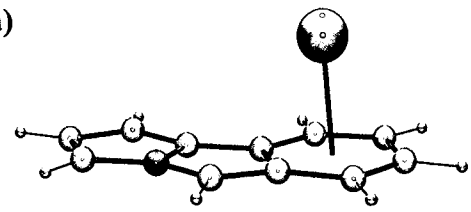

(XXI)

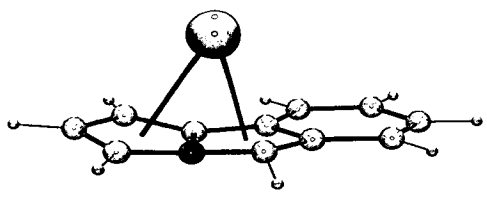

(XXId)

b)

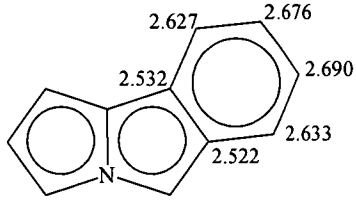

(XXIc)

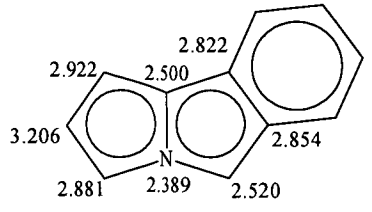

(XXId)

Figure 10. **a)** Optimised geometries of 5*H*-pyrrolo[2,1-a]isoindolyl sodium complexes **(XXIc)** and **(XXId)**.

b) Sodium – carbon/nitrogen lengths for 5*H*-pyrrolo[2,1-a]isoindolyl sodium complexes **(XXIc)** and **(XXId)** (all lengths in Å).

Structures **(XXIc)** and **(XXIb)** exhibit a slippage of the 5*H*-pyrrolo[2,1-a]isoindolyl anion similar to that observed in studied lithium structures. This slippage is more apparent in **(XXId)**; here the shorter individual sodium – anion bond lengths are associated with the central five membered ring of the anion. The slippage is also reflected in the unequivocal sodium – anion centroid lengths, Table 6. Whilst it may be plausible for the sodium cation to interact with both of the five membered rings of the 5*H*-pyrrolo[2,1-a]isoindolyl anion it is unlikely, especially when taking into consideration the individual sodium anion lengths. It is possible that the interaction between the sodium and the anion is one of an η^7 type where the sodium interacts with the C/N of the fused five membered rings except for those whose Na – C length is 2.922 and 3.206 Å. The similar bond lengths observed in **(XXIc)** indicate the possibility that an η^6 type interaction exists between the sodium centre and the six membered ring of the anion.

Table 6.

	(XXIc)	**(XXId)**
M-Ct_1† (Å)	-	2.54_5
M-Ct_2† (Å)	-	2.32_5
M-Ct_3† (Å)	2.19_2	-
Fold angle* (°)	1.6	13.3

* Bridgehead nitrogen – carbon dihedral angle.

† Ct_1 – centroid of terminal five membered ring, Ct_2 – centroid of internal five membered ring, Ct_3 – centroid of six membered ring.

Determination of the interaction between the anion and cation not only needs to take into account the metal – anion bond and centroid lengths but also any folding of the anion which may occur. This is apparent in structure **(XXId)** where a small degree of folding along the C/N bridgehead vector towards the sodium centre is observed, Table 6. In comparison minimal folding of the anion along this particular vector is observed for **(XXIc)**. This is simply due to the fact that the cation is no longer interacting with the two fused five membered rings but instead with the six membered ring of the heterocyclic anion. Folding of the 5*H*-pyrrolo[2,1-a]isoindolyl anion, in the case of structure **(XXId)**, enables an increased interaction between the terminal and internal five membered rings and the sodium centre. The formal hapticity of **(XXId)** is one which is difficult to define. When the dihedral angle along with the sodium – anion bond lengths, both individual and centroids, are all taken into consideration the most plausible interaction is η^7. This best describes the probable interaction and that which is chemically reasonable in regards to the individual bond lengths between the sodium and the two five membered rings of the heterocycle.

The final complexes in this series to be investigated were those of the 5*H*-pyrrolo[2,1-a]isoindolyl potassium. Optimisation of the three 5*H*-pyrrolo[2,1-a]isoindolyl potassium starting geometries led to the identification of one unique structure, **(XXIId)**, Figure 11a. Structure **(XXIId)** is noted to visually have a structural geometry similar to that of **(XXId)**. Variation in these two complexes arise from the different metal cation present in each complex and are reflected in the individual M-C/N bond lengths and hence the position of the cation over the C/N bridgehead vector.

a)

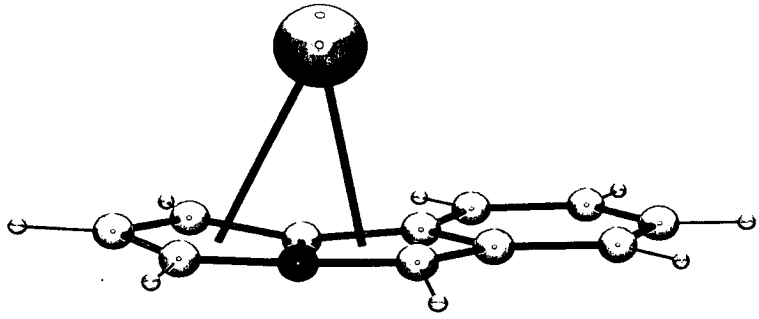

b)

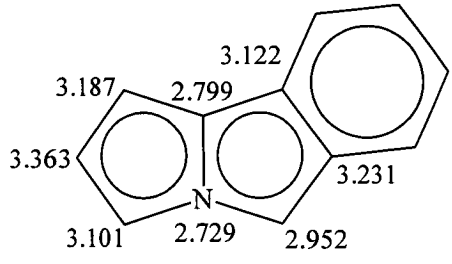

Figure 11. **a)** Optimised geometry of structure type D of 5*H*-pyrrolo[2,1-a]isoindolyl potassium, **(XXIId)**.

b) Potassium - anion interaction lengths of 5*H*-pyrrolo[2,1-a]isoindolyl potassium, **(XXIId)**, (all lengths in Å).

Whilst both the sodium and potassium complexes appear to be structurally similar on closer inspection it is noticed that there is a decrease in the slippage of the anion in the potassium complex. This is reflected in the individual M-C/N bond lengths in complex **(XXIId)**, Figure 11b, where they are observed to be of a similar length with only minimal variation. This is in comparison to the unequal lengths seen

earlier for the analogous sodium complex **(XXId)**. From this is can be stated that potassium cation is more centrally positioned between the fused five membered rings in comparison to that of the corresponding sodium complex, Figure 12. The lengthening of the individual potassium – anion bond lengths is as would be expected for a cation of a larger radius.

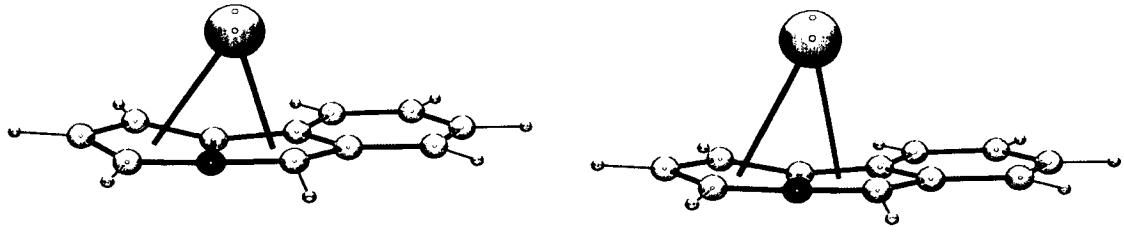

(XXIId) **(XXId)**

Figure 12.

The incorporation of the larger potassium cation was shown to alter the dihedral angle along the C/N bridgehead vector from 13.3 ° in **(XXId)** to 11.4 ° in **(XXIId).** The decrease in this fold angle is bought about by the increase in the radius of the cation, the anion decreases the degree of this fold to satisfy both the electronic and steric requirements of the complex. This in turn leads to the subsequent lengthening of the potassium – anion bond lengths which is observed in **(XXIId)**. The lengthening of the potassium – "wingtip" carbon bonds suggest that these particular bonds have a lesser influence on the overall bonding in the complex. Like that of the analogous 5*H*-pyrrolo[2,1-a]isoindolyl sodium complex, **(XXId)**, the formal hapticity of the potassium complex is unclear as to whether these wingtip carbon have any influence on the overall interaction. The potassium – 5*H*-pyrrolo[2,1-a]isoindolyl interaction is therefore most probably one of η^7 nature.

Comparison of the theoretically calculated structure of **(XXIId)** with that of the synthetically prepared substituted pentalendiyl complex $[K_2C_8H_4\{(Si^iPr_3\text{-}1,4)_2\}_2 K_2(C_6H_6)]$, **(XXIII)** Figure 13, reported by Cloke *et al.* in 2000,[60] indicates similarities in bond length and the dihedral angle of the bridgehead vector. Before directly comparing these two structures it should be noted that the structure of the synthetically prepared bimetallic sandwich structure of **(XXXIII)** contains the solvent molecule benzene in the crystal structure and was found to exist as a

polymer. Whilst this differs from the calculated geometry of **(XXIId),** which is monomeric and unsolvated, similarities are observed in the potassium-ring centroid lengths and the bridgehead dihedral angle. The potassium-ring centroid lengths observed in the known system **(XXIII)** are as follows: 2.69_1; 2.75_1 and 2.80_5 Å[60] with the value for a similar interaction in the theoretical system being 2.71_5 Å. Cloke *et al.* commented that the potassium – ring carbon lengths for K1 and K2 to the two five membered rings of the pentalendiyl ligand are comparable to the potassium ring carbon lengths in $[\{K(\eta^5\text{–}C_5H_5)\}_n]$.

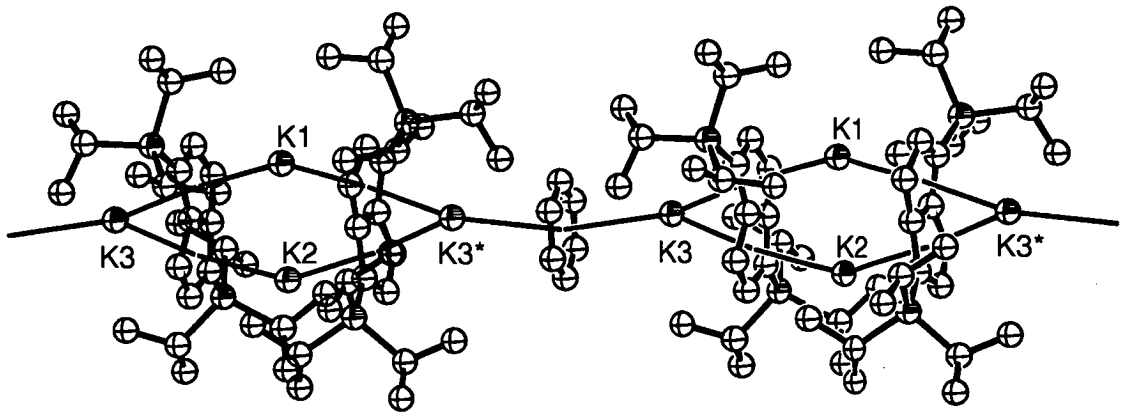

Figure 13. Single crystal X-ray structure of $[K_2C_8H_4\{(Si^iPr_3\text{-}1,4)_2\}_2K_2(C_6H_6)]$ **(XXIII),**[60] X-ray crystal structure reproduced from the CCDC database.[36,37] Thermal ellipsoids are shown with arbitrary radii, hydrogens have been removed for clarity.

A summary of the metal-centroid and dihedral fold angle of complexes **(XX)** – **(XXII)** is given in Table 10. This shows that the increase in the M-C/N bond and the subsequent lengthening of the metal-ring centroid interactions is related to the increasing radii of the metal cation on progressing down the Group 1 group. The complexes containing the smaller lithium centre resulted in the identification of three unique geometries where the 5*H*-pyrrolo[2,1-a]isoindolide was observed to have little to no folding of the anion along the C/N bridgehead vector. This maintained the aromaticity of the anion in the complex yet enabled the coordination sphere of the lithium centre to be satisfied. In comparison to the lithium complexes, only one unique geometry was found for the potassium complex. In this particular case the anion was observed to fold towards the larger potassium centre whilst still maintaining the aromaticity of the anion.

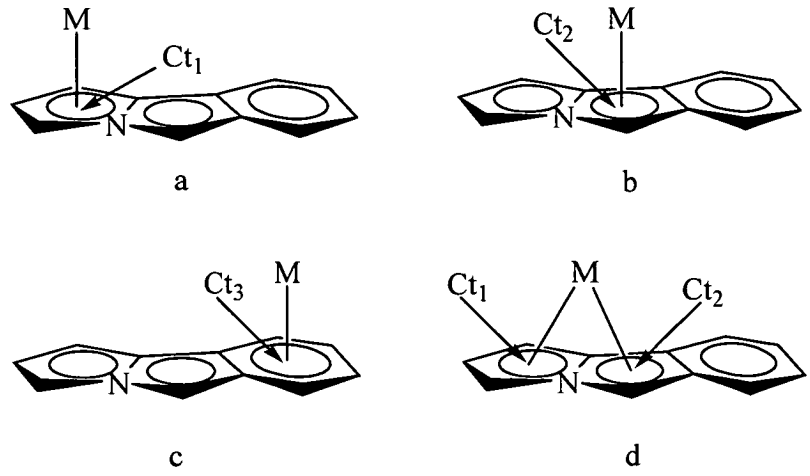

Table 6. Metal – ring centroid bond lengths and fold angles of 5*H*-pyrrolo[2,1-a]isoindolyl Group 1 metal complexes.

	(XXa)	**(XXb)**	**(XXc)**	**(XXIc)**	**(XXId)**	**(XXIId)**
M-Ct_1† (Å)	1.76_7	-	-	-	2.54_5	2.80_1
M-Ct_2† (Å)	-	1.78_0	-	-	2.32_5	2.71_5
M-Ct_3† Å)	-	-	1.69_8	2.19_2	-	-
Fold angle* (°)	2.8	3.3	0.3	1.6	13.3	11.4

* Between the terminal and internal five membered rings.

† Ct_1 – centroid of terminal five membered ring, Ct_2 – centroid of internal five membered ring, Ct_3 – centroid of six membered ring.

All optimised geometries of the 5*H*-pyrrolo[2,1-a]isoindolyl Group 1 metal complexes showed some degree of slippage of the anion. The most notable of these was observed to occur when the cation was interacting with the either one or both five membered rings in the system, complexes **(XXa)**, **(XXb)**, **(XXId)** and **(XXIId)**. The shortest bond lengths in these complexes are between the metal and the bridgehead nitrogen indicating a greater degree of bonding interaction between the metal and the anion at this particular point, with lesser interactions occurring with the "wingtip" carbons of the fused five membered rings of the anion.

4.2.2.2 Structural Studies of 9*H*-pyrrolo[1,2-a]indolyl Group 1 metal complexes

The Group 1 metal complexes investigated within this section at first glance appear to be similar to those studied in Section 4.2.2.1. There is however a subtle difference within the actual anion itself. The anion here is an isomer of the 5*H*-pyrrolo[2,1-a]isoindolyl anion, Figure 14. The structure of the 9*H*-pyrrolo[1,2-a]indolyl anion has no sp^2 carbon spacer between the bridgehead nitrogen and the carbon of the six membered ring. As with the investigation of 5*H*-pyrrolo[2,1-a]isoindolyl Group 1 complexes, three possible starting geometries were chosen, Figure 15. These were optimised and single point energy calculations were carried out on the obtained geometries, Figure 16, using the DFT methods previously described. Optimisation of the starting geometries led to the identification of the same number of geometries as for the 5*H*-pyrrolo[2,1-a]isoindolyl Group 1 complexes, that is three lithium, two sodium and one potassium geometry.

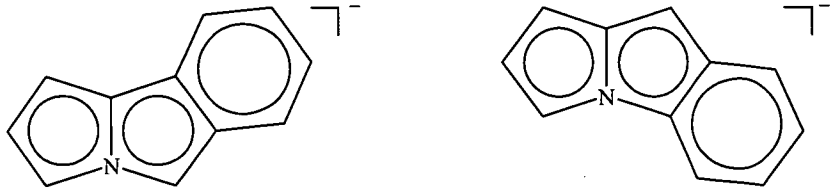

5*H*-pyrrolo[2,1-a]isoindolyl 9*H*-pyrrolo[1,2-a]indolyl

Figure 14.

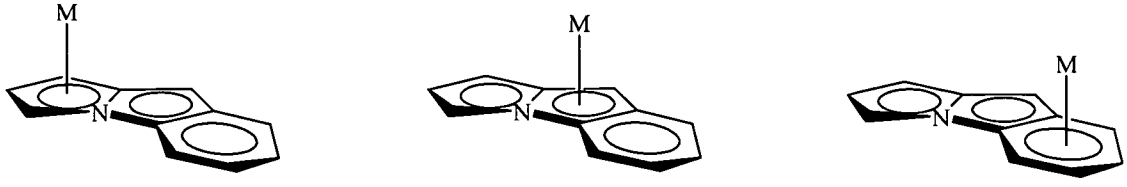

A **B** **C**

Figure 15. Starting geometries of 9*H*-pyrrolo[1,2-a]indolyl Group 1 metal complexes, M = Li, Na and K.

a)

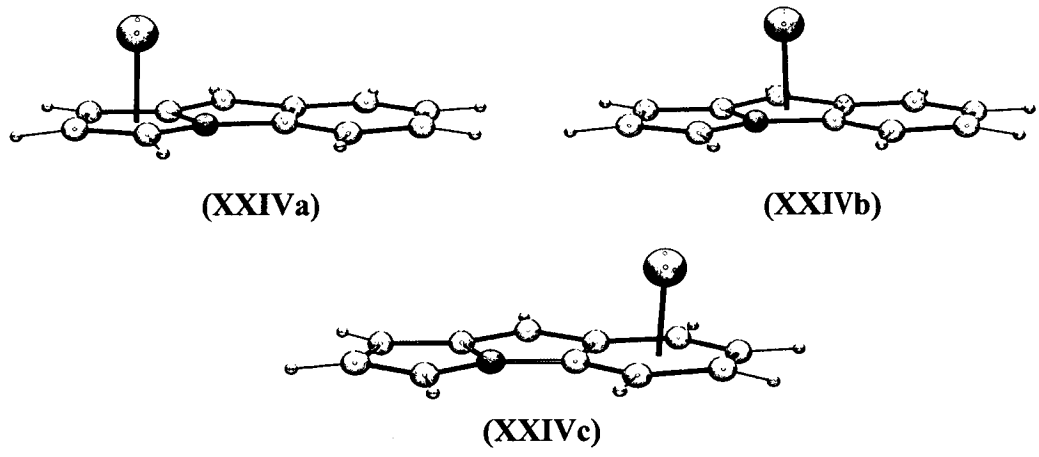

(XXIVa) (XXIVb)

(XXIVc)

b)

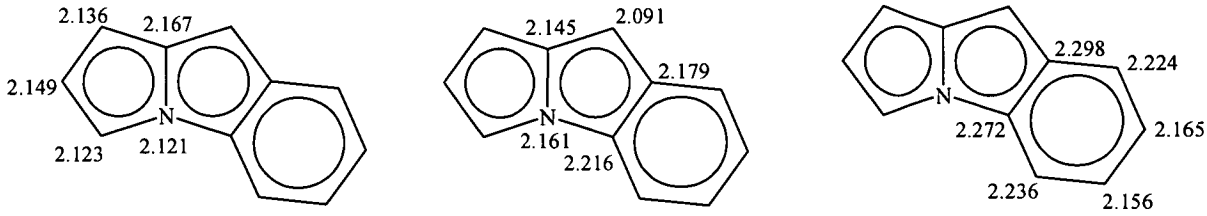

(XXIVa) (XXIVb) (XXIVc)

Figure 16. **a)** Optimised geometries of 9*H*-pyrrolo[1,2-a]indolyl lithium complexes.

b) Individual lithium - carbon/nitrogen lengths for the optimised 9*H*-pyrrolo[1,2-a]indolyl lithium complexes (all lengths in Å).

As before in the lithium structures **(XXa)** – **(XXc)** the anions of the three optimised geometries **(XXIVa)** - **(XXIVc)** are observed to be relatively planar; there is very little folding of the fused five membered ring towards the metal centre, 0.6 – 2.8 °, Table 12. The greatest fold angle of these three structures is observed for **(XXIVa)** where the lithium is situated over the terminal five membered ring of the anion. This structure also has the greatest dissociation energy of the three lithium complexes, 599.8 kJ/mol, and indeed the largest dissociation energy of any of the complexes investigated in Section 4.2.2.2.

Table 7. Lithium anion distances and angles for structures a – c of 9*H*-pyrrolo[1,2-a]indolyl lithium

	(XXIVa)	**(XXIVb)**	**(XXIVc)**
M-Ct_1 (Å)	1.76_7	1.78_4	1.71_0
Fold angle (°)	2.8	1.6	0.6

* Between the terminal and internal five membered rings.

† Ct_1 – centroid of terminal five membered ring, Ct_2 – centroid of internal five membered ring, Ct_3 – centroid of six membered ring.

The metal-ring centroid lengths in complexes **(XXIVa)** – **(XXIVc)** are of a similar value, with the shortest lithium – centroid interaction present in **(XXIVc)**. This shorter interaction enables the lithium to interact with all six carbons in an η^6 fashion satisfying the coordination sphere of the lithium. This shorter interaction along with the minimal bridgehead folding allows for the aromaticity of the heterocyclic system to be preserved. Overall the lithium - ring centroid interactions are similar in length with only minimal variation in these lengths being observed.

As observed in the earlier studied structures of **(XXb)** and **(XXc)**, **(XXIVb)** and **(XXIVc)** also exhibit a similar slippage of the 9*H*-pyrrolo[1,2-a]indolide. This is reflected in the varying individual Li-C/N bond lengths and the decrease in the bridgehead dihedral angle, Figure 16b and Table 7. The position of the lithium cation and the resulting individual bond lengths of **(XXIVb)** indicate a slipped η^5 type interaction between the lithium and the internal five membered ring is most probable.

Whilst the geometries of the lithium tautomers discussed in Sections 4.2.2.1 and 4.2.2.2 are similar, small differences are noted in the relative binding energies observed. The relative binding energies for the 5*H*-pyrrolo[2,1-a]isoindolyl lithium structures, Table 8, were observed to be quite similar in energy, with the greatest difference being 3.4 kJ/mol. In comparison a greater difference in these energies was observed for the 9*H*-pyrrolo[1,2-a]indolyl lithium structures, 11.2 kJ/mol.

Table 8. Comparison of relative dissociation energies of isomeric lithium complexes.

	Relative Dissociation Energies (kJ/mol)		
	a	**b**	**c**
(XX)	597.2	596.1	592.8
(XXIV)	599.8	588.6	580.4

The theoretical study of the 9*H*-pyrrolo[1,2-a]indolyl sodium complexes led to the identification of two unique structures of geometry type c and d, optimisation of the starting geometries A and B converged to give the single structure **(XXVd)**. As was the case in the previously described lithium complexes the obtained geometries are isostructural with the analogous 5*H*-pyrrolo[2,1-a]isoindolyl sodium structures discussed in Section 4.2.2.1. Of the two sodium complexes investigated **(XXVd)** was found to have the lowest dissociation energy, 482.0 kJ/mol, Table 9.

Table 9.

	Relative Dissocation Energies (kJ/mol)	
	c	**d**
(XXV)	482.0	499.8

The geometry of **(XXVc)** shows the sodium cation positioned over the terminal six membered ring of the heterocyclic anion, Figure 17a. The sodium cation is not centrally positioned above the terminal six membered ring, but instead appears to be situated over to one side. This is reflected in the uneven Na-C bond lengths present, Figure 17b, indicating a slippage of the anion occurs within the final obtained geometry of the complex. Minimal folding of the anion along the fused edge of the five and six membered ring is observed, the dihedral angle for this particular vector was determined to be 1.9 °. Whilst there is variance in the sodium anion bond lengths present in the structure the small degree of folding along the bridgehead vector of the five and six membered rings the interaction between the metal and anion is best described as η^6.

a)

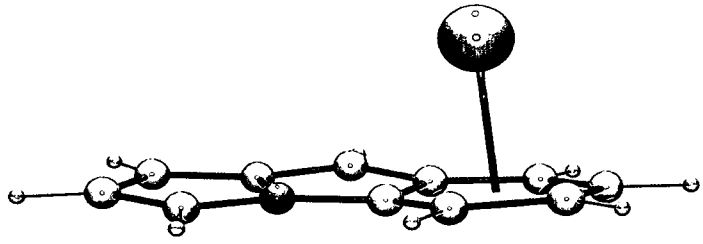

b)

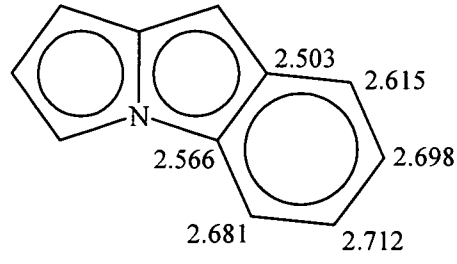

Figure 17. **a)** Optimised geometry 9*H*-pyrrolo[1,2-a]indolyl sodium **(XXVc)**.

b) Sodium - anion interaction lengths (all lengths in Å).

The visual geometry of **(XXVd)** is similar to that which was obtained for the earlier discussed **(XXId)**. Both structures resulted from the convergence of two different starting geometries to give one unique structure after optimisation. Complex **(XXVd)** shows the sodium cation situated over the bridgehead vector of the fused five membered rings of the heterocyclic anion, Figure 18a. A folding of the 9*H*-pyrrolo[1,2-a]indolide is observed to occur along the C/N bridgehead vector, with the

terminal five membered ring appearing to fold towards the sodium centre at a dihedral angle of 12.6 °.

a)

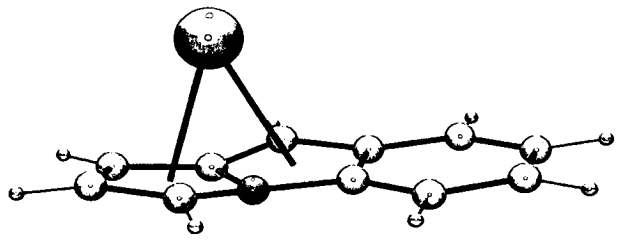

b)

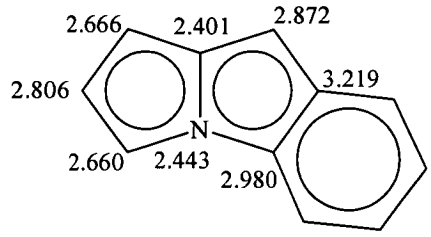

Figure 18. **a)** Optimised geometry of 9*H*-pyrrolo[1,2-a]indolyl sodium **(XXVd)**.

b) Sodium - anion interaction lengths (all lengths in Å).

As with previous structures containing the anion the shortest Na-C/N length occurs between the sodium and the bridgehead nitrogen of the anion. Longer M-C/N interactions occur with the atoms of the internal five membered ring and the wingtip carbon of the terminal five membered ring. The metal ring centroid bond length was calculated for each interaction between the sodium and each five membered ring, and these were found to vary by 0.22 Å. The shorter of the two interactions was between the sodium and the terminal five membered ring. The shortening of one centroid length in conjunction with the folding of the anion along the C/N bridgehead vector towards the sodium centre indicates that the metal centre interacts with both five membered rings. Variation in the Na-C/N bond lengths indicate that it is unlikely that the sodium interacts with the 9*H*-pyrrolo[1,2-a]indolide *via* an η^8 mode. Instead it is most likely that the sodium interacts with all atoms of the terminal five membered ring in an η^5 mode and the carbons adjacent to the bridgehead atoms of the internal five membered ring *via* an η^3 interaction.

Optimisation of the three starting geometries of the 9*H*-pyrrolo[1,2-a]indolyl potassium complex converged to give a single unique geometry **(XXVId)**, Figure 19. The convergence of the three starting geometries to give one unique geometry observed here was also noted to occur for the earlier studied 5*H*-pyrrolo[2,1-a]isoindolyl potassium, Section 4.2.2.1. Both **(XXVId)** and **(XXIId)** exhibit similar geometries, Figure 19, with the potassium metal situated over the C/N bridgehead vector interacting with both the internal and the terminal five membered rings of the heterocyclic system. The terminal five membered ring in both complexes is observed to fold towards the potassium centre whilst the internal ring remains relatively planar with respect to the six membered ring.

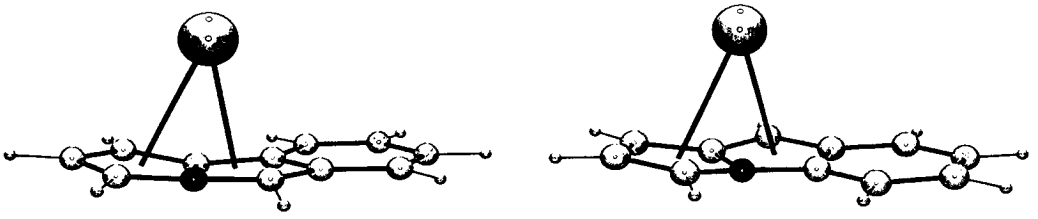

(XXIId) **(XXVId)**

Figure 19.

The individual K-C/N bond lengths indicate that the potassium cation is centrally positioned over the C/N bridgehead vector with only a slight slippage of the anion occurring, Figure 20b. The slippage of the anion is reflected in the slight difference in length of the potassium nitrogen and potassium bridgehead carbon interactions, 2.747 and 2.773 Å, respectively, Figure 20b. As with many of the complexes investigated in this Section, the shortest interaction between the metal and anion is that between the metal and the bridgehead nitrogen.

a)

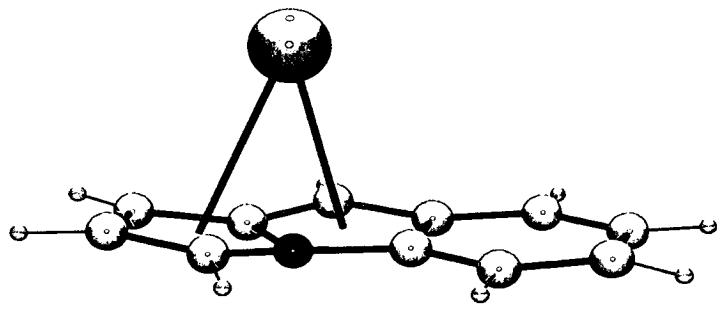

b)

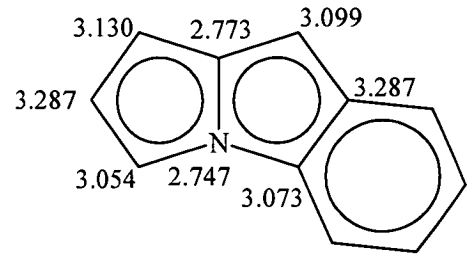

Figure 20. **a)** Optimised geometry of 9*H*-pyrrolo[1,2-a]indolyl potassium.

b) Potassium anion bond lengths

On moving from the bridgehead atoms to the adjacent carbons and the wingtip carbons an increase in the M-C/N interaction is observed. The greatly increased bond length between the potassium and the wingtip carbons sees a decrease in the possibility that the potassium and these atoms participate in the binding mode interaction. By this rationale alone it could be concluded that an η^6 binding mode is present in **(XXVId)**, however, the anion, as stated earlier, is observed to fold towards the potassium centre. The degree of folding in the anion was determined by measuring the C/N bridgehead dihedral vector which was found to be 11.3 °, this angle is almost identical to that of **(XXIId)** which was measured to be 11.4 °. When the degree of folding of the anion along with the K-C/N bond lengths and the radius of the metal centre is taken into consideration then it is plausible for the interaction between the potassium and the 9*H*-pyrrolo[1,2-a]indolide to be described as an η^8 binding mode involving all atoms of the fused five membered rings.

The metal-ring centroid lengths for structures **(XXIV)** – **(XXVI)** along with the C/N bridgehead vector dihedral angles are summarised in Table 10. This clearly shows that the increase in the metal atomic radius on descending the group

influences the metal-ring centroid lengths leading to overall increase in this particular measurement. The only two structures which show any significant folding of the anion are the sodium and potassium structures, **(XXVd)** and **(XXVId)**, respectively. Whilst the sodium structure was found to have varying metal - anion centroid lengths the analogous potassium structure was found to have centroid lengths which were near equal in length. The C/N bridgehead vector dihdedral angle of the 9*H*-pyrrolo[1,2-a]indolide was observed to decrease on going from the smaller sodium to the larger potassium containing structure. This in turn may have an effect on the position of the metal within the structure resulting in the aforementioned observations mentioned in regard to the slippage of the anion and the uneven metal-ring centroid lengths observed in **(XXVd)**.

Table 10. Metal – centroid bond length and fold angle of Group 1 metal 4-azapentalenyl complexes

	(XXIV)			**(XXV)**		**(XXVI)**
	a	**b**	**c**	**c**	**d**	**d**
M-Ct (Å)	1.76_7	1.78_4	1.71_0	2.21_4	2.30_5	2.75_6
M-Ct (Å)	-	-	-	-	2.52_7	2.74_9
Fold angle (°)	2.8	1.6	0.6	1.9	12.6	11.3

The relative dissociation energies for the identified geometries are given in Table 11. The highest dissociation energies are noted for the lithium complexes, which are some 100 kJ/mol higher in energy than the potassium and sodium complexes. The lower dissociation energies in the lithium and sodium complexes are those where the metal interacts with the terminal six membered ring of the tricyclic anion. The folded geometry of the sodium complex, **(XXV)**, indicates a more stable structure, however, with more energy required to achieve the C/N bridgehead dihedral angle observed.

Table 11. Relative dissociation energies of Group 1 metal with 9*H*-pyrrolo[1,2-a]indolyl complexes.

	Relative Dissociation Energies (kJ/mol)			
	a	**b**	**c**	**d**
(XXIV)	599.8	588.6	580.4	-
(XXV)	-	-	482.0	499.8
(XXVI)	-	-	-	454.4

4.2.3 DFT studies of Group 1 metal 4-azapentalenyl complexes

Two possible starting geometries for the Group 1 metal 4-azapentalenyl complexes with C_1 and C_s symmetry where chosen, **(XXVII)** and **(XXVIII)**, respectively. The optimisation of the energies of the complexes led to the identification of two unique geometries for the lithium complexes, **(XXIX)** and **(XXX)**, Figure 21. The optimisation of the structures and energies for the sodium and potassium complexes, with starting geometries of C_1 and C_s, converged to give a single geometry of C_s symmetry, **(XXXI)** and **(XXXII)**, respectively, in Figure 21. The dissociation energy of each unique geometry for the investigated complexes are calculated, using Equation 1 previously outlined, and is given in Table 12.

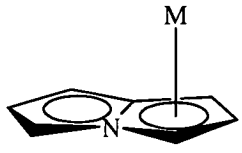

(XXVII)

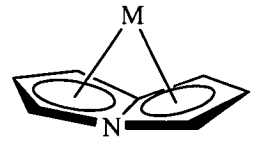

M = Li
Na
K

(XXVIII)

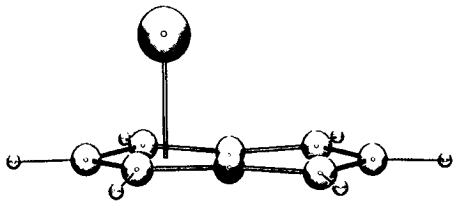

(XXIX)

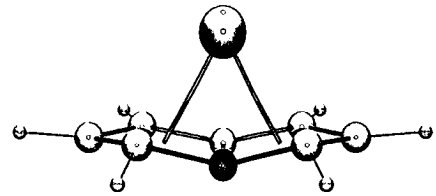

(XXX)

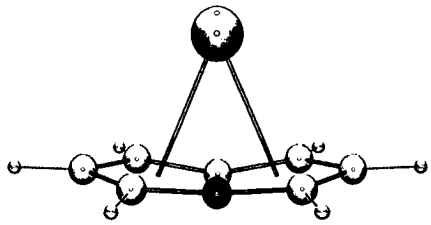

(XXXI)

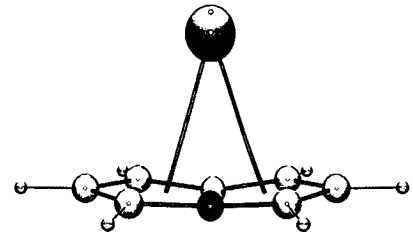

(XXXII)

Figure 21. Calculated geometries of Group 1 metal 4-azapentalenyl complexes.

Table 12. Dissociation energies (kJ/mol) for Group 1 metal 4-azapentalenyl complexes.

Metal Centre	**Structure ID**	**Symmetry**	
		C_1	C_s
Li^+	**(XXIX)** and **(XXX)**	642.7	621.7
Na^+	**(XXXI)**	-	537.2
K^+	**(XXXII)**	-	492.4

When comparing the calculated single point energies of the two lithium complexes, **(XXIX)** and **(XXX)**, it is noted that **(XXIX)** is lower in energy than **(XXX)**, this difference is calculated to be 21.0 kJ/mol. Subsequent frequency calculations carried out on **(XXIX)** and **(XXX)** showed that the geometry of **(XXIX)** is the global minimum of the lithium 4-azapentalenyl system, whilst **(XXX)** is a first order transition state on the energy surface of the structure. A trend in the dissociation energy of the complexes is also evident in Table 12 between those structures with C_s symmetry. This trend shows that as the group is descended a decrease in the dissociation energy occurs. The same trend was also in the reported in the theoretical study by Rayón and Frenkling in 2002 who investigated Group 1 metal cyclopentadienyl complexes of the type $[M(C_5H_5)]$ for Li – Cs.[18] On going down the group they noted that there was little difference between the Na – Cs dissociation energies with the M-(C_5H_5) bond strength remaining relatively constant, Table 13. The difference between the dissociation energy of $[Li(C_5H_5)]$ and the other Group 1 metal cyclopentadienyl complexes indicated that the Li-(C_5H_5) bond was much stronger than those of the other Group 1 complexes investigated.

Table 13. Dissociation energies for the $[M(C_5H_5)]$, $[M(C_5H_5)_2]^-$ and $[M(C_7H_6N)]$ systems (M = Li, Na, K, Rb or Cs).

Group 1 metal	**Dissociation Energy (kJ/mol)**		
	$[M(C_5H_5)]$ [a]	**$[M(C_5H_5)_2]^-$** [b]	**$[M(C_7H_6N)]$** [c]
Li	360	925	621.7 [d]
			642.7 [e]
Na	254	751	537.2 [d]
K	251	733	492.4 [d]
Rb	238	720	-
Cs	259	-	-

[a] Dissociation of $[M(C_5H_5)]$ to M and $(C_5H_5^-)$.[18]

[b] Dissociation of $[M(C_5H_5)_2]^-$ to M^+ and $2(C_5H_5^-)$.[17]

[c] Dissociation of $[M(C_7H_5N)]$ to M^+ and $(C_7H_6N^-)$.

[d] $[M(C_7H_6N]$ of C_s symmetry, [e] $[M(C_7H_6N]$ of C_1 symmetry.

Some years earlier in 1997 Bridgeman carried out a similar study investigating the dissociation energy of Group 1 metal bis(cyclopentadienyl)complexes of the type $[M(C_5H_5)_2]^-$.[17] These anionic complexes showed a decrease in dissociation energy on descending the group. Bridgeman extended the Group 1 metals investigated beyond those studied here to look at rubidium complexes as well. As was the case that was later observed by Rayón and Frenkling, Bridgeman noted that there was little difference in the dissociation energies of the Group 1 metal complexes of Na-Rb. The bis(cyclopentadienyl) lithium complex was once again found to have a much greater dissociation energy than the other Group 1 metal complexes. The differences in energies observed for **(XXXI)** and **(XXXII)** are comparable with those reported by Bridgeman, Rayón and Frenkling, though the differences here are much larger. As was the case in the Group 1 cyclopentadienyl complexes, the dissociation energy of both **(XXIX)** and **(XXX)** was much larger than the analogous sodium and potassium complexes indicating that the M-(C_7H_6N) interaction is greatest for the lithium complexes.

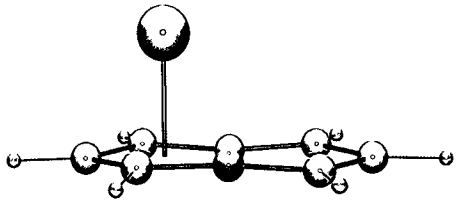

(XXIX)

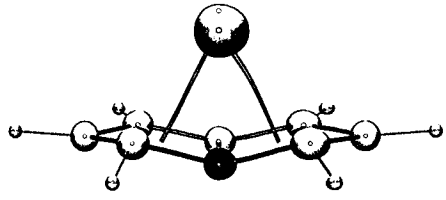

(XXX)

The geometries of the 4-azapentalenyl anion in the lithium structures **(XXIX)** and **(XXX)** are observed to be quite different. The 4-azapentalenyl anion in **(XXIX)** is observed to be relatively flat whilst the anion in **(XXX)** shows a folding of the anion along the bridgehead vector towards the lithium metal centre. The difference in the geometry of the anion is also reflected in the interaction that exists between the metal and anion. The relatively planar geometry of the anion in **(XXIX)** allows for the lithium centre to interact with only one of the five membered rings giving rise to an η^5- interaction. In comparison the folded structure of **(XXX)** allows the lithium to interact with both five membered rings of the 4-azapentalenyl anion. The anion is shown to fold towards the metal centre however the wingtip carbons are observed to be "pulling away" from the lithium centre. The interaction between the lithium and the 4-azapentalenyl anion is therefore best described as an η^6- interaction. The 4-

azapentalenyl anion folds out of the plane along the C-N bridgehead vector at an angle of 16 ° towards lithium centre. The folding of the anion towards the lithium centre allows for the electronic requirements of the lithium centre to be satisfied. This folding which occurs is, however, detrimental to the overall aromaticity of the anion: that is, in order to achieve an η^8- interaction between the lithium and the anion the energy required to fold the anion would be too great leading to the decrease of the anion's aromaticity. This type of folded interaction is therefore unfavourable due to the expense of energy required to fold the anion, hence, the η^5- interaction of **(XXIX)** is preferred.

The optimised geometries of the sodium and potassium complexes **(XXXI)** and **(XXXII)**, respectively, are of a similar structure. The metal cation in both complexes is shown to be situated over the bridgehead vector interacting with both five membered rings of the 4-azapentalenyl anion. The anion is observed to fold along the C-N bridgehead vector at 13.7 ° and 10.9 ° out of the plane of the bridgehead atoms towards the sodium and potassium centres, respectively. The dihedral angle measured for **(XXXI)** and **(XXXII)** is not as great as that which was measured for the lithium complex **(XXX)**, as evident in Table 14 where the various bond lengths and dihedral angles are listed. No structures with C_1 symmetry were located for either the sodium and potassium complexes indicating that there is only one minima on their energy surface, that where the structure of the complex has C_s symmetry.

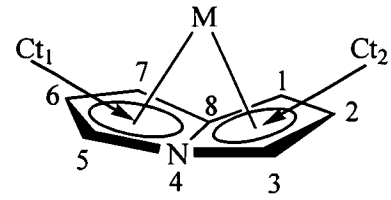

Figure 22. Defining the dihedral bridgehead angles for 4-azapentalenyl anion: positions 5-4-8-1 and 3-4-8-7.

Table 14. Metal – centroid bond lengths and fold angle of Group 1 metal 4-azapentalenyl complexes.

	Complex			
	(XXIX)	**(XXX)**	**(XXXI)**	**(XXXII)**
M-Ct_1† (Å)	1.758	1.954	2.363	2.728
M-Ct_2† (Å)	-	1.954	2.363	2.728
Fold angle‡ (°)	2.2	16.4	13.7	10.9

† See Figure 8 for definition of Ct_1 and Ct_2

‡ Bridgehead nitrogen – carbon dihedral angle (see Figure 22).

Some of the differences observed in the M-Ct and dihedral angles in Table 14 can be attributed to the varying atomic radii of the Group 1 metal cationic centres. As expected the lithium 4-azapentalenide complexes had the shortest M-C/N interactions whilst the longest M-C/N interactions are present in the potassium complex, **(XXXII)**. In the η^5- complex **(XXIX)**, minimal folding of the 4-azapentalenyl anion is observed. However, when the interaction between the metal centre and the anion is increased to an η^6- binding mode a dramatic increase in this fold angle is observed, an increase from 2.2 – 16.4 °.

Variation in the individual M-C/N bond lengths within structures **(XXIX)** – **(XXXII)** were observed and are shown in Figure 23. A small variation in these individual lengths is observed in **(XXIX)**, indicating the lithium is almost centrally positioned over one of the five membered rings of the bicyclic anion. In comparison to the near equal bond lengths observed in **(XXIX)**, the η^6/η^8- bound complexes of **(XXX)** – **(XXXII)** showed up to a 0.6 Å variation in bond length.

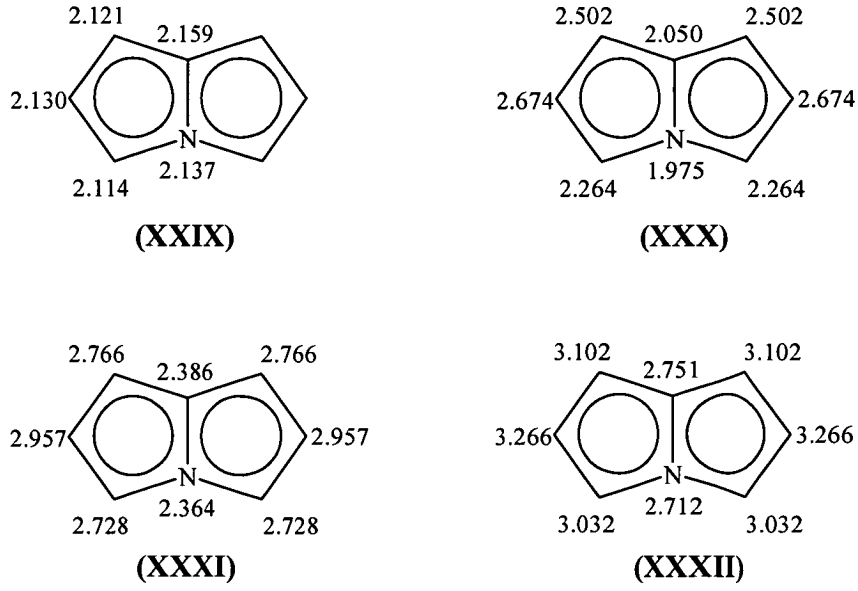

Figure 23. Metal – carbon/nitrogen bond lengths (Å).

From the bond lengths shown in Figure 23 it is evident that a slippage of the metal towards the nitrogen containing side of the anion occurs in all structures studied here. A similar type of slippage was observed in the theoretical studies carried out on alkali metal pyrrolides by Kryachko *et al.* in 2003.[61] Their calculations and subsequent investigations of the Mulliken charges showed that there were several key factors in the stabilisation of the π complexes of the alkali metal pyrrolides, **(XXXIII)**. The first of these was the formation of an ionic pair between the Group 1 metal and the nitrogen, the second relates to this ionic pair. Here the lithium reacts with the pyrrolide forming a π-cation interaction between the metal cation and the pyrrolide anion.

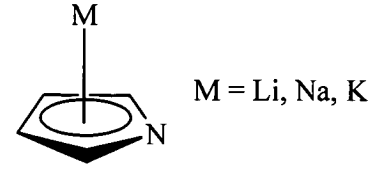

(XXXIII)

A comparison between the Group 1 metal 4-azapentalenyl complexes and other like complexes whose crystal structures are known is given in Table 15.

Table 15.

CCDC distances† (Å)		Ref.	Theoretical calculated distances (Å)	
$\{Li(C_5H_5)\}_n$	2.260 – 2.685	62	**(XXIX)** (C_1)	2.114 – 2.159
$[Li2(C_8H_8)_2(OEt_2)_2]$	2.196 – 3.323	63	**(XXX)** (C_s)	1.975 – 2.674
$\{Li(C_9H_7)\}_n$	2.258 – 2.417 (5)	64		
	2.269 – 4.168 (6)			
$[Li(C_{13}H_9)]$	2.235 – 3.497 (5)	65		
	2.311 – 5.118 (6)			
$\{Na(C_5H_5)\}_n$	2.585 – 3.139	62	**(XXXI)**	2.364 – 2.957
$\{Na(C_5Me_5)\}_n$	2.657 – 2.779	66		
$[(C_8H_8)Sm(C_8H_8)Na(THF_3)]$	2.858 – 3.050			
$[Na(C_9H_7)]$	2.793 – 3.041 (5)			
	2.879 – 4.401 (6)			
$\{(C_{13}H_9)Na(TMEDA)\}_n$	2.484 – 3.447 (5)	67		
	2.599 – 5.025 (6)			
$\{K(C_5H_5)\}_n$	2.843 – 3.301	62	**(XXXII)**	2.712 – 3.266
$\{(C_5Me_5)K(THF)\}_n$	2.949 – 3.371	68		
$\{(C_8H_8)K(THF)_2\}_n$	2.937 – 3.283	69		
$[K(C_8H_6)]$	2.732 – 3.189	60		
$\{(C_9H_7)K(PMDETA)\}_n$	3.046 – 3.151(5)	70		
	3.070 – 4.507 (6)			
$[(C_{13}H_9)K(C_6O_3H_{14})]_4$	3.029 – 3.370 (5)	71		
	3.068 – 4.647 (6)			

† Range of distances obtained from the Cambridge Crystal Data Centre, Cambridge Structural Database version 5.26 (November 2004),[36] ConQuest version 1.7 using Vista version 2.1.[37]

From the data in Table 15 it is shown that the M-C/N bond lengths of complexes **(XXIX)** – **(XXXII)** are overall slightly shorter than those of the known structures. The shortening of the M-C/N lengths may also be due to the incorporation of the nitrogen heteroatom into the heterocycle, as none of the synthetically prepared complexes in this comparison contain heteroatoms in their structures. It should be noted here that differences in the bond lengths between the real and theoretical systems may arise due to their surrounding environment and the subsequent actual structure of the synthetic complexes. The unsolvated Group 1 cyclopentadienyl complexes exist as polymeric structures whilst some of other synthetically prepared complexes, as is the case of the potassium pentadiyl, have solvent present in their crystal structure, which in turn affects the bond lengths, angles and overall geometry of the complex. The theoretical studies of the complexes here do not take into account any solvent effects and have the metal bonding to a single face of the anion; no polymeric species were investigated in this work.

4.2.4 Structural studies of 4-azapentalenyl Group 3 metal complexes.

4.2.4.1 Structural studies of 4-azapentalenyl Group 3 metal complexes.

The optimisation of the 4-azapentalenyl Group 3 metal dihalogen complexes, $[(C_7H_6N)MX_2]$, from the starting geometries A and B converged to give one unique structure of type C geometry, Figure 24. The dissociation energy of each complex was calculated using Equation 1, Section 4.2.1, and are given in Table 16. From this data it can be seen that two clear trends emerge, the first is a decrease in the dissociation energy on descending the group. The second is that the diflouride containing 4-azapentalenyl Group 3 complexes have smaller dissociation energies in comparison to the analogous dichloride complexes.

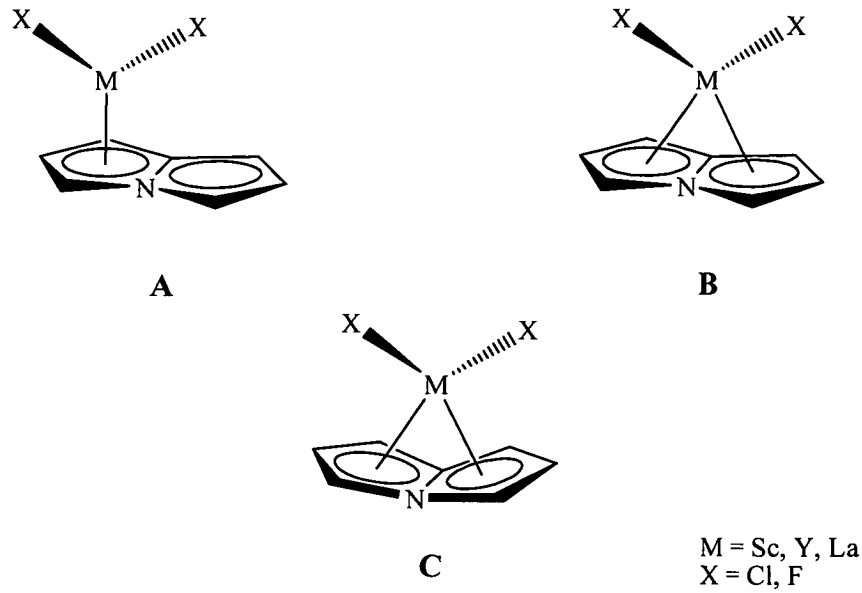

Figure 24. Starting geometries A and B were optimised to give a single unique geometry C.

Table 16. Relative dissociation energies for $[(C_7H_6N)MX_2]$ where M is Sc, Y or La and X is Cl or F.†

M		X	
		Cl^- (a)	F^- (b)
Sc^{3+}	(XXXIV)	924.8	920.5
Y^{3+}	(XXXV)	768.6	747.3
La^{3+}	(XXXVI)	695.0	544.8

† All energies are in kJ/mol.

The optimised geometries of the 4-azapentalenyl Group 3 dihalide complexes are shown in Figure 25a. Each complex shows the 4-azapentalenyl anion folding towards the Group 3 metal centre, in a similar way which was observed for the sodium and potassium complexes **(XXIV)** and **(XXV)**, respectively. From the structures in Figure 25a it is noted that the halogens in each complex are orientated in the same

direction, over the C/N bridgehead vector. The hydrogen atoms of the carbons adjacent to the bridgehead atoms are noted to fold away from the plane of the carbon to which they are attached.

a)

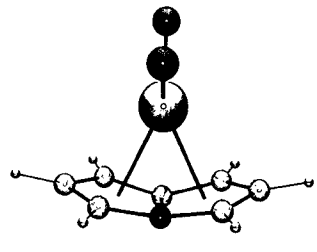

(XXXIVa)

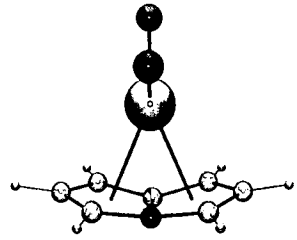

(XXXVa)

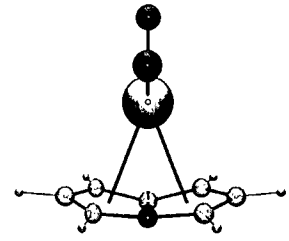

(XXXVIa)

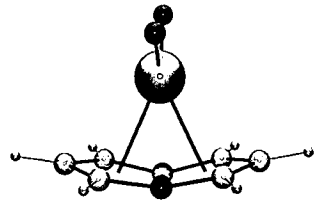

(XXXIVb)

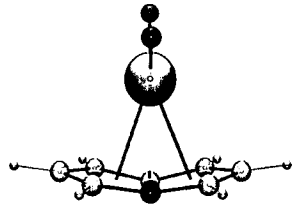

(XXXVb)

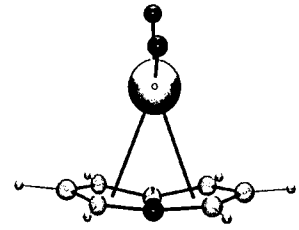

(XXXVIb)

b)

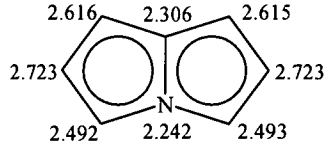

(XXXIVa)

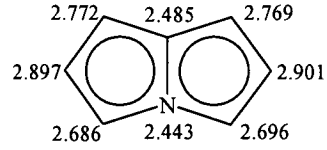

(XXXVa)

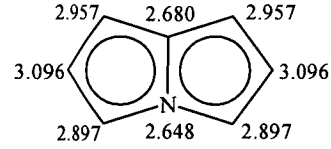

(XXXVIa)

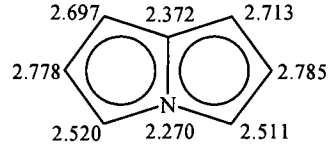

(XXXIVb)

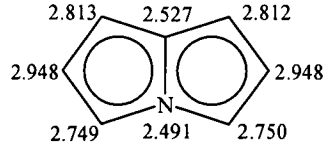

(XXXVb)

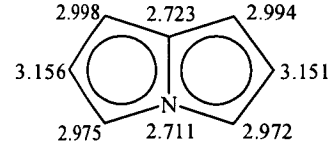

(XXXVIb)

Figure 25. **a)** Optimised geometry of 4-azapentalenyl Group 3 metal dihalide complexes.

b) Metal-anion bond lengths

The individual M-C/N bond lengths for complexes **(XXXIV)** - **(XXXVI)** are shown in Figure 25b. An increase in the M-C/N bond lengths is observed on descending Group 3 as would be expected due to the increasing atomic radii of the metal centre. Lengthening of the M-C/N also occurs on the exchange of the chloride substituents for fluoride substituents, this can be attributed to the nature of the difference in the respective electron negativities of the halogen substituents, fluorine 3.98 and chlorine 3.16 (these are Pauling electronegativity values).[72] This results in the metal centre being "pulled" towards the fluorine ligands and away from the 4-azapentalenyl anion hence resulting in the increased M-C/N bond lengths observed.

As with the potassium and sodium 4-azapentalenyl complexes discussed earlier, an increase in the individual Group 3 metal - C/N anion bond lengths is observed on moving from the bridgehead atoms out to the wingtip carbons. The lengthening of the individual M-C/N lengths leads to a corresponding lengthening of the metal-ring centroid (Ct) interactions on descent of the group and exchange of the chloride for fluoride, Table 17. A minor slippage of the 4-azapentalenyl anion is evident by the shortening of the M-N interaction in comparison to the M-C(bridgehead carbon) indicating that the metal is not exactly centrally positioned over the bridgehead vector.

Table 17. Metal – centroid bond lengths and fold angles of Group 3 metal 4-azapentalenyl complexes.

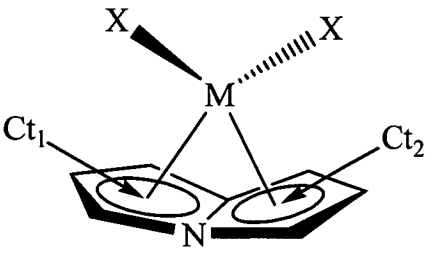

	Complex					
	(XXXIVa)	**(XXXI)**	**(XXXVa)**	**(XXX)**	**(XXXV)**	**(XXXVI**
M-Ct_1 (Å)	2.17_1	2.23_1	2.37_5	2.42_9	2.56_6	2.65_3
M-Ct_2 (Å)	2.17_1	2.23_5	2.37_7	2.43_0	2.59_5	2.65_7
Fold angle (°)	25.25	23.05	22.60	21.15	19.30	18.10

As with previously studied structures in this Chapter, the M-C/N bond lengths alone do not provide enough information to determine the binding mode. The 4-azapentalenyl anion in these complexes is observed to fold towards the Group 3 metal centre. The degree by which the anion folds towards the metal, Table 17, therefore needs to be taken into consideration when determining the formal binding mode. The bridgehead dihedral angle is observed to decrease on going from the small scandium centre through to the larger lanthanum centre. A decrease in this dihedral angle is also noted for complexes of the same metal centre when going from the dichloride species to the difluoride species; this angle is observed to decrease by as much as 2 °.

Taking into consideration the atomic radii of the metal centre, the individual M-C/N bond lengths, the M-Ct interactions and the degree of folding of the 4-azapentalenyl anion which occurs it becomes possible to determine the type of binding mode present in each complex. The smaller scandium cationic centre, which has a radius of 0.68 Å,[73] along with the elongated M-C/N bond lengths and folded anion is most likely to interact with the anion *via* an η^6 binding mode involving all atoms except the "wingtip" carbons. The folding of the anion is not great enough yet

to constitute the small scandium centre interacting with all eight atoms of the 4-azapentalenyl anion.

The significant increase in atomic radii of the yttrium and lanthanum cations, 1.04 Å and 1.17 Å, respectively,[73] along with the folding of the anion along the bridgehead vector towards the metal centre increases the probability that an η^8 binding mode may be achieved. Even though there is a decrease in the dihedral angle in comparison to the scandium complexes the folding of the anion is one still of significance. Of the yttrium and lanthanum complexes investigated it is most likely that an interaction of an η^8 nature exists for the lanthanum complexes **(XXXVIa)** and **(XXXVIb)** due to the larger atomic radius of the lanthanum cation. The dihedral angle of the yttrium complexes is unlikely to be great enough to achieve an η^8 interaction between the smaller yttrium and the anion. It is therefore more likely that an η^6 interaction exists in complexes **(XXXVa)** and **(XXXVb).**

4.2.4.2 Investigation of the relationship between relative energy and the bridgehead dihedral angle

The energetic effects inherent for the 4-azapentalenyl anion, **(XXXVII)**, to go from a planar geometry, with a dihedral angle of 0 °, to a folded geometry, which was observed for the 4-azapentalenyl Group 3 complexes, were investigated using DFT. In order to investigate these energetic effects a range of bridgehead dihedral angles from 0 – 40 ° were required to be fixed during the optimisation of each structure. The energies of the 4-azapentalenyl anion at various dihedral angles along with the relative energy with respect to the 4-azapentalenyl anion with a dihedral angle of 0 ° are shown in Figure 26.

The data obtained here indicate that in order to achieve folding of the 4-azapentalenyl anion significant energy is required. That is, as the dihedral angle is increased the relative energy of the system with respect to the planar geometry is observed to increase.

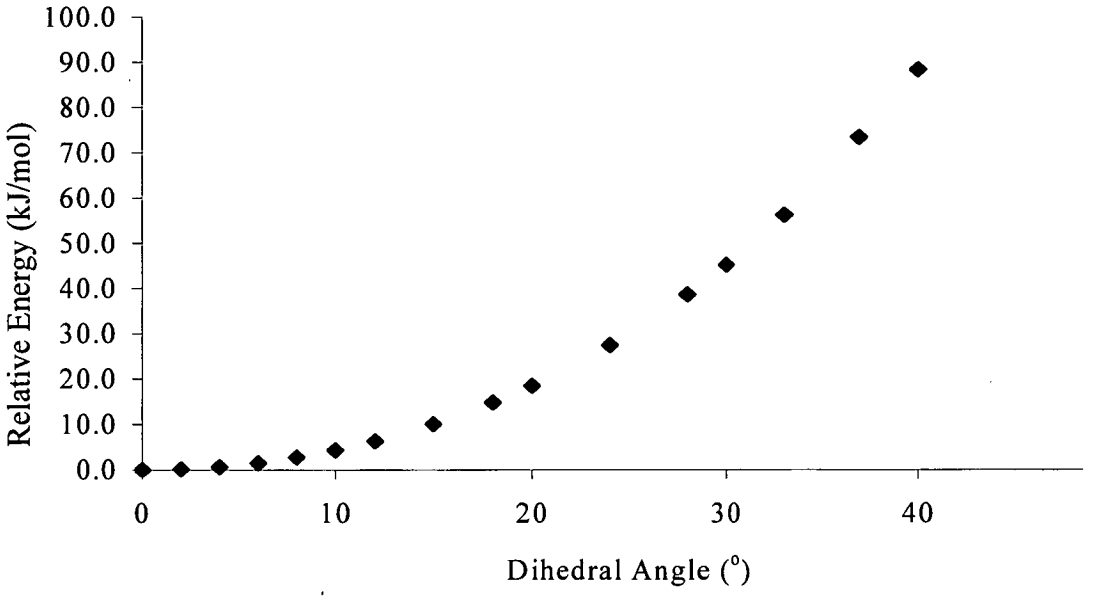

Figure 26.

In order to put these results in context with the results obtained earlier in Section 4.2.4.1, the single point energies of complexes **(XXXIV)** – **(XXXVI)** were determined. This time, however, the metal halide fragment of the complexes was removed and the geometry of the anion frozen. The calculated energies along with their corresponding dihedral angles and relative energies, with respect to the global minimum, are listed in Table 18.

Table 18. Relative Energy required to obtain various dihedral angle folding of the 4-azapentalenyl anion.

Compound	Dihedral angle (°)	Energy (kJ/mol)	Relative Energy (kJ/mol)
(XXXVII)	0.0	-853741.8249	0.0
(XXXIVa)	25.25	-853712.3824	30.44
(XXXIVb)	23.10	-853716.9092	25.92
(XXXVa)	22.60	-853719.0865	23.74
(XXXVb)	21.10	-853721.8134	21.01
(XXXVIa)	19.30	-853725.4365	17.39
(XXXVIb)	17.95	-853727.6604	15.16

From the data obtained in Table 18 it appears that the relative energies of the complexes occur within narrow range of relative energies, 15.1 – 30.5 kJ/mol.The greatest relative energies corresponded to the scandium complexes which have larger dihedral angles than the yttrium and lanthanum complexes. Figure 27 shows the overlap of the data from complexes **(XXXIV)** – **(XXXVI)** fitting to the trend which was determined by forcing the anion to fold at set values, in a narrow range of dihedral angle.

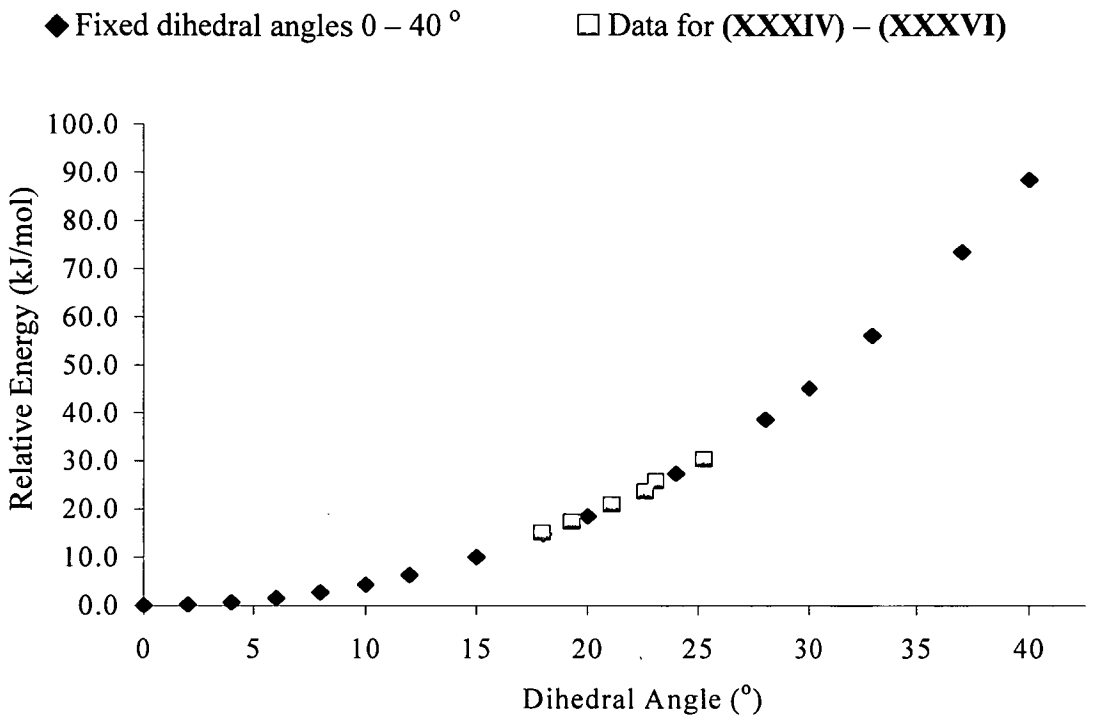

Figure 27.

An extended investigation was undertaken to determine if there was any energy advantage in the metal forming a complex of a higher coordination number, as may be the case when the anion folds towards the metal centre. In order to do this the two energies of the $[(C_7H_6N)MX_2]$ complexes given in Table 18 were required to be determined. The first of these energies relates to the effect the folding of the 4-azapentalenyl anion has on the total energy of the complex; for these calculations the dihedral bridgehead angle was fixed to be 0 °. The second energies calculated are those which relate to the folded structures from Section 4.2.4.1, which are seen here as energies relating to loss of aromaticity in the complex. The energy advantage in the metal forming a higher coordination number complex can then be calculated using Equation 2.

Energy Advantage = Total energy effect of folding – Loss of aromaticity energy

= Energy (fixed dihedral angle 0 °) – Energy (free optimisation)

Equation 2.

Table 19. The energy advantage in the formation of a complex with a higher metal coordination number.

Complex	Energy[a] (kJ/mol)	Energy[b] (kJ/mol)	Dihedral angle (°)	Energy advantage[c] (kJ/mol)
$[(C_7H_6N)ScCl_2]$	-5268181.0	-5268224.0	25.2	43.0
$[(C_7H_6N)ScF_2]$	-3375984.3	-3376003.9	23.2	19.5
$[(C_7H_6N)YCl_2]$	-3371562.1	-3371597.3	22.6	35.3
$[(C_7H_6N)YF_2]$	-1479328.3	-1479359.0	21.2	30.7
$[(C_7H_6N)LaCl_2]$	-4414822.8	-4414850.7	19.3	27.9
$[(C_7H_6N)LaF_2]$	-2522590.6	-2522613.6	18.1	23.0

[a] Bridgehead dihedral angle of 4-azapentalenyl anion in $[(C_7H_6N)MX_2)]$ was frozen to be 0 ° during optimisation.

[b] Free optimised of $[(C_7H_6N)MX_2)]$ complexes, see dihedral angle column for optimised bridgehead dihedral angle.

[c] Energy[a] – Energy[b]

From the data obtained in Table 19, it is clearly seen that there is a distinct energy advantage in Group 3 metal complexes of the type $[(C_7H_6N)MX_2)]$ to form complexes where the metal has a high coordination number. That is, these complexes have a greater preference to form complexes where the 4-azapentalenyl anion has a folded geometry and the Group 3 cation is coordinated to both five membered rings of the complex *via* η^6 or η^8 interactions.

4.2.5 Density functional theory studies of 4-azapentalenyl Group 4 metal complexes.

4.2.5.1 Density functional theory studies of neutral 4-azapentalenyl Group 4 trihalides, $[(C_7H_6N)MX_3]$

The geometries and relative binding energies of neutral 4-azapentalenyl Group 4 metal trihalide complexes were studied using B3LYP[51-53] density functional theory using the Gaussian 03 suite.[54] Two possible starting geometries for the Group 4 metal complexes were chosen, A and B, these are shown in Figure 28. Optimisation and subsequent single point energy calculations on these structures were carried out as outlined earlier in the general computational methods, Section 4.2.1.

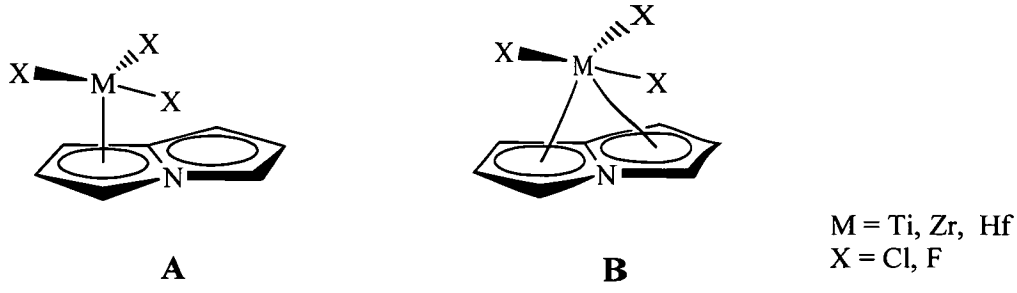

Figure 28. Starting geometries of neutral 4-azapentalenyl Group 4 complexes.

Optimisation of the starting geometries resulted in two unique final geometries, Figures 29 – 31, with the final symmetries outlined in Table 20. This is in contrast to the earlier Group 3 metal complexes studied where the optimisation of the two different starting symmetries resulted in a single converged structure. Optimisation of the halide containing complexes of C_1 symmetry resulted in final geometries where the C_1 symmetry was maintained. In these complexes the binding mode between the metal centre and the 4-azapentalenyl anion is best described as an η^5 interaction where the Group 4 metal interacts with one of the five membered rings of the bicyclic anion.

Table 20. Metal – 4-azapentalenyl binding mode of optimised structures starting from various symmetries.

		Cl^- (a)		F^- (b)	
	M	C_1	C_s	C_1	C_s
(XXXVII)	Ti^{4+}	η^5	η^5	η^5	η^5
(XXXVIII)	Zr^{4+}	η^5	η^5	η^5	η^4
(XXXIX)	Hf^{4+}	η^5	η^5	η^5	η^4

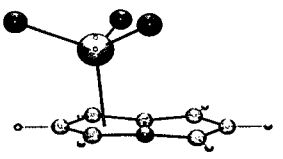

(XXXVIIa)-C_1

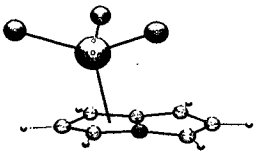

(XXXVIIa)-C_s

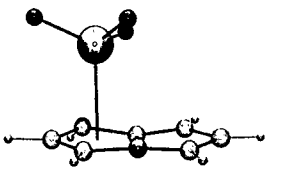

(XXXVIIb)-C_1

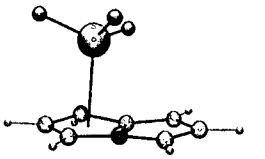

(XXXVIIb)-C_s

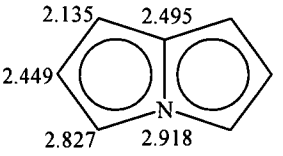

(XXXVIIa)-C_1

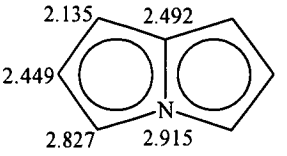

(XXXVIIa)-C_s

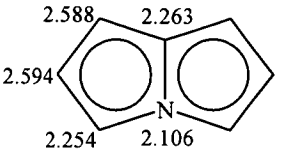

(XXXVIIb)-C_1

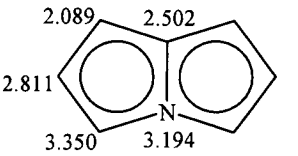

(XXXVIIb)-C_s

Figure 29.

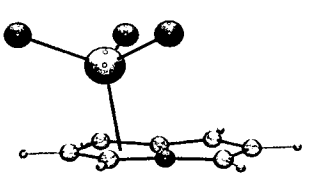

(XXXVIIIa)-C_1

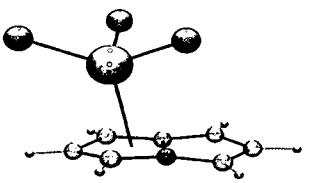

(XXXVIIIa)-C_s

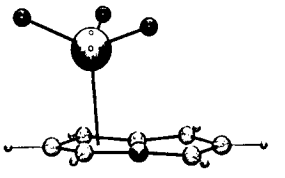

(XXXVIIIb)-C_1

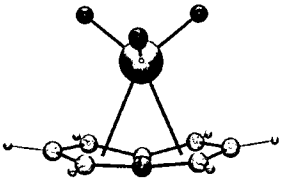

(XXXVIIIb)-C_s

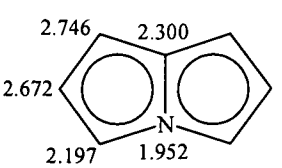

(XXXVIIIa)-C_1

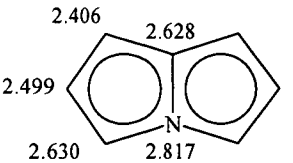

(XXXVIIIa)-C_s

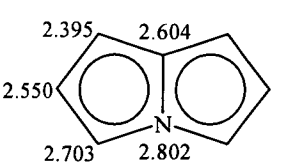

(XXXVIIIb)-C_1

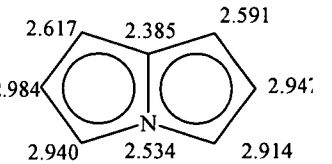

(XXXVIIIb)-C_s

Figure 30.

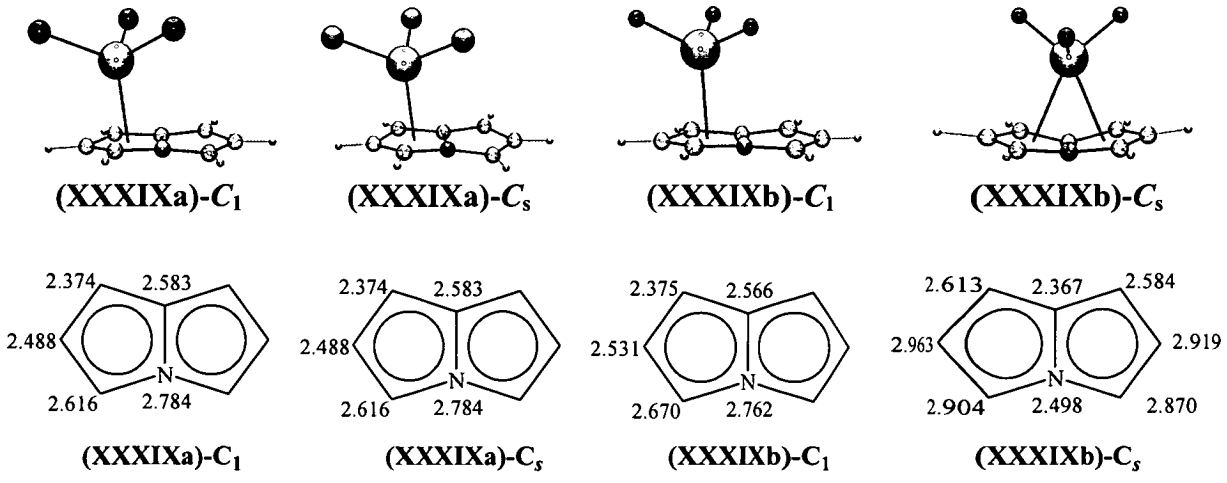

Figure 31.

The relative binding energies for the optimised structures **(XXXVII)** – **(XXXIX)** are given in Table 21. These relative binding energies are calculated using the equation given earlier, Equation 1. The relative energies indicate that those structures where the halide is a chloride have lower relative dissociation energies in comparison to their analogous fluoride complexes. When comparing the effect the different metal centres have on the energy of the complexes it is shown that those structures which had a zirconium metal centre had the lowest relative dissociation energy. Similarities in the relative binding energies are observed for the 4-azapentalenyl structures of titanium and hafnium trichloride, 917.0 and 914.4 kJ/mol, respectively. This closeness in relative binding energies is not observed between the analogous fluoride structures where the difference was found to be 51.6 kJ/mol.

Table 21. Relative binding energies for transition metal 4-azapentalenyl complexes.†

M		X	
		Cl^- (a)	F^- (b)
Ti^{4+}	(XXXVII)	917.0	986.2
Zr^{4+}	(XXXVIII)	898.9	919.9
Hf^{4+}	(XXXIX)	914.4	934.6

† All energies are in kJ/mol.

4.2.5.2 Density functional theory studies of 4-azapentalenyl Group 4 dihalide cationic, $[(C_7H_6N)MX_2]^+$

The relative binding energies and the optimised geometries of the 4-azapentalenyl Group 4 metal dihalogen cationic complexes were investigated using B3LYP[51-53] density functional theory using the Gaussian 03 suite.[54] The basis sets used during the geometry optimisation and the subsequent single point energy calculation have been previously outlined in Section 4.2.1. Optimisation of structures with geometry of type A and B converged to give a single structure of type C geometry.

The relative binding energies of the studied structures, Table 22, indicate that the dichloride complexes of titanium and zirconium are more readily formed than the analogous fluoride complexes. In comparison the corresponding hafnium difluoride complexes were found to have lower relative dissociation energy when compared to the analogous dichloride. The single point energies for each structure indicates the lowest energy complexes are those of the dichloride containing cationic species, Table 22; these complexes have a greater stability in comparison to their fluoride counter parts. In the series of dichloride containing complexes the most stable is that

of the 4-azapentalenyl titanium dichloride cationic complex, likewise the analogous titanium difluoride complex shows the greatest stability of the fluoride containing Group 4 complexes.

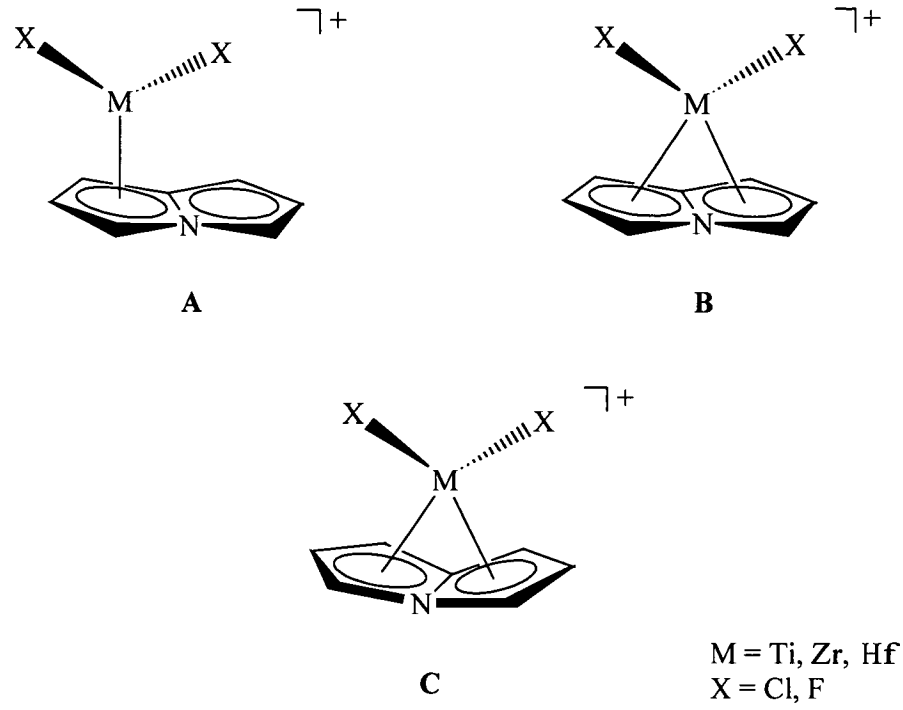

Figure 32. Structure types a – c for 4-azapentalenyl dihalide Group 4 cationic complexes, a – b starting geometry, c converged geometry.

Table 22. Single point and relative binding energies of 4-azapentalenyl Group 4 metal cationic complexes.

		Single Point Energies (kJ/mol)		Relative Binding Energies (kJ/mol)	
M				X	
		Cl^- (a)	F^- (b)	Cl^- (a)	F^- (b)
Ti^{4+}	(XL)	-3423296.1	-1531084.6	1878.5	2093.4
Zr^{4+}	(XLI)	-3393771.3	-1501544.7	1781.0	1908.6
Hf^{4+}	(XLII)	-3396868.8	-1504079.4	2358.0	1912.3

Figures 33a and 33b show the final optimised geometries and the metal – 4-azapentalenyl bond lengths of the Group 4 cationic complexes studied. The

structures exhibit a degree of folding of the 4-azapentalenyl anion along the bridgehead vector towards the metal centre, and this is observed to vary only when the Group 4 metal is changed. The metal cation in each complex is observed to be positioned over the bridgehead vector of the anion whilst the halides of each complex are orientated in a similar yet not identical direction. The metal cation – anion bonds of all complexes were found to be of an unequal interaction length, with the shortest length being that between the metal and bridgehead nitrogen.

a)

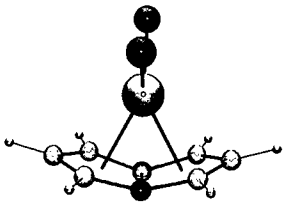

(XLa)

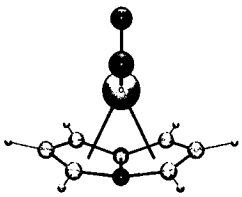

(XLIa)

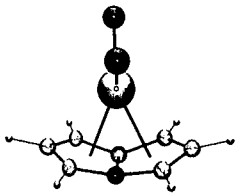

(XLIIa)

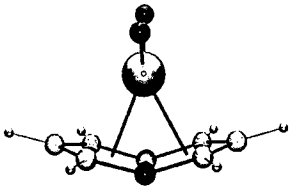

(XLb)

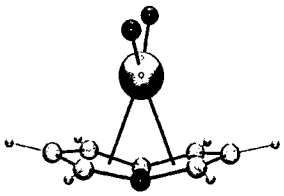

(XLIb)

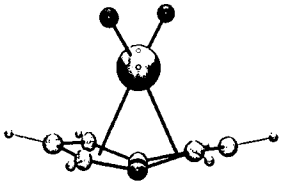

(XLIIb)

b)

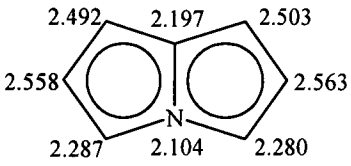

(XLa)

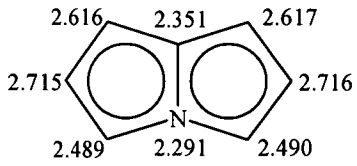

(XLIa)

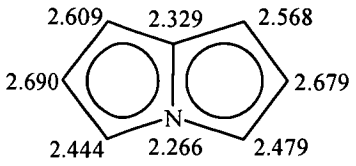

(XLIIa)

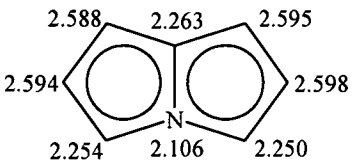

(XLb)

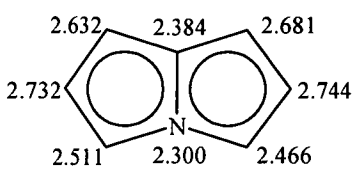

(XLIb)

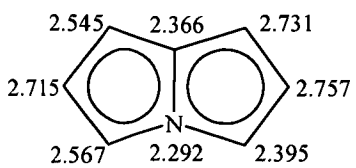

(XLIIb)

Figure 33.

The structures in Figure 33b indicate a lengthening of the metal anion interactions on going from the titanium to the zirconium complexes. This lengthening of the interactions is not observed when moving from the zirconium to the hafnium complexes. An exception to this is the hafnium fluoride complex where the length between the cation and the wingtip carbons is slightly longer than the analogous zirconium species.

Table 23. Metal – centroid bond length and fold angle of 4-azapentalenyl Group 4 metal complexes, $[(C_7H_6N)MX_2]^+$.

	(XLa)	**(XLb)**	**(XLIa)**	**(XLIb)**	**(XLIIa)**	**(XLIIb)**
M-Ct_1 (Å)	1.99_9	2.03_9	2.18_6	2.20_9	2.16_0	2.19_2
M-Ct_2 (Å)	2.00_1	2.04_1	2.18_7	2.21_3	2.15_4	2.20_6
M-Ct_3 (Å)	2.02_8	2.06_4	2.20_7	2.22_9	2.18_3	2.21_6
Fold angle (°)	32.5	31.7	29.3	28.8	30.4	29.1

The lengths between the metal and the anion are not the only parameters to vary between these structures, with a similar pattern also observed for the dihedral angle of the anion, Table 23. The largest dihedral angles observed in this selection of complexes are for the Group 4 metal dichloride complexes, with the largest dihedral angle observed being that for the titanium complex, **(XLa)**. A decrease in the fold angle is observed for the analogous zirconium and hafnium complexes. These complexes contain larger cations which force the anion away, leading to the decrease which is observed for this particular angle. Little or no variation in this particular angle is noted to occur when the zirconium metal centre is exchanged for the larger hafnium metal centre, Table 23.

4.2.5.3 Density functional theory study of neutral 4-azapentalenyl Group 4 dihalides, $[(C_7H_6N)MX_2]$

The geometries and relative binding energies of neutral 4-azapentalenyl Group 4 metal dihalogenated complexes were studied using B3LYP[51-53] density functional theory using the Gaussian 03 suite.[54] Two possible starting geometries for the Group 4 metal complexes were chosen, A and B, these are shown in Figure 34. Optimisation and subsequent single point energy calculations on these structures were carried out as outlined earlier in the general computational method Section, Section 4.2.1.

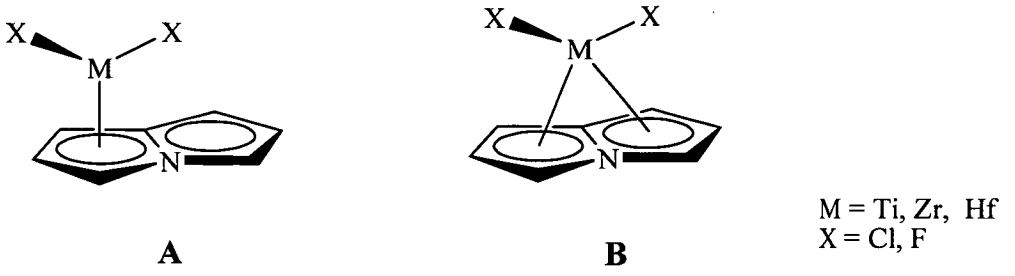

Figure 34. Starting geometries of neutral 4-azapentalenyl Group 4 complexes.

The optimisation of each starting geometry gave rise to a single, unique geometry of either C_1 or C_s symmetry, Figures 35 - 37. This is in contrast to the optimised geometries of the 4-azapentalenyl Group 4 metal dihalide cationic complexes in Section 4.2.3.2 where optimisation of the starting geometry resulted in a single converged geometry of C_s symmetry.

Table 24

		Relative Binding Energies (kJ/mol)			
		C_1		C_s	
		Cl^- (a)	F^- (b)	Cl^- (a)	F^- (b)
Ti^{3+}	(XLIII)	923.8	935.1	892.6	902.6
Zr^{3+}	(XLIV)	989.9	1032.5	985.3	1032.5
Hf^{3+}	(XLV)	941.0	973.2	937.9	973.2

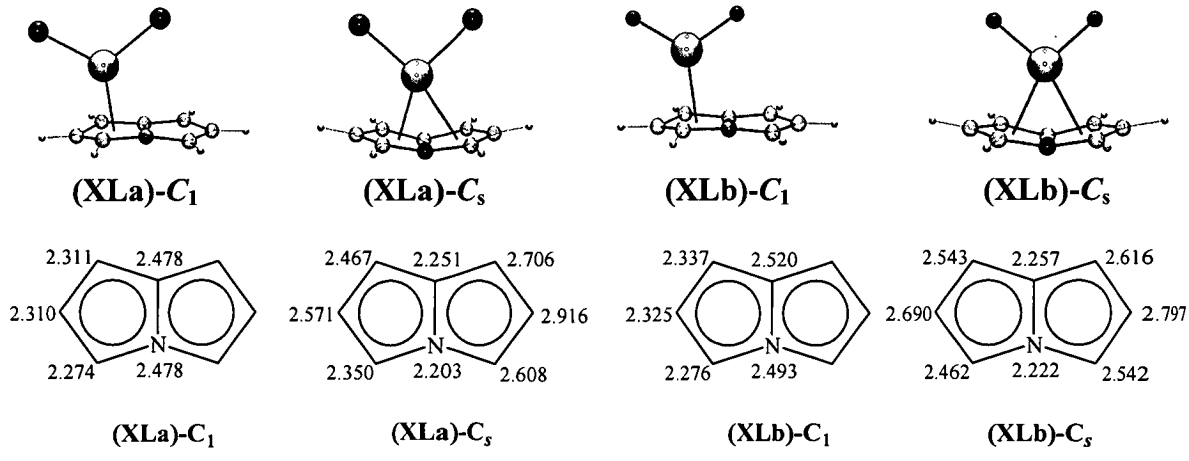

Figure 35.

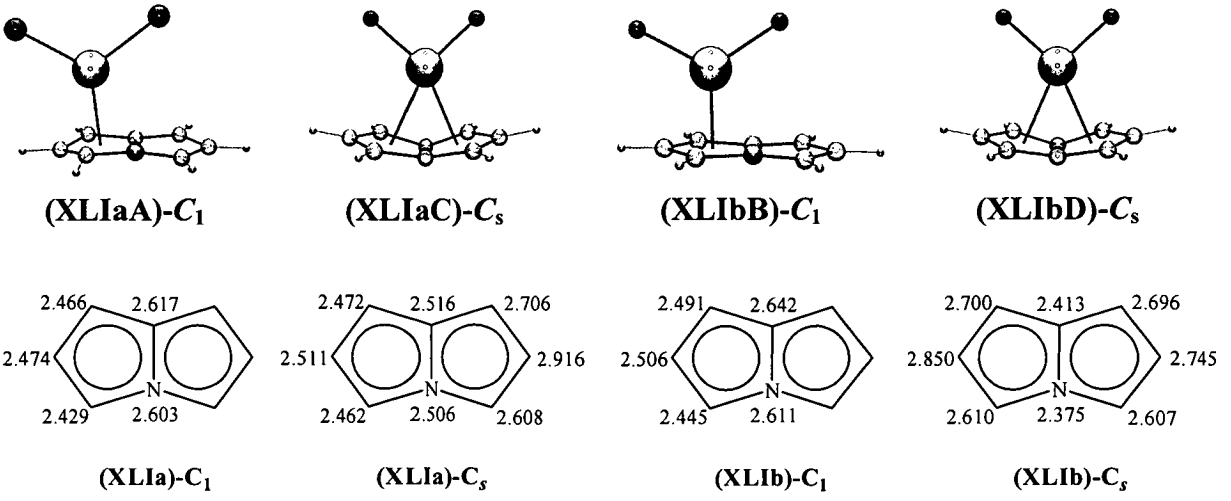

Figure 36.

Similar geometries to those of the optimised titanium dihalide complexes were observed for the analogous zirconium and hafnium complexes, Figures 34a and 35a, respectively. Optimisation of complexes of type A, C_1 symmetry, gave structures of the type A and B. As with the titanium complexes little folding of the anion towards the metal cation is observed; this is reflected in Table 25 where little difference is observed between the dihedral angles for titanium through to hafnium. The fold of the bridgehead dihedral angle for the zirconium and hafnium dichloride complexes is almost identical with only 0.1 ^{o} being the difference between the two.

While little change is observed in the dihedral angle a lengthening of the cation – 4-azapentalenyl anion interaction is observed between the zirconium and hafnium complexes. Both complexes exhibit an η^5 type interaction between the metal centre and the 4-azapentalenyl anion with the metal centre slipped more towards the extremity of one of the five membered rings. This is reflected in the individual cation – 4-azapentalenyl atom lengths shown in Figures 36b and 37b, where it is clearly noted that the length of the interactions of the cation with carbons 2, 3 and 4 are shorter than those with the bridgehead atoms. The overall individual lengths between the cationic centre and the atoms lengthens when moving from titanium to zirconium, and this length then shortens on moving from zirconium to

hafnium. This trend is not unusual and is seen often for complexes containing Group 4 metals.

Table 25. Metal – 4-azapentalenyl binding mode of optimised structures starting from various symmetries.

	C_1		C_s	
Metal	Cl	F	Cl	F
Ti	1.9	2.5	23.5	23.9
Zr	1.5	0	25.1	25.0
Hf	1.6	4.2	27.2	25.9

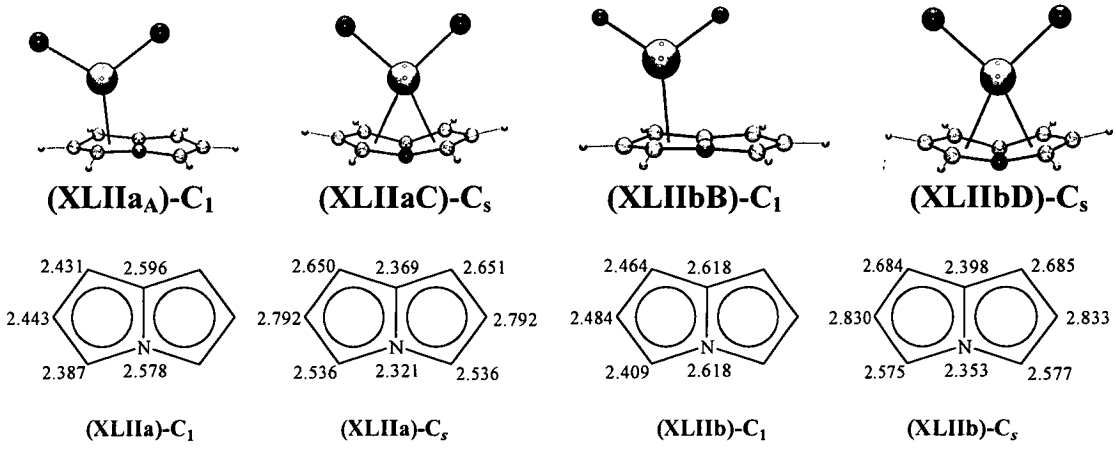

Figure 37.

The optimisation of the zirconium and hafnium dihalide complexes of the starting geometry type B gave structures of similar geometry to that of the earlier described analogous titanium complexes. The optimised geometries of the zirconium and hafnium complexes both exhibit a folding of the 4-azapentalenyl anion towards the metal centre, as shown in Figures 36a and 37a. The halogen substituents in these structures are seen to be perpendicular in relation to the dihedral vector of the bicyclic anion, similar to that observed to the analogous titanium complexes described earlier. The degree by which the bridgehead dihedral angle changes between the chloride to the fluoride complex is marginal in all optimised complexes,

Table 25. A small decrease of 1.3 ° in this angle is observed in the hafnium complexes when the chloride substituents are exchanged with fluorides.

The individual cation – C/N bond lengths for the zirconium and hafnium dihalide complexes of the type C and D vary depending on the metal cation present in the complex. An increase in the overall lengths is observed between titanium to zirconium, however, the lengths are shorter for hafnium. The shortest interaction length occurs between the metal cation and the bridgehead atoms, in particular the bridgehead nitrogen, which exhibits the shortest length in all six complexes of the folded geometry. The greatest lengths are observed to be between the wingtip carbons and the cation, for hafnium this length is 2.833 Å for the fluoride containing complex.

A slippage of the bicyclic anion is observed for the titanium and zirconium complexes of type C and D. The slippage of the 4-azapentalenyl anion leads to shorter interactions occurring between one of the five membered rings in comparison to the other. The shortest interactions between the cation and the 4-azapentalenyl are with the bridgehead atoms, the next shortest bond length after these is that with the carbon atom adjacent to the bridgehead nitrogen atom, indicating a slippage not only to one of the rings but also towards the nitrogen side of the heterocyclic anion. This slippage to one ring is not seen, however, in the analogous hafnium complexes, a slight slippage towards the nitrogen is still observed though. It can be noted that the individual hafnium 4-azapentalenyl anion lengths are more even than those of the previously mentioned titanium and zirconium complexes. This indicates that the hafnium cation is positioned over the bridgehead vector and not over one of the five membered rings.

The metal cation is seen to interact with the 4-azapentalenyl anion in these complexes in what may be described as either an η^6 or an η^8 fashion, depending whether the wingtip carbon interactions are included. For the smaller cationic centres of titanium and zirconium interaction with the wing tip carbons is likely to have little significance on the overall complex. The interaction between the metal centre and the anion is therefore best described as an η^6 type binding mode where the cation interacts with all atoms bar the wingtip carbons. However this is not the case for the

larger hafnium metal centre. The dihedral fold angle of the anion is similar to that seen for the titanium and zirconium and the lengths between the metal and anion are similar to those see for the analogous titanium complex. For the hafnium complexes it is therefore likely that the wingtip carbons are significant in the cation – anion interaction, that is the binding mode is best described as an η^8 interaction involving all atoms of the 4-azapentalenyl anion.

4.3 REFERENCES

(1) Pauson, P. L.; Kealy, T. J. *Nature* **1951**, *168*, 1039 - 1040.

(2) Jutzi, P. *Chem. Rev.* **1986**, *86*, 983 - 996.

(3) Jutzi, P. *J. Organomet. Chem.* **1990**, *400*, 1 - 17.

(4) Jutzi, P.; Burford, N. *Chem. Rev.* **1999**, *99*, 969 - 990.

(5) Jutzi, P.; Reumann, G.
J. Chem. Soc., Dalton Trans. **2000**, 2237 - 2244.

(6) Poli, R. *Chem. Rev.* **1991**, *91*, 509 - 551.

(7) Hou, Z. *Bull. Chem. Soc. Jpn* **2003**, *76*, 2253 - 2266.

(8) King, R. B. *Coord. Chem. Rev.* **1976**, *20*, 155-169.

(9) Geerlings, P.; Proft, F. D.; Langenaeker, W.
Chem. Rev. **2003**, *103*, 1793 - 1873.

(10) Hanusa, T. P. *Organometallics* **2002**, *21*, 2559 - 2571.

(11) Green, J. C.; Hohl, D.; Roesch, N.
Organometallics **1987**, *6*, 712 - 720.

(12) Niu, S.; Hall, M. B. *Chem. Rev.* **2000**, *100*, 353 - 405.

(13) Frunzke, J.; Lein, M.; Frenkling, G.
Organometallics **2002**, *21*, 3351 - 3359.

(14) Schumann, H.; Albrecht, I.; Loebel, J.; Hahn, E.; Hossain, M. B.;
van der Helm, D. *Organometallics* **1986**, *5*, 1296 - 1304.

(15) Sudupe, M.; Cano, J.; Royo, P.; Herdtweck, E.
Eur. J. Inorg. Chem. **2004**, 3074 - 3083.

(16) Braun, L. F.; Dreier, T.; Christy, M.; Petersen, J. L.
Inorg. Chem. **2004**, *43*, 3976 - 3987.

(17) Bridgeman, A. J. *J. Chem. Soc., Dalton Trans.* **1997**, 2887 - 2893.

(18) Rayón, V. M.; Frenking, G. *Chem. Eur. J.* **2002**, *8*, 4693 - 4707.

(19) Bénard, M.; Rohmer, M.-M.
J. Am. Chem. Soc. **1992**, *114*, 4785 - 4790.

(20) Harder, S.; Prosenc, M. H.; Rief, U. *Organometallics* **1996**, *15*, 118.

(21) Harder, S.; Prosenc, M. H.
Angew. Chem., Int. Ed. Engl. **1994**, *33*, 1744.

(22) Stalke, D. *Angew. Chem., Int. Ed. Engl.* **1994**, *33*, 2168 - 2171.

(23) Bunder, W.; Weiss, E. *J. Organomet. Chem.* **1975**, *92*, 1.

(24) Zerger, R.; Stucky, G. *J. Organomet. Chem.* **1974**, *80*, 7.

(25) Veiros, L. F. *Chem. Eur. J.* **2005**, *11*, 2505 - 2518.

(26) Calhorda, M. J.; Romão, C. C.; Veiros, L. F.
Chem. Eur. J. **2002**, *8*, 868 - 875.

(27) Calhorda, M. J.; Gamelas, C. A.; Gonçalves, I. S.; Herdtweck, E.; Romão, C. C.; Veiros, L. F. *Organometallics* **1998**, *17*, 2597 - 2611.

(28) Ascenso, J. R.; Gonçalves, I. S.; Herdtweck, E.; Romão, C. C.
J. Organomet. Chem. **1996**, *508*, 169.

(29) Stoll, M.; Belanzoni, P.; Calhorda, M. J.; Drew, M. G. B.; Félix, V.; Geiger, W. E.; Gamelas, C. A.; Gonçalves, I. S.; Romão, C. C.; Veiros, L. F. *J. Am. Chem. Soc.* **2001**, *123*, 10595 - 10606.

(30) Biagioni, R. N.; Lorkovic, I. M.; Skelton, J.; Hartung, J. B.
Organomeallics **1990**, *9*, 547 - 551.

(31) Forschner, T. C.; Cutler, A. R.; Kullnig, R. K.
Organometallics **1987**, *6*, 889 - 891.

(32) Merola, J. S.; Kacmarcki, R. T.; Van Engen, D. J.
J. Am. Chem. Soc. **1986**, *108*, 329 - 331.

(33) Kowalewski, R. M.; Rheingold, A. L.; Trogler, W. C.; Basolo, F.
J. Am. Chem. Soc. **1986**, *108*, 2460 - 2461.

(34) Brooks, J. J.; Wendell, R.; Stucky, G. D.
J. Am. Chem. Soc. **1972**, *94*, 7399 - 7346.

(35) Calhorda, M. J.; Gonçalves, I. S.; Herdtweck, E.; Romão, C. C.; Royo, B.; Veiros, L. F. *Organometallics* **1999**, *18*, 3956 - 3958.

(36) Allen, F. H. *Acta Crystallogr.* **2002**, *B58*, 380 - 388.

(37) Bruno, I. J.; Cole, J. C.; Edgington, P. R.; Kessler, M.; Macrae, C. F.; McCabe, P.; Pearson, J.; Taylor, R.
Acta Crystallogr. **2002**, *B58*, 389-397.

(38) Kirillov, E.; Toupet, L.; Lehmann, C. W.; Razavi, A.; Kahlal, S.; Saillard, J.-Y.; Carpentier, J.-F.
Organometallics **2003**, *22*, 4038 - 4046.

(39) Katz, T. J.; Rosenberger, M. *J. Am. Chem. Soc.* **1963**, 2030-2031.

(40) Katz, T. J.; Rosenberger, M. *J. Am. Chem. Soc.* **1962**, *84*, 865-866.

(41) Katz, T. J.; Acton, N. J. *J. Am. Chem. Soc.* **1972**, *94*, 3281.

(42) Katz, T. J.; Acton, N. J.; McGinnis, J.
J. Am. Chem. Soc. **1972**, *94*, 6205.

(43) Cloke, F. G. N.; Green, J. C.; Jardine, C. N.; Kuchta, M. C.
Organometallics **1999**, *18*, 1087 - 1090.

(44) Costuas, K.; Saillard, J.-Y. *Chem. Commun.* **1998**, 2047 - 2048.

(45) Kuchta, M. C.; Cloke, F. G. N.; Hitchcock, P. B.
Organometallics **1998**, *17*, 1934 - 1936.

(46) Jonas, K.; Kolb, P.; Kollbach, G.; Gabor, B.; Mynott, R.; Angermund, K.; Heinemann, O.; Krüger, C.
Angew. Chem., Int. Ed. Engl. **1997**, *36*, 1714 - 1718.

(47) Jonas, K.; Gabor, B.; Mynott, R.; Angermund, K.; Heinemann, O.; Krüger, C. *Angew. Chem., Int. Ed. Engl.* **1997**, *36*, 1712 - 1714.

(48) Gleiter, R.; Bethke, S.; Okubo, J.; Jonas, K.
Organometallics **2001**, *20,* 4274 - 4278.

(49) Young, D. C. *Computational Chemistry; A practical guide for applying techniques to real world problems*; John Wiley and Sons, Inc.: New York, 2001.

(50) Cloke, F. G. N.; Green, J. C.; Janesko, B. G.
Organometallics **1999**, *18*, 1080 - 1086.

(51) Becke, A. D. *J. Chem. Phys.* **1993**, *93*, 5648.

(52) Becke, A. D. *Phys. Rev. A.* **1998**, 3098.

(53) Lee, C.; Yang, W.; Parr, R. G. *Phys. Rev. B.* **1998**, *37*, 785.

(54) Frisch, M. J.; Trucks, G. W.; Schlegel, H. B.; Scuseria, G. E.; Robb, M. A.; Cheeseman, J. R.; Montgomery, J., J. A.; Vreven, T.; Kudin, K. N.; Burant, J. C.; Millam, J. M.; Iyengar, S. S.; Tomasi, J.; Barone, V.; Mennucci, B.; Cossi, M.; Scalmani, G.; Rega, N.; Petersson, G. A.; Nakatsuji, H.; Hada, M.; Ehara, M.; Toyota, K.; Fukuda, R.; Hasegawa, J.; Ishida, M.; Nakajima, T.; Honda, Y.; Kitao, O.; Nakai, H.; Klene, M.; Li, X.; Knox, J. E.; Hratchian, H. P.; Cross, J. B.; Bakken, V.; Adamo, C.; Jaramillo, J.; Gomperts, R.; Stratmann, R. E.; Yazyev, O.; Austin, A. J.; Cammi, R.; Pomelli, C.; Ochterski, J. W.; Ayala, P. Y.; Morokuma, K.; Voth, G. A.; Salvador, P.; Dannenberg, J. J.; Zakrzewski, V. G.; Dapprich, S.; Daniels, A. D.; Strain, M. C.; Farkas, O.; Malick, D. K.; Rabuck, A. D.; Raghavachari, K.; Foresman, J. B.; Ortiz, J. V.; Cui, Q.; Baboul, A. G.; Clifford, S.;

Cioslowski, J.; Stefanov, B. B.; Liu, G.; Liashenko, A.; Piskorz, P.; Komaromi, I.; Martin, R. L.; Fox, D. J.; Keith, T.; Al-Laham, M. A.; Peng, C. Y.; Nanayakkara, A.; Challacombe, M.; Gill, P. M. W.; Johnson, B.; Chen, W.; Wong, M. W.; Gonzalez, C.; Pople, J. A.; Revision C.02 ed.; Gaussian, Inc.: Wallingford CT, 2004.

(55) Frisch, M. J.; Pople, J. A.; Binkley, J. S. *J. Chem. Phys.* **1984**, *80*, 3265.

(56) Dunning, T. H.; Hay, P. J. *Modern Theoretical Chemistry*; Plenum: New York, 1976; Vol. 3.

(57) Hay, P. J.; Wadt, W. R. *J. Chem. Phys.* **1985**, *82*, 299.

(58) Dolg, M.; Wedig, U.; Stoll, H.; Preuss, H. *J. Chem. Phys.* **1987**, *86*, 866 - 872.

(59) Andrae, D.; Haeussermann, U.; Dolg, M.; Stoll, H.; Preuss, H. *Theor. Chem. Acc.* **1990**, *77*, 123.

(60) Cloke, F. G. N.; Kuchta, M. C.; Harker, R. M.; Hitchcock, P. B.; Parry, J. S. *Organometallics* **2000**, *19*, 5795.

(61) Somers, K. R. F.; Kryachko, E. S.; Ceulemans, A. *J. Phys. Chem. A* **2003**, *107*, 5427 - 5438.

(62) Dinnebar, R. E.; Behrens, U.; Olbrich, E. *Organometallics* **1997**, *16*, 3855.

(63) Stezowski, J. J.; Hoier, H.; Wilhlem, D.; Clark, T.; Schleyer, P. v. R. *Chem. Commun.* **1985**, *18*, 1263.

(64) Dinnebar, R. E.; Neander, S.; Behrens, U.; Olbrich, E. *Organometallics* **1999**, *18*, 2915.

(65) Uffing, C.; Koppe, R.; Schnockle, M. *Organometallics* **1998**, *17*, 3512.

(66) Tedesco, C.; Dinnebar, R. E.; Olbrich, E.; von Smaalen, S. *Acta Crystallogr., Sect. B: Struct. Sci.* **2001**, *57*, 673.

(67) Corbelin, S.; Kopf, J.; Weiss, E. *Chem. Ber.* **1991**, *124*, 2417.

(68) Evans, W. J.; Brady, J. C.; Fujimoto, C. H.; Giarikos, D. G.; Ziller, J. W. *Organometallics* **2002**, *649*, 252.

(69) Shu-Li, Z.; Zhong-Sheng, J.; Ge-Cheng, W.; Wen-Qi, C. *Jiegou Huaxue* **1991**, *10*, 31.

(70) Jordan, V.; Behrens, U.; Olbrich, E.; Weiss, E.

J. Organomet. Chem. **1996**, *517*, 18.

(71) Neander, S.; Kormich, J.; Olbrich, E.
J. Organomet. Chem. **2002**, *656*, 89.

(72) Allred, A. L. *J. Inorg. Nucl. Chem.* **1961**, *17*, 215.

(73) Cotton, F. A.; Wilkinson, G. *Advanced Inorganic Chemistry*; 5th ed.; John Wiley and Sons Inc.: New York, 1988.

CHAPTER 5
COMPUTATIONAL STUDIES OF CATALYTICALLY RELEVANT SYSTEMS

5.1 INTRODUCTION

The insertion of an alkene into a metal – hydride or metal alkyl bond has long been widely explored both synthetically and computationally in the polymerisation of alkenes.[1] In 1953 Karl Ziegler reported the production of a polyethylene *via* the polymerisation of ethylene at low pressures with a solid catalyst, in particular the reaction between triethylaluminium and titanium tetrachloride.[2] The reaction yielded a polyethylene that was more rigid and dense, as well as being more highly crystalline than previously obtainable. What was of great interest though was the polyethylene obtained had greater structural regularity in comparison to the polyethylene being produced in industry at the time that required higher temperatures and pressures.[2] A year later in 1954 Guilio Natta reported the synthesis of stereoregular polypropylene using catalytic systems that were similar to those of Ziegler.[3] The use of the heterogeneous catalytic systems developed by Ziegler produced isotactic polymers and only small amounts of syndiotactic polymers. To produce larger quantities of syndiotactic polymers homogenous catalysts based on vanadium that were activated by aluminium alkyls were used.[4]

Around the same time that Ziegler and Natta made their discovery the first transition metal metallocenes utilising the cyclopentadienyl anion (Cp) were reported in 1951 by Kealy and Paulson.[5] In 1957 Natta and his co-workers reported the use of bis(cyclopentadienyl)titanium dichloride in the presence of triethylaluminium in the successful polymerisation of ethylene.[6] This homogeneous catalyst system and other catalysts based on $Cp_2MCl_2/AlRCl_2$ system (where M = titanium, zirconium, R = methyl, ethyl) were shown to be less active catalysts than the traditional Ziegler catalysts.[4,6] It wasn't until much later in 1976 that Kaminsky and Sinn showed that these Group 4 metallocenes could be activated with methylaluminoxane (MAO) to provide a highly active catalyst towards the polymerisation of a range of terminal alkenes.[4,7] These cationic metallocenes reported by Kaminsky and later by

Brintzinger[7,8] showed great promise in polymerisation reactions, preliminary results indicating that they could be 100 times more active than the traditional Ziegler-Natta catalysts.[9]

While the activity of the cationic Group 4 metallocenes catalysts was shown to be superior to that of the Ziegler-Natta systems, they did not produce stereoregular polymers. In order to overcome this low stereoregulation the development of chiral and stereorigid metallocenes was required.[10-12] This lead to the investigation of other multihaptic ligands other than cyclopentadienyl to be used as ligands in metallocene like systems, these included indenyl and fluorenyl anions. These however did not provide the appropriate properties in order to obtain the desired stereoregular polymers. During the 1980s it was found that by placing substitutents at various positions on the ligand and in some cases bridging the two ligands *via* a suitable substituent, known as *ansa* metallocenes, a more stereorigid, chiral metallocene catalyst could be obtained. This in turn led to the realisation that these "constrained geometry" catalysts enhanced not only the activity but also the enantioselectivity in the alkene insertion reaction giving greater selectivity towards isotactic and syndiotactic polymers.[13]

There are several proposed mechanisms which alkene insertion in a Ziegler–Natta catalytic system is thought to follow. The first of these was proposed by Cossée and Arlman in 1964,[14-16] and became a widely accepted mechanism by which olefin polymerisation in heterogeneous Ziegler–Natta system, and later homogeneous, occurs. The Cossée–Arlman mechanism, Scheme 1, shows the active complex has a vacant coordination site, which during the insertion step is occupied by the alkene allowing the formation of a π- complex. The alkene then inserts into the metal carbon bond, in a migratory process passing through a cyclic four-membered transition state which then goes on to give the alkyl product. This product also contains a vacant coordination site allowing for further reaction with another alkene that hence leads to the propagation of the alkyl chain.

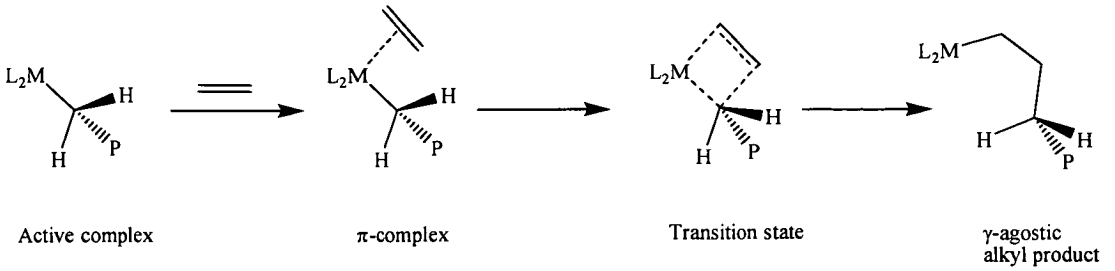

Scheme 1. Cossée – Arlman mechanism for alkene insertion polymerisation.

In 1983 Brookhart and Green proposed another mechanism by which olefin polymerisation could proceed.[17] Their slightly modified Cossée–Arlman mechanism implied that α-agostic interactions play an important role during the propagation of the alkyl chain, Scheme 2. This α-agostic interaction is thought to stabilise both the ground state alkene complex and the four-centre transition state.[17-20] Both mechanisms rely on an important aspect, that is that the insertion of the monomer is a two step process that comprises the coordination of the alkene followed by the insertion of the monomer into the metal – alkyl bond.[20]

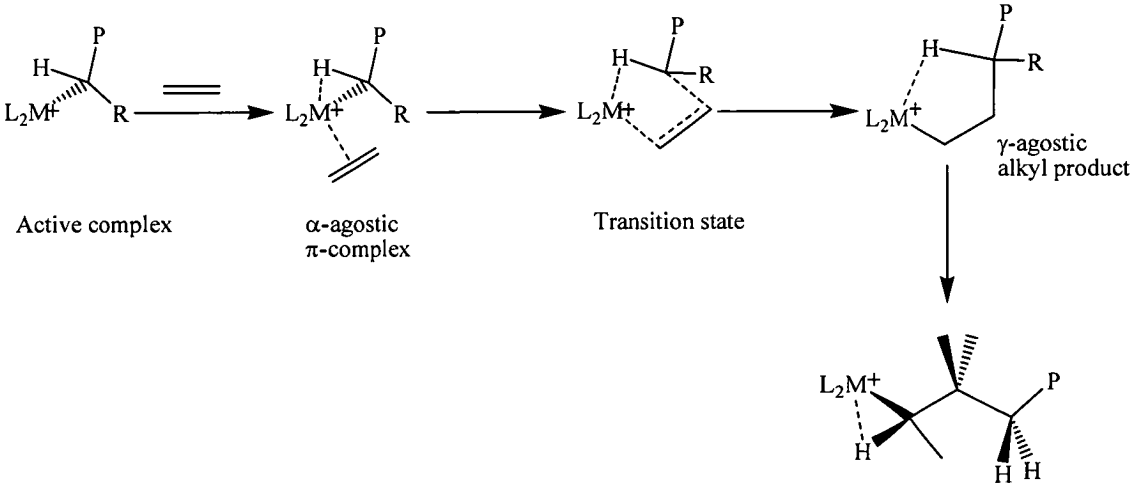

Scheme 2. Brookhart-Green mechanism for alkene insertion polymerisation

The use of early transition metals in these catalytically active species has not been limited to Group 4 metals, the application of *f*-block elements in metallocenes have been investigated as possible alternatives to the traditional heterogeneous Zeigler – Natta catalysts.[1,21,22] The use of lanthanides as a catalyst in a binary system for the polymerisation of butadiene was first reported by Shen and colleagues in 1964.[23] The lanthanide catalysts were of the type $LnCl_3$ and reacted in the presence

of an aluminium alkyl to produce highly stereospecific polymeric butadiene however the activity of these catalysts was low.[23,24] Over the following years, developments of the catalytic system were made in an attempt to increase the activity of these catalysts. Throckmorton increased the activity *via* the use of a ternary system, which had its own limitations as the cerium residues present needed to be completely removed.[25] During the 1970s the use of neodymium compounds or mixtures of neodymium and praseodymium were found to be highly active in the catalysis with butadiene. This led to the development of new ternary component systems, some of which contained lanthanide naphthenate, lanthanide carboxylates or lanthanide phosphates in the presence of an aluminium alkyl.[24] It was also shown by Yang *et al.* in 1980 that upon the addition of a known amount of alcohol to a $LnCl_3$ / aluminium alkyl system the activity of the catalyst was increased with no decrease in the stereospecificity.[26]

The lanthanide metals are known to form hydrides and alkyls when incorporated into cyclopentadienyl compounds and other similar compounds, some of which have been shown to be highly active catalysts for hydrogenation reactions.[27,28] In 1982 Watson reported the use of a bis(pentamethylcyclopentadienyl)lanthanide methyl complex (where the lanthanides used were lutetium and ytterbium) as a catalyst in the polymerisation of alkenes and alkynes.[29] In 1985 Marks and co-workers developed organolanthanide complexes which were shown to be extremely active homogeneous ethylene polymerisation catalysts.[28] The organolanthanide complexes of interest were comprised of the extensively utilised bis(pentamethylcyclopentadienyl) system. Also present in the highly active species was a bulky alkyl group that provided the steric bulk required to decrease the possibility of any unfavourable coordination of the metal centre to the halide moieties that were present during preparation.[28]

In 1990 Bercaw and co-workers reported the structure and reactivity of a single component scandium catalyst showing it to be capable of polymerising terminal alkenes to give regiospecific polymers.[30] Bercaw's group was able to show that these scandocene derivatives were able to undergo facile alkene insertion and β-hydride and β-alkyl elimination similar to that seen for Ziegler-Natta catalysts.[28] Two years later in 1992 he reported the first iso-specific, single component Ziegler-Natta

polymerisation catalyst, shown in Figure 1.[31] The inclusion of the bulky trimethyl silyl and *t*-butyl groups in the ligand design influences the way in which coordination to the yttrium centre occurs, thus leading to only the racemic isomer of the halide precursor. These bulky groups along with the constrained bridging silyl group led to a catalyst which has allowed for high stereospecificity during the polymerisation of terminal alkenes.[31]

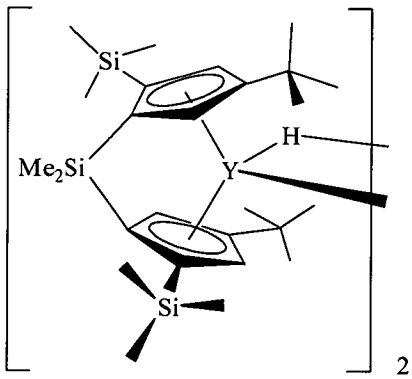

Figure 1. Single component Ziegler-Natta catalyst,

Many computational studies have been undertaken in order to gain a better understanding of the Ziegler-Natta polymerisation of alkenes and the actual geometry changes of the catalyst which occur during the approach and insertion of the alkene into the metal – carbon bond.[32] Morokuma and co-workers have carried out and reported the results of many *ab initio* calculations on various alkene insertion reactions.[33-38] His studies have focussed on the insertion of the olefin into the metal – carbon / metal – hydride bond of model and real systems.[33-35] One such theoretical study investigated the pathways and energetics of alkene insertion into the Zr-H bond of a bis(cyclopentadienyl)zirconium hydride system reported in 1993.[33] In this study Morokuma showed that of the two reaction pathways possible, the more favoured pathway was that where the alkene approached the metal centre *via* the vacant coordination site. This particular pathway was calculated to have a lower activation energy barrier. These theoretical results were found to be consistent with the previous experimental results for alkene insertion.[39-41]

In the mid 1990s Tom Ziegler's group had investigated the chain growth and chain terminating steps in alkene polymerisation by zirconcenes and scandocenes as well as constrained-geometry catalysts.[21,42,43] The density functional calculations carried out indicated that the metal in the complex and the charge of the system does

not greatly influence the alkene insertion barrier. The energy barrier was observed to remain unchanged when going from the unbridged zirconcene to a system containing a silylene bridge.[21,42] At about the same time, Siegbahn extended the investigation of alkene insertion into metal – hydrogen bonds to include other metals from the *5d* series of the transition metals.[44] He was able to show that the differences in the barrier height of alkene insertion depended on the metal centre and could be explained by the repulsion which exists between the electrons in the nonbonding metal *d*-orbital and the π-electrons of the alkene.[44]

In the late 1990s Ziegler and his colleagues undertook further investigations expanding their initial studies on the complexation of ethylene with zirconium and scandium metallocenes to include a number of d^0 and d^0f^n systems.[1,32,45] This systematic study investigated the effect that varying the metal centre and the ligand substituents had on the bond strength of the β-agostic interaction, the bond formed between the β carbon of the ethyl moiety and the metal centre. The agostic interactions in uncharged precursor complexes were found to be overall weaker in comparison to those charged precursor complexes studied.[32] He also noted that these agostic interactions became weaker on going down the series of Group 3 and 4 metals.[32] Ziegler also investigated the termination of a growing polymer chain *via* DFT calculations. The results from his studies showed that the β-hydrogen transfer to the monomer is the dominating chain termination mechanism and that β-hydrogen elimination is possible only if the concentration of the monomer is limited.[1,45]

Recent studies into the polymerisation of ethylene have focussed on the influence of the metal on the catalytic activity and selectivity.[46-49] In 2003 the groups of Eisenstein and Bercaw extended the range of metals in the bis(cyclopentadienyl) complexes studied in the alkene insertion process to include samarium, europium, ytterbium, niobium and tantalum.[47,48] Eisenstein's group concentrated on the divalent lanthanide metallocenes based on cyclopentadienyl and the bulkier pentamethylcyclopentadienyl ligand, investigating the trends shown in the interaction between not only ethylene but also H_2, N_2 and acetylene and the metallocenes. Their results suggested that the interaction of the above substrates and the metallocene was influenced by the *f*-electron count of the lanthocene.[48] Bercaw and Green investigated the exchange of hydrogen after alkene insertion in *ansa*-niobocene and

ansa-tantalocene complexes.[47] More specifically they looked at the effect that single and double *ansa* bridges have on the exchange rate of the hydrogens in the model systems shown in Figure 2.[47] Their calculations showed that the activation energy for the singly bridged system was much lower than the unbridged or doubly bridged systems. In addition to this, they found that rotation of the methyl groups influenced the energy barrier in the hydrogen exchange.

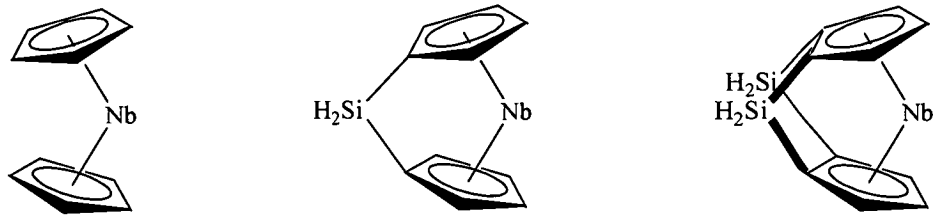

Figure 2. Model niobocene systems investigated by Bercaw and Green.

The relative instability of the 4-azapentalenyl anion and difficulties encountered during the synthesis of the 3*H*-pyrrolizine and subsequent metal complexes in this project meant that the catalytic potential of the system could not be investigated in this study. To explore the catalytic potential of the 4-azapentalenyl complexes we employed the use of DFT calculations on neutral Group 3 metal and cationic Group 4 metal complexes. A further study on a bis(4-azapentalenyl) scandium hydride complex was taken to investigate its geometry and energetics during the polymerisation of ethylene. In particular we probed the fluxionality of the 4-azapentalenyl ligand during high and low coordination steps of the catalysis.

5.2 RESULTS AND DISCUSSION

5.2.1 4-azapentalenyl Group 3 and Group 4 metal alkyl halide complexes

5.2.1.1 General computational methods

The geometries and relative binding energies of the complexes studied in this chapter were carried out using B3LYP[50-52] density functional theory using Gaussian 03.[53] Two possible starting geometries for the complexes to be studied were chosen and are illustrated in Figure 3. The ligands and alkyl/halide substituents in the complexes investigated in this Chapter were optimised by applying the basis set 6-31+G(d),; for the basis set applied to the metal centre see Table 2. The basis set LANL2DZ,[54,55] is a collection of double – zeta basis sets,[56] and was applied to the heavier metal centres.

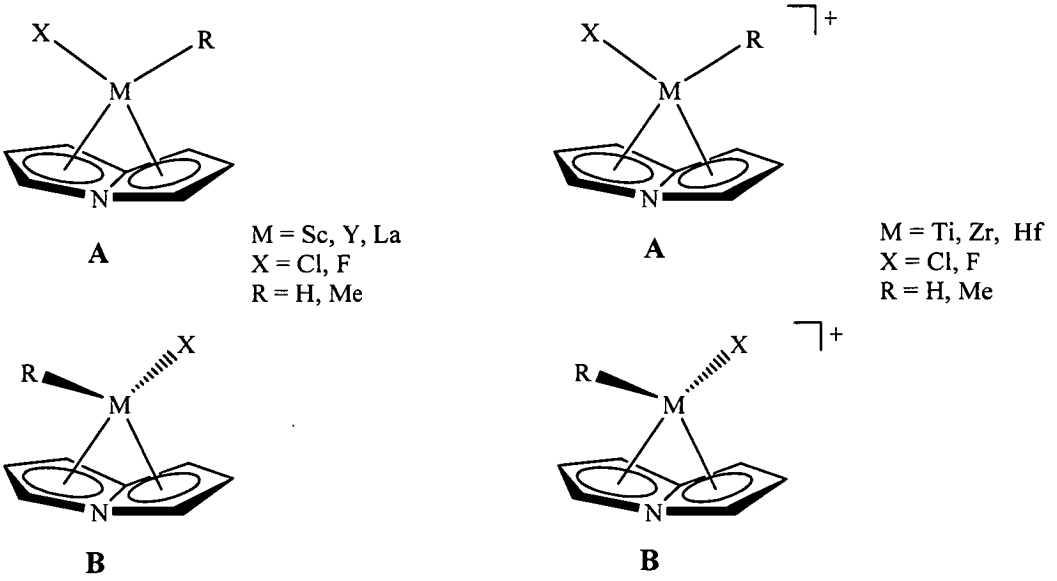

Figure 3. Starting geometries of 4-azapentalenyl Group 3 and 4 metal alkyl halides.

Table 1. Basis sets applied to metal centres during optimisation of geometries.

Metal	Basis Set	Reference
Sc	6-31+G(d)	[57]
Y, La	LANL2DZ	[54,55]
Group 4 metals (Ti – Hf)	LANL2DZ	[54,55]

Single point energy calculations for this Chapter were carried out by applying the basis set 6-311+G(d,p)[57] to the 4-azapentalenyl anion and the alkyl/halide substituents of the complexes. The basis sets applied to the metal centres for these calculations are outlined in Table 2.

Table 2. Basis sets applied to metal centres for single point energy calculations.

Metal	Basis Set	Reference
Sc	6-311+G(d,p)	[57]
Y, La	SDD	[58,59]
Group 4 metals (Ti – Hf)	SDD	[58,59]

The relative binding energy of all studied complexes was calculated to be the difference between the calculated energy of the complex and the sum of the individual calculated energies of the anion plus the metal alkyl/halide, Equation 1.

Binding Energy = Energy of complex - Σ(Energy of the individual components)

Equation 1. Calculation of Dissociation Energy of complexes.

The relative binding energies of the 4-azapentalenyl metal alkyl/halide complexes are given in Table 3.[1] The relative binding energies show a decrease in the calculated binding energy between the hydride and methyl metal halide containing. This may be due to steric effects from the methyl substituent. The difference in relative binding energy is most noticeable for the 4-azapentalenyl

Group 4 metal complexes of zirconium and hafnium where the binding energy difference is as large as 399.3 kcal mol^{-1}.

Table 3. Relative binding energies of optimised [$(C_7H_6N)MXR$)] complexes.†

	Relative Binding Energies (kcal mol^{-1})			
	Cl		F	
	H	Me	H	Me
$(C_7H_6N)Sc$	926.5	825.3	933.2	810.4
$(C_7H_6N)Y$	918.4	797.7	911.6	783.5
$(C_7H_6N)La$	849.5	743.6	827.3	718.1
$(C_7H_6N)Ti$	2033.3	1651.5	1929.2	1714.3
$(C_7H_6N)Zr$	1902.3	1573.4	1998.2	1598.9
$(C_7H_6N)Hf$	1910.6	1584.4	1985.1	1636.5

† Optimisation at B3LYP/LAN2DZ/6-31+G(d)

Single point at B3LYP/SDD/6-311+G(d,p)

There are smaller, yet still significant, differences observed in the relative binding energies when the halide substituent is varied. For the Group 4 metal complexes a slight increase in binding energy is observed when the chloride atom is substituted for a fluoride atom for the majority of these complexes. When comparing the effect of changing the halogen on relative binding energies of the Group 3 metal complexes two sets of trends emerge. The first trend observed sees a slight increase in the relative binding energy of the scandium and yttrium hydride halide complex when the chloride is exchanged for a fluoride. This increase in energy is not observed for the corresponding lanthanum hydride complex and the Group 3 methyl halide complexes. The binding energy of these complexes exhibit a slight decrease in the respective energies when moving from a chloride to a fluoride substituent.

Table 4. 4-azapentalenyl Group 3 metal and Group 4 metal complexes of the type $(C_7H_6N)MXH$ and $[(C_7H_6N)MXH]^+$ respectively.

Group 3 Complexes	**Structure ID**	**Group 4 Complexes**	**Structure ID**
(C_7H_6N)ScClH	**(I)**	$[(C_7H_6N)$TiClH$]^+$	**(XIII)**
(C_7H_6N)ScClMe	**(II)**	$[(C_7H_6N)$TiClMe$]^+$	**(XIV)**
(C_7H_6N)ScFH	**(III)**	$[(C_7H_6N)$TiFH$]^+$	**(XV)**
(C_7H_6N)ScFMe	**(IV)**	$[(C_7H_6N)$TiFMe$]^+$	**(XVI)**
(C_7H_6N)YClH	**(V)**	$[(C_7H_6N)$ZrClH$]^+$	**(XVII)**
(C_7H_6N)YClMe	**(VI)**	$[(C_7H_6N)$ZrClMe$]^+$	**(XVIII)**
(C_7H_6N)YFH	**(VII)**	$[(C_7H_6N)$ZrFH$]^+$	**(XIX)**
(C_7H_6N)YFMe	**(VIII)**	$[(C_7H_6N)$ZrFMe$]^+$	**(XX)**
(C_7H_6N)LaClH	**(IX)**	$[(C_7H_6N)$HfClH$]^+$	**(XXI)**
(C_7H_6N)LaClMe	**(X)**	$[(C_7H_6N)$HfClMe]	**(XXII)**
(C_7H_6N)LaFH	**(XI)**	$[(C_7H_6N)$HfFH$]^+$	**(XXIII)**
(C_7H_6N)LaFMe	**(XII)**	$[(C_7H_6N)$HfFMe$]^+$	**(XXIV)**

5.2.1.2 Structures of 4-azapentalenyl Group 3 metal alkyl halide complexes

The optimised geometries of the 4-azapentalenyl Group 3 metal alkyl halide complexes are shown in Figure 4. These structures all show a folding of the anion along the bridgehead dihedral vector towards the metal centre. In all cases studied the metal centre is situated over the bridgehead vector, slipped slightly towards the bridgehead nitrogen side of the anion. The alkyl substituent is positioned over the bridgehead nitrogen with the halide almost perpendicular to the bridgehead vector. After optimisation those complexes where a methyl substituent was present showed a similar rotation of the group, that is the hydrogens of the methyl group were noted to be of a similar orientation.

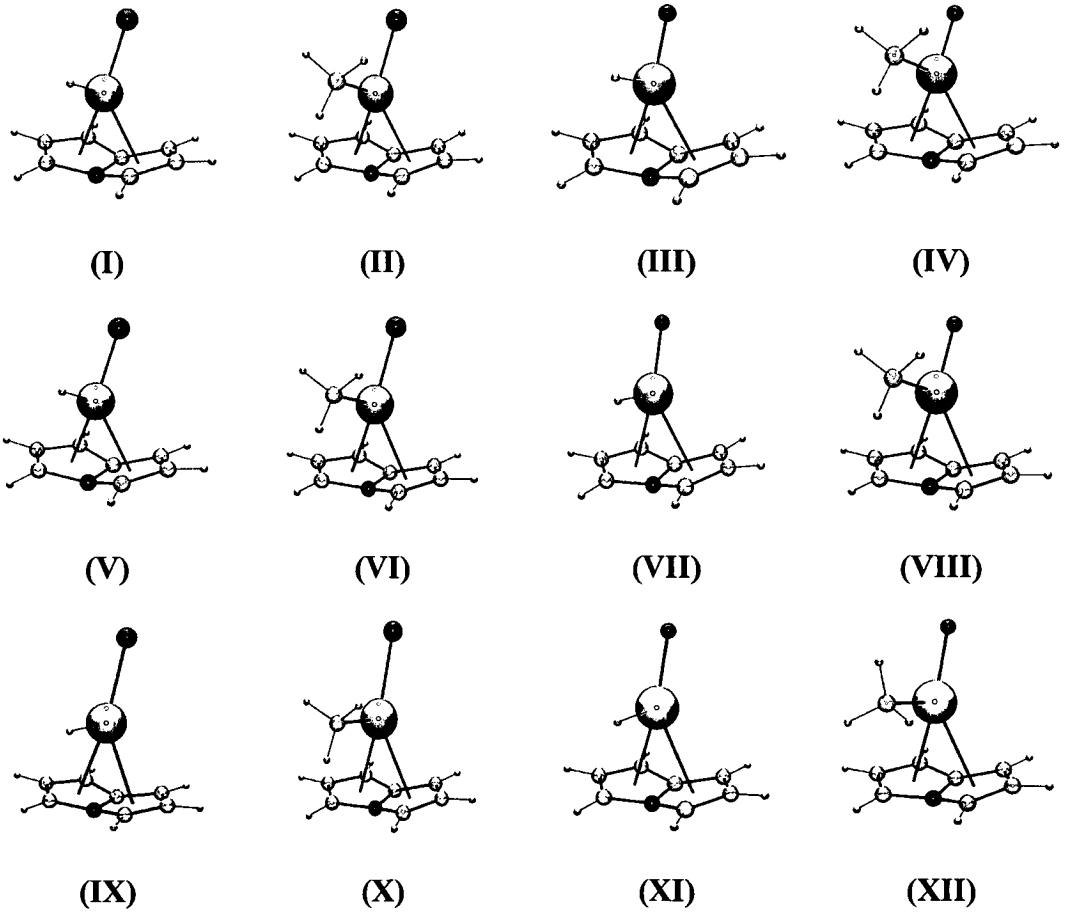

Figure 4. Optimised geometries of the 4-azapentalenyl Group 3 alkyl halide complexes.

The shortest metal – anion interaction distances were observed for the bridgehead carbon and nitrogen, with the shorter of these two distances being

between the metal centre and the bridgehead nitrogen. The greatest distance between the anion and the metal centre in all investigated complexes were those between the wingtip carbons and the Group 3 metal centre. The metal anion distances, the radii of the metal centres and the bridgehead dihedral angle influence the formal hapticity of the interaction between the Group 3 metal and the anion.

The 4-azapentalenyl scandium complexes, as expected, exhibit the shortest metal anion distances of the Group 3 metal complexes studied here. Small variations in these bond distances is observed when the halide substituent is exchanged for another. For example, there is little difference in the calculated distances between the 4-azapentalenyl scandium chloride hydride complex and 4-azapentalenyl scandium fluoride hydride complex. A shortening of the bridgehead atom – scandium bond distances is noted to occur when the hydride is exchanged for the bulkier electron donating methyl group. The other bond distances in the complex show little difference, with these distances being similar in the hydride and methyl complexes. This indicates that the alkyl substituent has the greater effect on the bond distances between the scandium with the bridgehead atoms and, curiously, only when the halide is the chloride substituent.

The position of the scandium metal centre can be best described as positioned above the bridgehead vector, however the anion is slipped so that the scandium centre is more towards the bridgehead nitrogen. The slippage of the anion in the complex is reflected in the various Sc-bridgehead atom distances, the Sc-N bond distance is shorter in comparison to the Sc-C(bridgehead) bond distance. The way in which the interaction in the scandium complexes is described is dependent on whether the wingtip carbons are perceived to have a significant interaction with the metal centre. The distances between the wingtip carbons and scandium in the studied complexes are so great that it is unlikely that bonding will occur. Without taking the bridgehead dihedral angle into account, this will be discussed later, the interaction present in the scandium complexes here is best described as an η^6 type interaction where the wingtip carbons are not involved.

The analogous 4-azapentalenyl yttrium and lanthanum complexes investigated show a similar trend to that of the scandium complexes. The shortest

metal – anion interactions were those with the bridgehead atoms, in particular the bridgehead nitrogen, with the longest distances again being between the metal and the wingtip carbons. The yttrium and lanthanum centres are positioned over the bridgehead vector, with some complexes exhibiting a slippage of the anion so that the distance between the cation and the bridgehead nitrogen is shorter than the distance between the cation and the bridgehead carbon. As observed in the scandium complexes there is little variation in the metal – anion distances when the halogens are exchanged, only a slight increase occurs in this distance when the chloride is exchanged for a fluoride. Once again a significant difference in the bond distances occurs when the hydride substituent is substituted for a methyl group. This confirms that the steric and electronic effects contributed by the incorporation of a methyl group in the Group 3 metal complex influences the final bond distances and in turn the type of interaction present within the complexes.

By comparing the theoretical complexes with similar complexes whose structures and binding modes have been determined by X-ray diffraction studies it is possible to describe the type of interaction occurring between the 4-azapenatalenyl complex and the Group 3 metal cation, Table 5. From the data obtained it was shown that the η^5 – cyclopentadienyl and pentamethylcyclopentadienyl Group 3 metal complexes were found to have a much narrower range of bond distances than those of the calculated 4-azapentalenyl Group 3 complexes. One of the more notable differences between the theoretical and experimental structures in Table 5 is the upper range of the metal – anion distances of the smaller Group 3 metal centres, scandium and yttrium. This observed increase, by as much as 0.2 Å in the calculated scandium complexes, indicates that the metal centres of the calculated scandium and yttrium complexes are unlikely to interact strongly with the wingtip carbons of the 4-azapentalenyl anion. The interaction between the 4-azapentalenyl anion and the scandium/yttrium alkyl halide complexes is therefore best described as an η^6 interaction, with all atoms of the 4-azapentalenyl anion involved except for the farthest wingtip carbons.

Table 5. Group 3 metal – ligand bond distance for complexes of the type M(π-L).

M(π-L) Fragment	Bonding Interaction	CCDC distances† (Å)	Theoretical calculated distances (Å)	
$Sc(C_5H_5)$	η^5	2.390 – 2.593	$Sc(C_7H_6N)$	2.267 – 2.782
$Sc(C_5Me_5)$	η^5	2.441 – 2.554		
$Sc(C_8H_8)$		2.381 – 2.450		
$Sc(C_9H_7)$	η^5	2.149 – 2.581		
$Y(C_5H_5)$	η^5	2.525 – 2.788	$Y(C_7H_6N)$	2.509 – 2.953
$Y(C_5Me_5)$	η^5	2.568 – 2.792		
$Y(C_8H_8)$		2.504 – 2.679		
$Y(C_9H_7)$	η^5	2.590 – 2.950		
$Y(C_{13}H_9)$	η^5	2.601 – 2.785		
$La(C_5H_5)$	η^5	2.560 – 2.999	$La(C_7H_6N)$	2.659 – 3.158
$La(C_5Me_5)$	η^5	2.725 – 2.975		
$La(C_8H_8)$		2.692 – 2.813		
$La(C_9H_7)$	η^5	2.756 – 3.081		
$La(C_{13}H_9)$	η^5	2.758 – 3.050		

† Range of distances obtained from the Cambridge Crystal Data Centre, Cambridge Structural Database version 5.26 (November 2004),[60] ConQuest version 1.7 using Vista version 2.1.[61]

When comparing the theoretical lanthanum complexes with those of known η^5 cyclopentadienyl and pentamethylcyclopentadienyl lanthanum complexes the degree of the variation in bond distances is decreased. The observed variation in the upper range of the bond distances of the lanthanum complexes is about 0.18 Å. While this difference is similar to that observed in the scandium and yttrium complexes, the increased size of the lanthanum metal centre along with the folding of the 4-azapentalenyl anion along the bridgehead vector now presents the possibility of the

metal interacting with the wingtip carbons of the anion. It is therefore quite plausible that an η^8 interaction exists between the lanthanum metal centre and the 4-azapentalenyl anion for complexes **(IX)** – **(XII)**.

The bridgehead dihedral angles in Table 6 show that the anion is indeed folding towards the Group 3 metal centre of each complex. As expected as the radius of the metal centre increases the degree of folding observed for this particular angle decreases and the metal – anion centroid distance increases. Little variation is observed in the bridgehead dihedral angle when the halide substituent is changed from a chloride to a fluoride, with the alkyl component of the complex kept constant, for example, $(NC_7H_6)ScClH$ **(I)** and $(NC_7H_6)ScFH$ **(III)**, Table 6. Lengthening of individual bond distances is only observed to occur when the alkyl group is exchanged, which in turn leads to a change in the bridgehead dihedral angle of the complex, for example, $(NC_7H_6)LaClH$ **(IX)** and $(NC_7H_6)LaClMe$ **(X)**, Table 6.

Table 6. Metal – centroid distances and bridgehead vector dihedral angle for complexes of the type $[(NC_7H_6)MXR]$.[†]
(M = Sc, Y or La, X = Cl or F and R = H or CH_3).

	Ct1	Ct2	dihedral angle
(I)	2.208	2.208	28.3
(II)	2.200	2.198	24.0
(III)	2.210	2.207	28.3
(IV)	2.230	2.230	23.2
(V)	2.377	2.377	22.7
(VI)	2.402	2.402	21.6
(VII)	2.407	2.407	22.1
(VIII)	2.402	2.431	21.1
(IX)	2.594	2.593	19.8
(X)	2.622	2.622	18.7
(XI)	2.625	2.625	19.4
(XII)	2.661	2.624	18.3

[†] All distances and angles are in Å and °, respectively.

The formal classification of the interaction between the metal and the 4-azapentalenyl anion is dependent on the observed bond distances and the subsequent determination of whether the wingtip carbons are involved. The smaller radii of scandium and yttrium metal centres decreases the likelihood of an η^8 interaction with the wingtip carbons of the 4-azapentalenyl anion in the respective complexes, even though the bridgehead dihedral fold angle is greater than those of the corresponding lanthanum complexes. The interaction between the smaller Group 3 metal centres and the 4-azapentalenyl anion is therefore best described as an η^6 type interaction with all atoms except for the wingtip carbons involved in bonding interactions in the complexes.

The work done here on the 4-azapentalenyl Group 3 metal alkyl halide complexes indicates that the particular halide present has little effect on the overall interaction that occurs in the complex. In comparison changing the alkyl substituent from the less sterically demanding hydride to the bulky methyl substituent was observed to decrease both the metal – anion bond distances and the bridgehead dihedral angle. It is unclear whether the electronic nature of the complexes or the sterics of the alkyl substituent influence the overall interactions and hence the final geometries of the 4-azapentalenyl Group 3 metal alkyl halide complexes.

5.2.1.3 Cationic 4-azapentalenyl Group 4 metal alkyl halide complexes

The optimised geometries of the 4-azapentalenyl Group 4 alkyl halide complexes are shown in Figure 5. The optimised structures of all the studied complexes show a folding of the 4-azapentalenyl anion towards the cationic Group 4 alkyl halide centre. Figure 6 shows the individual 4-azapentalenyl atom – Group 4 metal centre distances. For all cases studied here the shortest observed distance between the metal centre and the anion were those between the cation and the bridgehead atoms. The shortest distance was between the bridgehead nitrogen and the cationic metal centre. As would be expected the shortest interaction distances between the Group 4 metal and the 4-azapentalenyl anion were observed for the titanium chloride containing complexes. Little difference in individual metal anion bond distances of this complex were observed when the hydride group was exchanged for the methyl substituent, thus indicating that the alkyl substituent does not affect the metal anion interaction. Whilst the exchange of the alkyl substituent appeared to have little affect on the overall metal anion interaction distances the substitution of the chloride atom for the fluoride atom appears to lengthen the bridgehead – metal interactions for all the Group 4 complexes.

Complex	ID	Complex	ID	Complex	ID
$[(C_7H_6N)TiClH]^+$	**(XII)**	$[(C_7H_6N)ZrClH]^+$	**(XVII)**	$[(C_7H_6N)HfClH]^+$	**(XXI)**
$[(C_7H_6N)TiClMe]^+$	**(XIV)**	$[(C_7H_6N)ZrClMe]^+$	**(XVIII)**	$[(C_7H_6N)HfClMe]^+$	**(XXII)**
$[(C_7H_6N)TiFH]^+$	**(XV)**	$[(C_7H_6N)ZrFH]^+$	**(XIX)**	$[(C_7H_6N)HfFH]^+$	**(XXIII)**
$[(C_7H_6N)TiFMe]^+$	**(XVI)**	$[(C_7H_6N)ZrFMe]^+$	**(XX)**	$[(C_7H_6N)HfFMe]^+$	**(XXIV)**

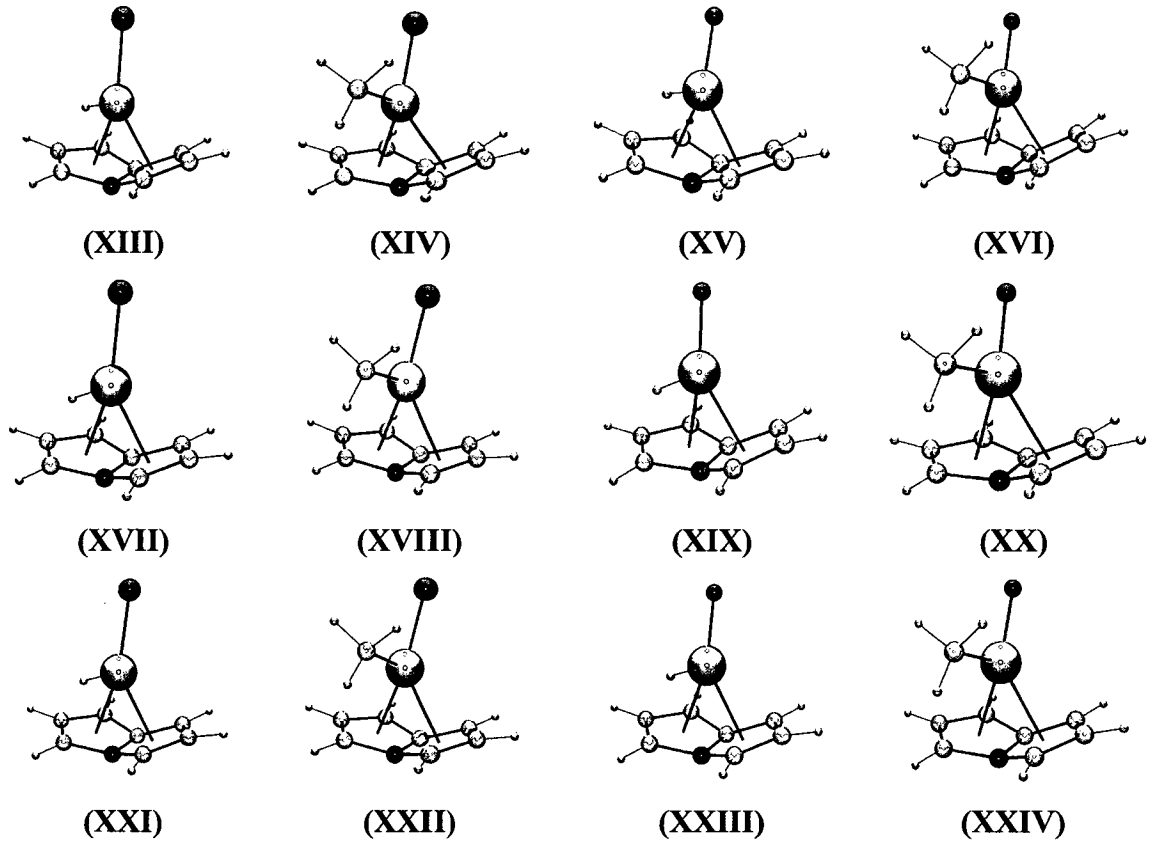

Figure 5. Optimised geometries of complexes of the type $[(C_7H_6N)MXR]^+$: where M = Ti, Zr or Hf; X = Cl or F and R = H or CH_3.

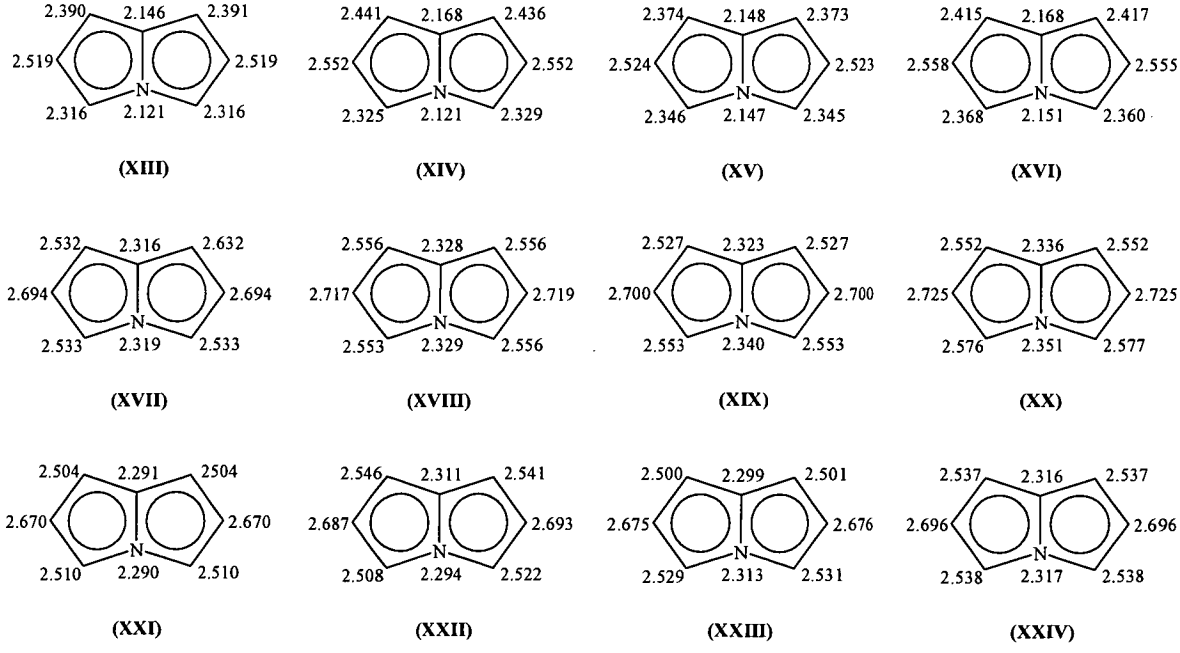

Figure 6. Individual metal – anion distances for cationic 4-azapentalenyl Group 4 metal alkyl halide complexes (distances are all Å).

The optimised geometries indicate that on going from the titanium metal centre to the zirconium metal centre a lengthening of the metal - anion interactions are observed. However when the zirconium centre is exchanged for a hafnium metal centre a further elongation of these distances does not occur. Instead a shortening of the individual hafnium – 4-azapentalenyl interactions is observed. These distances, however, are slightly longer than those observed for the titanium — 4-azapentalenyl anion interactions by about 0.15 Å on average.

As with previous complexes of analogous structure discussed in this Chapter, the type of interaction used to describe the bonding within the complex depends on whether the wingtip carbons are determined to be involved in the actual bonding. To determine the most probable binding mode present for each of the calculated geometries, data was collected from the Cambridge Structural Database (CSD)[60] for Group 4 metal complexes containing the following ligands: cyclopentadienyl (Cp); pentamethylcyclopentadienyl (Cp*) and cyclooctatetraenyl (COT). Table 7 gives the metal anion bonding interaction as well as the range of the bond distances for the known η^5 Cp and Cp* complexes and η^8 COT complex. Comparison of the range of distances between the metal and the anion of the known complexes allowed for the appropriate bonding interactions to be assigned to the 4-azapentalenyl complexes.

Table 7. Group 4 metal ligand distances for complexes of the type M(π-L) and $[MLXR]^+$.

M(π-L) Fragment †	Interaction	CCDC distances† (Å)	Theoretical calculated distances (Å)	
$Ti(C_5H_5)$	η^5	2.087 – 2.871	$[(C_7H_6N)TiXR]^+$	2.133 – 2.715
Ti (C_5Me_5)	η^5	2.159 – 2.598		
$Ti(C_8H_8)$		2.208 – 2.438		
$Ti(C_9H_7)$	η^5	2.102 – 2.652		
$Ti(C_{13}H_9)$	η^5	2.271 – 2.556		
$Zr(C_5H_5)$	η^5	2.395 – 2.746	$[(C_7H_6N)ZrXR]^+$	2.317 – 2.858
$Zr(C_5Me_5)$	η^5	2.431 – 2.737		
$Zr(C_8H_8)$		2.337 – 2.694		
$Zr(C_9H_7)$	η^5	2.405 – 2.722		
$Zr(C_{13}H_9)$	η^5	2.377 – 2.763		
$Hf(C_5H_5)$	η^5	2.361 – 2.640	$[(C_7H_6N)HfXR]^+$	2.294 – 2.828
$Hf(C_5Me_5)$	η^5	2.434 – 2.707		
$Hf(C_8H_8)$		2.329 – 2.486		
$Hf(C_9H_7)$	η^5	2.423 – 2.753		
$Hf(C_{13}H_9)$	η^5	2.384 – 2.693		

† Range of distances obtained from the Cambridge Crystal Data Centre, Cambridge Structural Database version 5.26 (November 2004),[60] ConQuest version 1.7 using Vista version 2.1.[61]

The interaction between the titanium metal and the 4-azapentalenyl anion wingtip carbons are much longer than those with the bridgehead atoms and the adjacent atoms as would be expected in such a complex. On comparing the titanium anion distances for the Cp, Cp*, COT and 4-azapentalenyl complexes it is observed that the longest distance is observed for an η^5 titanium Cp complex, 2.871 Å. The longest distance in the calculated titanium 4-azapentalenyl complexes was 2.715 Å. The interaction between the wingtip carbons and the titanium centre for all the halide alkyl complexes is thus likely to have any significance on the overall bonding of the

cationic complex and is therefore best described as an η^8 type interaction. The same type of η^8 interaction is most likely to be present in the cationic 4-azapentalenyl zirconium complexes. Again the bond distances between the cationic zirconium centre and the wingtip carbons is greater than those with the corresponding bridgehead and adjacent carbon atoms.

In comparison to the titanium and zirconium complexes, where the wingtip carbons are likely to have some effect on the bonding interactions, the wingtip carbons in the analogous hafnium complexes are likely to interact more with the metal centre. The metal 4-azapentalenyl anion interaction is therefore best described as an η^8 binding mode with all atoms of the anion to form bonds with the hafnium centre. The change in the description of the binding mode can be attributed to the larger atomic radii of hafnium in comparison with zirconium and titanium, therefore decreasing the interatomic distances that are observed in the optimised geometries.

The Group 4 metal – anion centroid lengths along with the bridgehead dihedral angle are given in Table 5. As would be expected from the individual metal 4-azapentalenyl distances as discussed previously, a increase in the metal – anion centroid distance is observed when moving down the Group 4 period from titanium to zirconium. There is very little difference observed in the metal – anion centroid distance when moving from zirconium to the larger hafnium cationic centre. As before, a change in substituents of the metal, either the alkyl or halide component, has little affect on the overall metal – anion centroid interactions.

Table 8. Group 4 metal 4-azapentalenyl anion centroid distances and bridgehead vector dihedral angle.[†]

	Ct1	Ct2	dihedral angle
(XIII)	1.963	1.963	35.4
(XIV)	1.991	1.990	33.1
(XV)	2.000	2.002	35.4
(XVI)	2.003	2.000	33.5
(XVII)	2.170	2.170	31.2
(XVIII)	2.191	2.168	29.7
(XIX)	2.181	2.181	31.6
(XX)	2.204	2.204	29.9
(XXI)	2.140	2.140	31.8
(XXII)	2.159	2.163	30.3
(XXIII)	2.152	2.153	32.2
(XXIV)	2.173	2.172	30.6

[†] All distances and angles are in Å and °, respectively.

Whilst the metal – anion distances were only slightly altered by changing the substitutents on the cationic metal centre in the Group 4 complexes, a change in the dihedral bridgehead angle was observed. On the exchange of the smaller hydride group of the 4-azapentalenyl titanium chloride complex for a larger methyl substituent a decrease in the bridgehead dihedral angle is observed, by 2.3 °. However, such a decrease in the same dihedral angle is not observed when the chloride is exchanged for a fluoride, the alkyl substituent is kept the same in this comparison. In fact, very little change in the dihedral bridgehead angle is observed when the one halide is exchanged for another halide in the titanium complexes. The trend observed in the titanium complexes for a decrease in the bridgehead dihedral angle when the alkyl substituent is exchanged for another is also seen in the other 4-azapentalenyl Group 4 alkyl halide complexes, Table 5.

5.2.2 Density functional theory study of catalytically relevant 4-azapentalenyl Group 3 and 4 metal complexes

5.2.2.1 General computational methods

The geometries and relative binding energies of the complexes studied in this Chapter were carried out using B3LYP[50-52] density functional theory using Gaussian 03.[53] Possible starting geometries for the complexes to be studied were chosen and are illustrated in Figure 7. The ligands, alkyl/halide substituents and ethylene moiety in the complexes investigated were optimised by applying the basis set 6-31+G(d), for the basis set applied to the metal centre, see Table 9.

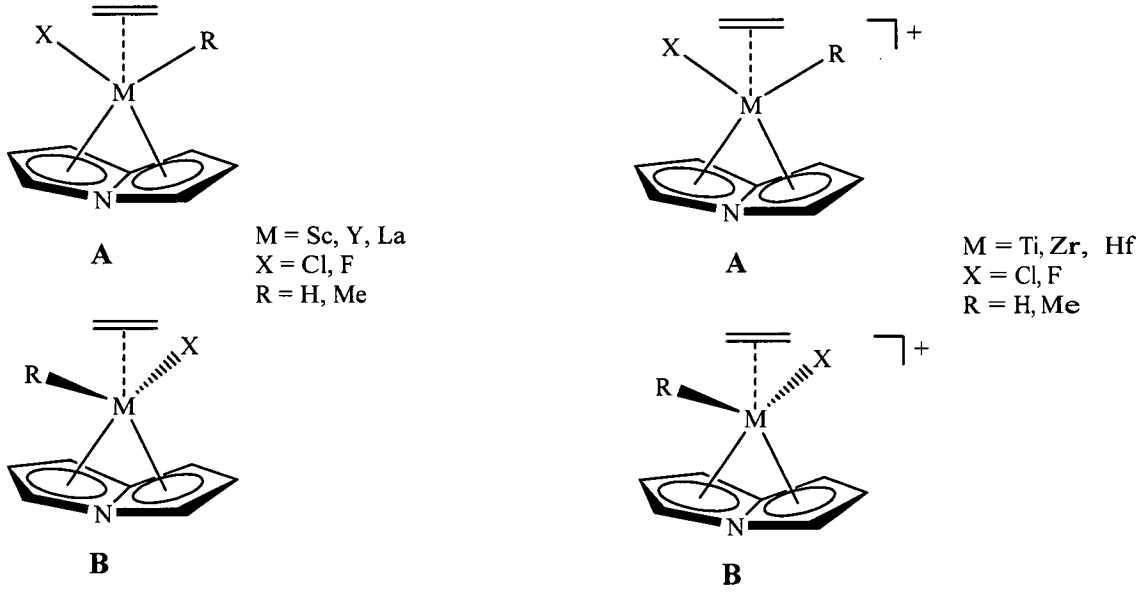

Figure 7. Starting geometries of 4-azapentalenyl Group 3and 4 metal alkyl halides

Table 9. Basis sets applied to metal centres during optimisation of geometries.

Metal	Basis Set	Reference
Sc	6-31+G(d)	57
Y, La	LANL2DZ	54,55
Group 4 metals (Ti – Hf)	LANL2DZ	54,55

Single point energy calculations for this Chapter were carried out by applying the basis set 6-311+G(d,p)[57] to the 4-azapentalenyl anion, alkyl/halide substituents and the ethylene moiety of the complexes. The basis sets applied to the metal centres for these calculations are outlined in Table 10.

Table 10. Basis sets applied to metal centres for single point energy calculations.

Metal	Basis Set	Reference
Sc	6-311+G(d,p)	57
Y, La	SDD	58,59
Group 4 metals (Ti – Hf)	SDD	58,59

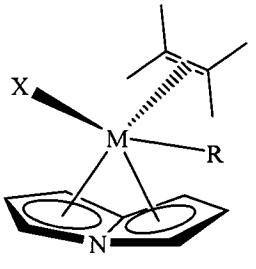

M = Sc, Y, La
X = Cl, F
R= H, Me

Group 3 metal complexes

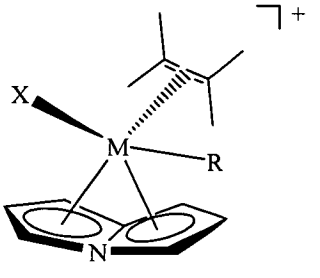

M = Ti, Zr, Hf
X = Cl, F
R = H, Me

Group 4 metal complexes

The relative binding energy of all complexes was calculated as per Equation 1 shown earlier and are given in Table 11.

Table 11. Relative binding energies[†]

	Relative Binding Energies (kJ/mol)			
	Cl		F	
	H	Me	H	Me
$[(C_7H_6N)Sc(C_2H_4)]$	20.6	2.1	22.1	8.8
$[(C_7H_6N)Y(C_2H_4)]$	22.2	18.7	22.2	20.2
$[(C_7H_6N)La(C_2H_4)]$	25.3	23.9	31.0	22.8
$[(C_7H_6N)Ti(C_2H_4)]^+$	40.0	10.9	49.7	17.3
$[(C_7H_6N)Zr(C_2H_4)]^+$	61.1	40.9	67.0	48.5
$[(C_7H_6N)Hf(C_2H_4)]^+$	64.2	43.8	91.0	51.7

[†] Optimisation at B3LYP/LAN2DZ/6-31+G(d)
Single point at B3LYP/SDD/6-311+G(d,p)

A general observation of the complexes which contain a methyl group is that they have a significantly lower relative binding energy than those of the analogous hydrogen complexes, in some cases this energy is halved. The greatest difference in the relative binding energies, however is noted for those complexes which contain the smaller metal cations of titanium and scandium. The following structure identification has been given to the complexes studied within this Section, Table 12.

Table 12.

Group 3 Complexes	Structure ID	Group 4 Complexes	Structure ID
$[(C_7H_6N)ScClH(C_2H_4)]$	**(XXV)**	$[(C_7H_6N)TiClH(C_2H_4)]^+$	**(XXXVII)**
$[(C_7H_6N)ScClMe(C_2H_4)]$	**(XXVI)**	$[(C_7H_6N)TiClMe(C_2H_4)]^+$	**(XXXVIII)**
$[(C_7H_6N)ScFH(C_2H_4)]$	**(XXVII)**	$[(C_7H_6N)TiFH(C_2H_4)]^+$	**(XXXIX)**
$[(C_7H_6N)ScFMe(C_2H_4)]$	**(XXIII)**	$[(C_7H_6N)TiFMe(C_2H_4)]^+$	**(XL)**
$[(C_7H_6N)YClH(C_2H_4)]$	**(XXIX)**	$[(C_7H_6N)ZrClH(C_2H_4)]^+$	**(XLI)**
$[(C_7H_6N)YClMe(C_2H_4)]$	**(XXX)**	$[(C_7H_6N)ZrClMe(C_2H_4)]^+$	**(XLII)**
$[(C_7H_6N)YFH(C_2H_4)]$	**(XXXI)**	$[(C_7H_6N)ZrFH(C_2H_4)]^+$	**(XLIII)**
$[(C_7H_6N)YFMe(C_2H_4)]$	**(XXXII)**	$[(C_7H_6N)ZrFMe(C_2H_4)]^+$	**(XLIV)**
$[(C_7H_6N)LaClH(C_2H_4)]$	**(XXXIII)**	$[(C_7H_6N)HfClH(C_2H_4)]^+$	**(XLV)**
$[(C_7H_6N)LaClMe(C_2H_4)]$	**(XXXIV)**	$[(C_7H_6N)HfClMe(C_2H_4)]^+$	**(XLVI)**
$[(C_7H_6N)LaFH(C_2H_4)]$	**(XXXV)**	$[(C_7H_6N)HfFH(C_2H_4)]^+$	**(XLVII)**
$[(C_7H_6N)LaFMe(C_2H_4)]$	**(XXXVI)**	$[(C_7H_6N)HfFMe(C_2H_4)]^+$	**(XLVIII)**

5.2.2.2 4-azapentalenyl Group 3 metal alkyl halide ethylene complexes of the type $[(C_7H_6N)MXR(C_2H_4)]$

The optimisation of the 4-azapentalenyl Group 3 alkyl halide ethylene complexes gave the unique geometries shown in Figure 8. The optimised geometries of the studied complexes show the Group 3 metal positioned above the bridgehead dihedral vector, the metal centre is situated towards the bridgehead nitrogen along this particular vector. In all of the complexes the orientation of the alkyl and halide groups is the same, with the alkyl group being perpendicular with the bridgehead nitrogen. The exception to this is seen in the structure of compound **(XXVIII)** where the fluoride atom is found to be perpendicular to the bridgehead nitrogen. The

ethylene moiety was found to approach the Group 3 metal centre *via* one of the wingtip carbons of the 4-azapentalenyl anion.

The optimised geometries of the 4-azapentalenyl Group 3 metal alkyl halide ethylene complexes indicate a clear folding of the anion towards the metal centre, similar to that seen in the Group 3 metal alkyl halide complexes in Section 5.2.1.2. The degree of folding of the 4-azapentalenyl anion along the bridgehead N-vector is observed to vary by as much as 9.2 °. The variation in dihedral angle is thought to arise from the differing radii of the metal centre as well as the properties of the alkyl and halide groups, which are interacting with the metal. The degree of folding of the 4-azapentalenyl anion along the dihedral vector along with the individual metal – anion distances are influential in the bonding interaction present in the complex, this will be discussed later.

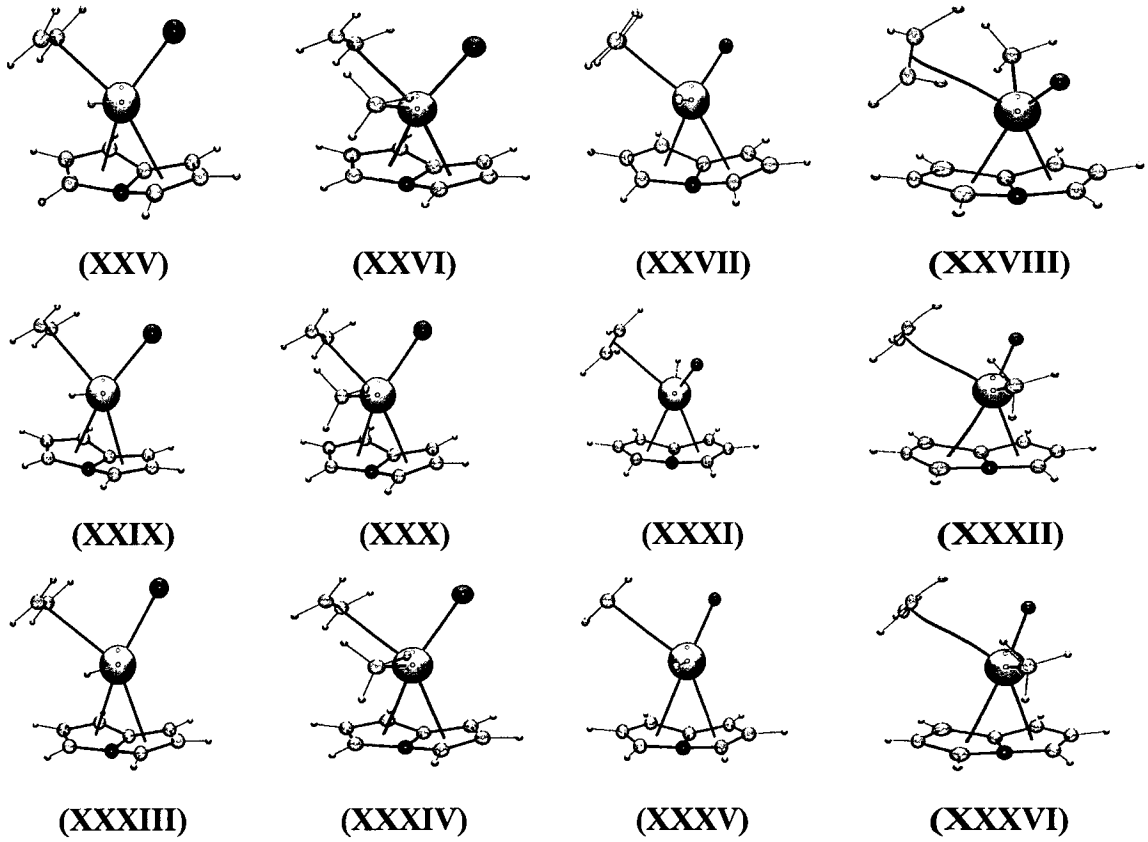

Figure 8. Optimised geometries of Group 3 metal complexes of the type $[(C_7H_6N)MXR(C_2H_4)]$: M = Sc, Y, L; X = Cl, F and R = H, Me.

While the 4-azapentalenyl Group 3 metal alkyl halides discussed in Section 5.2.1.2 were observed to have metal - wingtip carbon bond distances that were near equal, the incorporation of an ethylene moiety into these structures is observed to cause these distances to become unequal. The longer of these two distances can be attributed to the approach of the sterically demanding ethylene moiety anion causing the anion to fold away from the metal centre slightly. The shorter interaction is due to the less sterically demanding halide positioned above the relevant wingtip carbon resulting in an increase of the folding of the anion towards the metal. An increase in the electron count by two with the ethylene bond hints at a fluxional binding mode in response to substrate binding.

On descending the Group 3 metal series the determined metal – 4-azapentalenyl centroid distances are observed to increase, these are given in Table 13. It is noted that one centroid distance is greater than the other in all of the structures investigated here, **(XXV)** – **(XXXVI)**. This difference in centroid distances is reflected in the differing metal wingtip carbon distances discussed earlier in this Section. The lengthening of one of these distances follows the same rationale applied earlier to the unequal metal – wingtip distances, that is the lengthening is believed to occur due to the approaching ethylene moiety to counter the increasing steric bulk whilst maintaining the interaction between the metal and both rings of the 4-azapentalenyl anion.

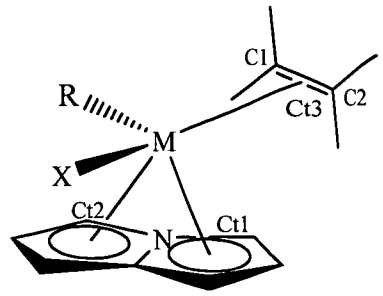

Table 13. Centroid distances and bridgehead vector dihedral angles for $[(C_7H_6N)MXR(C_2H_4)]$: M=Sc, Y, La; X=Cl, F and R=H, Me.†

	Ct1	Ct2	Ct3 (M-Et)	Dihedral
(XXV)	2.208	2.298	2.653	25.9
(XXVI)	2.204	2.284	3.055	21.2
(XXVII)	2.212	2.304	2.651	25.7
(XXVIII)	2.272	2.309	3.035	21.1
(XXIX)	2.429	2.380	2.930	20.9
(XXX)	2.473	2.401	3.018	19.5
(XXXI)	2.474	2.424	2.946	20.7
(XXXII)	2.430	2.506	3.018	18.9
(XXXIII)	2.642	2.590	3.156	18.2
(XXXIV)	2.613	2.681	3.215	17.2
(XXXV)	2.683	2.616	3.167	17.8
(XXXVI)	2.641	2.719	3.229	16.7

† All distances and angles are in Å and °, respectively.

5.2.2.3 Cationic 4-azapentalenyl Group 4 metal alkyl halide ethylene complexes of the type $[(C_7H_6N)MXR(C_2H_4)]^+$

The optimised geometries of the cationic 4-azapentalenyl Group 4 alkyl halide ethylene complexes are given in Figure 9a. These geometries show the cationic metal centre positioned above the bridgehead dihedral vector of the 4-

azapentalenyl anion with the alkyl substituent at a right angle to the bridgehead nitrogen. The halide is positioned over one of the two wingtip carbons with the ethylene component of the complex approaching the metal centre *via* the vacant coordination site over the other wingtip carbon. The 4-azapentalenyl anion is observed to have folded towards the cationic metal centre along the bridgehead vector.

To determine whether the metal – 4-azapentalenyl anion interaction is η^6 or η^8 the individual metal – 4-azapentalenyl bond distances, Figure 9b, and the dihedral fold angle need to be taken into consideration. As has been observed for all the 4-azapentalenyl complexes investigated in this Chapter, the shortest metal – anion distances are observed for the M-C/N bridgehead atoms in particular the bridgehead nitrogen. As with the Group 3 structures discussed in Section 5.2.2.1 it is also noted that the individual metal anion distances are greater for one of the five membered rings of the bicyclic 4-azapentalenyl anion compared to the other. The increasing metal anion distances are determined to be influenced by the folding of the anion where one of the rings appears to be folding more towards the metal centre than the other. The approach of the ethylene moiety towards the metal centre leads to a decrease in the folding of the ring over where it approaches due to the steric effect of the ethylene, thus leading to increased metal – anion bond distances.

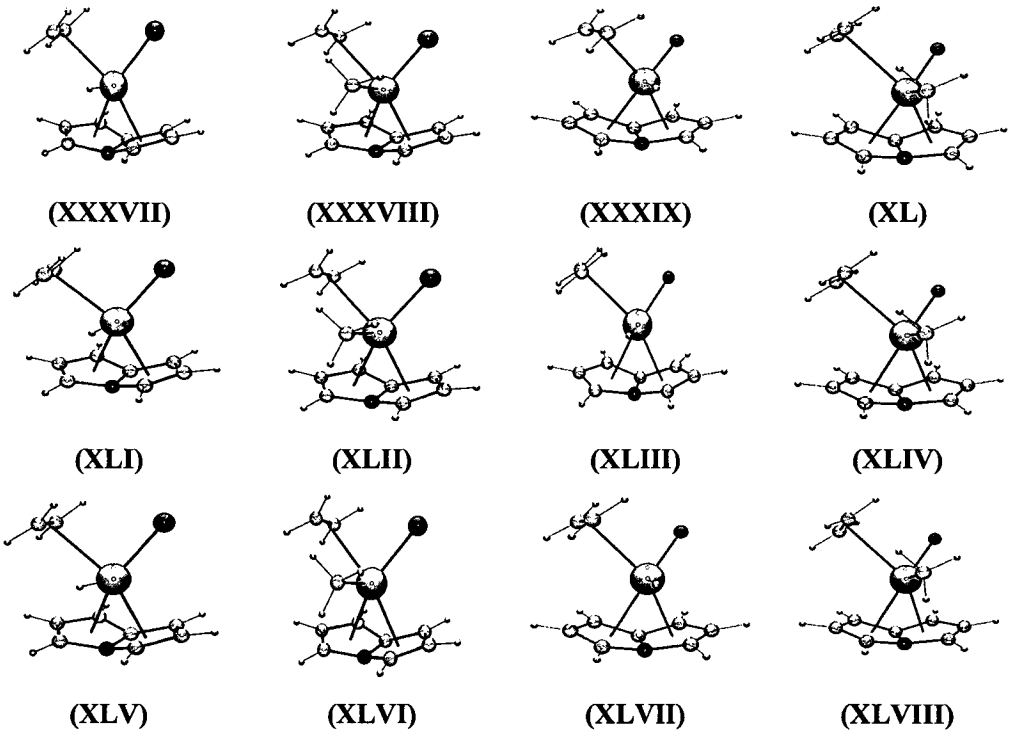

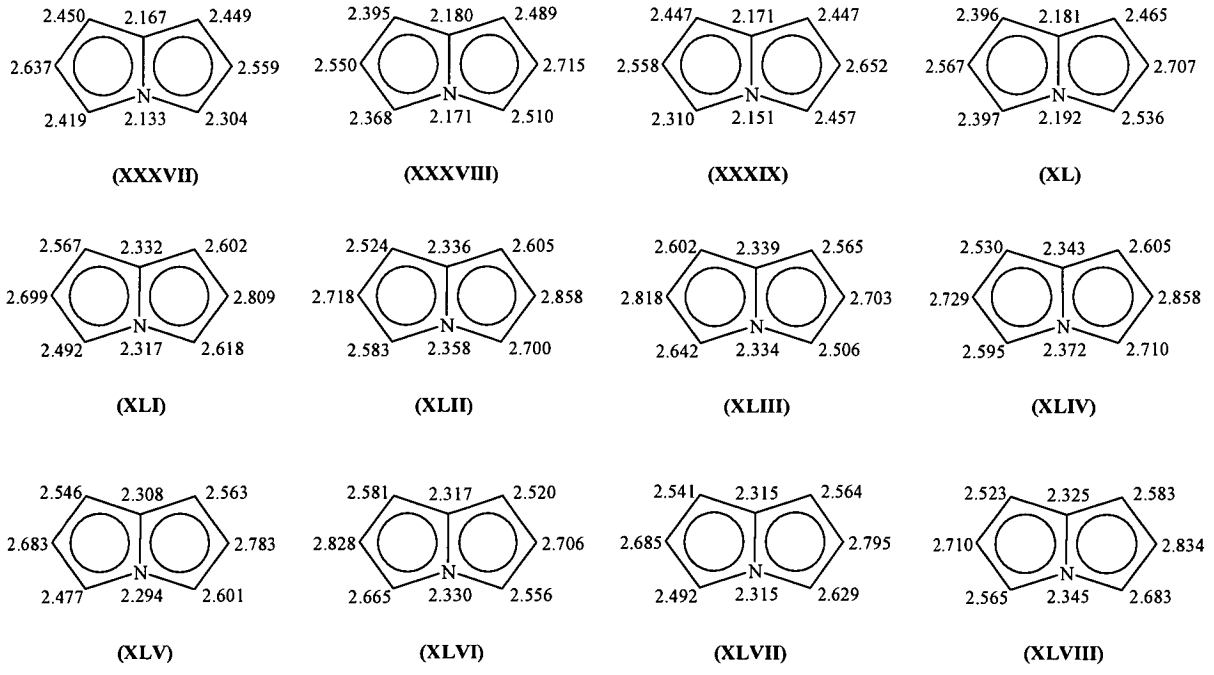

Figure 9a. Optimised geometries of Group 4 metal complexes of the type $[(C_7H_6N)MXR(C_2H_4)]^+$: M = Zr, Ti, Hf; X = Cl, F and R = H, Me.

Figure 9b. Individual metal – anion distances for cationic 4-azapentalenyl Group 4 alkyl halide ethylene complexes (distances are all in Å).

The metal anion bond distances in the optimised geometries here show the same trend as the cationic complexes discussed in Section 5.2.1.2, with the Group 4 metals. On going from titanium to zirconium an increase in the M-C/N bridgehead distances is observed, however on going from a zirconium to hafnium metal centre a subsequent increase in this distance is not observed due to the influence of the lanthanide contraction phenomenon. This particular trend is observed to occur for the metal – anion centroid distances shown in Table 14. The ring over which the ethylene moiety approaches is observed to have an increased M-Ct distance. Like the analogous Group 3 complexes discussed in Section 5.2.2.1, the ring over which the ethylene is approaching is observed to fold less towards the metal centre than the other ring of the 4-azapentalenyl anion due to the decreased steric bulk.

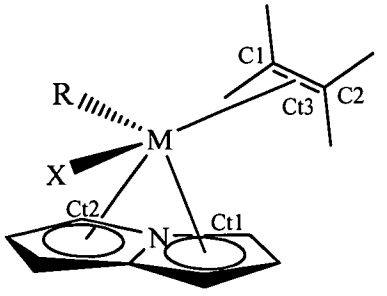

Table 14. Centroid distances and bridgehead vector dihedral angle $[(C_7H_6N)MC(C_2H_4)]^+$: M=Sc, Y, La; X=Cl, F; R=H, Me.†

	Ct1	Ct2	Ct3 (M-Et)	dihedral
(XXXVII)	2.041	1.993	2.539	31.2
(XXXVIII)	2.004	2.103	2.867	29.2
(XXXIX)	1.998	2.057	2.490	31.1
(XL)	2.020	2.106	2.795	29.3
(XLI)	2.174	2.239	2.702	27.9
(XLII)	2.200	2.281	2.830	26.3
(XLIII)	2.252	2.182	2.692	27.9
(XLIV)	2.211	2.288	2.812	26.3
(XLV)	2.151	2.210	2.672	28.6
(XLVI)	2.250	2.179	2.788	26.7
(XLVII)	2.160	2.226	2.665	28.6
(XLVIII)	2.188	2.261	2.770	26.8

† All bond distances and angles are in Å and °, respectively.

Subsequent changes in the bridgehead dihedral angle are also observed to occur along with the lengthening and shortening of the bond and centroid distances, Table 14. These results indicate that the anion folds more towards the titanium metal centre complexes than it does for the other analogous Group 4 cationic complexes in order to achieve the bonding interaction required to satisfy the titanium centre. Of the

four cationic 4-azapentalenyl titanium alkyl halide complexes investigated, the largest dihedral angle is observed for those of the hydride complexes, **(XXXVII)** and **(XXXIX)**. The same trend was found in the analogous zirconium and hafnium structures studied. For all structures studied it was shown that substitution of one halide for another had little effect on the dihedral fold angle. Instead it was shown that the alkyl group present influenced the final dihedral angle of the structure. In most cases, the substitution of the hydride for the larger methyl group saw a decrease by as much as 2 ^{o} of the dihedral angle.

Whilst the titanium complexes show the greatest folding of the bridgehead dihedral angle of the Group 4 cationic complexes it is unlikely that the wingtip carbons have any significant influence in the final bonding interaction due to the distance between the metal and these atoms. The cationic 4-azapentalenyl titanium complexes are therefore best described as having an η^6 type bonding interaction. Whilst containing a larger metal centre, the cationic zirconium complexes have both a decreased bridgehead dihedral angle and increased M- C/N bond distances. The combination of the above two factors along with the size of the zirconium centre make it unlikely that wingtip carbons will have a significant effect on the overall zirconium 4-azapentalenyl anion interaction. The interaction in the cationic 4-azapentalenyl zirconium complex is therefore best described as an η^6 interaction.

In comparison to the structures containing the smaller Group 4 metal centres of titanium and zirconium the larger hafnium metal centre exhibits a different binding mode. When compared to the analogous zirconium complexes the individual Hf-C/N bond distances along with the hafnium anion centroid distances are slightly shortened. This, along with the increased bridgehead dihedral angle of the anion, indicates a greater interaction between the hafnium cationic centre and the 4-azapentalenyl anion. It therefore becomes possible to include the wingtip carbons in the overall bonding interaction allowing the binding mode for the hafnium complexes to be described as an η^8 type interaction.

5.2.3 Density functional theory study of the catalytic cycle of a bis(4-azapentalenyl)scandium complex

The migratory insertion of hydrogen into ethylene is a known and utilised process in the catalytic polymerisation of alkanes. Many of these processes involve the use of metallocene, di(cyclopentadienyl), complexes, as the catalyst which have been both experimentally and theoretically investigated. In order to study the possibility of using bis(4-azapentalenyl) complexes in the polymerisation of alkanes *via* migratory hydrogen insertion we undertook a computational study using DFT of the reaction pathway.

The migratory insertion of hydride from the bis(4-azapentalenyl)scandium hydride complex, **(LI)**, onto an ethylene molecule, as shown in Figure 10, was investigated using DFT. The geometries and energies were studied using B3LYP[50-52] density functional theory using the Gaussian 03 suite.[53] The optimisation of all geometries was carried out using the basis set 6-31+G(d).[57] Single point energies were determined using the basis set 6-311+G(d,p).[57]

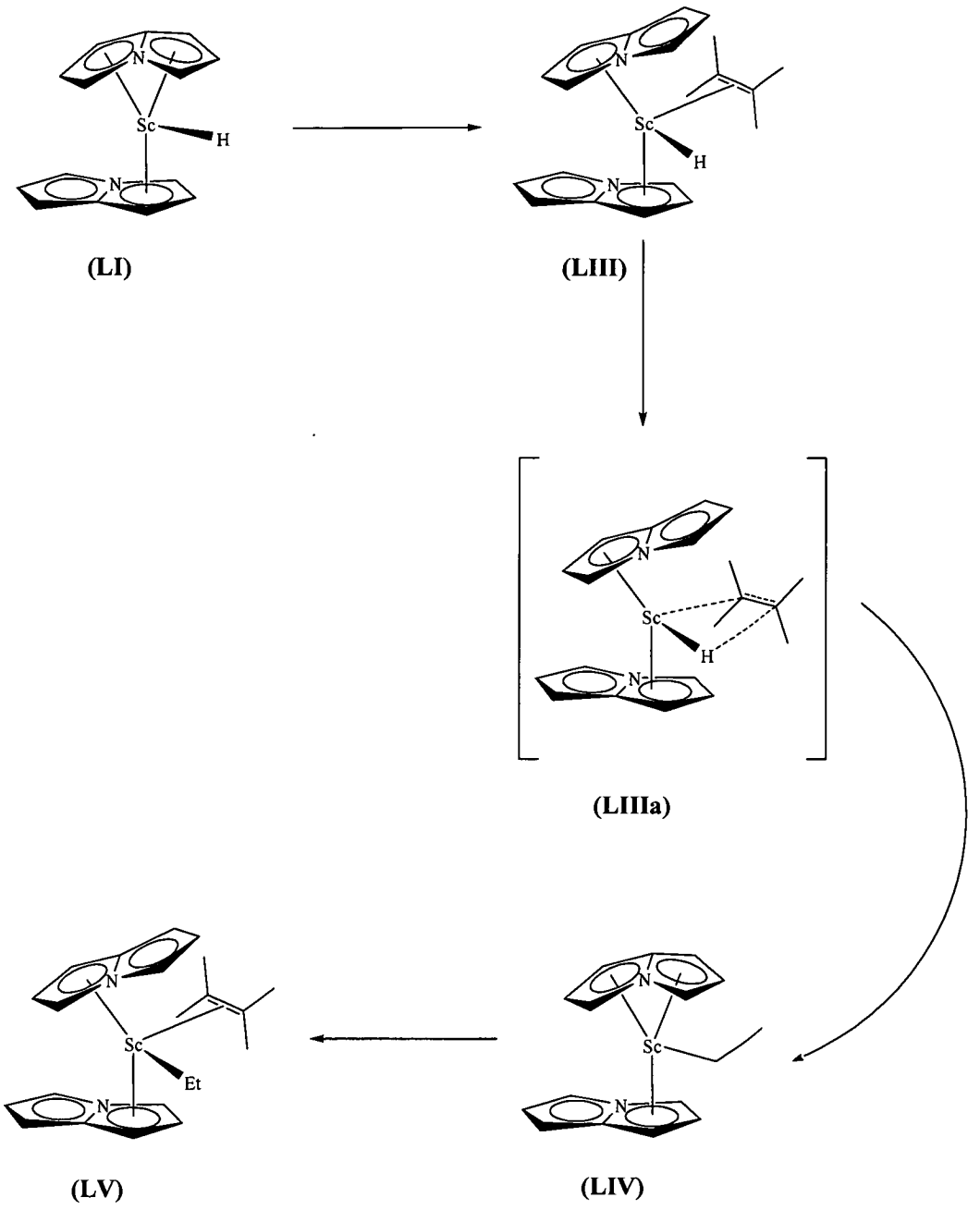

Figure 10.

To determine the starting geometry of the bis(4-azapentalenyl)scandium hydride three possible geometries were chosen, Figure 11, and optimised using the methods outlined previously giving the geometries shown in Figure 12. Two of the three optimised structures, **(IL)** and **(LI)**, are observed to have a similar overall geometry, the main difference between the two structures being the orientation of one of the 4-azapentalenyl anions. Both these structures show two unique geometries for the 4-azapentalenyl anion, one anion is relatively planar whilst the second is seen to have a folded geometry. The bridgehead dihedral angle of the folded 4-azapentalenyl anion falls into a narrow range of 26.9 – 27.5 °. The hydride

substituent of these scandium complexes was found to be approximately 105.1 ° out of the plane of the planar 4-azapentalenyl anion.

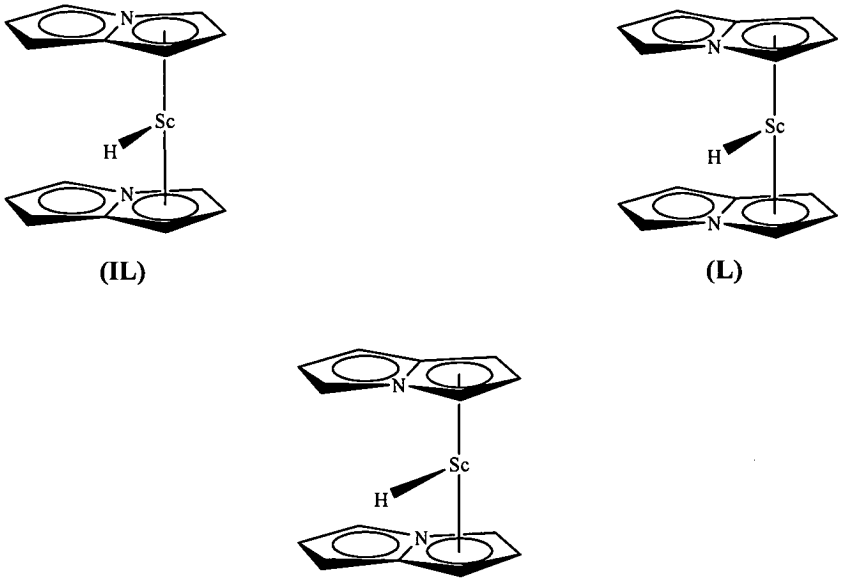

Figure 11. Starting geometries for DFT studies of bis(4-azapentalenyl)scandium hydride.

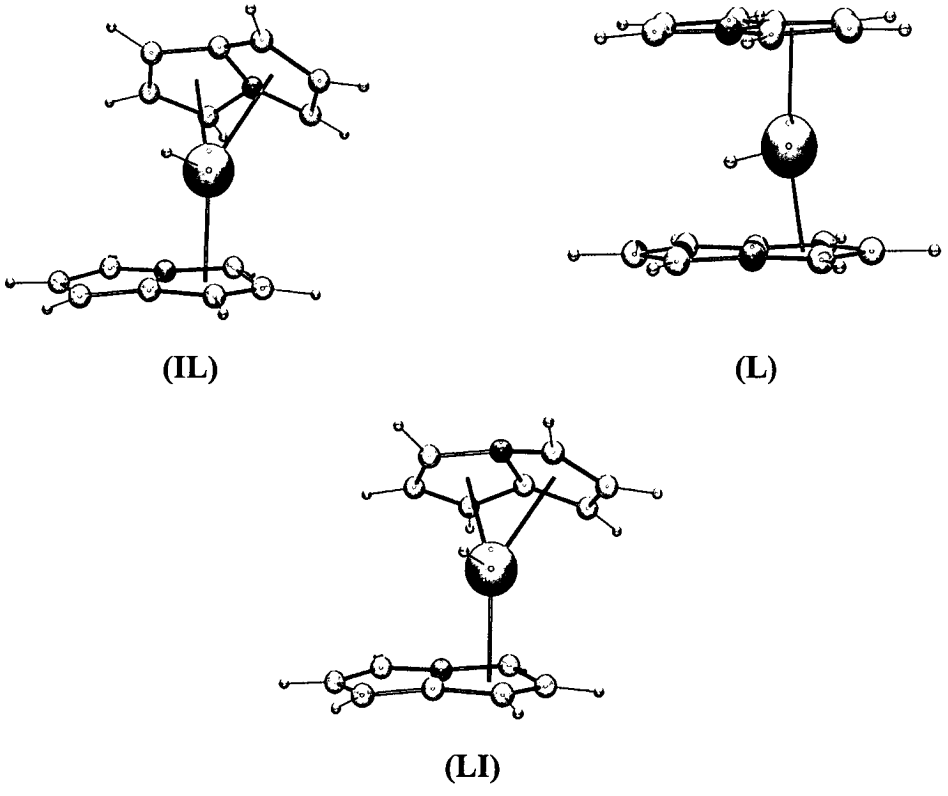

Figure 12. Optimised geometries of bis(4-azapentalenyl)scandium hydride

The observed interaction between the scandium metal centre and each 4-azapentalenyl anion in the structure shows two unique binding modes present. The scandium appears to interact with both five membered rings of the folded 4-azapentalenyl anion whilst it clearly interacts with only one five membered ring of the planar anion. In order to best describe the binding modes present in the complex the position of the scandium centre relative to the two anions as well as the relevant bond distances need to be taken into consideration. The binding mode between the scandium and the planar anion in the structures is best described as an η^5 mode. In those geometries where the metal centre is observed to be interacting with both rings of the anion and where folding of the anion occurs, the bonding is best described by an $\eta^6/\ \eta^8$ mode. The bridgehead dihedral angles observed for structures **(IL)** and **(LI)** are similar to those seen in Sections 5.2.

In comparison to structures **(IL)** and **(LI)**, structure **(L)** shows a unique geometry in which both anions in the complex exhibit a relatively planar geometry. The hydride moiety of the complex is positioned at a 90 $^{\circ}$ angle in relation to both of the anions in the complex. Unlike the geometries of structures **(IL)** and **(LI)**, where two different binding modes are present structure **(L)** only exhibits one type of binding mode. In this structure the scandium interacts with both anions *via* one of the five membered rings in an η^5 type fashion.

Of the three optimised geometries structures **(IL)** and **(LI)** were chosen to use as the starting geometries for the second step in the catalytic cycle as they exhibited two different binding modes of the azapentalenyl ligands. The second step in the catalytic cycle is the approach of the ethylene moiety towards the bis(4-azapentalenyl)scandium hydride complex. The geometries of the starting structures for this part of the cycle are shown in Figure 12. These structures were optimised to give the two unique geometries shown in Figures 13 and 14, with structure **(IL)** minimising to **(LII)** and structure **(LI)** being optimised to **(LIII)**.

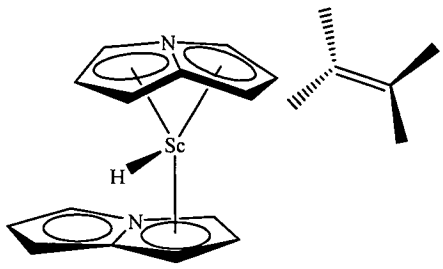

(ILa)

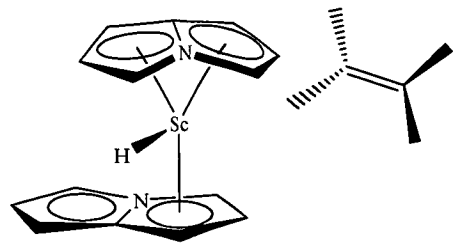

(LIa)

Figure 13.

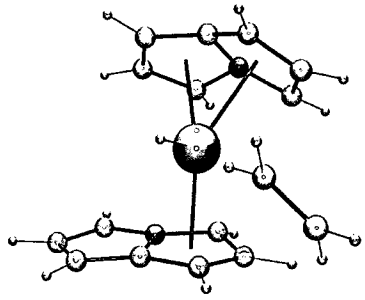

(LII)

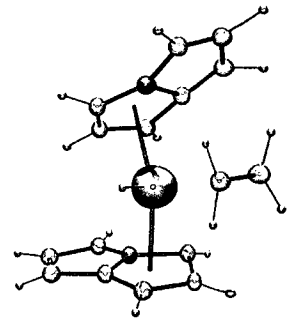

(LIII)

Figure 15

The optimisation of structure **(IL)** gave the minimised geometry **(LII)**. This structure shows minimal change in the geometry of the two 4-azapentalenyl anions between structures **(IL)** and **(LII)**. Both structures comprise one folded anion and one relatively planar anion which exhibits a slight fold away from the scandium centre. This structure like that of (IL), has two different scandium anion binding modes present in the complex. The scandium centre is observed to interact with the relatively flat anion in what is best described as an η^5 interaction with one of the five membered rings. The second interaction is between the scandium and the folded 4-azapentalenyl anion. This interaction can be described as either an η^6 or an η^8 interaction depending whether the wingtip carbons are seen to be involved in the interaction. The ethylene moiety is not π-bound to this particular complex and is thus not valid to consider in the following migration step.

The minimisation of the starting geometry of **(LI)** gave the optimised structure **(LIII)**. This structure exhibits a different geometry and metal – anion

interaction to that of the previously described **(LII)**. The complex shows two relatively planar 4-azapentalenyl anions interacting with the scandium metal centre *via* one of the five membered rings of each the bicyclic anions. The interaction between the scandium and each anion is best described as an η^5 binding mode. The anions have a staggered geometry, the structure with a distinct folding of the anion away from the metal occurring on the side of the complex where the ethylene moiety is observed to approach the scandium metal centre. This folding away of the anion allows for the change in the binding mode from the starting η^8 geometry of **(LI)** to the η^5 geometry observed here. This structure was chosen to be the starting geometry for the hydride insertion step as it had the lowest energy and in this case the complex was shown to exhibit a change in the binding modes between the scandium and the 4-azapentalenyl anions on the approach of the ethylene.

The optimisation of the hydride insertion product to give the bis(4-azapentalenyl) scandium ethyl is shown below in Figure 15, **(LIV)**. The minimised structure shows each anion has a different geometry, that is one anion is observed to fold towards the metal centre whilst the second anion is relatively planar in comparison. The scandium is observed to interact with the anions *via* two different binding modes, an η^5 interaction with the relatively planar anion and an η^6 interaction with the folded anion, this was also observed earlier for structure **(LI)**. This shows that a change in the binding modes occur between the approach of the ethylene towards the complex and the insertion product.

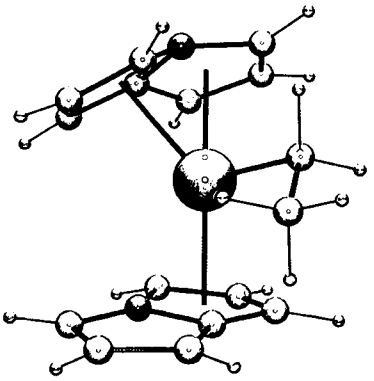

Figure 15. Hydride inserted product, bis-4azapentalenyl scandium ethane **(LIV)**.

Between structures **(LI)** and **(LIII)** and **(LIII)** and **(LIV)** in the hydride insertion cycle, it is possible that transition structures, or intermediates, exist. In order to find these transition structures the "left" and "right" pathways from structure **(LIII)** were required to be followed. The tracing of the "right" pathway allowed for the determination of the optimised geometry of the transition state, **(LIIIa)**. This particular transition state is involved in the migration of the hydrogen from the scandium metal centre to ethylene molecule. The optimised geometry of **(LIIIa)** along with the structure of **(LIII)** are shown in Figure 16.

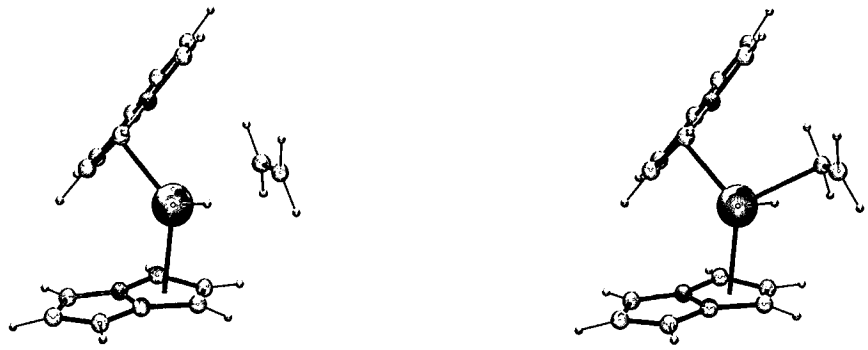

(LIII) **(LIIIa)**

Figure 16. Optimised geometries of structures **(LIII)** and **(LIIIa)**

The binding modes of the optimised scandium - 4-azapentalenyl structures **(LIII)** and **(LIIIa)** show the scandium centre interacting with the each anion *via* one of the five membered rings in an η^5 fashion. As with some of the earlier investigated structures, including **(LIII)**, one of the anions in the complex is observed to fold away from the metal centre as the ethylene moiety approaches the complexes. A comparison of those bond distances and angles in structures **(LIII)** to **(LIIIa)** that were expected to lengthen or shorten during the approach and subsequent interaction of the ethylene with the scandium complex are given in Table 15.

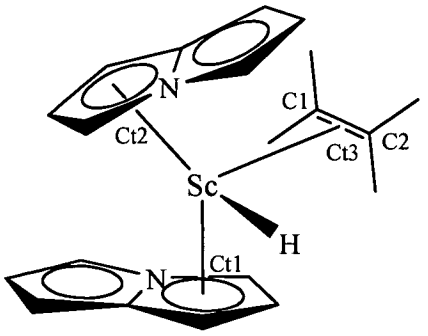

Table 15. Bond lengths and angles of optimised structures in the hydrogen insertion reaction, all measurements are in (Å) and (°)

	(LIII)	(LIIIa)
Sc-H	1.842	1.843
Sc-C1	2.710	2.562
Sc-C2	2.730	2.725
C2-H	2.458	2.081
C1-C2	1.369	1.362
C1-Sc-H	90.44	79.33
Sc-H-C2	77.36	87.76

From Table 15 it is shown that there is negligible difference in the scandium hydrogen bond distance between the two structures studied here. As is expected as the ethylene approaches the bis(4-azapentalenyl)scandium hydride a shortening of the scandium – ethylene carbons is observed. This decreased bond distance is not uniform with the scandium C1 distance showing a much greater decrease in this distance than the scandium C2 distance. The most significant of these decreases occurs for the distance between C2 and the hydrogen that shortens by 0.377 Å thus indicating the migration of the hydrogen to the ethylene moiety. The other significantly shortened distance is between the scandium metal centre and C1 of the ethylene moiety, decreasing by 0.15 Å. The shortening of this particular bond indicates the beginning of the formation of a new bond between the scandium centre and the carbon of the ethylene moiety.

Variation in certain metal - anion angles between **(LIII)** and **(LIIIa)** is observed to occur. A decrease of the angle C1-Sc-H from 90.44 °, **(LIII)**, to 79.33 °, **(LIIIa)**, is observed to occur. This decrease in angle complements the previously mentioned shortening of the Sc – C1 and C2 – H interaction distances. A second angle is observed to vary as the distance between the scandium complex and the ethylene decreases, Sc-H-C2 is shown to increase from 77.36 ° to 87.76 °. This increase in angle not only occurs due to the decrease in the C2-H distance but also because of the minimal change in the Sc-H and Sc-C2 distances. These variations between structures **(LIII)** and **(LIIIa)** clearly indicate that the hydrogen is migrating towards C2 of the ethylene moiety in preparation for insertion to give the final product **(LIV)**. The decreased distance between C1 of the ethylene and the scandium centre indicates the beginning of the formation of a bond which leads to the hydrogen insertion product **(LIV)**.

The mapping of the "left" pathway from complex **(LI)** lead to the determination of the first transition state, TS1, whose structure is located on the energy surface between complexes **(LI)** and **(LIII)**. Figure 17 shows the transition state geometry of the scandium hydride complex on the approach of the ethylene moiety in comparison with that of the structure of **(LIII)**.

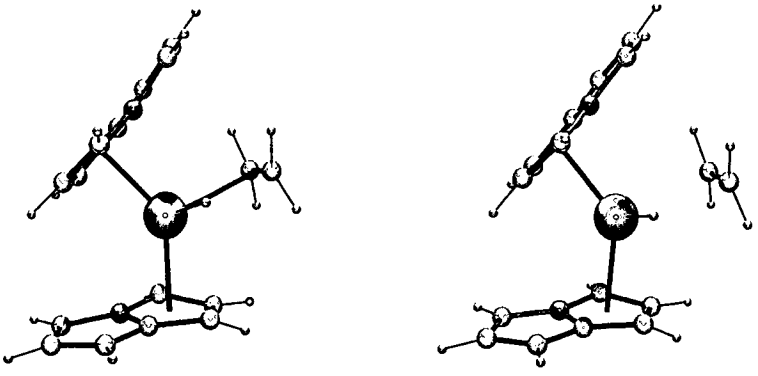

(LIa) **(LIII)**

Figure 17.

The two structures in Figure 17 show little difference visually, both TS1 and **(LIII)** show the scandium metal centre interacting with each 4-azapentalenyl anion in an η^5 fashion. While visually the geometries of the two structures look identical subtle differences in bond distances and angles are present, these are listed in Table

16. Of these differences, variation is observed in the scandium – ethylene, scandium – hydrogen and C2 – hydrogen distances. A decrease is observed in the scandium – C1 / C2 distances when comparing TS1 to structure **(LIII)** as would be expected as the ethylene moiety approaches the complex. The lengthening of the scandium – hydrogen distance is mirrored by a shortening of the C2 – hydrogen distance as the hydrogen migrates towards the ethylene for the insertion step of the cycle. Only a slight variation in some of the angles occurs during the approach of the ethylene moiety to the bis(4-azapentalenyl) scandium hydride complex. These changes occur primarily to the angles involving the ethylene carbons, the scandium centre and the hydrogen of the scandium.

Table 16. Bond lengths and angles of optimised structures in the hydrogen insertion reaction, all measurements are in (Å) and (°)

	(LIa)	**(LIII)**
Sc-H	1.828	1.842
Sc-C1	2.776	2.710
Sc-C2	2.836	2.730
C2-H	2.501	2.458
C1-C2	1.348	1.369
C1-Sc-H	87.87	90.44
Sc-H-C2	80.22	77.36

Table 17 gives the relative energies of each optimised structure in relation to the energy of structure **(LI)**, the starting complex of the catalytic cycle, Figure 10. A small energy barrier of 13.81 kJ/mol is required to be overcome to go from the starting geometry of structure **(LI)** to the transition state 1. This energy barrier is most likely due to the change in binding mode in the bis(4-azapentalenyl)scandium hydride that occurs on the approach of the ethylene moiety. The binding mode between the scandium and the anions is observed to change from an η^5, η^6 interaction to η^5, η^5 interaction. The energy barrier between structure **(LI)** and TS1 is the only large positive energy barrier that must be overcome in the catalytic cycle, a

smaller energy barrier of 0.4 kJ/mol is present between structures **(LIII)** and TS2 also.

Table 17.

Structure	**Relative energy (kJ/mol)**	**Energy Difference (kJ/mol)**
(LVI)	0	-
(LVIa)	13.8	13.8
(LIII)	-43.9	-57.7
(LIIIa)	-43.5	0.4
(LIV)	-110.0	-66.5

The energetics of the overall pathway is best described as a downhill process as is clearly shown in Figure 18. The relative energy of the hydrogen insertion product, **(LV)**, was found to be 26.3 kJ/mol lower than that of the energy of the starting complex, **(LI)**. Figure 18 also shows a very small increase in energy going from structure **(LI)** and first transition structure, **(LIa)** during the approach of the ethylene moiety towards the scandium metallocene, 3.3 kJ/mol. This increase in energy of the system is most probably due to the change in geometry of one of the 4-azapentalenyl anions which is observed on the approach of the ethylene moiety. Here the anion concerned is observed to go from the folded geometry of **(LI)** to the relatively flat geometry observed in **(LIa)**. It is noted that the anion of concern in structure **(LIa)** is observed to be folding away from the approaching ethylene molecule, Figure 18.

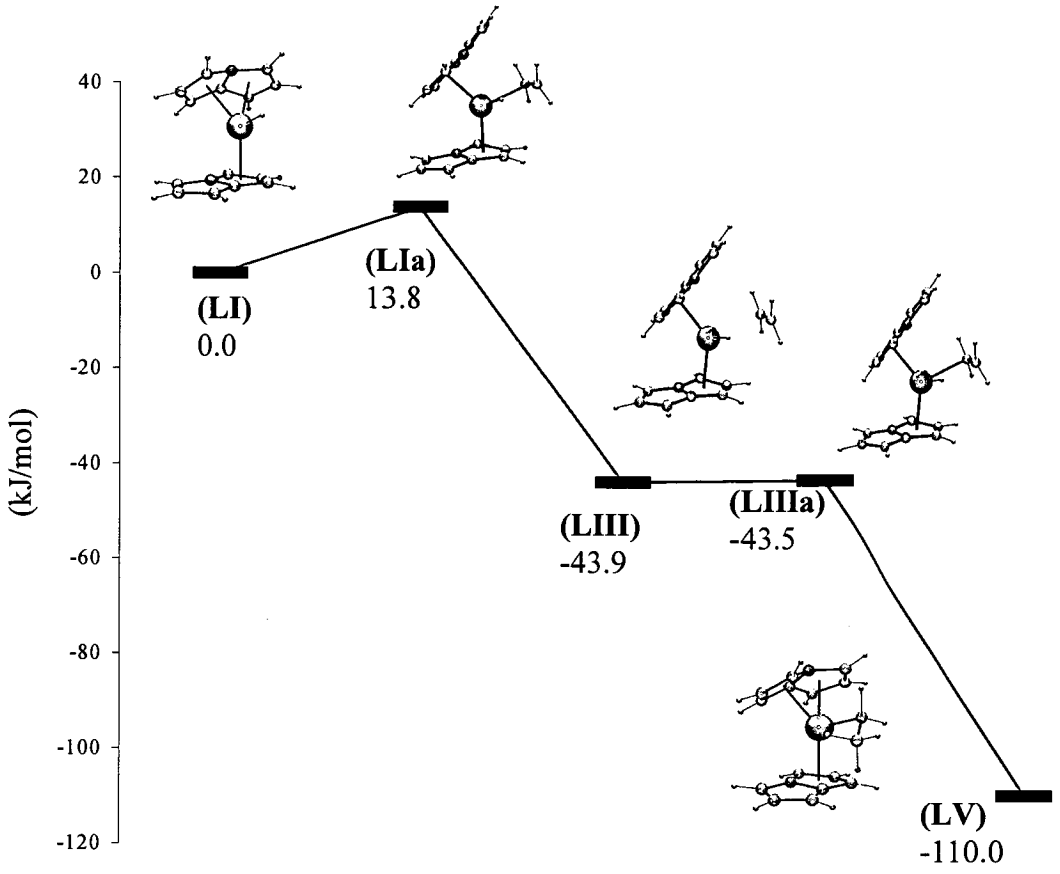

Figure 18.

† Optimisation at B3LYP/6-31+G(d), single point at B3LYP/SDD/6-311+G(d,p)

During the course of the hydrogen migration process a notable change in the geometry of one 4-azapentalenyl anion occurs, as previously stated. This change in the geometry of the bis(4-azapentalenyl)scandium complex is seen to take place on the approach of the ethylene and subsequent insertion of the hydrogen into the ethylene molecule. The change in geometry of the anion in turn brings about the lengthening and shortening of certain bonds as well as variation of certain bond angles. These changes in both length and angle are given Table 18 with Figure 19 showing the labelling used for the bis(4-azapentalenyl)scandium complex.

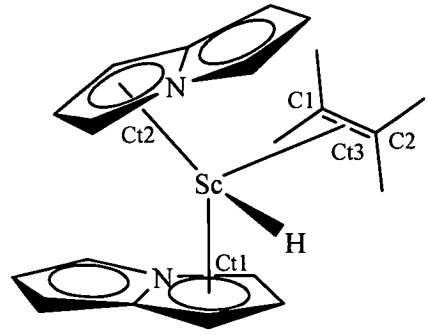

Figure 19.

Table 18. Bond lengths and angles of optimised structures in the hydrogen insertion reaction, all measurements are in (Å) and (°)

	(LI)	(LIa)	(LIII)	(LIIIa)	(LV)
Sc-H	1.832	1.828	1.842	1.843	3.220
Sc-C_1	NA	2.776	2.710	2.562	2.210
Sc-C_2	NA	2.836	2.730	2.725	3.079
Sc-C_{t3}	NA	2.724	2.632	2.556	NA
C_1-C_2	NA	1.348	1.369	1.362	1.500
C_2-H	NA	2.501	2.458	2.081	1.117
C_{t1}-Sc-C_{t2}	138.94	133.54	130.34	133.17	138.94
C_{t1}-Sc-H	104.90	106.52	105.75	106.98	92.00
C_{t2}-Sc-H	106.68	102.46	111.01	103.14	94.17
C_{t1}-Sc-C_{t3}	NA	111.36	106.92	110.14	NA
Ct_2-Sc-C_{t3}	NA	111.11	113.47	115.01	NA
C_1-Sc-H (°)	NA	87.87	90.44	79.33	42.04
C_{t3}-Sc-H (°)	NA	73.95	75.89	64.06	NA

When comparing the bond lengths there is no noticeable change in those lengths corresponding to the scandium metal centre and centroids of the 4-azapentalenyl centroids. Where the major lengthening and shortening of bonds is observed to correspond to those components of the complex which are involved in

the hydrogen insertion reaction. During the catalytic cycle the scandium hydrogen length is observed to increase indicating the migration of the hydrogen to the ethylene molecule. The initial lengthening is quite slight however the final structure, **(LIV)**, clearly indicates that the hydrogen is no longer bonded to the scandium but to C2 of the ethylene.

A lengthening of the ethylene C1-C2 bond occurs as the ethylene moiety approaches the scandium complex. The C1-C2 bond is observed to lengthen from 1.348 Å in **(LIa)** to 1.500 Å the in the final product, **(LIV)**. The bond length of C1 - C2 in final structure is similar to bond lengths which have been reported for a single carbon – carbon bond, of 1.500 Å, indicating that the double bond is no longer present between C1 and C2. The shortening of the distance between the scandium metal centre and C1 of the ethylene over the course of the hydrogen migration indicate the formation of a new bond. The final scandium – C1 bond length was found to be 2.210 Å, which is similar to other scandium – carbon bond lengths, for ethyl groups, that have been reported *via* single crystal XRD structure determination.[62,63]

The results from the migratory insertion of ethylene into the scandium complex show that the structures are close to the insertion free barrier for polymerisation. This can be accounted for by the reversible $\eta 6/8 \leftrightarrow \eta 5$ fluxionaltity of the 4-azapentalenyl anion in response to the overall electronic saturation of the species through the insterion process.

5.3 REFERENCES

(1) Margl, P.; Deng, L.; Ziegler, T. *Topics in Catalysis* **1999**, *7*, 187 - 208.

(2) Corrandini, P. *J. Polym. Sci. Part A: Polym. Chem.* **2004**, *42*, 391 - 395.

(3) Natta, G.; Pino, P.; Corrandini, P.; Danusso, F.; Mantica, E.; Mazzanti, G.; Moragoli, G. *J. Am. Chem. Soc.* **1955**, *77*, 1708.

(4) Corrandini, P.; Guerra, G.; Cavallo, L. *Acc. Chem. Res.* **2004**, *37*, 231 - 241.

(5) Kealy, T. J.; Paulson, P. L. *Nature (London)* **1951**, *168*, 1039-1040.

(6) Natta, G.; Pino, P.; Mazzanti, G.; Giannini, U. *J. Am. Chem. Soc.* **1957**, *79*, 2975 - 2976.

(7) Anderson, A. A.; Cordes, H. G.; Herwig, J.; Kaminsky, W.; Merck, A.; Mottweiler, R.; Pein, J.; Sinn, H.; Vollmer, H. J. *Angew. Chem., Int. Ed. Engl.* **1976**, *15*, 630 - 632.

(8) Kaminsky, W.; Kulper, K.; Brintzinger, H. H.; Wild, F. R. W. P. *Angew. Chem., Int. Ed. Engl.* **1992**, *31*.

(9) Alt, H. G.; Köppl, A. *Chem. Rev.* **2000**, *100*, 1205 - 1221.

(10) Wild, F.; Wasiucionek, M.; Huttner, G.; Brintzinger, H. H. *J. Organomet. Chem.* **1985**, *288*, 63.

(11) Wild, F.; Zsolnai, L.; Huttner, G.; Brintzinger, H. H. *J. Organomet. Chem.* **1982**, *232*, 233.

(12) Schnutenhaus, H.; Brintzinger, H. H. *Angew. Chem., Int. Ed. Engl.* **1979**, *18*, 777.

(13) Schmid, R.; Ziegler, T. *Organometallics* **2000**, *19*, 2756 - 2765.

(14) Cossee, P. *J. Catal.* **1964**, *3*, 80.

(15) Arlman, E. J. *J. Catal.* **1964**, *3*, 89.

(16) Arlman, E. J.; Cossee, P. *J. Catal.* **1964**, *3*, 99.

(17) Brookhart, M.; Green, M. L. H. *J. Organomet. Chem.* **1983**, *250*, 395.

(18) Laverty, D. T.; Rooney, J. J. *J. Chem. Soc., Faraday Trans. 1* **1983**, *79*, 869.

(19) Dawoodi, Z.; Green, M. L. H.; Mtetwa, V. S. B.; Prout, K. *J. Chem. Soc., Chem. Commun.* **1982**, 1410.

(20) Resconi, L.; Cavallo, L.; Fait, A.; Piemontesi, F. *Chem. Rev.* **2000**, *100*, 1253 - 1345.

(21) Woo, T. K.; Fan, L.; Ziegler, T. *Organometallics* **1994**, *13*, 2252 - 2261.

(22) Brintzinger, H. H.; Fischer, D.; Muelhaupt, R.; Waymouth, R. M. *Angew. Chem., Int. Ed. Engl.* **1995**, *34*, 1143.

(23) Shen, Z.; Gong, Z.; Zhong, C.; Ouyang, J. *Sci. Sin. (Engl. Transl.)* **1964**, *23*, 172.

(24) Yang, J.-H.; Tsutsui, M.; Chen, Z.; Bergreiter, D. E. *Macromolecules* **1982**, *15*, 230 - 233.

(25) Throckmorton, M. C. *Kautsch. Gummi, Kunstst.* **1969**, *22*, 293.

(26) Yang, J.-H.; Hu, J.; Feng, S.; Pan, E.; Xie, D.; Zhong, Y.; Ouyang, J. *Sci. Sin. (Engl. Transl.)* **1980**, *23*, 734.

(27) Cotton, F. A.; Wilkinson, G. *Advanced Inorganic Chemistry*; Fifth ed.; John Wiley & Sons, Inc.: New York, 1988.

(28) Jeske, G.; Lauke, H.; Mauermann, H.; Swepston, P. N.; Schaumannn, H.; Marks, T. J. *J. Am. Chem. Soc.* **1985**, *107*, 8091 - 8103.

(29) Watson, P. L. *J. Am. Chem. Soc.* **1982**, *104*, 337 - 339.

(30) Shapiro, P. J.; Bunei, E.; Schäfer, W. P.; Bercaw, J. E. *Organometallics* **1990**, *9*, 867 - 869.

(31) Coughlin, E. B.; Bercaw, J. E. *J. Am. Chem. Soc.* **1992**, *114*, 7606 - 7607.

(32) Margl, P.; Deng, L.; Ziegler, T. *Orangometallics.* **1998**, *17*, 933 - 946.

(33) Endo, J.; Koga, N.; Morokuma, K. *Organometallics* **1993**, *12*, 2777 - 2787.

(34) Koga, N.; Morokuma, K. *Chem. Rev.* **1991**, *91*, 823 - 842.

(35) Kawamura-Kuribayashi, H.; Koga, N.; Morokuma, K. *J. Am. Chem. Soc.* **1992**, *114*, 2359 - 2366.

(36) Kawamura-Kuribayashi, H.; Koga, N.; Morokuma, K. *J. Am. Chem. Soc.* **1992**, *114*, 8687.

(37) Yoshida, T.; Koga, N.; Morokuma, K. *Organometallics* **1995**, *14*, 746.

(38) Yoshida, T.; Koga, N.; Morokuma, K. *Organometallics* **1996**, *15*, 746.

(39) Hart, D. W.; Blackburn, T. F.; Schwartz, J. *J. Am. Chem. Soc.* **1975**, *97*, 679 - 680.

(40) Hart, D. W.; Schwartz, J. *J. Am. Chem. Soc.* **1974**, *96*, 8115 - 8116.

(41) Schwartz, J.; Labinger, J. A. *Angew. Chem., Int. Ed. Engl.* **1976**, *15*, 333 - 340.

(42) Woo, T. K.; Fan, L.; Ziegler, T. *Organometallics* **1994**, *13*, 432-433.

(43) Ziegler, T.; Folga, E.; Berces, A. *J. Am. Chem. Soc.* **1993**, *115*, 636 - 646.

(44) Siegbahn, P. E. M. *J. Am. Chem. Soc.* **1993**, *115*, 5803 - 2812.

(45) Margl, P.; Deng, L.; Ziegler, T. *J. Am. Chem. Soc.* **1999**, *121*, 154 - 162.

(46) Borrelli, M.; Busico, V.; Cipullo, R.; Ronca, S.; Budzelaar, P. H. M. *Macromolecules* **2002**, *35*, 2835 - 2844.

(47) Ackerman, L. J.; Green, M. L. H.; Green, J. C.; Bercaw, J. E. *Organometallics* **2003**, *22*, 188 -194.

(48) Perrin, L.; Maron, L.; Eisenstein, O.; Schwartz, D. J.; Burns, C. J.; Anderson, R. A. *Organometallics* **2003**, *22*, 5447 - 5453.

(49) Tobisch, S.; Ziegler, T. *J. Am. Chem. Soc.* **2004**, *126*, 9059 - 9071.

(50) Becke, A. D. *J. Chem. Phys.* **1993**, *93*, 5648.

(51) Becke, A. D. *Phys. Rev. A* **1998**, 3098.

(52) Lee, C.; Yang, W.; Parr, R. G. *Phys. Rev. B.* **1998**, *37*, 785.

(53) Frisch, M. J.; Trucks, G. W.; Schlegel, H. B.; Scuseria, G. E.; Robb, M. A.; Cheeseman, J. R.; Montgomery, J., J. A.; Vreven, T.; Kudin, K. N.; Burant, J. C.; Millam, J. M.; Iyengar, S. S.; Tomasi, J.; Barone, V.; Mennucci, B.; Cossi, M.; Scalmani, G.; Rega, N.; Petersson, G. A.; Nakatsuji, H.; Hada, M.; Ehara, M.; Toyota, K.; Fukuda, R.; Hasegawa, J.; Ishida, M.; Nakajima, T.; Honda, Y.; Kitao, O.; Nakai, H.; Klene, M.; Li, X.; Knox, J. E.; Hratchian, H. P.; Cross, J. B.; Bakken, V.; Adamo, C.; Jaramillo, J.; Gomperts, R.; Stratmann, R. E.; Yazyev, O.; Austin, A. J.; Cammi, R.; Pomelli, C.; Ochterski, J. W.; Ayala, P. Y.; Morokuma, K.; Voth, G. A.; Salvador, P.; Dannenberg, J. J.; Zakrzewski, V. G.; Dapprich, S.; Daniels, A. D.; Strain, M. C.; Farkas, O.; Malick, D. K.; Rabuck, A. D.; Raghavachari, K.; Foresman, J. B.; Ortiz, J. V.; Cui, Q.; Baboul, A. G.; Clifford, S.; Cioslowski, J.; Stefanov, B. B.; Liu, G.; Liashenko, A.; Piskorz, P.; Komaromi, I.; Martin, R. L.; Fox, D. J.; Keith, T.; Al-Laham, M. A.; Peng, C. Y.; Nanayakkara, A.; Challacombe, M.; Gill, P. M. W.; Johnson, B.; Chen, W.; Wong, M. W.; Gonzalez, C.; Pople, J. A.; Revision C.02 ed.; Gaussian, Inc.: Wallingford CT, 2004.

(54) Hay, P. J.; Wadt, W. R. *J. Chem. Phys.* **1985**, *82*, 299.

(55) Dunning, T. H.; Hay, P. J. *Modern Theoretical Chemistry*; Plenum: New York, 1976; Vol. 3.

(56) Young, D. C. *Computational Chemistry; A practical guide for applying techniques to real world problems*; John Wiley and Sons, Inc.: New York, 2001.

(57) Frisch, M. J.; Pople, J. A.; Binkley, J. S. *J. Chem. Phys.* **1984**, *80*, 3265.

(58) Andrae, D.; Haeussermann, U.; Dolg, M.; Stoll, H.; Preuss, H. *Theor. Chem. Acc.* **1990**, *77*, 123 .

(59) Dolg, M.; Wedig, U.; Stoll, H.; Preuss, H. *J. Chem. Phys.* **1987**, *86*, 866.

(60) Allen, F. H. *Acta Crystallogr.* **2002**, *B58*, 380 - 388.

(61) Bruno, I. J.; Cole, J. C.; Edgington, P. R.; Kessler, M.; Macrae, C. F.; McCabe, P.; Pearson, J.; Taylor, R. *Acta Crystallogr.* **2002**, *B58*, 389-397.

(62) Hayes, P. G.; Piers, W. E.; Lee, L. W. M.; Knight, L. K.; Parvez, M.; Elsegood, M. R. J.; Clegg, W. *Organometallics* **2001**, *20*, 2533.

(63) Fryzuk, M. D.; Giesbricht, G.; Rettig, S. J. *Organometallics* **1996**, *15*, 3329.

CHAPTER 6

pK_A STUDIES OF MODIFIED 3*H*-PYRROLIZINES

6.1 INTRODUCTION

In 1967 Okamura and Katz determined the pK_a of 3*H*-pyrolizine using experimental methods.[1] This involved measuring the proton exchange rate with D_2O (5 M in N,N-dimethylformamide) in the presence of 1 M triethylamine. From the rate of exchange of the protons observed they were able to calculate that the pK_a of the system to about 29, this they noted to be higher when compared to those compounds who where isostructural and isoelectronic; indene, cyclopentadiene and fluorine. To date no further studies have been reported into the determination of the pK_a of the 3*H*-pyrrolizine system to confirm the value obtained by Okamura and no studies have been done on benzannulated systems such as those discussed here.

The measurement of acid dissociation constants, pK_a values, has allowed for the greater understanding of the chemistry which molecules undergo. The pK_a of a compound can be defined using the mathematical equation shown in (1). Due to the small free-energy differences, which control the dissociation of the molecules in solution, it is essential that the methods that measure pK_a values are highly accurate. The physical methods, which are currently used, do not always give the highly accurate pK_a measurements that are desired. The accuracy of physical methods rely on the precision and accuracy of the multiple measurements which are required as well as the purity of the material being analysed.[2] Some methods that are used for the determination of pK_a values are potentiometric titrations and conductivity measurements. These methods, though, have varying degrees of selectivity, sensitivity, accuracy and precision.[3] Whilst these methods have shown to be successful they both have their limitations. In the case of conductivity measurements the method is limited to a narrow range of pK_a values for partially dissociated acids.

$$pK_a = -\log K_a \qquad (1)$$

As mentioned earlier Okamura and Katz measured the pK_a of 3*H*-pyrrolizine by looking at the proton exchange rate *via* NMR spectroscopy. Due to the ability of this particular method to distinguish between different species in solution it has been possible to monitor the extent of ionisation in solution. This particular method is most suitable for weak acids and weak acids which are unsuitable for spectrophotometric studies, however high concentrations of the compound are required.[4]

While the physical methods discussed here briefly have been shown to give accurate pK_a determination for simple systems the same does not hold true for more complex systems such as enzyme – substrate complexes. Theoretical methods, both macro and microscopic, have been developed allowing for the highly accurate determination of the solvation free energies, ΔG_s, of the components which make up the thermodynamic cycle, as shown in Scheme 1.[5] In this thermodynamic cycle the free energy of deprotonation for the gas and aqueous phases are represented by ΔG^0_{gas} and ΔG^0_{aq}, respectively. By calculating these values using the appropriate computational methods it is possible to determine the pK_a of the system being investigated, equations (1) – (4).

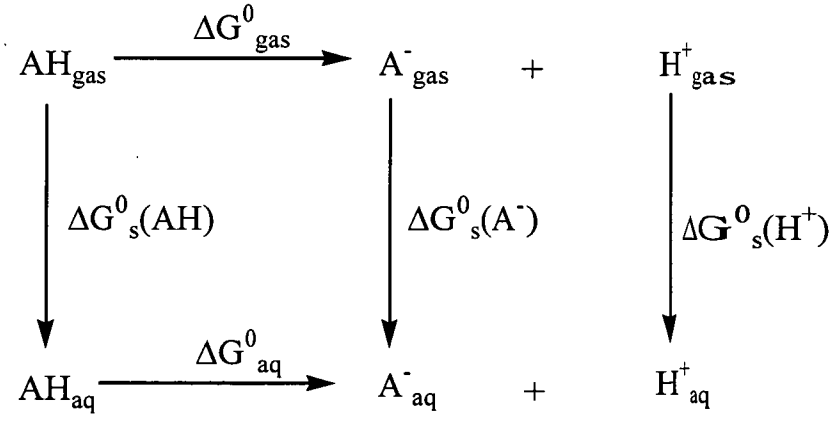

Scheme 1: Thermodynamic cycle used in the calculation of pK_a values.

$$pK_a = -\log K_a \quad (1)$$

$$pK_a = \Delta G^0_{aq} / 2.303RT \quad (2)$$

$$\Delta G^0_{aq} = -2.303RT \log K_a \quad (3)$$

$$\begin{aligned}\Delta G^0_{aq} &= G^0(A^-_{aq}) + G^0(H^+_{aq}) - G^0(HA_{aq}) \\ &= G^0(A^-_{gas}) + \Delta G^0_s(A^-) + G^0(H^+_{gas}) + \Delta G^0_s(H^+) \\ &\quad - G^0(HA_{gas}) - \Delta G^0_s(HA) \quad (4)\end{aligned}$$

The determination of ΔG values through out the cycle shown in Scheme 1 requires different levels of computational theory to be applied. Gas phase ΔG values are calculated by applying high level *ab initio* or density functional with a solvation method used to calculate the solvation ΔG values, a continuum dielectric method is the most commonly used. The development of the methods being applied in these calculations has increased the accuracy, obtaining values within 4.2 kJ/mol of known experimental values.[6] The accuracy of these calculations is highly important in the determination of a compound's pK_a value as an error as little as 5.7 kJ/mol in the calculation of Gibb's free energy of formation can lead to a discrepancy of 1 pK_a unit.[6]

In order to calculate the ΔG^0 values for equation (4) high level energy calculations must be carried out using an appropriate level of theory. Some of these levels of theory which have been applied to such calculations by previous groups include DFT calculations,[7] post Hartree Fock methods (HF) with large basis sets,[8] complete basis set method (CBS) and Gaussian methods.[5,6,9] Of these methods a study by Liptak and Shields in 2001 concluded that the CBS-QB3 method[10] gave the most accurate results of all the methods which they investigated during the calculation of the pK_a of a set of six carboxylic acids.[5] The CBS methods[10-16] were developed by Petersson and his colleagues during a period from the late 1980s to the mid 1990s. The CBS methods use "complete basis set extrapolation of the correlation energy based on the asymptotic convergence of pair natural orbital expansions" (Liptak and Shields 2001).[6] While *ab initio* based calculations provide highly accurate results. As with any calculation of molecular energies there are associated errors. One of the major sources of error is the truncation of the one electron basis set. CBS methods are defined to take into account these truncation errors resulting in the extremely accurate calculation of molecular energies.[9,17]

The free energies of solvation, however, must be calculated in a different manner to those of the gas phase calculations. The solvent surrounding a molecule can have a stabilising effect on the charge of the molecule, thus there is a possibility that the electron density of the molecule may be altered. The most commonly applied method for this type of calculation has been the conductor-like polarisable continuum model, CPCM.[18] The CPCM method is based on an earlier method called the polarised continuum model, PCM, which was developed by Tomasi and colleagues.[19-25] In the CPCM method the cavities in which the solute molecules are embedded in are modelled on molecular shape with optimised parameters with electrostatic and non-electrostatic contributions being taken into account. The total free energy of solvation is calculated from the sum of the energies obtained from the various interactions (electrostatic, dispersion and repulsion) and formation of the cavity. This, however, is not the only method available for calculating the free energies of solvation. Other methods which have been utilised include a cluster continuum model,[8] an alternate continuum-solvation approach,[7] and a method known as SM5.42R,[26,27] a combination of a self consistent reaction field with a solvation shell calculation.[9]

In 2001 Shields *et al.* reported their investigation and determination of pK_a values for a series of carboxylic acids applying six different methods to calculate the gas phase energies and two different methods to calculate the free energies of solvation in order to find out which combination of methods gave the most accurate relative pK_a values.[9] The initial geometries of the carboxylic acids were optimised using HF then the following methods were applied to calculate the gas phase energies: CBS-4;[13] CBS-QB3;[10] CBS-APNO;[13,14] G3;[28] G2[29] and G2MP2.[30] The last three methods are Gaussian methods that were developed by Pople and his colleagues during the 1990s; these methods are of a similar chemical model to that of the CBS methods. After the calculation of the gas phase energies of the six acids and their corresponding anions was completed the free energy of solvation was calculated using two different methods, SM5.42R[26,27] and CPCM.[18]

The results of the study by Shields *et al.* indicated that the CBS methods, CBS-QB3 and CBS-APNO, gave mean errors of 1.7 kJ/mol in the gas phase calculations. This was half that of the mean error of the energies calculated by the

Gaussian based methods and a third of the mean error in the CBS-4 calculations. Of all the gas phase calculations the CBS-QB3 method was found to be the most desirable as not only did it give accurate results but it also required less computation time than any of the other gas phase methods investigated. The free energies of solvation calculated using the CPCM calculations with diffuse functions had a lower mean error than the calculations when the SM5.42R method was applied, 7.5 kJ/mol in comparison to 2.1 kJ/mol for CPCM diffuse function methods. On combining the CBS-QB3 gas phase calculations with the CPCM diffuse functions calculations the pK_a value of unknown molecule from a known molecule deviated 0.5 pK_a units and had an average mean error of 0.4 pK_a units.[9]

By determining the best methods to use in the calculation of highly accurate pK_a values, the method developed by Shields and co-workers has been applied in the calculation of pK_a values for various organic compounds and ligand systems used in organometallic chemistry.[31,32] One such important system investigated was the imidazolium salt / carbene system by Yates *et al.*[33] Imidazole, a carbene based compound, has been extensively used as a ligand in ruthenium based olefin metathesis. The work by Yates *et al.* determined the pK_a of a series of nucleophilic carbenes[33] using the Liptak – Shields method, as it has been postulated that increased catalytic activity may be due to an increase in basicity of the ligand system.[34] The study of Yates and co-workers found that substitution at the four and five position of the imidazole ring resulted in a significantly altered pK_a value, as did the inclusion of substitutents at the nitrogen of the imidazole. The pK_a of the system was observed to have decreased on the addition of electron withdrawing phenyl rings at the nitrogen positions. The calculated pK_a values were in good agreement with the experimentally known pK_a values for those carbene compounds whose value was available.

We have sought to determine the pK_a values of the 3*H*-pyrrolizine and our modified compounds using the highly accurate Liptak – Shields method in order to understand the chemistry of these systems. The reductive coupling of the 5*H*-pyrrolo[2,1-a]isoindolyl anion in the presence of mercury(II) chloride will also be discussed in relation to the pK_a value calculated for 5*H*-pyrrolo[2,1-a]isoindole.

6.2 RESULTS AND DISCUSSION

6.2.1 Studies of reductively coupled species

6.2.1.1 General Computational Methodology

The chosen starting geometries of the dimerised 3*H*-pyrrolizine and 5*H*-pyrrolo[2,1-a]isoindole were optimised by applying B3LYP[36-38] density functional theory using the 6-31+G(d)[39] basis set. Single point calculations were carried out on the structures utilising the expanded 6-311+G(d,p)[39] basis set. All density functional calculations were carried out using the Gaussian 03 suite.[40] Subsequent relative dissociation energies were calculated using Equation 5.

Dissociation Energy = Energy of complex - Σ(Energy of the individual components)

Equation 5. Calculation of dissociation energy of complexes.

6.2.1.2 Density functional calculations of bis(3*H*-pyrrolizine) compounds

Three possible starting geometries of isomers were chosen for the optimisation and determination of the relative binding energies of the 3*H*-pyrrolizine dimer, structures **(I)** – **(III)** in Figure 1a. The optimisation of those starting geometries resulted in the geometries shown in Figure 1b. The relative dissociation energies of each were determined with **(I)** found to have the lowest relative dissociation energy of the studied structures, Table 1. This lowest dissociation energy indicated that structure **(I)** was the preferred dimeric geometry of the three structures studied. The relative energy of **(II)** and **(III)** was then compared to that of **(I)**, Table 1. This indicates that **(III)** is 9.0 kJ/mol higher in energy than **(I)** whilst **(II)** is even higher in energy than **(I)** at 20.9 kJ/mol.

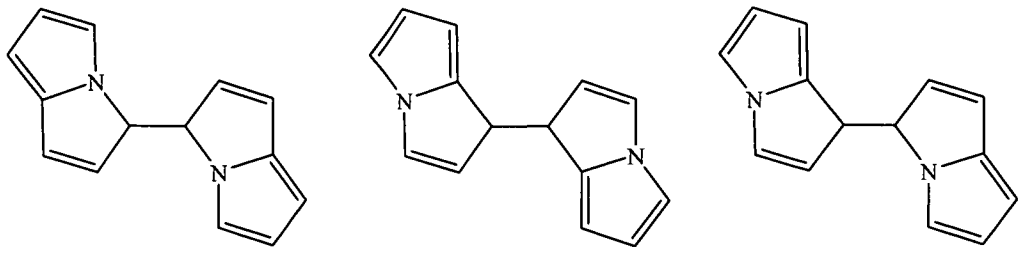

I II III

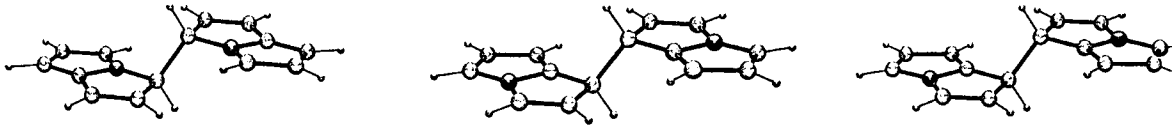

(I) (II) (III)

Figure 1a. Starting geometries for structures **(I)** – **(III)** for bis-3*H*-pyrrolizine.

Figure 1b. Optimised geometries for structures **(I)** – **(III)** for bis-3*H*-pyrrolizine.

Table 1. Dissociation energies of bis-3*H*-pyrrolizine structures **(I)** – **(III)**.†

Compound	Relative Dissociation Energy	Relative Energy
(I)	78.3	0.0
(II)	99.1	-20.9
(III)	87.3	-9.0

† Energies reported in kJ/mol.

Visually little difference is observed in the orientation and the geometry of the three optimised structures, especially between **(II)** and **(III)**. The carbon and nitrogen atoms of the 3*H*-pyrrolizine units are positioned in two separate planes which were found to be parallel to each other. The hydrogen atoms bonded to the bridging carbons are observed to fold away and out of the plane of the carbon and nitrogen atoms in each 3*H*-pyrrolizine unit. The angle between the bridgehead carbons and their adjacent hydrogens, the C-C-H angle, in each structure is observed to be similar, Table 2. The two C-C-H angles present in both **(I)** and **(II)** are identical, however **(III)** has two different C-C-H angles reported with one slightly larger than the other, Table 2. This particular orientation of the hydrogens attached to the bonded bridged atoms is similar to that observed in the structurally authenticated (dihydro-1,1'-bipentalenyl)iron, Figure 2.[41,42,43]

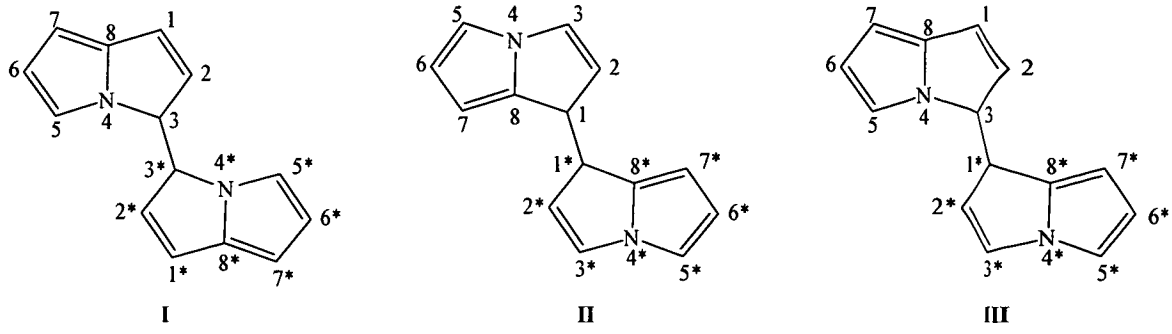

Table 2. Bond length and angle of bridging C-C of the –3*H*-pyrrolizine dimers.

	(I)	(II)	(III)	(IV)
C-C (Å)*	1.561	1.564	1.560	1.568
C-C-H (°)†	107.91	107.14	108.38, 106.78	115.26, 109.24
Dihedral angle (°)‡	0.0	0.0	0.5, 1.8	N/A

* **(I)** – C3-C3*, **(II)** – C1-C1*, **(III)** – C3-C1*

† **(I)** – C3-C3*-H3*, **(II)** – C1-C1*-H1*, **(III)** – C1*-C3-H3, C3-C1*-H1*

‡ **(I)** – N4-C3-C1*-N4*, **(II)** – C8-C1-C1*-C8*, **(III)** – N4-C3-C1*-C2* C2-C3-C1*-C8*

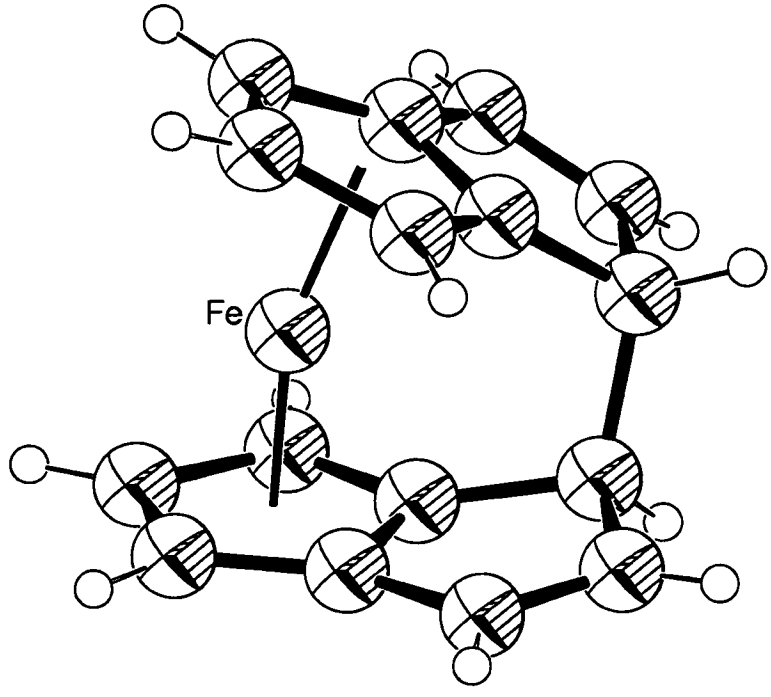

Figure 2. Single crystal X-ray structure of (dihydro-1,1'-bipentalenyl)iron **(IV)**, X-ray crystal structure reproduced from the CCDC database. Thermal ellipsoids are with arbitrary radii.

The bond lengths of the bridging carbon atoms in all three structures were found to be of a similar length with only a difference of 0.004 Å between the longest and shortest C-C bond, Table 2. This bridging bond length was found to be comparable with those of reported crystal structures of similar dimeric compounds.[41,44,45] In particular the bridging C-C length of the calculated structures compares well with that reported in the X-ray crystal structure of (dihydro-1,1'-bipentalenyl)iron by Churchill and Lin in 1973 a1 1.568 Å, Figure 2.[41] Similarity in the observed orientation of the bridging carbon hydrogens and the bridging carbon bond lengths of **(I)** – **(III)** with those reported for (dihydro-1,1'-bipentalenyl)iron indicate that the determined geometries of the 3*H*-pyrrolizine dimers are indeed plausible.

6.2.1.3 Density Functional Calculations of bis-5H-pyrrolo[2,1-a]isoindole dimers

Two possible starting geometries, **(V)** and **(VI)** Figure 3a, were chosen for bis-5*H*-pyrrolo[2,1-a]isoindole and optimised using the DFT methods outlined in Section 6.2.2.1 giving two unique geometries, Figure 3b. The relative binding energies of each structure were calculated using Equation 5 on page 276 and are given in Table 3. From these values it is noted that structure **(V)** has the lowest relative binding energy of the two optimised isomeric structures, indicating structure **(VI)** is the preferred dimeric species. The relative energy of structure **(V)** was then compared to that of **(VI)**, Table 3, and was found to be 23.3 kJ/mol higher in energy than that of **(VI)**.

3a

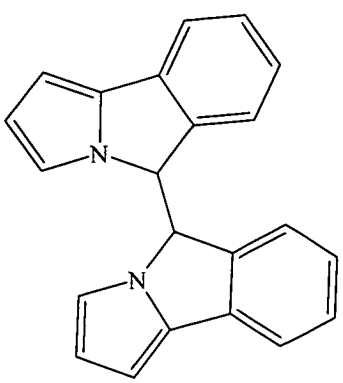

V

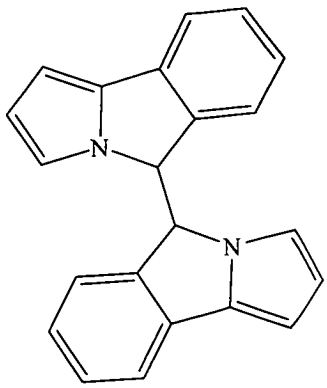

VI

3b

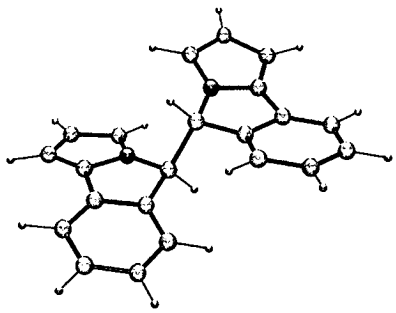

(V)

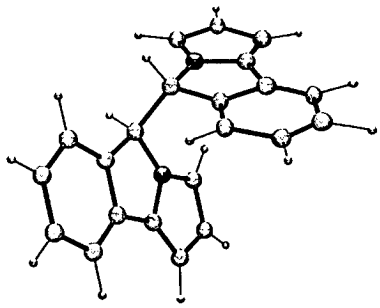

(VI)

Figure 3a. Starting geometries for structures **(V)** – **(VI)** for bis-5*H*-pyrrolo[2,1-a]isoindole.

Figure 3b. Optimised geometries for structures **(V)** – **(VI)** for bis-5*H*-pyrrolo[2,1-a]isoindole.

Table 3. Binding energies of bis(5*H*-pyrrolo[2,1-a]isoindole) structures, **(V)** and **(VI)**.†

Compound	Relative binding energy	Relative energy
(V)	-101.9	-23.3
(VI)	-78.6	0.0

† Energies reported in kJ/mol.

Visually the geometry of the optimised structures of the 5*H*(pyrrolo[2,1-a]isoindole) dimers are quite different. Structure **(V)** shows geometrical similarities to those structures **(I)** – **(III)** discussed earlier in this Chapter, where it was observed that the pyrrolizine units of the dimer lay in two distinct planes that were perpendicular to each other. A centre of symmetry is present in structure **(V)** through the centre of the C – C bond bridging the two tricyclic components of the dimer giving rise to the structure showing C_{2h} symmetry. The external five and six membered rings of the **(V)** are observed to fold out of the plane of the sp_3 carbon giving each (5*H*pyrrolo[2,1-a]isoindole) unit a curved appearance, which is clearly shown in Figure 4. As was also observed in structure **(I)** – **(III)** the hydrogens of the bridging carbons are noted to fold away from the central axis and out of the plane of their respective sp_3 carbon.

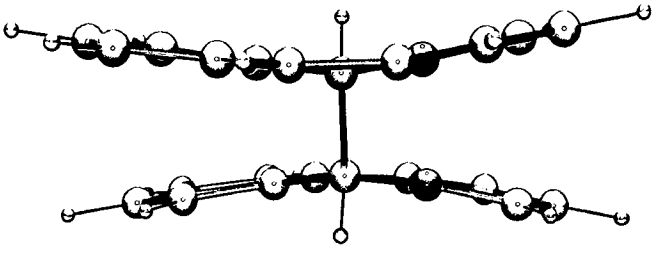

Figure 4. Folding of structure **(V)**.

Whilst **(V)** displays an optimised geometry similar to that of **(I)** – **(III)** the optimised structure of **(VI)** exhibits a vastly different geometry, Figure 5. Like **(V)** the heterocyclic units of **(VI)** are observed to lie in different planes, however the two components are not in parallel planes. The heterocyclic units were calculated to lie at a dihedral angle of 67.7 ° (N-C-C-N) angle, N-C-C 114.2 ° and C-C-C 116.6 °. The

optimised geometry of each 5*H*-pyrrolo[2,1-a]isoindole unit in **(VI)** is observed to be different when compared to those in **(V)**. While the 5*H*-pyrrolo[2,1-a]isoindole units in **(V)** were observed to be folding away from the central axis out of the plane of the sp^3 carbon, **(VI)** they are observed to be relatively "flat", Figure 5.

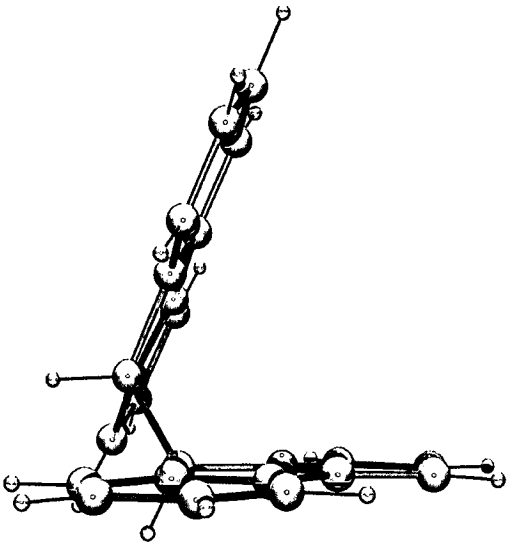

Figure 5. Optimised geometry of bis-5*H*- pyrrolo[2,1-a]isoindole, structure **(VI)**, showing angle between the two heterocycles.

The geometry observed for the bis-5*H*- pyrrolo[2,1-a]isoindole structure **(VI)** is similar to that for 9,9'-bifluorenyl, **(VII)**, Figure 6, which was reported to have the two fluorenyl units in two distinct planes. Like **(VI)** these planes are not parallel to each other, the bite angle between the two fluorenyl units was found to be 113.61 °. The hydrogens of the bridging carbons are noted to be orientated away from the plane of their respective fluorenyl unit. This same characteristic was observed to occur in all the other dimeric structures discussed in this Chapter. These particular angles, at which the hydrogens fold away from the bridging C-C bond, and the bridging C-C bond length for structures **(V)**-**(VI)** are given in Table 4. [42,43]

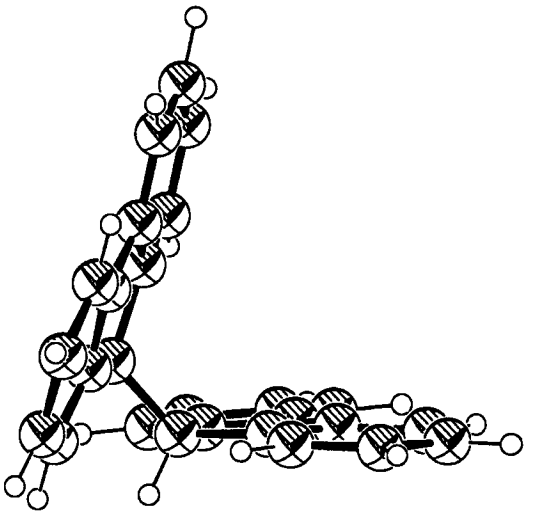

Figure 6. Single crystal X-ray structure of 9,9'-bifluorenyl **(VII)**, X-ray crystal structure reproduced from the CCDC database. Thermal ellipsoids are shown with arbitrary radii.

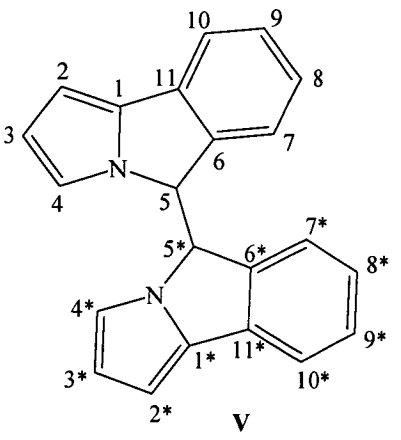

V

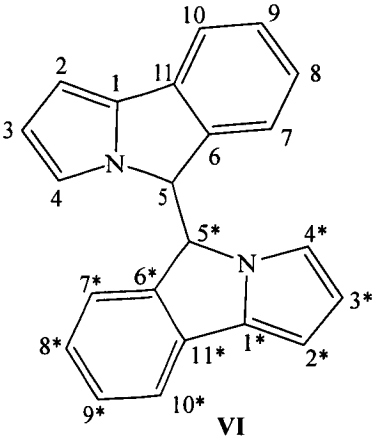

VI

Table 4. Bond length and angle of bridging C-C of bis(5*H*- pyrrolo[2,1-a]isoindole).

	(V)	**(VI)**	**(VII)**
C-C (Å)*	1.581	1.553	1.542
C-C-H (°)†	108.06	106.95, 107.04	108.06, 108.67
Dihedral angle (°)‡	7.0	112.3, 111.5	118.6, 117.9

* **(V)** – C5-C5*, **(VI)** – C5-C5*

† **(V)** – C5-C5*-H5*, **(VI)** – C5-C5*-H5*, C5*-C5-H5

‡ **(V)** – N-C5-C5*-C6*, **(VI)** – N-C5-C5*-N*, C6-C5-C5*-C6*

The three structures given in Table 4 show little variation in the C-C-H angle, that is the angle between the bridging carbon vector and the hydrogens of the bridging carbons. Small variations are observed in bridging carbon distances between the three structures with the greater bond distance occurring for **(V)**, this particular bond distance is 0.028 Å greater than that of structure **(VI)**. The bond distance of the bridging carbons is most similar between **(VI)** and the structurally determined **(VII)**, a 0.011 Å variation in distance. The variation in the bond distance between **(V)** and **(VI)** is due to the difference in the orientation of the 5*H*-pyrrolo[2,1-a]isoindole units within each optimised structure. By twisting of one of the pyrrolo[2,1-a]isoindole units in **(VI)** a decrease in any steric interactions occurs, thus allowing for the observed shorter bond distance. This twisting of one of the units in the dimeric structure is also observed in **(VII)** but is not present in **(V)**. The lengthening of this particular bond in **(V)** appears to occur in order to decrease any unfavourable steric interactions.

Further investigation of the dimeric 5*H*-pyrrolo[2,1-a]isoindole involved the dehydrogenation of each unit and the formation of a double bond between each 5*H*-pyrrolo[2,1-a]isoindolenyl unit. Two possible starting geometries were chosen, **(VIII)** and **(IX)**, and their geometries optimised and energies calculated as outlined in Section 6.2.2.1. The optimisation of the **(VIII)** and **(XI)** gave two unique structures of similar geometry, Figure 7. The relative binding energies, calculated *via* Equation 5, and the relative energy of **(IX)** with respect to **(VIII)** are given in Table 5.

Table 5. Binding and relative energies of 5*H*-pyrrolo[2,1-a]isoindolene dimers.†

Compound	Relative binding energy	Relative energy
(VIII)	772.4	0.0
(IX)	772.0	-0.5

† Energies reported in kJ/mol.

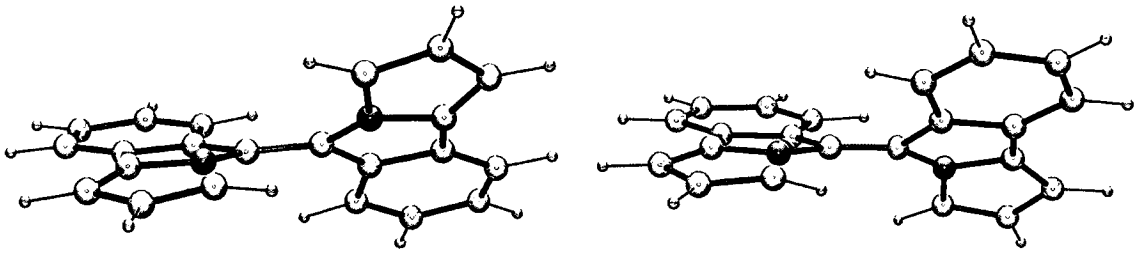

(VIII) **(IX)**

Figure 7. Optimised geometries of bis 5*H*- pyrrolo[2,1-a]isoindolene.

Both structures show each 5*H*-pyrrolo[2,1-a]isoindolenyl unit with a flat geometry with no folding of the dianion that was observed in **(V)** present. Each 5*H*-pyrrolo[2,1-a]isoindolenyl unit is in a unique plane, these planes are not parallel to each other as was the case for the bis(3*H*-pyrrolizine) structures and **(V)**. One of the two units in each structure is observed to be twisting out of the plane of the other unit. It is, however, not perpendicular to the other unit. Table 6 gives the dihedral angles measured for structures **(VIII)** and **(IX)**.

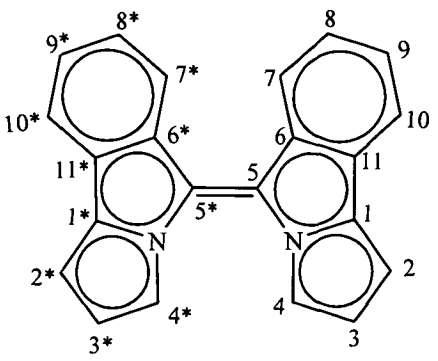

VIII

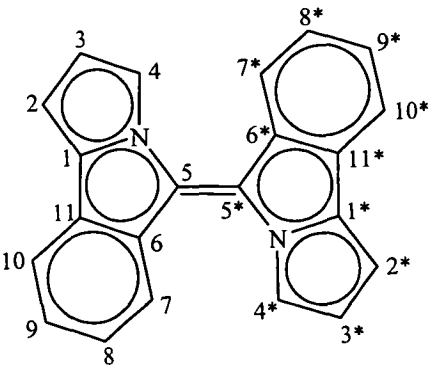

IX

Table 6. Bond length and dihedral angles of bis(5*H*-pyrrolo[2,1-a]isoindolene)

	(VIII)	**(IX)**	**(X)**
C-C (Å) *	1.372	1.372	1.364
Dihedral angle (°) ‡	28.9	23.9, 36.2	38.9, 28.0

* **(V)** – C5-C5*, **(VI)** – C5-C5*

‡ **(V)** – N-5-5*-6*, **(VI)** – N-5-5*-N*, C6-C5-C5*-C6*

In 1985 Lee and Nyburg reported the X-ray crystal structure of 9,9'-bifluorenylidene, **(X)**, Figure 8, a dimeric compound with a similar geometry to **(VIII)** and **(IX)**.[46] This particular compound exhibits the same twisting out of the plane as was found in structures **(VIII)** and **(IX)**, with one of the bifluorenyl units observed to twist out of the plane. Like structures **(VIII)** and **(IX)** the determined single crystal X-ray structure of **(X)** shows each bifluorenyl unit with a relatively flat geometry. The dihedral angle of the bridging carbons calculated for structures **(VIII)** and **(IX)** are similar in magnitude to that measured in **(X)** as is the corresponding bond length between the two bridging carbons, C5-C5*, Table 6. The twisting of one of the units away from the plane of the other in all three structures allows for the decrease in any undesired interactions that may occur within the dimeric species.[42,43]

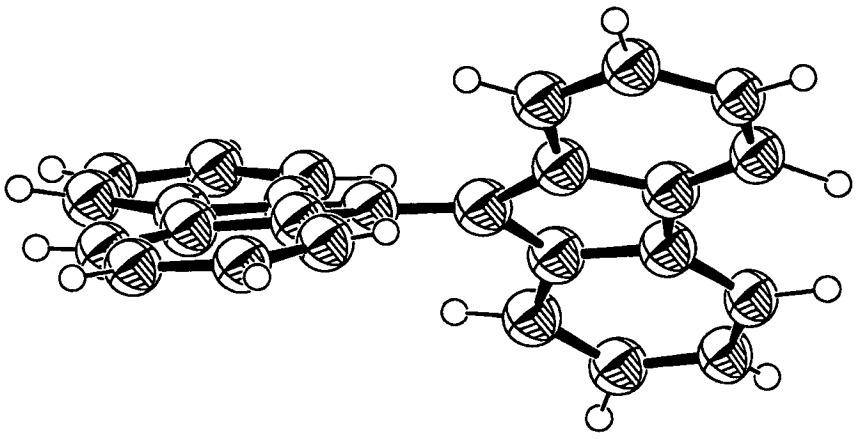

Figure 8. Single crystal X-ray structure of 9,9'-bifluorenylidene, X-ray crystal structure reproduced from the CCDC database. Thermal ellipsoids are shown with abitrary radii.

The similarity of the calculated geometries of **(VI)**, **(VIII)** and **(IX)** with the determined X-ray crystal structures of 9,9'-bifluorenyl, **(VII)**, and 9,9'-bifluorenylidene, **(X)**, provide a good indication of what may occur in the real system for dimeric structures of this type. Similarities in the bridging unit bond distances and the dihedral angles between the dimers determined for the calculated structures further reinforce this idea. We have determined the relative binding energy for each structure and in doing so have shown that the lowest energy conformer of the bis(5*H*-pyrrolo[2,1-a]isoindole) and bis(5*H*-pyrrolo[2,1-a]isoindolene) are the structures where one of the units is observed to twist out of the plane of the bridging C-C vector. The twisting observed allows for a lowering of any steric interactions which may be present thus leading to the conformers of the lowest energy.

6.2.2 Determination of pK_a

6.2.2.1 General Computational Methodology

The pK_a of structures **(XI)** – **(XIII)** were determined using Complete Basis Set, CBS, and Gaussian methods combined with the conductor-like polarised continuum method, CPCM. This particular method has been successfully used to accurately calculate the pK_a of a wide range of structures including carboxylic acids,[5] substituted phenols,[47] and carbenes.[33]

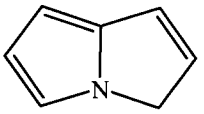

XI

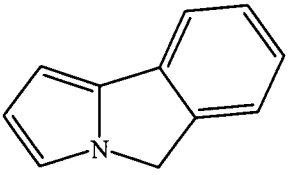

XII

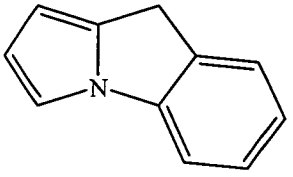

XIII

The geometries of both the acid and anion form of each structures were first optimised using the 6-31+G(d) basis set using Hartree Fock, HF, level of theory. The gas phase energy calculations were carried out at the CBS-QB3 level with the solution phase geometries calculated using the conductor-like polarised continuum method, CPCM, developed by Barone and Cossi,[18] at the CPCM/HF/6-31+G(d) level of theory. The standard free energies of solvation in water were then calculated by performing single point calculations at the CPCM/HF/6-31+G(d), CPCM/HF/6-31+G(d)//HF/6-31+G(d) and CPCM/HF/6-31+G(d)//CBS-QB3. Three different solvent regimes were used to calculate the energy of solvation and are referred to as S1, S2 and S3. For these solvation calculations the number of tesserae on each sphere and the area of each tesserae were set at 240 and 0.3 $Å^2$, respectively.

The 3*H*-pyrrolozine derived compounds and their corresponding 4-azapentalenyl anions were initially optimised in the gas phase at the B3LYP density functional theory using 6-31+G(d) basis set. The high level gas phase free energies, G^0, were then calculated using the complete basis set method, CBS-QB3.[10] The CBS-

QB3 method performs the initial geometry optimisation at B3LYP/CBSB7 level followed by single point calculations at CCSD(T)/6-31+G(d), MP4SDQ/CBSB4 and MP2/CBSB3 levels of theory. The final single point energy calculation includes extrapolation of the complete basis set method applied. The CBS-QB3 method includes a zero point vibrational energy correction from the B3LYP/CBSB7 frequency calculation which is scaled by 0.9899. The value used for $G^0(H^+)_{gas}$ was taken as -18.4 kJ/mol. This number was derived from the value of $G^0(H^+)_{gas}$ obtained in the Sackur-Tetrode equation, -26.3 kJ/mol, this equation takes into account the change of the reference state from atmospheres to moles per litre.[47]

The calculated free energies and solvation energies for both the anion and the acid forms of each compound are given in Tables 7 to 9. From these it becomes possible to calculate the absolute pK_a of each compound, see Scheme 1, the results are given in Table 10.

Table 7: CBS-QB3 free energies, G^0 (hartrees).

	Acid	Anion
(XI)	-325.102629	-324.529108
(XII)	-478.484494	-477.910968
(XIII)	-478.483340	-477.917159

Table 8: Solvation energies of acids (kJ/mol)[a]

	S1	**S2**	**S3**
(XI)	-25.4	-25.3	-26.4
(XII)	-25.0	-24.9	-25.9
(XIII)	-17.3	-17.2	-17.9

[a] **S1** = CPCM/HF/6-31+G(d), **S2** = CPCM/HF/6-31+G(d) // HF/6-31+G(d), **S3** = CPCM/HF/6-31+G(d) // CBS-QB3

Table 9: Solvation energies of anions (kcal/mol) [a]

	S1	S2	S3
(XI)	-216.1	-216.1	-216.4
(XII)	-196.8	-196.7	-197.2
(XIII)	-197.0	-197.0	-197.0

[a] **S1** = CPCM/HF/6-31+G(d), **S2** = CPCM/HF/6-31+G(d) // HF/6-31+G(d), **S3** = CPCM/HF/6-31+G(d) // CBS-QB3

Table 10: Absolute pK_a's for 4-azapentalenyl systems in H_2O [a]

	S1	S2	S3	Average	Deviation[b]
(XI)	35.46	35.43	35.57	35.50	0.07
(XII)	38.77	38.76	38.85	38.90	0.05
(XIII)	34.00	33.98	34.11	34.03	0.07

[a] **S1** = CPCM/HF/6-31+G(d), **S2** = CPCM/HF/6-31+G(d) // HF/6-31+G(d), **S3** = CPCM/HF/6-31+G(d) // CBS-QB3. [b] Mean unsigned deviation from average pK_a.

The pK_a of *3H*-pyrolizine, **(XI)**, was determined in 1967 by Okamura and Katz by measuring the proton exchange rate of the compound with D_2O in triethylamine. The measured rate of proton exchange enabled the pK_a of the system to be calculated and found to be about 29 pK_a units.[1] In comparison the pK_a calculated by the methods here give a value of 35.5. This is comparable with the work carried out by Chipman who showed that the absolute pK_a values he calculated in water for a range of compounds was also found to be higher than that which had been measured experimentally.[48] Table 10 also shows that the three different calculations methods utilised for the calculation of the pK_a of each compound gave very similar results.

The calculated pK_a values of the investigated compounds clearly indicate that all are weak acids with **(XIII)** being the strongest weak acid of the three, **(XIII)** < **(XI)** < **(XII)**. The high pK_a values explain the instability exhibited by the organometallic derivatives and the preference of the compound to remain as the protonated acid. Hence the instability of the anion and the subsequent reversion to

the protonated base which has been observed experimentally in some of the Group 1 metal complexes synthesised within in Chapter 3 of this thesis can somewhat be explained through the high pK_a values that have been calculated.

6.3 REFERENCES

(1) Okamura, W. H.; Katz, T. J. *Tetrahedron* **1967**, *23*, 2941-2957.

(2) Perrin, C. L.; Fabian, M. A. *Anal. Chem.* **1996**, *68*, 2127 - 2134.

(3) Bates, R. G. *Determination of pH: Theory and Practice*; 2nd ed. ed.; Wiley: New York, 1973.

(4) Cookson, R. F. *Chem. Rev.* **1974**, *74*, 5-28.

(5) Liptak, M. D.; Shields, G. C. *J. Am. Chem. Soc.* **2001**, *123*, 7314-7319.

(6) Liptak, M. D.; Shields, G. C. *Int. J. Quantum Chem.* **2001**, *85*, 727-741.

(7) Jang, Y. H.; Sowers, L. C.; Cagin, T.; Goddard III, W. A. *J. Phys. Chem. A* **2001**, *105*, 274-280.

(8) Pliego Jr., J. R.; Riveros, J. M. *J. Phys. Chem. A* **2002**, *106*, 7434-7439.

(9) Toth, A. M.; Liptak, M. D.; Phillips, D. L.; Shields, G. C. *J. Chem. Phys.* **2001**, *114*, 4595-4606.

(10) Montgomery, J. A.; Frisch, M. J.; Ochterski, J. W.; Petersson, G. A. *J. Chem. Phys.* **1999**, *110*, 2822 - 2827.

(11) Montgomery, J. A.; Ochterski, J. W.; Petersson, G. A. *J. Chem. Phys.* **1994**, *101*.

(12) Nyden, M. R.; Petersson, G. A. *J. Chem. Phys.* **1981**, *75*, 1843.

(13) Ochterski, J. W.; Petersson, G. A.; Montgomery, J. A. *J. Chem. Phys.* **1996**, *104*, 2598.

(14) Petersson, G. A.; Bennett, A.; Tensfeldt, T. G.; Al-Laham, M. A.; Shirley, W. A.; Mantzaris, J. *J. Chem. Phys.* **1988**, *89*, 2193.

(15) Petersson, G. A.; Al-Laham, M. A. *J. Chem. Phys.* **1991**, *94*, 6081.

(16) Petersson, G. A.; Malick, D. K.; Wilson, W. G.; Ochterski, J. W.; Montgomery, J. A.; Frisch, M. J. *J. Chem. Phys.* **1998**, *109*, 10570.

(17) Young, D. C. *Computational Chemistry: A Practical Guide for Applying Techniques to Real-World Problems*; John Wiley and Sons, Inc.: New York, 2001.

(18) Barone, V.; Cossi, M. *J. Phys. Chem. A* **1998**, *102*, 1995-2001.

(19) Barone, V.; Cossi, M.; Tomasi, J. *J. Comput. Chem.* **1998**, *19*, 404.

(20) Barone, V.; Cossi, M.; Mennucci, B.; Tomasi, J. *Chem. Phys. Lett.* **1997**, *107*, 3210.

(21) Cossi, M.; Barone, V.; Cammi, R.; Tomasi, J.

Chem. Phys. Lett. **1996**, *255*, 327.

(22) Cossi, M.; Barone, V.; Mennucci, B.; Tomasi, J. *Chem. Phys. Lett.* **1998**, *286*, 253.

(23) Miertus, S.; Tomasi, J. *Chem. Phys.* **1981**, *65*, 239.

(24) Miertus, S.; Scrocco, E.; Tomasi, J. *Chem. Phys. Lett.* **1996**, *255*, 327.

(25) Cances, M. T.; Mennucci, V.; Tomasi, J. *J. Chem. Phys.* **1997**, *107*, 3032.

(26) Li, J.; Zhu, T.; Hawkins, G. D.; Liotard, D. A.; Cramer, C. J.; Truhlar, D. G. *Theor. Chem. Acc.* **1999**, *103*, 9.

(27) Li, J.; Cramer, C. J.; Truhlar, D. G. *Chem. Phys. Lett.* **1998**, *288*, 293.

(28) Curtiss, L. A.; Raghavachari, K.; Redfern, P. C.; Rassolov, V.; Pople, J. A. *J. Chem. Phys.* **1998**, *109*, 7764.

(29) Curtiss, L. A.; Raghavachari, K.; Trucks, G. W.; Pople, J. A. *J. Chem. Phys.* **1991**, *94*, 7221.

(30) Curtiss, L. A.; Raghavachari, K.; Jones, C.; Pople, J. A. *J. Chem. Phys.* **1993**, *98*, 1283.

(31) Leal, J. P.; Cachata, V.; Carvalho, A. *Eur. J. Inorg. Chem.* **2001**, 1587 - 1591.

(32) am Busch, M. S.; Knapp, E.-W. *Chem. Phys. Chem.* **2004**, *5*, 1513 - 1522.

(33) Magill, A. M.; Cavell, K. J.; Yates, B. F. *J. Am. Chem. Soc.* **2004**, *126*, 8717 - 8724.

(34) Denk, K.; Sirsch, P.; Herrmann, W. A. *J. Organomet. Chem.* **2002**, *649*, 219 - 224.

(35) Canty, A. J.; Minchin, N. J. *Aust. J. Chem.* **1986**, *39*, 1063 - 1069.

(36) Becke, A. D. *J. Chem. Phys.* **1993**, *93*, 5648.

(37) Becke, A. D. *Phys. Rev. A.* **1998**, *38*, 3098.

(38) Lee, C.; Yang, W.; Parr, R. G. *Phys. Rev. B.* **1998**, *37*, 785.

(39) Frisch, M. J.; Pople, J. A.; Binkley, J. S. *J. Chem. Phys.* **1984**, *80*, 3265.

(40) Frisch, M. J.; Trucks, G. W.; Schlegel, H. B.; Scuseria, G. E.; Robb, M. A.; Cheeseman, J. R.; Montgomery, J. A.; Vreven, T.; Kudin, K. N.; Burant, J. C.; Millam, J. M.; Iyengar, S. S.; Tomasi, J.; Barone, V.; Mennucci, B.; Cossi, M.; Scalmani, G.; Rega, N.; Petersson, G. A.; Nakatsuji, H.; Hada, M.; Ehara, M.; Toyota, K.; Fukuda, R.; Hasegawa, J.; Ishida, M.; Nakajima, T.; Honda, Y.; Kitao, O.; Nakai, H.; Klene, M.; Li, X.; Knox, J. E.; Hratchian, H. P.; Cross, J. B.; Bakken, V.; Adamo, C.; Jaramillo, J.; Gomperts, R.; Stratmann, R. E.; Yazyev, O.; Austin, A. J.; Cammi, R.; Pomelli, C.;

Ochterski, J. W.; Ayala, P. Y.; Morokuma, K.; Voth, G. A.; Salvador, P.; Dannenberg, J. J.; Zakrzewski, V. G.; Dapprich, S.; Daniels, A. D.; Strain, M. C.; Farkas, O.; Malick, D. K.; Rabuck, A. D.; Raghavachari, K.; Foresman, J. B.; Ortiz, J. V.; Cui, Q.; Baboul, A. G.; Clifford, S.; Cioslowski, J.; Stefanov, B. B.; Liu, G.; Liashenko, A.; Piskorz, P.; Komaromi, I.; Martin, R. L.; Fox, D. J.; Keith, T.; Al-Laham, M. A.; Peng, C. Y.; Nanayakkara, A.; Challacombe, M.; Gill, P. M. W.; Johnson, B.; Chen, W.; Wong, M. W.; Gonzalez, C.; Pople, J. A.; Revision C.02 ed.; Gaussian, Inc.: Wallingford CT, 2004.

(41) Churchill, M. R.; Lin, K.-K. G. *Inorg. Chem.* **1973**, *12*, 1973.

(42) Bruno, I. J.; Cole, J. C.; Edgington, P. R.; Kessler, M.; Macrae, C. F.; McCabe, P.; Pearson, J.; Taylor, R. *Acta Crystallogr.* **2002**, *B58*, 389-397.

(43) Allen, F. H. *Acta Crystallogr.* **2002**, *B58*, 380 - 388.

(44) Grindley, T. B.; Macleod, P. J.; Pincock, J. A.; Cameron, T. S. *Can. J. Chem.* **1996**, *74*, 1795.

(45) Schaefer, W. P.; Henling, L. M.; McBay, H. C.; Abulu, J. *Acta. Crystallogr., Sect. C: Cryst. Struct. Commun.* **1996**, *52*, 104.

(46) Lee, J.-S.; Nyburg, S. C. *Acta. Crystallogr., Sect. C: Cryst. Struct. Commun.* **1985**, *41*, 560.

(47) Liptak, M. D.; Gross, K. C.; Seybold, P. G.; Feldgus, S.; Shields, G. C. *J. Am. Chem. Soc.* **2002**, *124*, 6421-6427.

(48) Chipman, D. M. *J. Phys. Chem. A* **2002**, *106*, 7413-7422.

CHAPTER 7
CONCLUSION

The studies of the 4-azapentalenyl anion and its derivatives within this thesis have indicated a number of interesting properties. In particular structural studies of the Group 1 metal complexes have shown these ring fused anions to be capable of various multi-hapto binding modes that can adapt to match the requirements of the metals and their ancillary ligands. In addition, the complexes have cyclopentadienyl-type overall structural motifs, which has allowed us to direct our further efforts in line with this trend. The information we gained from the theoretical studies has shown that the 4-azapentalenyl anion can act as a fluxional ligand during a catalytic process. Theoretical studies have also aided in our understanding of the relative instability of the deprotonated 4-azapentalenyl anion and its derivatives by through their high pK_a values.

We were able to successfully synthesise the parent 3*H*-pyrrolizine and some of its derivatives including 5*H*-pyrrolo[2,1-a]isoindole in reasonable yield. Group 1 metal complexes of deprotonated 5*H*-pyrrolizine and 5*H*-pyrrolo[2,1-a]isoindole were successfully synthesised. In particular potassium complexes of the latter class, coordination of various Lewis bases aided in stabilising the complexes. These potassium salts were able to be crystallised and successful characterisation indicated that the potassium interacted with the anion in a variety of binding modes including η^1, η^3, η^5 and η^6. No folding of the tricyclic anion was observed within the crystal structures. The synthesis and subsequent characterisation of many of the Group 1 metal compounds proved to be somewhat more problematic than first thought. Deprotonation of the parent compound was observed to occur, more readily in some cases than in others, to give the corresponding anion. The subsequent instability of the anion led to the reprotonation of the species and in some cases a reductively coupled product was observed, this was the case the reaction of the 3*H*-pyrrolizine with the samarium pentamethylcyclopentadienyl compounds discussed in Chapter 3 The tendency of the heterocycle to reprotonate or form these coupled species meant that characterisation of several of the complexes was limited to NMR spectroscopic studies, in some cases this was limited as well.

Theoretical studies using density functional theory, DFT, was used to gain further insight into the 4-azapentalenyl anion and the effect of extending the ring system. Studies of the 4-azapentalenyl anion indicated that it has the potential to interact with metal centres in variety binding modes ranging from η^1 through to $\eta^{6/8}$. Study of the interaction between Group 1 metals and the 4-azapentalenyl anion showed folded geometries for the larger potassium and sodium cations. On proceeding to the complexes of the 4-azapentalenyl anion with Group 3 and 4 metals it became evident that in order to form a stable complex the wingtip carbons of the anion become involved in the bonding similar to that which had been observed in pentalendiyl complexes. It was difficult however to fully determine whether the metal-ligand interactions occurring within these complexes was η^6 or η^8.

Theoretical investigations into the deprotonated 5*H*-pyrrolo[2,1-a]isoindole Group 1 metal salts showed that the size and the nature of the metal centre influences the type of interaction which is observed. The metal centre was also noted to affect the extent to which the anion was able to fold along the N-C bridgehead vector. The degree of this folding, in turn, affects the type of interaction or hapticity which was noted, which is compensated by loss in aromatic character of the anion.

One of the most interesting aspects to come out of this work is the fluxionality which was observed in the DFT calculations for a catalytically relevant process in Chapter 5. Here we were able to show that the hapticity of the anion changes during the migratory insertion of ethylene into a scandium hydride in a bis(4-azapentalenyl) complex. The results of this migratory insertion of ethylene into the scandium hydride complex show that the complex has close to an energy free insertion barrier for ethylene polymerisation. This can be accounted for by the reversible $\eta^{6/8} \leftrightarrow \eta^5$ fluxionality of the 4-azapentalenyl anion in response to the overall electronic saturation of the species through the insertion process. This was indeed what we hoped to observe from this particular process. We were not able to synthetically achieve this catalysis in the laboratory, however, due to the proven instability of the anion, as discussed earlier. Nevertheless, this concept remains

important in a general sense and ought to be further explored for related synthetically accessible ligand systems.

Further evidence of the instability of the anions in these complexes became evident when theoretical calculations of pK_a were undertaken. These studies employing DFT methods determined that 3*H*-pyrrolizine and its benzannulated derivatives that were synthesised have relatively high pK_a values. This indicated that these ligands prefer to remain as a protonated acid, hence confirming that the reprotonation we observed during the attempted Group 1 metal complex synthesis of these compounds related to issues of low acidity.

APPENDIX I

EXPERIMENTAL PROCEDURES

Unless otherwise stated all manipulations of complexes were carried out under argon, high purity, by using standard Schlenk techniques. Solvents for the preparation of complexes were dried over Na or Na/K. Storage of complexes and preparation of samples for various analyses required the use of a dry atmosphere glove box (Innovative Technologies) fitted with O_2 (CuO) and H_2O (molecule sieve) removal columns, filled with a pre-dried, recirculating atmosphere of high purity nitrogen. For the preparation of organic intermediates or ligands, solvents including, ethanol, dichloromethane, toluene, 40 – 60 °C or 60 – 80 °C petroleum ether, diethyl ether, N,N dimethyl acetamide were used as received or after degassing in some cases. All chemicals were obtained from Aldrich and used as received except pyrrole, which was used in subsequent reactions after being freshly redistilled, TMEDA and PMDETA which were pre-dried prior to use. 18-crown-6 was dried.

NMR spectra were recorded in $CDCl_3$, acetone-d^6 or appropriately dried C_6D_6, THF-d^8 and pyridine-d^5 using a Varian-Gemini 200 spectrometer operating at 199.975 (^{1}H) and 50.290 (^{13}C) MHz or a Varian Gemini Mercury Plus 300 spectrometer operating at 299.905 (^{1}H) and 75.417 (^{13}C) MHz at room temperature. The ^{1}H NMR spectra were referenced to following the residual ^{1}H resonances (δ, ppm): $CDCl_3$ (7.26); C_6D_6 (7.15); THF-d^8 (1.85 or 3.76) and pyridine-d^5 (8.62). The ^{13}C NMR spectra were referenced to the following ^{13}C resonances (δ, ppm): $CDCl_3$ (77.0); C_6D_6 (128.0); THF-d^8 (68.0) and pyridine-d^5 (149.9). GC/MS spectra were performed using a HP5890 gas chromatograph equipped with an HP5790 Mass Selective Detector and a 25 m x 0.32 mm HPI column. Elemental analyses were performed by the Central Science Laboratory at the University of Tasmania with a Carlo Erba EA1108 Elemental Analyser or at the Chemical and Analytical Services Pty. Ltd. Melbourne. X-ray crystal structure determinations were carried out by Professor Allan H. White and Dr. Brian W. Skelton of the University of Western

Australia, Professor Peter C. Junk Monash University, Dr Peter B. Hitchcock, University of Sussex, UK and Dr Michael G. Gardiner.

APPENDIX II
CRYSTALLOGRAPHIC DATA

Summary of X-Ray Diffraction Data

X-Ray diffraction data for 5*H*-pyrrolo[2,1-a]isoindole, **(9)**

White crystals of 5*H*-pyrrolo[2,1-a]isoindole, **(9)**, suitable for X-ray structure determination were obtained by sublimation (80 °C, 2.6 x 10^{-2} mbar). The crystals of **(9)** belong to the monoclinic space group $P2_1/n$ (No. 14), a = 10.1227(7), b = 5.6528(4), c = 14.1174(9) Å, β = 97.300(2)°. The asymmetric unit contains one molecule of **(9)**, and the unit cell consists of four molecules of **(9)**. The molecular structure of **(9)** is shown in Figure 1.

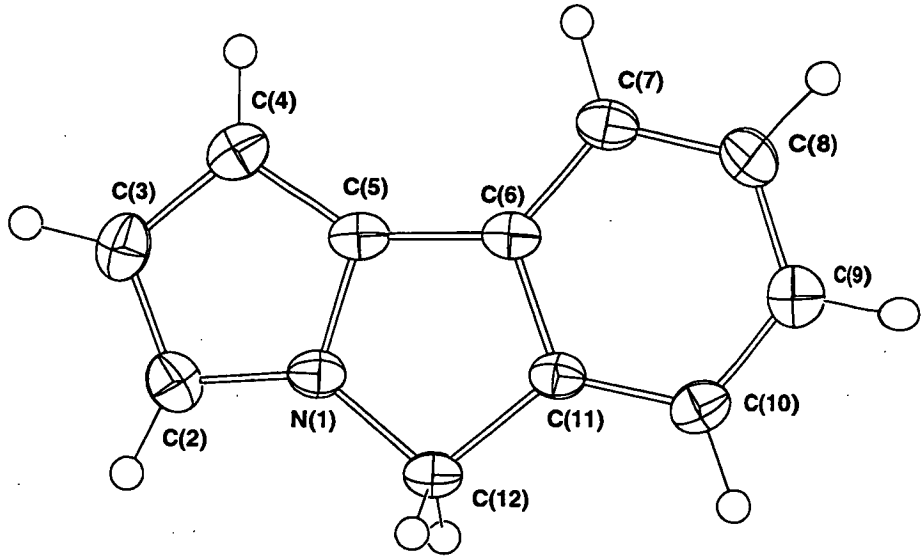

Figure 1: Molecular structure of 5*H*-pyrrolo[2,1-a]isoindole, **(9)**, with thermal ellipsoids are drawn at the level of 50% probability.

Compound **(9)** adopts a planar 5:5:6 ring structure which exhibits little deviation from the crystallographic plane, this is similar to the crystal structure for compound **(11)**. Compound **(11)** adopts a 6:5:5:6 ring structure however unlike **(9)** a crystallographic disorder in the solid state structure exists. A 50% occupational disorder of the central C and the bridgehead N positions and sp^2 and the sp^3 positions adjacent to these was reported by Frey.[25]

Figure 2 is a representation of the unit cell contents of compound **(9)** showing that the molecules stack one above the other.

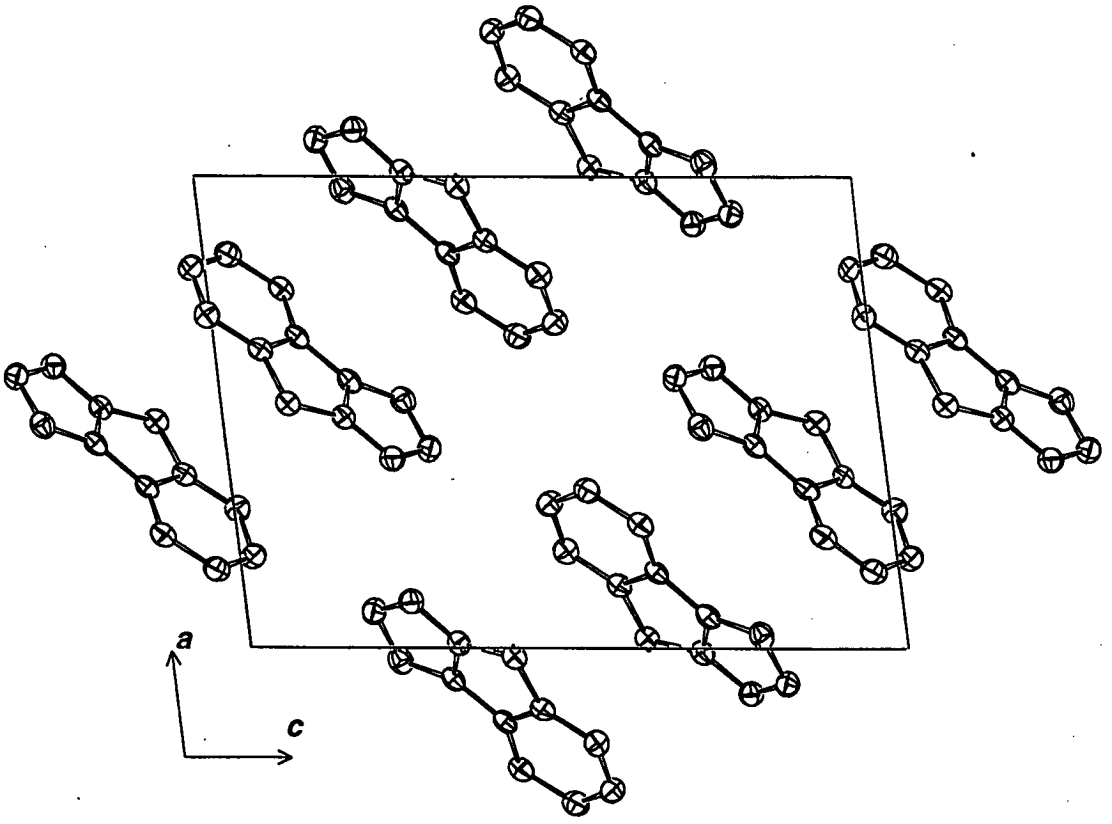

Figure 2: Unit cell packing diagram of 5*H*-pyrrolo[2,1-a]isoindole, **(9)**, with thermal ellpisoids are drawn at the level of 50% probability, protons have been removed for clarity.

X-Ray diffraction data for $[(C_{11}H_8N)K(THF)_{1/2}]$, **(19)**.

The complex $[(C_{11}H_8N)K(THF)_{1/2}]$, **(19)**, crystallises as red prisms from a concentrated THF at ambient temperature over two weeks in the monoclinic space group *C2/c*. Complex **(19)** has 8 molecules in the unit cell with the asymmetric unit being comprised of 2 independent halves of molecules. The complex comprises two K cations which are bridged by a THF molecule, each potassium coordinates to three anions ($C_{11}H_8N$), Figure 3 a = 17.6808(2), b = 10.2199(2), c = 12.4844(4) Å, β = 102.1350(10) °. The crystals were isolated and mounted in sealed thin-walled glass capillaries under an argon atmosphere. The diffraction data was collected by Gary Fallon at the Department of Chemistry, Monash University and the structure solution and refinement carried out by Dr Michael Gardiner.

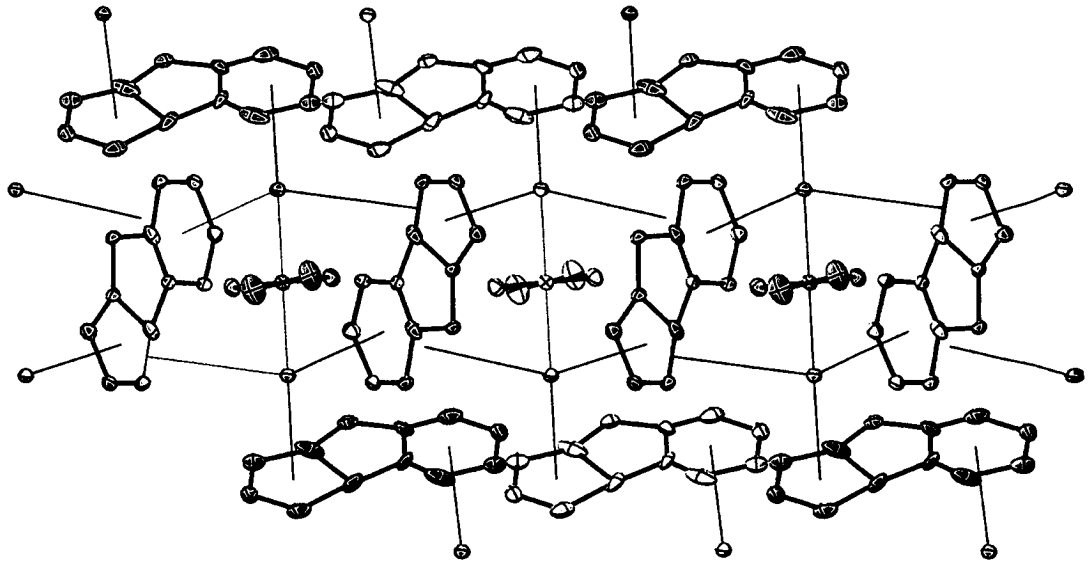

Figure 3. Molecular structure of $[(C_{11}H_8N)K(THF)_{1/2}]_n$, **(19)**, thermal ellipsoids are drawn at the level of 50% probability, hydrogens have been removed for clarity.

Table 1. Atomic coordinates (x 10^4) and equivalent isotropic displacement parameters (Å2x 103) for $[(C_{11}H_8N)K(THF)_{1/2}]$, **(19)**.

	x	y	z	*U(eq)
K(1)	3713(1)	490(1)	2019(1)	50(1)
N(1)	4829(3)	-1195(6)	675(4)	44(1)
C(2)	4326(2)	-2195(2)	997(2)	58(1)
C(3)	3610(1)	-1815(2)	383(2)	54(1)
C(4)	3607(1)	-724(2)	-260(2)	56(1)
C(5)	4341(2)	-198(3)	-191(2)	64(1)
C(6)	4994(3)	-548(6)	322(4)	44(1)
C(7)	5021(4)	-1652(7)	997(5)	47(2)
C(8)	5626(2)	-990(4)	922(3)	46(1)
N(2)	2691(2)	3015(4)	1287(5)	108(1)
C(9)	2519(2)	2699(3)	2290(3)	72(1)
C(10)	2067(2)	1596(3)	2236(2)	63(1)
C(11)	1848(2)	998(4)	1237(4)	88(1)
C(12)	2228(7)	1864(12)	336(13)	79(5)
C(13)	2528(6)	2543(12)	-572(8)	70(3)
C(14)	2691(2)	3015(4)	1287(5)	108(1)
C(15)	2017(6)	1315(11)	413(12)	69(4)
C(16)	3070(3)	3875(5)	676(4)	55(1)
O(1)	5000	2091(2)	2500	48(1)
C(17)	4933(2)	2914(2)	3423(2)	61(1)
C(18)	4902(3)	4278(3)	3012(3)	110(1)

* U(eq) is defined as one third of the trace of the orthogonalized Uij tensor.

Table 2. Anisotropic displacement parameters ($Å^2 x\ 10^3$)for $[(C_{11}H_8N)K(THF)_{1/2}]$, **(19)**.

	U11	U22	U33	U23	U13	U12
K(1)	40(1)	56(1)	53(1)	-7(1)	9(1)	2(1)
N(1)	39(3)	46(4)	44(3)	-2(2)	2(2)	18(2)
C(2)	59(2)	59(1)	58(2)	-7(1)	18(1)	-3(1)
C(3)	47(1)	65(2)	53(1)	-10(1)	16(1)	-10(1)
C(4)	45(1)	75(2)	44(1)	-9(1)	2(1)	18(1)
C(5)	77(2)	61(2)	64(2)	-21(1)	39(2)	-12(1)
C(6)	45(3)	49(3)	38(3)	-2(2)	7(2)	10(2)
C(7)	42(3)	50(4)	51(4)	-1(3)	10(3)	15(3)
C(8)	39(2)	50(2)	46(2)	2(2)	1(2)	11(2)
N(2)	61(2)	84(2)	189(4)	73(3)	51(2)	37(2)
C(9)	58(2)	66(2)	90(2)	5(2)	10(2)	18(1)
C(10)	61(2)	70(2)	60(2)	16(1)	21(1)	20(1)
C(11)	52(2)	89(2)	113(3)	-26(2)	-3(2)	23(2)
C(12)	73(10)	94(13)	56(8)	-13(8)	-18(6)	50(8)
C(13)	65(6)	94(9)	38(6)	-15(4)	-16(4)	53(6)
C(14)	61(2)	84(2)	189(4)	73(3)	51(2)	37(2)
C(15)	45(4)	87(8)	82(7)	21(6)	29(4)	23(4)
C(16)	40(2)	51(3)	67(3)	-8(2)	0(2)	7(2)
O(1)	50(1)	45(1)	51(1)	0	16(1)	0
C(17)	65(2)	58(1)	62(2)	-12(1)	21(1)	-6(1)
C(18)	169(4)	56(2)	121(3)	-14(2)	66(3)	13(2)

The anisotropic displacement factor exponent takes the form: $-2\pi^2[\ h^2a^{*2}U^{11} + ... + 2\ h\ k\ a^*\ b^*\ U^{12}\ ]$

Table 3. Hydrogen coordinates (x 10^4) and isotropic displacement parameters ($Å^2$x 10^3) for $[(C_{11}H_8N)K(THF)_{1/2}]$, **(19)**.

	x	y	z	U(eq)
H(2)	4454	-2908	1490	69
H(3)	3149	-2283	407	65
H(4)	3152	-366	-704	67
H(7)	5491	-1990	1420	57
H(8)	6027	-1449	1400	55
H(9)	2694	3189	2941	86
H(10)	1914	1261	2867	75
H(11)	1538	234	1083	105
H(14)	3011	3749	1239	129
H(16)	3381	4573	1028	65
H(17A)	5384	2791	4035	73
H(17B)	4457	2699	3686	73
H(18A)	4374	4638	2950	132
H(18B)	5268	4833	3528	132

Table 4. Bond lengths [Å] and angles [°] for $[(C_{11}H_8N)K(THF)_{1/2}]$, **(19)**.

K(1)-O(1)	2.7648(13)
K(1)-C(8)#1	3.000(4)
K(1)-C(4)	3.073(2)
K(1)-C(3)	3.097(2)
K(1)-C(9)	3.157(3)
K(1)-N(2)	3.173(3)
K(1)-C(10)	3.186(2)
K(1)-C(13)#2	3.233(8)
K(1)-C(5)	3.260(2)
K(1)-C(11)	3.278(3)
K(1)-C(2)	3.304(2)
N(1)-C(8)	1.392(7)
N(1)-C(2)	1.466(7)
N(1)-C(5)	1.600(6)
C(2)-C(7)	1.349(7)
C(2)-C(3)	1.391(4)
C(3)-C(4)	1.373(3)
C(4)-C(5)	1.391(4)
C(4)-K(1)#3	3.450(2)
C(5)-C(6)	1.249(6)
C(5)-C(6)#4	1.439(6)
C(5)-C(8)#4	1.527(5)
C(5)-K(1)#3	3.439(3)
C(6)-C(6)#4	1.383(12)
C(6)-C(7)	1.403(8)
C(6)-C(5)#4	1.439(6)
C(8)-C(5)#4	1.527(5)
C(8)-K(1)#1	3.000(4)
N(2)-C(9)	1.387(5)
N(2)-C(16)	1.422(6)
C(9)-C(10)	1.375(4)
C(10)-C(11)	1.369(4)

C(11)-C(15)	1.176(12)
C(11)-C(12)	1.679(16)
C(12)-C(13)#2	0.766(12)
C(12)-C(13)	1.517(16)
C(12)-C(12)#2	1.91(3)
C(13)-C(12)#2	0.766(12)
C(13)-C(14)#2	1.062(8)
C(13)-C(13)#2	1.45(2)
C(13)-K(1)#2	3.233(8)
C(15)-C(16)#2	1.350(15)
C(16)-C(15)#2	1.350(15)
O(1)-C(17)#1	1.452(3)
O(1)-C(17)	1.452(3)
O(1)-K(1)#1	2.7648(13)
C(17)-C(18)	1.483(4)
C(18)-C(18)#1	1.393(7)

O(1)-K(1)-C(8)#1	87.56(8)
O(1)-K(1)-C(4)	109.11(5)
C(8)#1-K(1)-C(4)	121.80(10)
O(1)-K(1)-C(3)	121.67(5)
C(8)#1-K(1)-C(3)	98.05(10)
C(4)-K(1)-C(3)	25.72(6)
O(1)-K(1)-C(9)	95.27(6)
C(8)#1-K(1)-C(9)	114.68(11)
C(4)-K(1)-C(9)	118.41(8)
C(3)-K(1)-C(9)	131.78(8)
O(1)-K(1)-N(2)	88.51(8)
C(8)#1-K(1)-N(2)	138.81(13)
C(4)-K(1)-N(2)	98.14(12)
C(3)-K(1)-N(2)	118.54(12)
C(9)-K(1)-N(2)	25.31(9)
O(1)-K(1)-C(10)	119.75(6)
C(8)#1-K(1)-C(10)	107.72(10)

C(4)-K(1)-C(10)	110.05(7)
C(3)-K(1)-C(10)	113.43(7)
C(9)-K(1)-C(10)	25.03(7)
N(2)-K(1)-C(10)	42.33(7)
O(1)-K(1)-C(13)#2	100.6(3)
C(8)#1-K(1)-C(13)#2	152.7(2)
C(4)-K(1)-C(13)#2	80.30(15)
C(3)-K(1)-C(13)#2	99.52(16)
C(9)-K(1)-C(13)#2	39.17(17)
N(2)-K(1)-C(13)#2	19.05(14)
C(10)-K(1)-C(13)#2	45.8(2)
O(1)-K(1)-C(5)	84.27(5)
C(8)#1-K(1)-C(5)	118.41(10)
C(4)-K(1)-C(5)	25.16(7)
C(3)-K(1)-C(5)	42.39(6)
C(9)-K(1)-C(5)	126.82(8)
N(2)-K(1)-C(5)	101.92(11)
C(10)-K(1)-C(5)	128.93(8)
C(13)#2-K(1)-C(5)	88.46(19)
O(1)-K(1)-C(11)	134.54(8)
C(8)#1-K(1)-C(11)	121.43(12)
C(4)-K(1)-C(11)	85.80(8)
C(3)-K(1)-C(11)	90.47(7)
C(9)-K(1)-C(11)	42.69(8)
N(2)-K(1)-C(11)	46.28(9)
C(10)-K(1)-C(11)	24.40(7)
C(13)#2-K(1)-C(11)	38.1(3)
C(5)-K(1)-C(11)	106.43(9)
O(1)-K(1)-C(2)	104.70(5)
C(8)#1-K(1)-C(2)	79.16(10)
C(4)-K(1)-C(2)	42.97(6)
C(3)-K(1)-C(2)	24.83(6)
C(9)-K(1)-C(2)	156.40(7)
N(2)-K(1)-C(2)	141.05(12)

C(10)-K(1)-C(2)	135.02(7)
C(13)#2-K(1)-C(2)	122.68(15)
C(5)-K(1)-C(2)	45.27(7)
C(11)-K(1)-C(2)	114.08(7)
C(8)-N(1)-C(2)	133.5(5)
C(8)-N(1)-C(5)	115.4(5)
C(2)-N(1)-C(5)	110.9(4)
C(8)-N(1)-K(1)	119.3(3)
C(2)-N(1)-K(1)	76.3(2)
C(5)-N(1)-K(1)	73.6(2)
C(7)-C(2)-C(3)	127.6(4)
C(7)-C(2)-N(1)	26.8(2)
C(3)-C(2)-N(1)	100.9(3)
C(7)-C(2)-K(1)	91.8(3)
C(3)-C(2)-K(1)	69.25(13)
N(1)-C(2)-K(1)	78.1(2)
C(4)-C(3)-C(2)	116.1(2)
C(4)-C(3)-K(1)	76.13(13)
C(2)-C(3)-K(1)	85.92(14)
C(3)-C(4)-C(5)	112.9(2)
C(3)-C(4)-K(1)	78.15(13)
C(5)-C(4)-K(1)	84.99(14)
C(3)-C(4)-K(1)#3	129.61(15)
C(5)-C(4)-K(1)#3	77.92(15)
K(1)-C(4)-K(1)#3	151.44(9)
C(6)-C(5)-C(4)	132.1(4)
C(6)-C(5)-C(6)#4	61.4(5)
C(4)-C(5)-C(6)#4	166.3(4)
C(6)-C(5)-C(8)#4	112.8(4)
C(4)-C(5)-C(8)#4	115.0(3)
C(6)#4-C(5)-C(8)#4	51.4(3)
C(6)-C(5)-N(1)	33.0(3)
C(4)-C(5)-N(1)	99.2(3)
C(6)#4-C(5)-N(1)	94.4(4)

C(8)#4-C(5)-N(1)	145.8(3)
C(6)-C(5)-K(1)	94.0(3)
C(4)-C(5)-K(1)	69.86(13)
C(6)#4-C(5)-K(1)	114.4(2)
C(8)#4-C(5)-K(1)	113.4(2)
N(1)-C(5)-K(1)	78.3(2)
C(6)-C(5)-K(1)#3	124.2(3)
C(4)-C(5)-K(1)#3	78.78(15)
C(6)#4-C(5)-K(1)#3	91.6(2)
C(8)#4-C(5)-K(1)#3	60.56(19)
N(1)-C(5)-K(1)#3	130.0(2)
K(1)-C(5)-K(1)#3	141.32(10)
C(5)-C(6)-C(6)#4	66.1(4)
C(5)-C(6)-C(7)	116.8(5)
C(6)#4-C(6)-C(7)	177.1(7)
C(5)-C(6)-C(5)#4	118.6(5)
C(6)#4-C(6)-C(5)#4	52.5(4)
C(7)-C(6)-C(5)#4	124.7(4)
C(2)-C(7)-C(6)	114.5(5)
N(1)-C(8)-C(5)#4	98.7(4)
N(1)-C(8)-K(1)#1	117.4(3)
C(5)#4-C(8)-K(1)#1	93.1(2)
C(9)-N(2)-C(16)	147.8(5)
C(9)-N(2)-K(1)	76.70(15)
C(16)-N(2)-K(1)	110.7(2)
C(10)-C(9)-N(2)	112.5(3)
C(10)-C(9)-K(1)	78.64(15)
N(2)-C(9)-K(1)	77.99(16)
C(11)-C(10)-C(9)	117.5(3)
C(11)-C(10)-K(1)	81.59(16)
C(9)-C(10)-K(1)	76.33(15)
C(15)-C(11)-C(10)	126.8(7)
C(15)-C(11)-C(12)	19.4(9)
C(10)-C(11)-C(12)	107.4(5)

C(15)-C(11)-K(1)	83.0(6)
C(10)-C(11)-K(1)	74.01(15)
C(12)-C(11)-K(1)	76.3(4)
C(13)#2-C(12)-C(13)	70.6(18)
C(13)#2-C(12)-C(11)	116(2)
C(13)-C(12)-C(11)	173.8(13)
C(13)#2-C(12)-C(12)#2	48.4(14)
C(13)-C(12)-C(12)#2	22.2(5)
C(11)-C(12)-C(12)#2	164.0(14)
C(13)#2-C(12)-K(1)	77.5(12)
C(13)-C(12)-K(1)	108.2(6)
C(11)-C(12)-K(1)	74.1(4)
C(12)#2-C(12)-K(1)	99.3(7)
C(12)#2-C(13)-C(14)#2	146(3)
C(12)#2-C(13)-C(13)#2	79.6(16)
C(14)#2-C(13)-C(13)#2	134.8(19)
C(12)#2-C(13)-C(12)	109.4(18)
C(14)#2-C(13)-C(12)	105.0(15)
C(13)#2-C(13)-C(12)	29.8(6)
C(12)#2-C(13)-K(1)#2	89.2(12)
C(14)#2-C(13)-K(1)#2	77.3(5)
C(13)#2-C(13)-K(1)#2	114.1(6)
C(12)-C(13)-K(1)#2	113.5(5)
C(11)-C(15)-C(16)#2	147.7(11)
C(11)-C(15)-K(1)	76.6(6)
C(16)#2-C(15)-K(1)	117.7(6)
C(15)#2-C(16)-N(2)	119.0(5)
C(17)#1-O(1)-C(17)	109.2(2)
C(17)#1-O(1)-K(1)	111.81(11)
C(17)-O(1)-K(1)	108.31(11)
C(17)#1-O(1)-K(1)#1	108.31(11)
C(17)-O(1)-K(1)#1	111.81(11)
K(1)-O(1)-K(1)#1	107.40(7)
O(1)-C(17)-C(18)	105.8(2)

O(1)-C(17)-K(1)	48.52(9)
C(18)-C(17)-K(1)	121.2(2)
C(18)#1-C(18)-C(17)	108.64(17)

Symmetry transformations used to generate equivalent atoms:

#1 -x+1,y,-z+1/2 #2 -x+1/2,-y+1/2,-z #3 x,-y,z-1/2

#4 -x+1,-y,-z

X-Ray diffraction data for $\{(C_{11}H_8N)K(TMEDA)\}_n$, **(20)**.

The complex $\{(C_{11}H_8N)K(TMEDA)\}_n$, **(20)**, crystallised as red prisms from TMEDA at – 4 °C over two days in the triclinic space group P$\bar{1}$ (No. 2). Complex **(20)** has a polymeric structure with eight molecules in the unit cell and the asymmetric unit comprising of four molecules, as shown in Figure 27. The complex consists of a two crystallographically independent, though similar, linear zigzag polymeric strands where planar heterocyclic anions alternate with TMEDA coordinated potassium cations, (a = 10.1459(2), b = 17.4901(4), c = 20.997(5) Å, α = 77.0870(10), β = 82.899(2), γ = 82.0080(10) °). The crystals were isolated and mounted in a sealed thin-walled glass capillary under an argon atmosphere and the data collected at –100 °C. The diffraction data was collected by Dr. P. B. Hitchcock at the School of Chemistry, University of Sussex, United Kingdom.

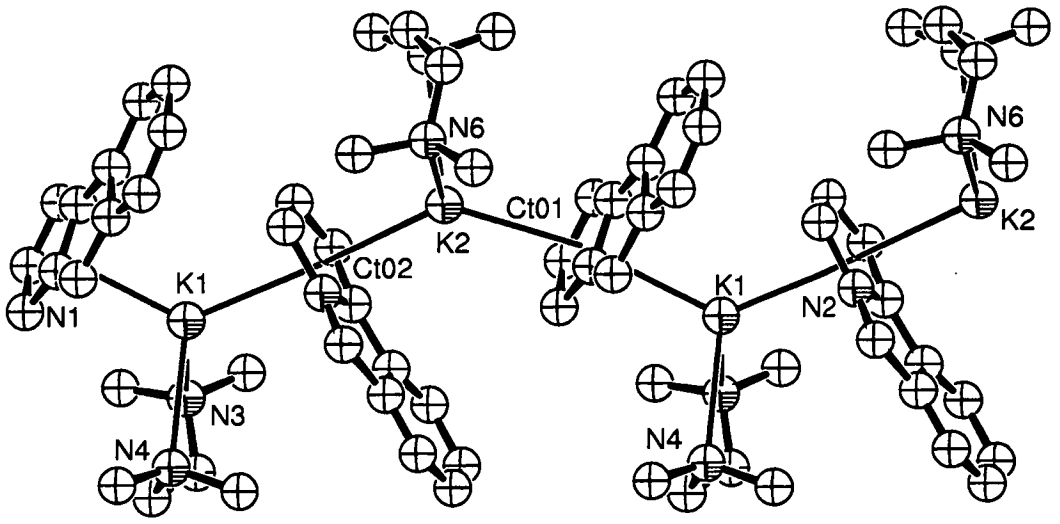

Figure 4: Molecular structure of $[(C_{11}H_8N)K(TMEDA)]_n$, **(20)**, Thermal ellipsoids are drawn at the level of 50% probability, hydrogens have been removed for clarity.

Table 5. Atomic coordinates (x 10^4) and equivalent isotropic displacement parameters ($Å^2$ x 10^3) for $[(C_{11}H_8N)K(TMEDA)]_n$, **(20)**.

	x	y	z	*U(eq)
K(1)	6717(1)	11550(1)	-3846(1)	47(1)
K(2)	1705(1)	10486(1)	-2784(1)	48(1)
N(1)	4579(4)	10592(3)	-3375(2)	73(1)
N(2)	-473(4)	10810(2)	-3602(2)	75(1)
N(3)	6261(3)	13132(2)	-4569(2)	49(1)
N(4)	6771(3)	11701(2)	-5227(2)	55(1)
N(5)	1118(3)	10133(2)	-1383(2)	49(1)
N(6)	1901(3)	8848(2)	-2180(2)	50(1)
C(1)	3793(4)	11272(3)	-3751(2)	69(1)
C(2)	3525(4)	11785(3)	-3316(2)	66(1)
C(3)	4071(5)	11460(3)	-2726(2)	63(1)
C(4)	4734(4)	10720(3)	-2753(2)	53(1)
C(5)	5530(4)	10057(2)	-2408(2)	54(1)
C(6)	6006(4)	9861(3)	-1787(2)	63(1)
C(7)	6795(4)	9158(3)	-1626(2)	66(1)
C(8)	7050(5)	8686(3)	-2077(3)	72(1)
C(9)	6672(6)	8845(4)	-2662(4)	89(2)
C(10)	5877(4)	9525(3)	-2876(3)	77(2)
C(11)	5278(6)	9903(4)	-3454(3)	81(2)
C(12)	-1263(4)	10590(3)	-2977(2)	68(1)
C(13)	-1448(5)	11280(3)	-2746(2)	68(1)
C(14)	-851(5)	11886(3)	-3169(2)	68(1)
C(15)	-228(4)	11604(2)	-3705(2)	56(1)
C(16)	594(4)	11798(3)	-4317(2)	60(1)
C(17)	1127(5)	12478(3)	-4654(3)	76(1)
C(18)	1909(5)	12449(4)	-5231(3)	87(2)
C(19)	2097(5)	11739(5)	-5441(3)	87(2)
C(20)	1622(6)	11094(5)	-5121(4)	99(2)
C(21)	871(5)	11061(4)	-4563(3)	87(2)
C(22)	179(5)	10498(3)	-4088(3)	84(2)
C(23)	6654(4)	13136(2)	-5270(2)	58(1)
C(24)	6160(4)	12491(3)	-5509(2)	59(1)
C(25)	7134(5)	13586(3)	-4333(3)	74(1)

C(26)	4866(4)	13457(3)	-4466(3)	69(1)
C(27)	8176(4)	11572(3)	-5458(3)	76(1)
C(28)	6055(5)	11111(3)	-5393(3)	76(1)
C(29)	1086(5)	9280(3)	-1138(2)	68(1)
C(30)	2042(5)	8758(3)	-1479(2)	65(1)
C(31)	-138(5)	10549(3)	-1152(2)	69(1)
C(32)	2233(5)	10403(3)	-1157(3)	78(1)
C(33)	3045(5)	8370(3)	-2446(3)	85(2)
C(34)	685(5)	8589(3)	-2306(3)	82(2)
K(3)	4462(1)	6537(1)	1151(1)	50(1)
K(4)	9426(1)	5517(1)	2217(1)	48(1)
N(7)	6839(4)	5604(3)	1621(2)	74(1)
N(8)	11819(4)	5800(3)	1359(3)	89(2)
N(9)	4476(3)	8134(2)	450(2)	46(1)
N(10)	5001(3)	6726(2)	-229(2)	50(1)
N(11)	9939(4)	3882(2)	2772(2)	62(1)
N(12)	9439(3)	5143(2)	3609(2)	52(1)
C(35)	7470(4)	6266(3)	1238(2)	62(1)
C(36)	7267(5)	6789(3)	1662(2)	68(1)
C(37)	6574(5)	6493(3)	2264(3)	71(1)
C(38)	6308(4)	5770(3)	2233(2)	55(1)
C(39)	5638(4)	5081(3)	2587(2)	62(1)
C(40)	4943(5)	4898(3)	3217(3)	75(1)
C(41)	4389(5)	4179(3)	3405(3)	71(1)
C(42)	4594(5)	3702(3)	2951(3)	70(1)
C(43)	5232(5)	3878(3)	2347(3)	81(2)
C(44)	5793(4)	4562(3)	2135(3)	74(1)
C(45)	6511(5)	4917(3)	1548(3)	75(1)
C(46)	12427(4)	5592(3)	2007(3)	90(2)
C(47)	12153(5)	6303(3)	2224(2)	69(1)
C(48)	11498(4)	6891(3)	1791(2)	68(1)
C(49)	11272(4)	6601(2)	1253(2)	58(1)
C(50)	10658(4)	6801(2)	650(2)	56(1)
C(51)	9982(5)	7484(3)	302(3)	68(1)
C(52)	9529(5)	7436(4)	-266(3)	88(2)
C(53)	9772(7)	6720(6)	-458(3)	98(2)
C(54)	10343(8)	6108(6)	-146(5)	114(3)
C(55)	10812(5)	6103(4)	391(3)	86(2)
C(56)	11519(6)	5488(3)	849(5)	111(3)

C(57)	4366(4)	8161(2)	-245(2)	50(1)
C(58)	5300(4)	7534(2)	-516(2)	52(1)
C(59)	3283(5)	8588(3)	718(2)	68(1)
C(60)	5665(5)	8465(3)	535(2)	67(1)
C(61)	3752(4)	6584(3)	-437(3)	68(1)
C(62)	6086(5)	6170(3)	-436(3)	72(1)
C(63)	9405(6)	4293(3)	3834(2)	79(1)
C(64)	10265(6)	3797(3)	3442(3)	82(2)
C(65)	8210(5)	5549(4)	3886(3)	85(2)
C(66)	10594(5)	5403(3)	3808(2)	74(1)
C(67)	11077(6)	3475(4)	2419(4)	102(2)
C(68)	8736(6)	3555(4)	2719(4)	106(2)

* U(eq) is defined as one third of the trace of the orthogonalized U^{ij} tensor.

Table 6. Anisotropic displacement parameters ($Å^2 x\ 10^3$) for $[(C_{11}H_8N)K(TMEDA)]_n$, **(20)**.

	U^{11}	U^{22}	U^{33}	U^{23}	U^{13}	U^{12}
K(1)	38(1)	54(1)	48(1)	-2(1)	-11(1)	-10(1)
K(2)	38(1)	56(1)	47(1)	1(1)	-8(1)	-12(1)
N(1)	56(2)	98(3)	70(2)	-26(2)	12(2)	-35(2)
N(2)	58(2)	75(3)	99(3)	-27(2)	-36(2)	9(2)
N(3)	43(2)	48(2)	57(2)	-11(1)	-5(1)	-10(1)
N(4)	54(2)	64(2)	51(2)	-22(2)	-14(2)	1(2)
N(5)	46(2)	51(2)	46(2)	-11(1)	-3(1)	2(1)
N(6)	49(2)	50(2)	52(2)	-14(1)	0(1)	-9(1)
C(1)	43(2)	109(4)	49(2)	14(2)	-13(2)	-31(2)
C(2)	57(3)	61(3)	69(3)	4(2)	3(2)	-11(2)
C(3)	65(3)	67(3)	59(3)	-11(2)	3(2)	-24(2)
C(4)	43(2)	79(3)	42(2)	-12(2)	-1(2)	-26(2)
C(5)	38(2)	57(2)	67(3)	-18(2)	9(2)	-17(2)
C(6)	47(2)	61(3)	83(3)	-19(2)	12(2)	-17(2)
C(7)	50(2)	72(3)	67(3)	9(2)	-8(2)	-12(2)
C(8)	54(3)	63(3)	90(4)	-2(3)	8(2)	-10(2)
C(9)	72(3)	81(4)	114(5)	-25(3)	12(3)	-22(3)
C(10)	42(2)	55(3)	134(5)	-30(3)	29(3)	-20(2)
C(11)	70(3)	114(5)	69(3)	-25(3)	-3(3)	-39(3)
C(12)	40(2)	73(3)	80(3)	27(2)	-23(2)	-19(2)
C(13)	57(3)	90(4)	55(3)	-9(2)	-19(2)	4(2)
C(14)	71(3)	63(3)	77(3)	-18(2)	-31(2)	-1(2)
C(15)	48(2)	39(2)	82(3)	-1(2)	-32(2)	-6(2)
C(16)	46(2)	68(3)	69(3)	-17(2)	-24(2)	5(2)
C(17)	58(3)	90(4)	83(3)	-20(3)	-31(3)	8(2)
C(18)	59(3)	107(4)	80(4)	23(3)	-20(3)	-21(3)
C(19)	55(3)	144(6)	54(3)	-15(3)	-10(2)	9(3)
C(20)	75(4)	124(5)	102(5)	-35(4)	-36(4)	13(4)
C(21)	45(2)	143(5)	82(3)	-61(4)	-31(2)	37(3)
C(22)	63(3)	77(3)	115(5)	-9(3)	-37(3)	-8(3)
C(23)	50(2)	56(2)	60(2)	4(2)	-4(2)	-11(2)
C(24)	51(2)	74(3)	50(2)	-11(2)	-11(2)	2(2)
C(25)	71(3)	59(3)	101(4)	-25(3)	-25(3)	-13(2)

C(26)	54(2)	61(3)	88(3)	-15(2)	4(2)	-6(2)
C(27)	51(3)	88(3)	96(4)	-43(3)	-18(2)	10(2)
C(28)	79(3)	87(3)	76(3)	-35(3)	-14(3)	-14(3)
C(29)	94(3)	55(2)	47(2)	-5(2)	3(2)	-3(2)
C(30)	81(3)	54(2)	59(3)	-6(2)	-16(2)	-3(2)
C(31)	59(3)	82(3)	62(3)	-22(2)	-1(2)	17(2)
C(32)	68(3)	96(4)	74(3)	-17(3)	-11(2)	-25(3)
C(33)	62(3)	89(4)	99(4)	-26(3)	10(3)	-3(3)
C(34)	66(3)	78(3)	111(4)	-25(3)	-29(3)	-12(2)
K(3)	35(1)	56(1)	51(1)	1(1)	-2(1)	-2(1)
K(4)	34(1)	56(1)	49(1)	-2(1)	-5(1)	-1(1)
N(7)	53(2)	82(3)	89(3)	-25(2)	-31(2)	14(2)
N(8)	53(2)	54(2)	142(4)	-7(3)	31(3)	-6(2)
N(9)	43(2)	46(2)	49(2)	-12(1)	-6(1)	-2(1)
N(10)	47(2)	48(2)	55(2)	-18(1)	8(1)	-5(1)
N(11)	63(2)	48(2)	81(2)	-20(2)	-29(2)	5(2)
N(12)	49(2)	58(2)	50(2)	-11(2)	-5(1)	-10(1)
C(35)	38(2)	78(3)	57(2)	11(2)	-6(2)	-6(2)
C(36)	59(3)	67(3)	69(3)	2(2)	-16(2)	4(2)
C(37)	64(3)	77(3)	71(3)	-20(2)	-16(2)	12(2)
C(38)	36(2)	80(3)	53(2)	-29(2)	-11(2)	12(2)
C(39)	42(2)	62(2)	79(3)	-2(2)	-23(2)	1(2)
C(40)	56(3)	66(3)	109(4)	-23(3)	-39(3)	10(2)
C(41)	51(2)	83(3)	73(3)	0(3)	-16(2)	-1(2)
C(42)	53(3)	59(3)	93(4)	7(2)	-24(2)	-7(2)
C(43)	65(3)	76(3)	94(4)	-2(3)	-19(3)	10(2)
C(44)	47(2)	59(3)	116(4)	-10(3)	-37(3)	4(2)
C(45)	55(3)	85(3)	83(3)	-16(3)	-13(2)	0(2)
C(46)	24(2)	84(4)	123(4)	57(3)	-4(2)	0(2)
C(47)	60(3)	83(3)	59(3)	1(2)	-1(2)	-23(2)
C(48)	54(2)	62(3)	78(3)	-7(2)	15(2)	-7(2)
C(49)	36(2)	46(2)	77(3)	6(2)	10(2)	0(2)
C(50)	43(2)	52(2)	72(3)	-18(2)	15(2)	-15(2)
C(51)	54(2)	70(3)	80(3)	-18(2)	8(2)	-23(2)
C(52)	64(3)	99(4)	85(4)	27(3)	-9(3)	-27(3)
C(53)	90(4)	163(7)	55(3)	-25(4)	10(3)	-76(5)
C(54)	100(5)	130(6)	124(7)	-53(5)	45(5)	-58(5)
C(55)	64(3)	113(5)	103(4)	-72(4)	43(3)	-53(3)
C(56)	62(3)	51(3)	202(8)	-27(4)	57(4)	-7(3)

C(57)	52(2)	43(2)	54(2)	-4(2)	-13(2)	-4(2)
C(58)	49(2)	58(2)	49(2)	-10(2)	3(2)	-12(2)
C(59)	61(3)	64(3)	79(3)	-27(2)	5(2)	4(2)
C(60)	61(3)	63(3)	80(3)	-19(2)	-22(2)	-5(2)
C(61)	55(2)	70(3)	84(3)	-28(2)	6(2)	-17(2)
C(62)	64(3)	65(3)	87(3)	-31(2)	5(2)	7(2)
C(63)	100(4)	72(3)	60(3)	5(2)	-2(3)	-25(3)
C(64)	99(4)	52(3)	92(4)	1(2)	-39(3)	-2(2)
C(65)	57(3)	127(5)	73(3)	-38(3)	-4(2)	4(3)
C(66)	63(3)	102(4)	63(3)	-14(3)	-7(2)	-34(3)
C(67)	78(4)	82(4)	151(6)	-47(4)	-13(4)	9(3)
C(68)	68(3)	79(4)	182(7)	-30(4)	-56(4)	-2(3)

The anisotropic displacement factor exponent takes the form: $-2\pi^2[h^2a^{*2}U^{11} + ... + 2 h k a^* b^* U^{12}]$

Table 7. Hydrogen coordinates (x 10^4) and isotropic displacement parameters ($Å^2$x 10^3) for $[(C_{11}H_8N)K(TMEDA)]_n$, **(20)**.

	x	y	z	U(eq)
H(1)	3532	11345	-4182	83
H(2)	3031	12293	-3412	79
H(3)	4001	11708	-2362	76
H(6)	5788	10204	-1487	76
H(7)	7155	9002	-1214	79
H(8)	7559	8189	-1945	87
H(9)	6951	8486	-2944	107
H(11)	5357	9699	-3843	98
H(12)	-1574	10096	-2777	82
H(13)	-1934	11332	-2338	82
H(14)	-868	12407	-3102	82
H(17)	956	12951	-4491	91
H(18)	2308	12898	-5478	104
H(19)	2612	11724	-5848	104
H(20)	1824	10631	-5297	118
H(22)	184	9963	-4117	101
H(23A)	7642	13086	-5346	69
H(23B)	6307	13652	-5534	69
H(24A)	5179	12515	-5401	71
H(24B)	6340	12586	-5992	71
H(25A)	8066	13359	-4403	111
H(25B)	6893	13567	-3864	111
H(25C)	7028	14136	-4575	111
H(26A)	4294	13147	-4625	103
H(26B)	4747	14007	-4707	103
H(26C)	4621	13436	-3997	103
H(27A)	8545	11037	-5255	113
H(27B)	8661	11959	-5339	113
H(27C)	8269	11632	-5936	113
H(28A)	5107	11195	-5235	115
H(28B)	6434	10581	-5185	115
H(28C)	6144	11163	-5870	115
H(29A)	174	9156	-1162	81
H(29B)	1251	9153	-669	81

H(30A)	2959	8855	-1431	78
H(30B)	1941	8203	-1257	78
H(31A)	-888	10368	-1309	104
H(31B)	-135	11118	-1322	104
H(31C)	-235	10439	-671	104
H(32A)	3074	10123	-1313	116
H(32B)	2143	10296	-676	116
H(32C)	2236	10972	-1329	116
H(33A)	3876	8538	-2360	127
H(33B)	3018	8438	-2920	127
H(33C)	3009	7812	-2235	127
H(34A)	-89	8907	-2131	123
H(34B)	657	8032	-2094	123
H(34C)	662	8653	-2781	123
H(35)	7912	6330	807	74
H(36)	7570	7296	1552	81
H(37)	6338	6750	2622	85
H(40)	4852	5252	3507	90
H(41)	3900	4029	3820	86
H(42)	4254	3205	3077	85
H(43)	5292	3519	2063	98
H(45)	6725	4702	1166	90
H(46)	12879	5103	2214	109
H(47)	12397	6370	2629	83
H(48)	11237	7417	1848	81
H(51)	9846	7963	456	81
H(52)	9057	7881	-525	106
H(53)	9475	6698	-864	117
H(54)	10433	5635	-307	137
H(56)	11742	4955	807	133
H(57A)	4558	8687	-504	60
H(57B)	3435	8097	-300	60
H(58A)	5259	7635	-997	63
H(58B)	6226	7581	-438	63
H(59A)	2478	8367	662	102
H(59B)	3240	9141	484	102
H(59C)	3338	8557	1186	102
H(60A)	5716	8435	1003	100
H(60B)	5620	9018	301	100

H(60C)	6462	8164	359	100
H(61A)	3565	6043	-237	101
H(61B)	3831	6657	-916	101
H(61C)	3020	6958	-297	101
H(62A)	5887	5629	-244	108
H(62B)	6921	6255	-286	108
H(62C)	6180	6251	-915	108
H(63A)	9659	4140	4290	95
H(63B)	8472	4179	3846	95
H(64A)	10232	3239	3670	98
H(64B)	11196	3915	3427	98
H(65A)	7431	5374	3750	127
H(65B)	8201	6121	3726	127
H(65C)	8177	5424	4366	127
H(66A)	11414	5132	3624	112
H(66B)	10562	5280	4289	112
H(66C)	10584	5975	3647	112
H(67A)	11901	3692	2451	153
H(67B)	10919	3554	1956	153
H(67C)	11165	2909	2616	153
H(68A)	8585	3636	2255	159
H(68B)	7974	3818	2953	159
H(68C)	8834	2988	2912	159

Table 8. Bond lengths [Å] and angles [°] for $[(C_{11}H_8N)K(TMEDA)]_n$, **(20)**.

K(1)-N(4)	2.847(3)
K(1)-N(3)	2.850(3)
K(1)-N(1)	2.868(4)
K(1)-C(12)'	2.991(4)
K(1)-N(2)'	3.018(4)
K(1)-C(1)	3.047(4)
K(1)-C(13)'	3.059(4)
K(1)-C(4)	3.099(4)
K(1)-C(15)'	3.167(4)
K(1)-C(14)'	3.178(4)
K(1)-C(2)	3.292(5)
K(1)-C(11)	3.305(6)
K(1)-C(3)	3.339(4)
K(2)-N(6)	2.852(3)
K(2)-N(5)	2.871(3)
K(2)-N(2)	2.882(4)
K(2)-C(1)	3.001(4)
K(2)-N(1)	3.039(4)
K(2)-C(2)	3.058(4)
K(2)-C(12)	3.062(4)
K(2)-C(15)	3.097(4)
K(2)-C(3)	3.161(4)
K(2)-C(4)	3.167(4)
K(2)-C(22)	3.303(6)
K(2)-C(13)	3.304(5)
K(2)-C(14)	3.353(5)
N(1)-C(11)	1.344(7)
N(1)-C(4)	1.405(5)
N(1)-C(1)	1.465(7)
N(2)-C(22)	1.326(8)
N(2)-C(15)	1.410(6)
N(2)-C(12)	1.454(7)
N(3)-C(26)	1.459(5)
N(3)-C(25)	1.463(5)
N(3)-C(23)	1.475(5)
N(4)-C(27)	1.451(6)

N(4)-C(24)	1.460(5)
N(4)-C(28)	1.465(6)
N(5)-C(32)	1.453(6)
N(5)-C(31)	1.461(5)
N(5)-C(29)	1.469(5)
N(6)-C(34)	1.446(6)
N(6)-C(33)	1.462(6)
N(6)-C(30)	1.468(5)
C(1)-C(2)	1.396(7)
C(2)-C(3)	1.392(7)
C(3)-C(4)	1.383(6)
C(4)-C(5)	1.425(6)
C(5)-C(6)	1.400(7)
C(5)-C(10)	1.480(6)
C(6)-C(7)	1.369(6)
C(7)-C(8)	1.368(7)
C(8)-C(9)	1.292(8)
C(9)-C(10)	1.360(8)
C(10)-C(11)	1.413(8)
C(12)-C(13)	1.379(7)
C(13)-C(14)	1.380(7)
C(14)-C(15)	1.377(7)
C(15)-C(16)	1.442(7)
C(16)-C(17)	1.385(7)
C(16)-C(21)	1.473(7)
C(17)-C(18)	1.369(8)
C(18)-C(19)	1.390(9)
C(19)-C(20)	1.300(9)
C(20)-C(21)	1.311(9)
C(21)-C(22)	1.429(9)
C(23)-C(24)	1.498(6)
C(29)-C(30)	1.470(6)
K(3)-N(10)	2.836(3)
K(3)-N(9)	2.852(3)
K(3)-N(7)	2.868(4)
K(3)-C(46)"	2.988(4)
K(3)-C(35)	3.045(4)
K(3)-C(47)"	3.046(5)
K(3)-N(8)"	3.076(4)

K(3)-C(38)	3.076(4)
K(3)-C(48)"	3.176(4)
K(3)-C(49)"	3.205(4)
K(3)-C(36)	3.280(5)
K(3)-C(45)	3.283(5)
K(3)-C(37)	3.342(5)
K(4)-N(11)	2.838(4)
K(4)-N(12)	2.851(3)
K(4)-N(8)	2.870(4)
K(4)-C(35)	2.994(4)
K(4)-N(7)	3.016(4)
K(4)-C(36)	3.037(4)
K(4)-C(46)	3.039(4)
K(4)-C(49)	3.087(4)
K(4)-C(38)	3.130(4)
K(4)-C(37)	3.151(5)
K(4)-C(47)	3.260(5)
K(4)-C(48)	3.313(5)
K(4)-C(56)	3.360(7)
N(7)-C(45)	1.335(7)
N(7)-C(38)	1.407(6)
N(7)-C(35)	1.435(6)
N(8)-C(56)	1.388(10)
N(8)-C(49)	1.412(6)
N(8)-C(46)	1.513(8)
N(9)-C(60)	1.455(5)
N(9)-C(57)	1.468(5)
N(9)-C(59)	1.475(5)
N(10)-C(62)	1.455(5)
N(10)-C(61)	1.459(6)
N(10)-C(58)	1.466(5)
N(11)-C(68)	1.444(6)
N(11)-C(64)	1.457(6)
N(11)-C(67)	1.478(7)
N(12)-C(66)	1.452(5)
N(12)-C(63)	1.459(6)
N(12)-C(65)	1.469(6)
C(35)-C(36)	1.391(7)
C(36)-C(37)	1.396(7)

C(37)-C(38)	1.345(7)
C(38)-C(39)	1.474(6)
C(39)-C(40)	1.411(7)
C(39)-C(44)	1.434(7)
C(40)-C(41)	1.405(7)
C(41)-C(42)	1.381(7)
C(42)-C(43)	1.341(8)
C(43)-C(44)	1.357(7)
C(44)-C(45)	1.413(8)
C(46)-C(47)	1.400(8)
C(47)-C(48)	1.367(7)
C(48)-C(49)	1.393(7)
C(49)-C(50)	1.431(7)
C(50)-C(51)	1.392(7)
C(50)-C(55)	1.426(6)
C(51)-C(52)	1.354(8)
C(52)-C(53)	1.380(10)
C(53)-C(54)	1.233(10)
C(54)-C(55)	1.275(11)
C(55)-C(56)	1.446(10)
C(57)-C(58)	1.509(5)
C(63)-C(64)	1.456(8)

N(4)-K(1)-N(3)	65.31(10)
N(4)-K(1)-N(1)	101.25(11)
N(3)-K(1)-N(1)	122.01(12)
N(4)-K(1)-N(2)'	101.58(12)
N(3)-K(1)-N(2)'	120.04(11)
N(1)-K(1)-N(2)'	117.90(14)
N(6)-K(2)-N(5)	64.54(9)
N(6)-K(2)-N(2)	107.53(11)
N(5)-K(2)-N(2)	118.99(12)
N(6)-K(2)-N(1)	99.35(12)
N(5)-K(2)-N(1)	119.72(11)
N(2)-K(2)-N(1)	121.22(13)
C(11)-N(1)-C(4)	109.5(5)
C(11)-N(1)-C(1)	139.7(5)
C(4)-N(1)-C(1)	110.6(4)
C(11)-N(1)-K(1)	96.6(3)

C(4)-N(1)-K(1)	85.8(2)
C(1)-N(1)-K(1)	82.6(2)
C(11)-N(1)-K(2)	115.2(3)
C(4)-N(1)-K(2)	82.1(2)
C(1)-N(1)-K(2)	74.5(2)
K(1)-N(1)-K(2)	148.16(18)
C(22)-N(2)-C(15)	108.8(5)
C(22)-N(2)-C(12)	141.1(5)
C(15)-N(2)-C(12)	109.9(4)
C(22)-N(2)-K(2)	96.3(3)
C(15)-N(2)-K(2)	85.0(2)
C(12)-N(2)-K(2)	82.8(2)
C(22)-N(2)-K(1)"	114.3(3)
C(15)-N(2)-K(1)"	82.8(2)
C(12)-N(2)-K(1)"	75.0(2)
K(2)-N(2)-K(1)"	149.23(18)
C(26)-N(3)-C(25)	110.4(3)
C(26)-N(3)-C(23)	110.9(3)
C(25)-N(3)-C(23)	109.6(3)
C(26)-N(3)-K(1)	111.3(2)
C(25)-N(3)-K(1)	106.3(3)
C(23)-N(3)-K(1)	108.3(2)
C(27)-N(4)-C(24)	112.3(4)
C(27)-N(4)-C(28)	109.3(4)
C(24)-N(4)-C(28)	109.4(3)
C(27)-N(4)-K(1)	105.2(3)
C(24)-N(4)-K(1)	108.6(2)
C(28)-N(4)-K(1)	112.1(3)
C(32)-N(5)-C(31)	109.7(4)
C(32)-N(5)-C(29)	111.0(4)
C(31)-N(5)-C(29)	108.9(4)
C(32)-N(5)-K(2)	102.7(3)
C(31)-N(5)-K(2)	113.9(2)
C(29)-N(5)-K(2)	110.5(2)
C(34)-N(6)-C(33)	108.8(4)
C(34)-N(6)-C(30)	113.5(4)
C(33)-N(6)-C(30)	106.8(4)
C(34)-N(6)-K(2)	104.5(3)
C(33)-N(6)-K(2)	114.4(3)

C(30)-N(6)-K(2)	108.9(2)
C(2)-C(1)-N(1)	102.4(4)
C(3)-C(2)-C(1)	111.6(4)
C(4)-C(3)-C(2)	109.2(4)
C(3)-C(4)-N(1)	106.1(4)
C(3)-C(4)-C(5)	144.7(4)
N(1)-C(4)-C(5)	109.2(4)
C(6)-C(5)-C(4)	134.4(4)
C(6)-C(5)-C(10)	121.1(4)
C(4)-C(5)-C(10)	104.5(4)
C(7)-C(6)-C(5)	117.8(4)
C(8)-C(7)-C(6)	118.0(5)
C(9)-C(8)-C(7)	126.9(5)
C(8)-C(9)-C(10)	120.3(6)
C(9)-C(10)-C(11)	137.3(6)
C(9)-C(10)-C(5)	115.8(6)
C(11)-C(10)-C(5)	106.8(4)
N(1)-C(11)-C(10)	110.0(5)
C(13)-C(12)-N(2)	102.5(4)
C(12)-C(13)-C(14)	112.9(4)
C(15)-C(14)-C(13)	108.1(4)
C(14)-C(15)-N(2)	106.6(4)
C(14)-C(15)-C(16)	144.6(4)
N(2)-C(15)-C(16)	108.8(4)
C(17)-C(16)-C(15)	133.6(4)
C(17)-C(16)-C(21)	121.2(5)
C(15)-C(16)-C(21)	105.2(4)
C(18)-C(17)-C(16)	118.0(5)
C(17)-C(18)-C(19)	117.5(5)
C(20)-C(19)-C(18)	124.9(6)
C(19)-C(20)-C(21)	122.0(7)
C(20)-C(21)-C(22)	138.5(7)
C(20)-C(21)-C(16)	116.3(7)
C(22)-C(21)-C(16)	105.2(5)
N(2)-C(22)-C(21)	112.0(5)
N(3)-C(23)-C(24)	114.1(3)
N(4)-C(24)-C(23)	113.7(3)
N(5)-C(29)-C(30)	116.5(4)
N(6)-C(30)-C(29)	115.3(4)

N(10)-K(3)-N(9)	65.25(9)
N(10)-K(3)-N(7)	102.50(11)
N(9)-K(3)-N(7)	121.91(12)
N(10)-K(3)-N(8)"	100.08(14)
N(9)-K(3)-N(8)"	118.16(11)
N(7)-K(3)-N(8)"	119.90(13)
N(11)-K(4)-N(12)	65.27(10)
N(11)-K(4)-N(8)	101.80(12)
N(12)-K(4)-N(8)	121.83(15)
N(11)-K(4)-N(7)	102.31(11)
N(12)-K(4)-N(7)	119.40(11)
N(8)-K(4)-N(7)	118.77(16)
C(45)-N(7)-C(38)	111.5(5)
C(45)-N(7)-C(35)	138.9(5)
C(38)-N(7)-C(35)	109.3(4)
C(45)-N(7)-K(3)	95.8(3)
C(38)-N(7)-K(3)	84.7(2)
C(35)-N(7)-K(3)	82.9(2)
C(45)-N(7)-K(4)	115.7(3)
C(38)-N(7)-K(4)	81.3(2)
C(35)-N(7)-K(4)	75.3(2)
K(3)-N(7)-K(4)	148.45(17)
C(56)-N(8)-C(49)	107.8(5)
C(56)-N(8)-C(46)	143.6(5)
C(49)-N(8)-C(46)	108.4(5)
C(56)-N(8)-K(4)	98.1(3)
C(49)-N(8)-K(4)	85.1(2)
C(46)-N(8)-K(4)	81.5(2)
C(56)-N(8)-K(3)'	116.5(3)
C(49)-N(8)-K(3)'	82.2(2)
C(46)-N(8)-K(3)'	72.4(2)
K(4)-N(8)-K(3)'	145.3(2)
C(60)-N(9)-C(57)	111.3(3)
C(60)-N(9)-C(59)	109.1(3)
C(57)-N(9)-C(59)	109.2(3)
C(60)-N(9)-K(3)	111.8(2)
C(57)-N(9)-K(3)	108.5(2)
C(59)-N(9)-K(3)	106.8(2)
C(62)-N(10)-C(61)	109.4(3)

C(62)-N(10)-C(58)	109.4(3)
C(61)-N(10)-C(58)	110.8(3)
C(62)-N(10)-K(3)	114.1(3)
C(61)-N(10)-K(3)	103.5(2)
C(58)-N(10)-K(3)	109.5(2)
C(68)-N(11)-C(64)	114.4(5)
C(68)-N(11)-C(67)	108.6(4)
C(64)-N(11)-C(67)	107.4(4)
C(68)-N(11)-K(4)	104.9(3)
C(64)-N(11)-K(4)	108.3(3)
C(67)-N(11)-K(4)	113.4(4)
C(66)-N(12)-C(63)	111.9(4)
C(66)-N(12)-C(65)	109.5(4)
C(63)-N(12)-C(65)	108.4(4)
C(66)-N(12)-K(4)	111.2(3)
C(63)-N(12)-K(4)	108.2(3)
C(65)-N(12)-K(4)	107.5(3)
C(36)-C(35)-N(7)	102.1(4)
C(35)-C(36)-C(37)	113.3(5)
C(38)-C(37)-C(36)	106.1(4)
C(37)-C(38)-N(7)	109.4(4)
C(37)-C(38)-C(39)	144.4(4)
N(7)-C(38)-C(39)	106.2(4)
C(40)-C(39)-C(44)	122.4(4)
C(40)-C(39)-C(38)	132.8(4)
C(44)-C(39)-C(38)	104.8(4)
C(41)-C(40)-C(39)	118.4(5)
C(42)-C(41)-C(40)	116.2(5)
C(43)-C(42)-C(41)	125.7(5)
C(42)-C(43)-C(44)	121.1(6)
C(43)-C(44)-C(45)	135.1(6)
C(43)-C(44)-C(39)	116.2(5)
C(45)-C(44)-C(39)	108.8(4)
N(7)-C(45)-C(44)	108.6(5)
C(47)-C(46)-N(8)	102.2(4)
C(48)-C(47)-C(46)	112.8(5)
C(47)-C(48)-C(49)	109.4(4)
C(48)-C(49)-N(8)	107.2(5)
C(48)-C(49)-C(50)	143.6(4)

N(8)-C(49)-C(50)	109.1(5)
C(51)-C(50)-C(55)	118.2(5)
C(51)-C(50)-C(49)	134.8(4)
C(55)-C(50)-C(49)	107.0(5)
C(52)-C(51)-C(50)	117.0(5)
C(51)-C(52)-C(53)	118.0(6)
C(54)-C(53)-C(52)	125.5(7)
C(53)-C(54)-C(55)	120.5(8)
C(54)-C(55)-C(50)	120.7(8)
C(54)-C(55)-C(56)	132.5(7)
C(50)-C(55)-C(56)	106.8(6)
N(8)-C(56)-C(55)	109.3(5)
N(9)-C(57)-C(58)	113.5(3)
N(10)-C(58)-C(57)	114.1(3)
C(64)-C(63)-N(12)	116.0(4)
C(63)-C(64)-N(11)	115.9(4)

Symmetry transformations used to generate equivalent atoms:
‘ x+1,y,z “ x-1,y,z

X-Ray diffraction data for $[(C_{11}H_8N)K(PMDETA)]$, **(21).**

Red needle shaped crystals of $[(C_{11}H_8N)K(PMDETA)]$, **(21)**, suitable for X-ray structure determination were grown from a heated PMDETA solution cooled slowly to ambient temperature over 2 days. The crystals were isolated and mounted in a sealed thin-walled glass capillary under an argon atmosphere. The crystals belong to the orthorhombic $P2_12_12_1$ space group, a = 10.3397(16), b = 11.4447(17), c = 17.755(3) Å, with four molecules in the unit cell, the asymmetric unit consisting of one molecule of $[(C_{11}H_8N)K(PMDETA)]$, **(21)**, as shown in Figure 5.

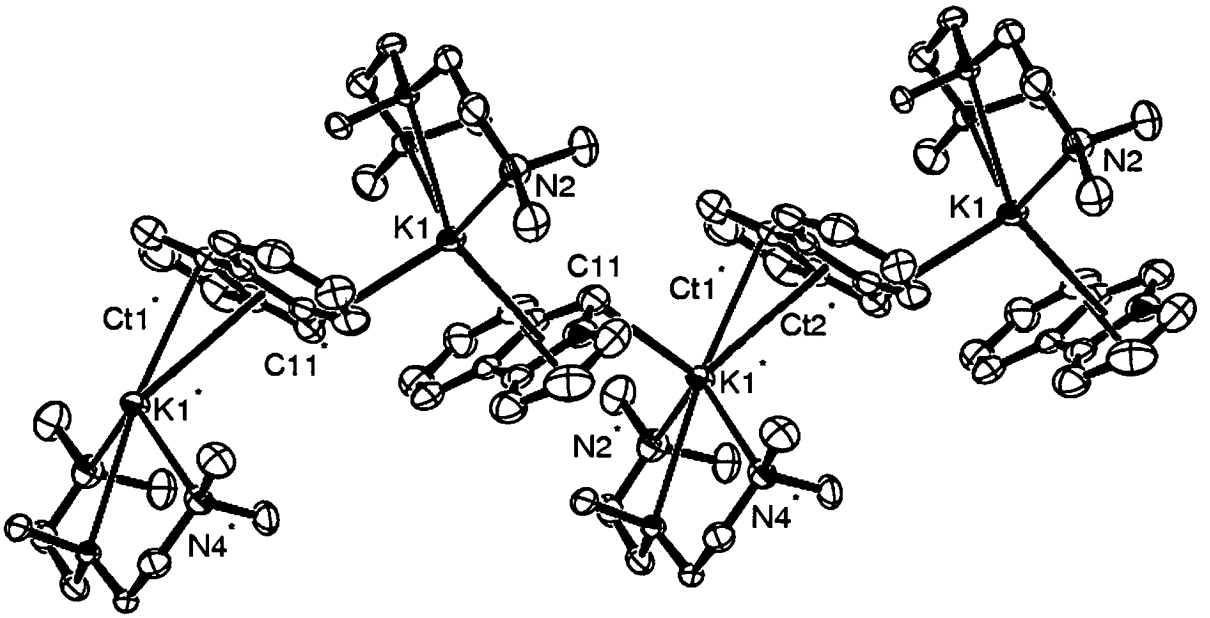

Figure 5: Molecular structure of $[(C_{11}H_8N)K(PMDETA)]_n$, **(21)**, thermal ellipsoids are drawn at the level of 50% probability, hydrogens have been removed for clarity.

Table 9. Atomic coordinates (x 10^4) and equivalent isotropic displacement parameters ($Å^2$x 10^3) for $[(C_{11}H_8N)K(PMDETA)]$, **(21)**.

	x	y	z	*U(eq)
K(1)	1550(1)	3202(1)	2250(1)	68(1)
N(1)	-145(6)	5357(6)	1894(5)	95(2)
C(1)	148(10)	5370(10)	1109(6)	103(3)
N(2)	3423(6)	3350(5)	1040(3)	76(2)
C(2)	-504(11)	4454(13)	826(7)	131(4)
N(3)	4160(4)	2391(4)	2509(3)	51(1)
C(3)	-1197(9)	3840(9)	1377(7)	101(3)
N(4)	2608(5)	3359(5)	3743(3)	65(2)
C(4)	-986(7)	4419(6)	2022(5)	69(2)
C(5)	-1200(6)	4454(6)	2818(6)	74(2)
C(6)	-1945(7)	3786(7)	3297(7)	92(3)
C(7)	-2079(9)	4119(9)	4049(7)	98(3)
C(8)	-1491(10)	5048(8)	4337(6)	97(3)
C(9)	-710(9)	5694(9)	3889(6)	104(3)
C(10)	-538(6)	5430(6)	3107(5)	67(2)
C(11)	140(8)	5993(7)	2503(6)	93(3)
C(12)	4557(7)	2602(6)	1146(5)	80(2)
C(13)	5088(6)	2641(6)	1924(4)	67(2)
C(14)	4698(6)	2598(5)	3257(4)	62(2)
C(15)	3680(7)	2584(7)	3880(4)	72(2)
C(16)	3757(9)	4595(6)	1160(5)	97(3)
C(17)	2839(9)	3180(8)	314(5)	103(3)
C(18)	3666(6)	1174(5)	2438(5)	77(2)
C(19)	1575(8)	3192(7)	4308(5)	97(2)
C(20)	3002(7)	4583(6)	3741(5)	82(2)

* U(eq) is defined as one third of the trace of the orthogonalized U_{ij} tensor.

Table 10. Anisotropic displacement parameters ($Å^2 x\ 10^3$) for $[(C_{11}H_8N)K(PMDETA)]$, **(21)**.

	U_{11}	U_{22}	U_{33}	U_{23}	U_{13}	U_{12}
K(1)	45(1)	62(1)	97(1)	0(1)	-9(1)	7(1)
N(1)	64(4)	67(4)	153(9)	-11(5)	-18(5)	20(4)
C(1)	104(7)	131(8)	73(7)	21(6)	30(6)	34(7)
N(2)	91(4)	80(4)	58(4)	1(3)	-3(3)	-6(4)
C(2)	98(8)	171(11)	123(10)	-40(9)	8(7)	24(8)
N(3)	38(2)	42(2)	72(4)	4(2)	-6(2)	0(2)
C(3)	80(6)	97(6)	127(9)	-10(7)	-1(6)	14(5)
N(4)	62(3)	61(4)	72(4)	1(3)	6(3)	5(3)
C(4)	54(4)	61(5)	94(7)	-15(5)	-18(4)	18(3)
C(5)	44(3)	48(4)	132(8)	5(5)	-15(4)	12(3)
C(6)	60(5)	80(5)	135(9)	11(6)	-17(5)	20(4)
C(7)	81(6)	108(7)	106(9)	19(6)	6(6)	-2(5)
C(8)	93(6)	113(7)	86(7)	22(6)	4(6)	-17(6)
C(9)	89(6)	123(8)	100(8)	-9(7)	-41(6)	19(6)
C(10)	48(4)	67(4)	86(6)	6(4)	-8(4)	13(3)
C(11)	65(5)	68(5)	145(9)	-7(6)	-3(5)	14(4)
C(12)	78(5)	61(4)	102(7)	-6(4)	10(5)	9(4)
C(13)	58(4)	61(4)	81(6)	-1(4)	10(4)	6(3)
C(14)	50(4)	49(3)	87(6)	-12(4)	-23(4)	7(3)
C(15)	73(5)	79(5)	64(5)	4(4)	-8(4)	0(4)
C(16)	125(7)	54(4)	111(7)	-2(4)	6(6)	-9(5)
C(17)	138(7)	105(6)	66(6)	3(5)	-12(5)	-11(6)
C(18)	58(4)	41(3)	132(7)	1(4)	-18(4)	-10(3)
C(19)	82(5)	110(6)	100(6)	13(6)	32(5)	-6(6)
C(20)	83(5)	50(4)	113(7)	-7(4)	14(4)	1(4)

The anisotropic displacement factor exponent takes the form: $-2\pi^2[\ h^2a^{*2}U^{11} + ... + 2\ h\ k\ a^*\ b^*\ U^{12}\ ]$

Table 11. Hydrogen coordinates (x 10^4) and isotropic displacement parameters ($Å^2$x 10^3) for [($C_{11}H_8N$)K(PMDETA)], **(21)**.

	x	y	z	U(eq)
H(1)	677	5901	848	123
H(2)	-496	4248	314	157
H(3)	-1702	3166	1309	122
H(6)	-2360	3110	3118	110
H(7)	-2609	3666	4366	118
H(8)	-1615	5255	4844	117
H(9)	-268	6335	4097	125
H(11)	667	6661	2529	111
H(12A)	5234	2844	793	96
H(12B)	4321	1794	1025	96
H(13A)	5797	2076	1962	80
H(13B)	5452	3419	2014	80
H(14A)	5136	3357	3260	74
H(14B)	5348	1997	3364	74
H(15A)	3350	1786	3935	87
H(15B)	4093	2803	4357	87
H(16A)	4397	4834	792	145
H(16B)	4106	4696	1663	145
H(16C)	2986	5070	1104	145
H(17A)	3397	3502	-72	154
H(17B)	2007	3572	300	154
H(17C)	2717	2351	225	154
H(18A)	3095	1121	2006	116
H(18B)	3194	965	2891	116
H(18C)	4388	642	2372	116
H(19A)	1358	2369	4340	146
H(19B)	815	3633	4159	146
H(19C)	1873	3465	4795	146
H(20A)	3455	4760	4206	123

H(20B)	2243	5076	3700	123
H(20C)	3571	4726	3317	123

Table 12. Bond lengths [Å] and angles [°] for $[(C_{11}H_8N)K(PMDETA)]$, **(21)**.

K(1)-N(4)	2.874(5)
K(1)-N(3)	2.890(5)
K(1)-N(2)	2.898(6)
K(1)-C(4)	2.997(6)
K(1)-N(1)	3.091(6)
K(1)-C(11)#1	3.104(8)
K(1)-C(3)	3.317(9)
K(1)-C(5)	3.340(7)
K(1)-C(10)#1	3.399(7)
K(1)-C(1)	3.517(10)
K(1)-C(11)	3.541(8)
N(1)-C(11)	1.336(11)
N(1)-C(4)	1.400(9)
N(1)-C(1)	1.426(11)
C(1)-C(2)	1.344(15)
N(2)-C(17)	1.437(9)
N(2)-C(12)	1.464(9)
N(2)-C(16)	1.481(9)
C(2)-C(3)	1.402(14)
N(3)-C(13)	1.442(8)
N(3)-C(14)	1.460(8)
N(3)-C(18)	1.489(7)
C(3)-C(4)	1.340(12)
N(4)-C(15)	1.441(8)
N(4)-C(20)	1.458(9)
N(4)-C(19)	1.477(9)
C(4)-C(5)	1.431(12)
C(5)-C(6)	1.379(11)

C(5)-C(10)	1.407(10)
C(6)-C(7)	1.396(12)
C(7)-C(8)	1.327(12)
C(8)-C(9)	1.353(12)
C(9)-C(10)	1.432(11)
C(10)-C(11)	1.435(12)
C(10)-K(1)#2	3.399(7)
C(11)-K(1)#2	3.104(8)
C(12)-C(13)	1.487(10)
C(14)-C(15)	1.527(9)

N(4)-K(1)-N(3)	61.19(15)
N(4)-K(1)-N(2)	115.21(16)
N(3)-K(1)-N(2)	60.82(16)
N(4)-K(1)-C(4)	115.4(2)
N(3)-K(1)-C(4)	170.98(17)
N(2)-K(1)-C(4)	117.2(2)
N(4)-K(1)-N(1)	110.8(2)
N(3)-K(1)-N(1)	144.87(16)
N(2)-K(1)-N(1)	100.4(2)
C(4)-K(1)-N(1)	26.54(18)
N(4)-K(1)-C(11)#1	97.8(2)
N(3)-K(1)-C(11)#1	104.01(19)
N(2)-K(1)-C(11)#1	121.9(2)
C(4)-K(1)-C(11)#1	84.5(2)
N(1)-K(1)-C(11)#1	111.1(2)
N(4)-K(1)-C(3)	138.0(2)
N(3)-K(1)-C(3)	160.8(2)
N(2)-K(1)-C(3)	102.3(3)
C(4)-K(1)-C(3)	23.8(2)
N(1)-K(1)-C(3)	40.8(2)
C(11)#1-K(1)-C(3)	76.3(3)
N(4)-K(1)-C(5)	91.1(2)
N(3)-K(1)-C(5)	152.2(2)

N(2)-K(1)-C(5)	140.2(2)
C(4)-K(1)-C(5)	25.4(2)
N(1)-K(1)-C(5)	40.2(2)
C(11)#1-K(1)-C(5)	80.1(2)
C(3)-K(1)-C(5)	47.0(2)
N(4)-K(1)-C(10)#1	110.37(18)
N(3)-K(1)-C(10)#1	91.01(14)
N(2)-K(1)-C(10)#1	97.00(18)
C(4)-K(1)-C(10)#1	98.00(19)
N(1)-K(1)-C(10)#1	122.13(19)
C(11)#1-K(1)-C(10)#1	25.0(2)
C(3)-K(1)-C(10)#1	81.7(2)
C(5)-K(1)-C(10)#1	101.23(16)
N(4)-K(1)-C(1)	130.1(2)
N(3)-K(1)-C(1)	134.67(19)
N(2)-K(1)-C(1)	78.9(2)
C(4)-K(1)-C(1)	39.9(2)
N(1)-K(1)-C(1)	23.83(19)
C(11)#1-K(1)-C(1)	115.1(3)
C(3)-K(1)-C(1)	38.9(2)
C(5)-K(1)-C(1)	61.3(2)
C(10)#1-K(1)-C(1)	115.1(3)
N(4)-K(1)-C(11)	89.0(2)
N(3)-K(1)-C(11)	130.83(18)
N(2)-K(1)-C(11)	108.4(2)
C(4)-K(1)-C(11)	40.3(2)
N(1)-K(1)-C(11)	21.9(2)
C(11)#1-K(1)-C(11)	119.02(5)
C(3)-K(1)-C(11)	60.5(2)
C(5)-K(1)-C(11)	39.10(19)
C(10)#1-K(1)-C(11)	137.64(18)
C(1)-K(1)-C(11)	42.8(2)
C(11)-N(1)-C(4)	115.1(9)
C(11)-N(1)-C(1)	137.5(9)

C(4)-N(1)-C(1)	107.3(8)
C(11)-N(1)-K(1)	98.3(5)
C(4)-N(1)-K(1)	73.0(3)
C(1)-N(1)-K(1)	95.1(5)
C(2)-C(1)-N(1)	104.6(10)
C(2)-C(1)-K(1)	82.6(7)
N(1)-C(1)-K(1)	61.1(4)
C(17)-N(2)-C(12)	111.9(6)
C(17)-N(2)-C(16)	110.9(7)
C(12)-N(2)-C(16)	110.9(6)
C(17)-N(2)-K(1)	112.1(5)
C(12)-N(2)-K(1)	113.9(4)
C(16)-N(2)-K(1)	96.1(4)
C(1)-C(2)-C(3)	112.7(11)
C(13)-N(3)-C(14)	111.7(5)
C(13)-N(3)-C(18)	110.7(5)
C(14)-N(3)-C(18)	111.0(5)
C(13)-N(3)-K(1)	116.3(4)
C(14)-N(3)-K(1)	116.6(3)
C(18)-N(3)-K(1)	88.1(3)
C(4)-C(3)-C(2)	105.4(10)
C(4)-C(3)-K(1)	64.6(4)
C(2)-C(3)-K(1)	90.0(6)
C(15)-N(4)-C(20)	112.1(5)
C(15)-N(4)-C(19)	111.2(6)
C(20)-N(4)-C(19)	109.1(6)
C(15)-N(4)-K(1)	114.2(4)
C(20)-N(4)-K(1)	99.5(4)
C(19)-N(4)-K(1)	110.0(4)
C(3)-C(4)-N(1)	110.0(9)
C(3)-C(4)-C(5)	146.3(9)
N(1)-C(4)-C(5)	103.5(7)
C(3)-C(4)-K(1)	91.6(5)
N(1)-C(4)-K(1)	80.5(3)

C(5)-C(4)-K(1)	90.8(4)
C(6)-C(5)-C(10)	119.1(9)
C(6)-C(5)-C(4)	132.8(8)
C(10)-C(5)-C(4)	107.9(7)
C(6)-C(5)-K(1)	115.1(4)
C(10)-C(5)-K(1)	92.1(4)
C(4)-C(5)-K(1)	63.8(3)
C(5)-C(6)-C(7)	119.6(9)
C(8)-C(7)-C(6)	122.8(9)
C(7)-C(8)-C(9)	119.1(10)
C(8)-C(9)-C(10)	121.9(9)
C(5)-C(10)-C(9)	117.5(8)
C(5)-C(10)-C(11)	108.7(8)
C(9)-C(10)-C(11)	133.7(9)
C(5)-C(10)-K(1)#2	121.5(4)
C(9)-C(10)-K(1)#2	86.9(5)
C(11)-C(10)-K(1)#2	65.9(4)
N(1)-C(11)-C(10)	104.6(8)
N(1)-C(11)-K(1)#2	115.7(5)
C(10)-C(11)-K(1)#2	89.1(5)
N(1)-C(11)-K(1)	59.7(4)
C(10)-C(11)-K(1)	83.7(4)
K(1)#2-C(11)-K(1)	169.9(3)
N(2)-C(12)-C(13)	113.4(6)
N(3)-C(13)-C(12)	114.7(6)
N(3)-C(14)-C(15)	113.3(5)
N(4)-C(15)-C(14)	113.7(5)

Symmetry transformations used to generate equivalent atoms:

#1 -x,y-1/2,-z+1/2 #2 -x,y+1/2,-z+1/2

Appendix III has been removed for copyright or proprietary reasons.

It is the following published article: Bermingham, M. J., Cloke, F. G. N., Gardiner, M. G., Hitchcock, P. B., Wise, L. E., Yates, B. F., Structural studies of Group 1 metal 4-azapentalenyl complexes, Dalton transactions, 2005, 7, 1157-1158